STABILITY OF THIN PRECAST CONCRETE WALL PANELS SUBJECTED TO GRAVITY AND SEISMIC FORCES

A thesis submitted in partial fulfillment of the
requirements for the degree of
Master of Civil Engineering
at the
University of Canterbury,
Christchurch, New Zealand

by

Methee Chiewanichakorn

November, 1999

ABSTRACT

The stability of thin reinforced concrete cantilever walls with lateral displacement restraint at roof level designed for limited ductility under gravity and in-plane seismic loading is investigated in this project.

A large number of innovative designs of very tall and slender reinforced concrete walls have been developed in New Zealand ahead of the design standard in the past five years. In order to understand the actual wall behaviour and obtain the quantitative design verifications, limited experimental work has been performed for the past few years at the University of Canterbury. The test results of the previous experimental work are reviewed.

Four slender precast concrete 1:2.5 scale walls were tested up to failure under reversed cyclic loading regime with increased displacement level. The walls were 3.75 m high, 1 m long and 50 mm thick. The aspect and slenderness ratios were 3.75 and 75, respectively. The two main variables investigated were in effect the eccentric axial load ratios and the ratio between the lap splice length of the starter bars and the height to the point of inflection.

Only one of the test units, which had longer lap-splice and imposed eccentric vertical load, was susceptible to lateral buckling failure due to a significant cracking in the lower half of the wall and the excessive out-of-plane displacement. The units with an artificial lap-splice (welded connection) performed well and failed due to loss of strength caused by fracturing of starter bars after being buckled under the effects of reversed cyclic loading. Failure was observed near the welds along an artificial lap splice. Twisting of the walls at the base of the walls was observed in the tests.

A continuum method for the seismic design and assessment of thin precast concrete walls is proposed. The method can be applied to walls of structures designed for the range of elastic to limited ductility response.

ACKNOWLEDGEMENTS

The research presented in this report was carried out in the Department of Civil Engineering, University of Canterbury, New Zealand, under the supervision of Mr. D. K. Bull and Dr. J. I. Restrepo.

A gratefully thanks to my supervisors Mr. D. K. Bull and Dr. J. I. Restrepo for their support, advice and patience throughout this research. Additional thanks to Dr. John Smaill from Mechanical Engineering Department for his assistance of steel testing.

The financial support of the Cement & Concrete Association of New Zealand and the Department of Civil Engineering is gratefully acknowledged.

I would like to thank all the technical staffs of the Civil Engineering Department, in particular to P. Murphy and S. Toase, who were involved in the construction of the test apparatus and the specimens used in this research. Melody Callahan produced the superb graphical presentation.

Thanks also to all my colleagues and friends, Jeff Matthews, Kazu Tsuno, Kueh Hsueh Lyn and Maree Stockman for their help and support over my research period.

Finally, I would like to give my special thanks to my family for their continuous support and encouragement during the years I spent at university.

TABLE OF CONTENTS

LIST OF FIGURES

LIST OF TABLES

NOTATIONS

A_g = gross section area.

A_s = cross-section area of non-prestressed tension reinforcement.

A_v = cross-section area of non-prestressed shear reinforcement.

b = wall thickness.

b_c = critical wall thickness.

b_w = wall width.

C_c = internal compressive force carried by concrete.

$C_{h,provided}$ = provided strength from design process.

$C_{h\,(450)}$ = design strength for 450 year return period earthquake.

C_{si} = internal compressive force of non-prestressed reinforcement.

c = neutral axis depth.

d = distance from extreme compression fibre to centroid of tension reinforcement.

d_b = nominal bar diameter.

E_c = modulus of elasticity of concrete

E_s = modulus of elasticity of non-prestressed reinforcement.

F_{w1} = uniformly distributed load due to inertia of the panel over full height of the wall.

F_{w2} = point load applied at the top of the wall.

f'_c = specified compressive concrete strength at 28 days.

$f'_{c,eff}$ = effective specified concrete compressive strength.

f_c = compressive concrete strength.

f_r = modulus of rupture of concrete.

f_s = stress in non-prestressed reinforcement.

f_u = ultimate strength of non-prestressed reinforcement.

f_y = lower characteristic yield strength of non-prestressed reinforcement.

f_{yt} = lower characteristic yield strength of non-prestressed shear reinforcement..

G = dead load.

h_w = wall height.

I_e = effective second moment of inertia.

I_g = gross second moment of inertia.

k_{75} = stiffness at 75% of the nominal in-plane flexural strength.

k^*_{calc} = theoretical in-plane stiffness.

k_{expt} = experimental in-plane stiffness.

L_{db} = basic development length of a straight bar.

l^* = buckling length.

l_p = theoretical potential plastic hinge length.

l'_p = actual potential plastic hinge length.

l_w = wall length.

M_n = nominal flexural strength.

M_x = applied moment at distance x below the top of the wall.

M'_y = first yield flexural strength.

n = number of stories.

N = applied axial force.

N^* = design axial force.

P_{75} = applied shear force at 75% of the nominal capacity.

P_{crack} = in-plane lateral load at cracking strength.

P_{crit} = critical buckling in-plane lateral load.

P_n = theoretical nominal capacity.

P_{yield} = in-plane lateral load at first-yield capacity.

p = steel ratio.

p_{min} = minimum allowable steel ratio.

p_{max} = maximum allowable steel ratio.

p_l = steel ratio of the section.

Q_u = reduced live load for the ultimate limit state.

$S_{a(450)}$ = design lateral force.

S_p = structural performance factor.

s_h = vertical spacing of the shear reinforcement.

s_v = horizontal spacing of vertical reinforcement along the length of the section.

T_{si} = internal tensile force of non-prestressed reinforcement.

t_{gap} = height of the gap between the wall and the foundation beam.

t_w = wall thickness.

V^* = design shear force.

V_d = shear force component due to dowel action.

V_E = demand horizontal shear capacity.

V_f = shear force component due to friction.

V_n = nominal shear strength.

$V_{provided}$ = provided base shear capacity from post-design assessment.

V_{wall} = design shear force.

W = total building weight imposed on the wall.

x_i = distance from the extreme compression fibre of the section.

α_a = parameter used in determining development lengths.

β = angular rotations for a given crack width.

ε_{si} = strain of non-prestressed reinforcement.

ε_{cc} = strain of concrete.

ε_{cu} = ultimate strain of concrete.

ε_{sm} = estimated maximum tensile strain.

ξ = critical eccentricity.

λ = amplification factor.

μ_f = coefficient of friction.

μ_ϕ = curvature ductility.

μ_Δ = displacement ductility.

$\mu_{\Delta,twist}$ = displacement ductility level when twisting of the base occurs.

ρ = concrete density.

ϕ = strength reduction factor.

ϕ'_y = first yield curvature.

$\phi_{o,w}$ = overstrength factor.

ϕ_u = ultimate limit state curvature.

ω_v = dynamic magnification factor.

v_c = concrete shear stress.

v_n = nominal shear stress.

Δ_{75} = average horizontal displacement at 75% of the nominal capacity.

Δ_c = crack width.

Δ'_y = reference yield displacement.

Δ_u = predicted ultimate displacement.

CHAPTER 1
INTRODUCTION

1.1 OVERVIEW OF STRUCTURAL DESIGN FOR SEISMIC RESISTING SYSTEM

Earthquakes have occurred for millions of years and will continue in the future as they have in the past. It is impossible to prevent earthquakes from occurring, but it is possible to mitigate the effects of strong earthquake shaking and to prevent the structural collapse to reduce loss of life, injuries and loss of operation.

The study of earthquakes dates back many centuries. Written records of earthquakes in China date as far back as 3000 years. In the United States the historical record of earthquakes is much shorter, about 350 years. On the seismically active west coast of the United States earthquakes records go back only about 200 years. In New Zealand archives describing seismic events are dated back about 150 years.

In New Zealand, the likelihood of getting a major earthquake in a major populated area is reasonably high. To design structures to resist earthquakes without any damage is difficult to achieve even if these structures are designed for elastic response. Elastic design can be uneconomical for a large number of earthquake resisting structures. Lower seismic loading can be used instead for seismic design and the structures are allowed to respond into the post-elastic range without a great reduction in lateral load capacity or support gravity loads. To achieve this, the critical regions in the structure must be detailed for ductility. Such structures must have only minimal, typically repairable, damage during earthquake corresponding to the serviceability limit state, i.e. the relatively frequent earthquakes inducing comparatively minor intensity of ground shaking should not interfere with functionality such as the normal operation of a building or the plant it contains.

"Limited ductility" can be defined as a design seismic level, which lies between elastic response and those of fully ductile response. Certain structures or individual elements may be considered to be of limited ductility and designed accordingly if this performance better suits the structural nature of the building [N1]. Figure 1.1 illustrates different levels of ductility response corresponding to variations of seismic design force levels. The straight line represents elastic response, or design ductility of 1.0. At the lower design seismic force, the design ductility gradually increases. In a structure designed for limited ductility response, see line *B-B'*, in Figure 1 the elastic and inelastic displacements are comparatively similar.

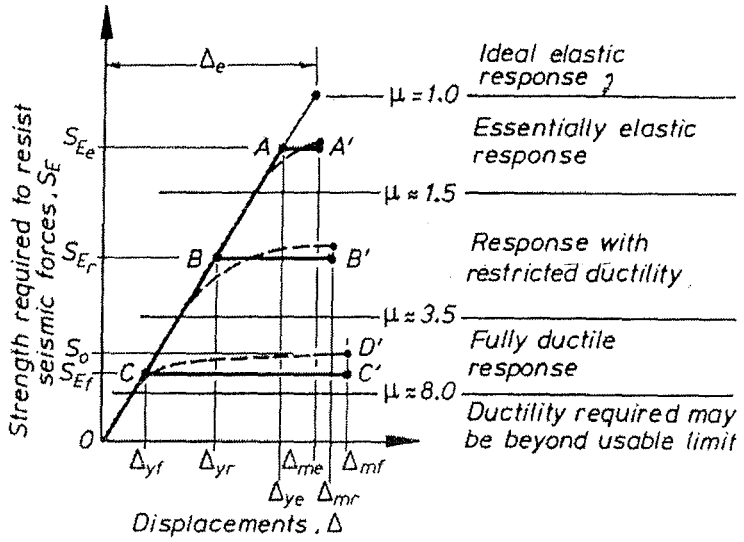

Figure 1.1: Range of design ductility level [P1]

Seismic design in New Zealand follows a "Capacity Design" procedure. The basis of this procedure was described for the first time in 1969 in paper by Hollings [H1] and further developed in 1975 in reference [P2]. Capacity design ensures that the most suitable mechanism of post-elastic deformation is developed and maintained in a structure during a major earthquake. In the capacity design of structures, elements of the primary lateral earthquake load resisting systems are chosen and suitably designed and detailed for adequate strength and ductility for a major earthquake. All other structural elements and other possible failure modes are then provided with sufficient strength, over and above the strengths generated in the inelastic mechanisms, so that the chosen means for achieving ductility can be maintained through out the deformations that may occur.

1.2 GENERAL OUTLINE OF PRECAST CONCRETE CONSTRUCTION IN NEW ZEALAND

Since the early 1960s, the use of structural precast concrete for structural components in buildings has become widespread in New Zealand. In the mid 1980s, there was a significant increase in the use of precast concrete in moment resisting frames and structural walls. Precast concrete technology had a major development because it has the advantages of high quality control, a reduction in site formwork and site labour, increased speed of construction and cost advantage.

New Zealand is in an active seismic zone, therefore the increase in the use of precast concrete required a great deal of innovation. This is because the past New Zealand Concrete Structures Standard [N4], same as the design concrete standards of many other countries, contained provisions for the seismic design of cast-in-place concrete structures but rather limited provisions for the seismic design precast concrete structures. The design methods that were introduced in New Zealand in the 1980s for frames and structural walls of buildings with precast concrete elements generally aimed to achieve monolithic behaviour representing cast-in-place concrete structures.

1.3 STRUCTURAL WALLS IN PRECAST CONCRETE CONSTRUCTION

In New Zealand, structural reinforced concrete walls have been recognised as the very efficient structural systems for resisting horizontal forces due to wind and earthquakes in buildings. Most structural walls in multi-storey buildings have been of cast-in-place reinforced concrete, but in the past decade significant precast concrete walls has been used, particularly in low rise construction, see Figures 1.2 to 1.4.

Tall and slender precast concrete wall panels are being commonly used in factory construction. Most panels are designed to resist both gravity and in-plane lateral forces without having any intermediate floors for the additional out-of-plane lateral supports.

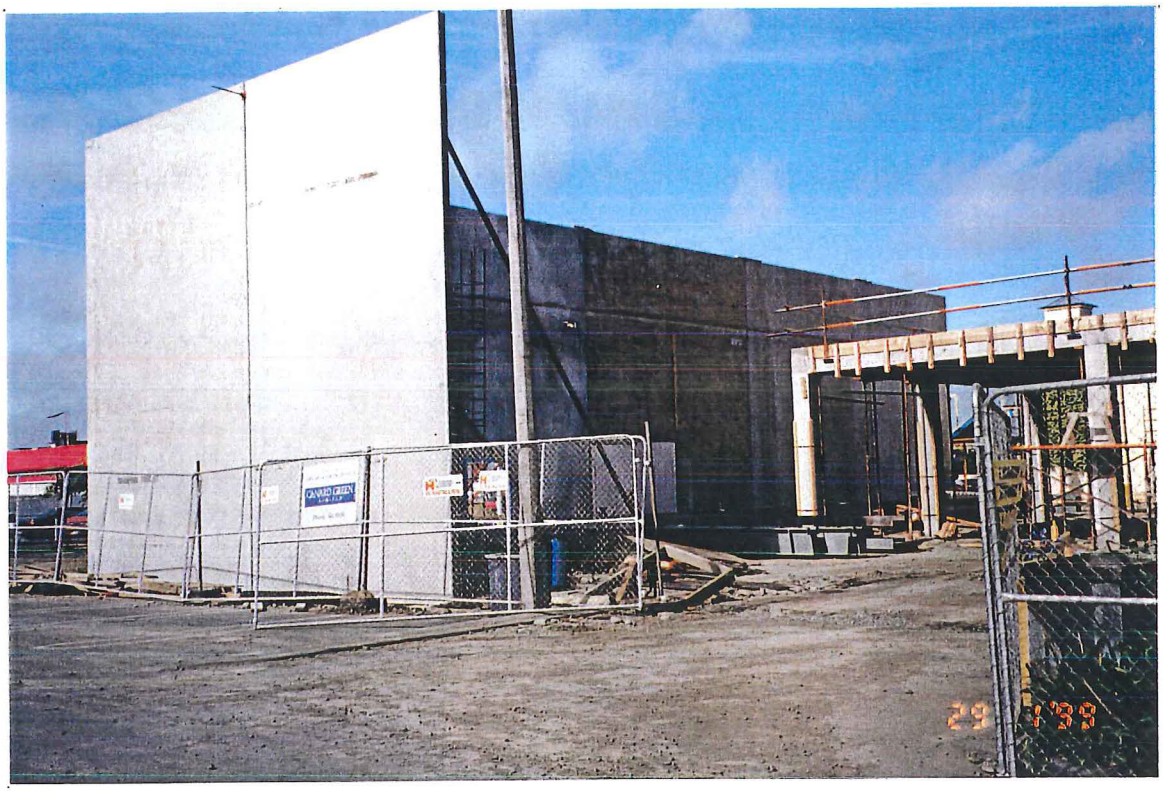

Figure 1.2: The use of thin precast concrete panel for factory construction

Figure 1.3: Low-rise apartment building with precast concrete wall panels

For precast concrete wall construction, relatively large reinforced concrete panels are cast horizontally on top of concrete floor slabs or casting either on site or alternatively in a precast concrete yard. When the concrete has reached sufficient strength for the panels to remain uncracked during lifting process, the wall panels are tilted up and lifted into their permanent position.

Unfortunately, the recent New Zealand Concrete Structures Standard [N1] does not have seismic design recommendations to cover all aspects of construction incorporating precast-concrete panels. As a result, designers have to come up with methods for connecting the elements together and to the foundations, which goes beyond the current scope of the New Zealand Concrete Structures Standard. Therefore, further research is required to give the designers' confidence in the design and construction with this structural system.

Figure 1.4: The use of precast concrete wall panel for Christchurch hospital car-park building

1.4 RESEARCH PROJECT ON PRECAST-CONCRETE WALL PANELS

The objective of this research is to investigate the seismic behaviour of thin slender precast concrete walls (with height-to-thickness ratio h_w/t_w of 75) as they are designed and built in common practice. This research is also a continuation of McMenamin's research [M1] on "The Performance of Slender Precast Reinforced Concrete Cantilever Walls with Roof Level Lateral Displacement Restraint under Simulated In-Plane Seismic Loading", which was undertaken at University of Canterbury in 1996-98.

This research project has been conducted by testing of four 1:2.5 scale wall specimens. Summary details of the four specimens are: -

1) A single wall with in-plane lateral loading only (normal lap-splice at the base of the wall to starter bars out of the foundation)
2) A single wall with in-plane lateral and eccentric vertical loading (normal lap-splice at the base of the wall to starter bars out of the foundation)
3) A single wall with in-plane lateral loading only (shorter lap-splice at the base of the wall to starter bars out of the foundation)
4) A single wall with in-plane lateral and eccentric vertical loading (shorter lap-splice at the base of the wall to starter bars out of the foundation)

Varying axial load with eccentricity was investigated to determine if out-of-plane moments (in the order expected in a real structure) were going to accelerate or initiate any out-of-plane instability that may occur.

The lap length was used to determine if the actual magnitude of the lap length had a beneficial effect on precluding failure modes seen in earlier research [M1]. These modes included spalling of the end zones of the walls, immediately above the foundation and out-of-plane flexure-shear failure in the compression zones of the base of the walls.

The effective length or height of the zone of plasticity ("plastic hinge zone") at the base of the walls is influenced by the physical length of the lapped bars at that

location. Another aim of varying the lengths of the laps in the tests was to establish if the restricting effect of the laps (binding the base of the walls in a less damaged zone) had an influence on when and if out-of-plane instability occurred in the extensively cracked zones immediately above the laps.

This research will only focus on the use of precast-concrete wall panels in one storey factories and warehouses, although they are also being used for low-rise apartments and offices which is beyond the scope of this studies.

CHAPTER 2
BACKGROUND AND LITERATURE REVIEW

2.1 INTRODUCTION

A large amount of research has been undertaken around the world during the past two decades about the behaviour of various connection details for precast concrete units. However, the amount of research work on the seismic behaviour of thin slender precast concrete wall construction is rather limited. Due to cranage limitations and material costs, precast concrete panels are manufactured as slender as practicable. Hence, panel stability and connection details are the most concerning issues in precast concrete wall construction.

2.2 STABILITY OF WALLS UNDER GRAVITY AND IN-PLANE HORIZONTAL LOADS

In general, precast concrete walls can be built reasonable slender. The slenderness ratio, defined as the height-to-thickness ratio h_w/t_w is generally much greater than that of normal cast-in-place reinforced concrete structural walls. Therefore, stability is a very important design criteria for precast concrete walls if the chosen ductility level is to be achieved.

Instability failure mode in structural walls can be classified into four main categories: -

(a) Elastic buckling of thin plate (Vlasov's solution)
(b) Goodsir and Paulay [G2] plastic hinge buckling
(c) Concrete compression failure – without buckling
(d) Flexural-shear failure associated with out-of-plane deformations

The instability types (b) to (d) can be defined as the loss of gravity and in-plane loading capacity caused by material failure.

Goodsir and Paulay [G2] found that the potential for out-of-plane buckling in thin sections of ductile walls depends more on the magnitude of the inelastic tensile strains imposed in the plastic hinge region of the wall, which on subsequent moment reversal is subjected to compression. Figures 2.1 (a) and (c) represents an idealised-cracked pattern for walls with thickness b. During the subsequent reversal of wall displacements, the tensile stresses in these bars reduce to zero while the width of cracks remains large. With the development of internal compression forces on the wall, compressive stresses will eventually be induced in the bars. Until the cracks close, the internal compression force within the wall section must be resisted by the vertical reinforcement only.

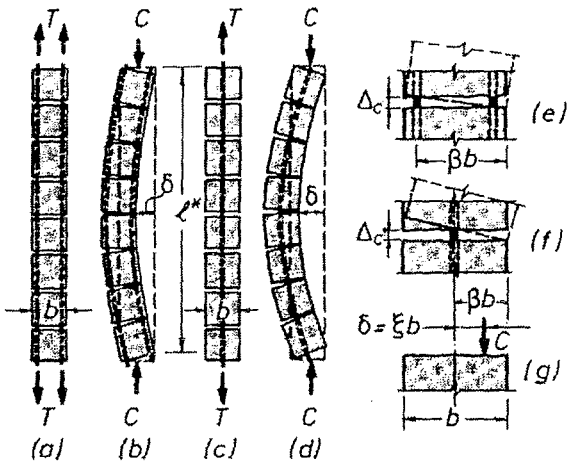

Figure 2.1: Deformations leading to out-of-plane buckling [P1]

At this stage the flexural compression force C within the thickness b of the wall may not coincide with the centroid of the vertical reinforcement as shown in Figures 2.1 (b) and (d). The eccentricity may result in rotation of blocks of concrete bound by adjacent horizontal cracks as depicted in Figures 2.1 (e) and (f). Hence, significant out-of-plane curvature may develop. The bending moment $M = \delta C$ at the centre of the wall strip, shown in Figures 2.1 (b) and (d) may cause an out-of-plane buckling failure of the wall well before cracks would fully close and before the in-plane flexural strength of the wall section could be developed [P1].

Goodsir and Paulay [G2] also found that the initiation of out-of-plane displacement δ would depend primarily on the crack width Δ_c and the arrangement of the vertical reinforcement within the thickness of the wall as suggested in Figures 2.1 (e) and (f). The crack width depends on the maximum tensile strain ε_{sm} imposed on the vertical bars in the preceding displacement cycle.

The combination of analytical concepts by Paulay and Priestley [P1] and experimental results by Goodsir and Paulay confirmed that this form of failure of the wall could occur when the thickness of the wall is less than the critical wall thickness b_c as shown in Equation 2-1.

$$b \le b_c = l^* \sqrt{\varepsilon_{sm} / 8\xi\beta} \qquad [2\text{-}1]$$

where

ξ = critical eccentricity in term of b

b_c = critical wall thickness

b = wall thickness

β = angular rotations for a given crack width

ε_{sm} = estimated maximum tensile strain

l^* = buckling length, usually assumes to be $0.5l_w$

l_w = wall length

With the conservative estimation for the extrapolated yield curvature in accordance with Figure 2.2 (a), the maximum steel strains ε_{sm} can be predicted as a function of the curvature ductility demand μ_ϕ. Goodsir and Paulay have shown that when out-of-plane displacements δ are relatively small, they reduce or disappear upon complete closure of cracks. However, with increased curvature ductility, increased displacements δ do not recover completely, and with repeated load cycles, out-of-plane displacements increase progressively. The threshold of critical displacement was found to be in the order of $\delta = b/3$. Hence by taking $\xi = 1/3$ it can be shown that

the critical wall thickness in the compressed end of the wall section in the plastic hinge region as in Equations 2-2 and 2-3.

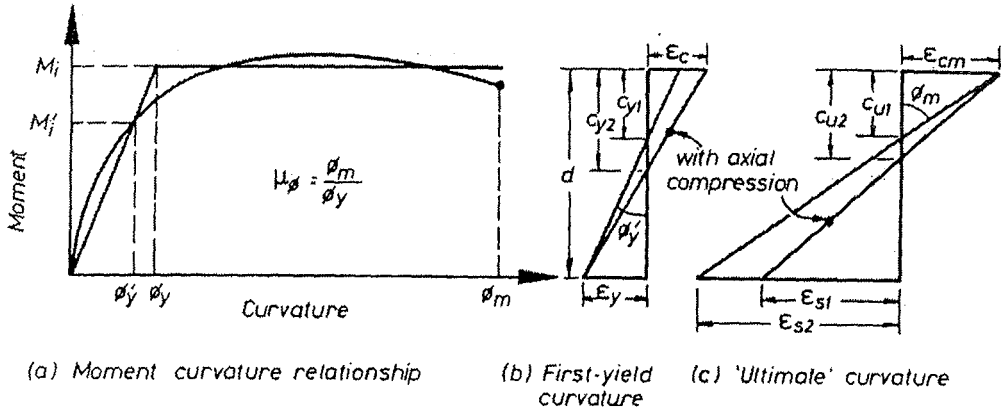

Figure 2.2: Definition of curvature ductility [P1]

$$b_c = 0.017 l_w \sqrt{\mu_\phi} \qquad \text{when } \beta = 0.8 \qquad [2\text{-}2]$$

$$b_c = 0.022 l_w \sqrt{\mu_\phi} \qquad \text{when } \beta = 0.5 \qquad [2\text{-}3]$$

where

b_c = critical wall thickness

l_w = wall length

μ_ϕ = demand curvature ductility

β = angular rotations for a given crack width (see Figure 2.1)

The relationship between curvature and displacement ductility of cantilever wall is shown in Equation 2-4. This relationship based on a plastic hinge length expression in Equation 2-5. Goodsir and Paulay have also produced a design curve to relate the critical wall thickness and the demand displacement ductility for both singly and doubly reinforced wall [G2].

$$\mu_\phi = 1 + \frac{(\mu_\Delta - 1)}{3(l_p/h_w)[1 - 0.5(l_p/h_w)]} \qquad [2\text{-}4]$$

$$l_p = 0.2 l_w + 0.044 h_w \qquad [2\text{-}5]$$

where

μ_ϕ = demand curvature ductility

μ_Δ = demand displacement ductility

l_p = potential plastic hinge length for wall

h_w = cantilever wall height

l_w = wall length

Additional factors affecting the stability of plastic hinge region in walls described by Goodsir and Paulay were:

1. The effect of disturbance of aggregate particles was believed to influence the transverse stability of slender sections. During tensile loading, aggregate may partially block full closure of the attendant horizontal cracks. On load reversal, the uneven closure of these cracks may result in an eccentricity of axial load which induces a transverse moment on the section.

2. The effect of cyclic loading or strain history of longitudinal reinforcement was believed to be a critical parameter causing out-of-plane instability. The most important aspect of strain history is the magnitude of the tensile strain which occurs prior to compression of the potentially unstable zone. It may be sufficient to allow large steel compression stresses and a very low tangent modulus to develop while tensile cracks are not yet fully closed.

3. Axial load level was another important parameter quoted. The sections with low axial forces are undoubtedly prone to out-of-plane buckling. High axial load will be more likely to cause the compression failures which accelerated by transverse instability.

4. McMenamin [M1] stated that this method by Goodsir and Paulay may not be able to predict the flexure-shear failure due to the difference in the wall configuration (boundary conditions).

In 1989 Saatchioglu, Wood and French [S1] verified that the deformability of structural walls under the in-plane loading are affected by a number of design parameters. The amount of longitudinal reinforcement, axial load level, loading history and wall geometry all play important roles.

Flexural failures were observed in the walls with small amounts of longitudinal reinforcement. These walls had low flexural capacities relative to their shear strengths. The available displacement ductility of approximately 6 was achieved by the lightly reinforced concrete wall panels. The available displacement ductility decreased as the amount of reinforcement increased. The available displacement ductility also decreased when the axial load level became greater for unconfined boundary elements.

Azizinamini, Glikin and Oesterle [A4] conducted an experiment on precast-concrete walls with slenderness ratio i.e. height-to-thickness ratio of 50 and 60. Test specimens were subjected to out-of-plane lateral and constant eccentric vertical loads. The top and bottom of each panel were allowed to rotate without translation. The lateral load capacity continually decreased while the out-of-plane displacement increased. The wall which was reinforced with two layers of reinforcement provided a stiffer wall with higher ductility, when compared to the wall with a single layer of reinforcement. No predicting methods concerning wall buckling were proposed by these researches.

Brown [B1] proposed with a design method, to ensure the stability of wall panels is adequate. The procedure applied to a typical boundary wall cantilever panel with in-plane seismic forces. In-plane bending moments at distance x below top of the panel are shown in Equation 2-6.

$$M_x = \frac{(F_{W1})x^2}{2h} + F_{W2}x \qquad [2\text{-}6]$$

where

M_x = bending moment at distance x below top of the wall

F_{w1} = uniformly distributed load due to inertia of the panel over full height of vertical cantilever

F_{w2} = point load applied at top of the wall, due to roof reaction

x = distance below the top of the wall

h = wall height

Brown [B1] presented an empirical solution to the buckling problem based on an equivalent column approach with an amplified earthquake in-plane lateral load. A design method assumes that buckling does not occur when the seismic lateral loads do not exceed some upper bound estimated from the New Zealand Loading Standard [N3].

Panel stability subjected to in-plane bending condition can also be analysed using either: -

(a) Flexural torsional buckling method based on calculation of a reference buckling moment M_o as discussed by McMenamin [M1].

(b) Empirical method for long column struts.

This method is based on an Euler elastic-buckling model. However, there are uncertainties in establishing parameters for this method and further this "elastic" approach, for determining instability, does not account for the flexure-shear failure which was observed by McMenamin [M1]. Therefore, it is believed that this approach requires further investigation.

2.3 CONNECTION BETWEEN PRECAST CONCRETE WALL PANEL AND FOUNDATION BEAM

2.3.1 Connection Systems for Precast Concrete Units

Connections between precast concrete walls and their foundations can be classified into two broad categories. They are "monolithic" and "jointed" connection details [G1]. "Monolithic" connection details have high degree of fixity providing

strong connection between the wall panel to the foundation. The precast elements are joined by reinforced concrete connection possessing stiffness, strength and ductility approaching that of cast-in-place concrete monolithic construction. In "monolithic" wall systems, connections are designed as "strong" connections, so their elastic limit is not exceeded in satisfying the building's ductility demands. Additionally, potential plastic hinge tends to spread into the structural members.

In "Jointed" connection details, the connection between the wall panels and the foundation are weak, such that there is a significant reduction in strength and stiffness at the wall-foundation interface. This governs the performance of the building during the earthquake. The purpose of utilising this "jointed" connection details is to maintain the integrity of the wall panel by providing an appropriate failure mechanism for the formation of potential plastic hinge, such as the starter bars, welded plates and so on. A common type of jointed connection in wall construction is precast concrete construction, which is extensively used in New Zealand for factories and warehouses. This type of connection may be designed as "ductile" with energy dissipation occurring at the connection.

2.3.2 Typical Wall-Foundation Connection

There are many different types of wall-foundation connection details which are employed by local structural engineers. The appropriate choice is made depending on the desired behaviour of walls under the event of major earthquake. The wall-foundation connections for the precast concrete wall can be divided into two subcategories depending on the degree of fixity of the connection [C1].

1) Cantilever
2) Pinned Connection

Figures 2.3 and 2.4 show the two subcategories of the typical wall-foundation connection detail of precast concrete wall construction in New Zealand.

In 1996, a seismic test carried out by Crisafulli et al. [C1] on a precast concrete wall panel connected to the foundation with vertical starter bars was able to achieve moderate to large displacement ductility factors without strength degradation. A brittle wire mesh, which was placed in the potential plastic hinge region as defined

by the New Zealand Concrete Structures Standard [N1], had no effect on the performance of the test unit.

Crisafulli et al. verified that precast concrete wall panel with a "construction joint" at the base, i.e. with starter bars (similar to Figure 2.3 (e)), can be designed as a structure of limited ductility. The design has to ensure that the ultimate in-plane flexural strength at the wall-foundation connection is less than the cracking moment of the wall panel because the plasticity would be able to concentrate at connection region without spreading through the wall panel. Without any panel cracking, out-of-plane instability was minimised.

Three components of in-plane lateral displacement found in Crisafulli et al.'s research were: -

1) Fixed-end rotation
2) Sliding shear
3) Wall deformation

Shear capacity at the horizontal joint, V^*, results from a combined mechanism due to friction between the wall panel and the base and dowel action in the reinforcing bars crossing the joint. Consequently, the shear force can be expressed as [C1]:

$$V^* = V_f + V_d \qquad [2\text{-}7]$$

where V_f and V_d are the components due to friction and dowel action, respectively.

From the design point of view, the shear capacity of the horizontal joint is usually assumed to be equal to the friction strength which can be expressed as Equation 2-8.

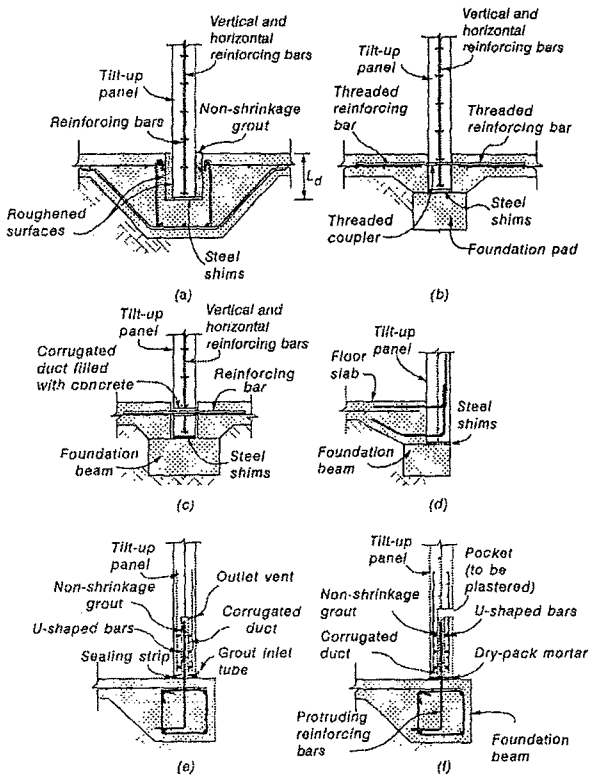

Figure 2.3: Wall-foundation connection designed as cantilever wall [C1]

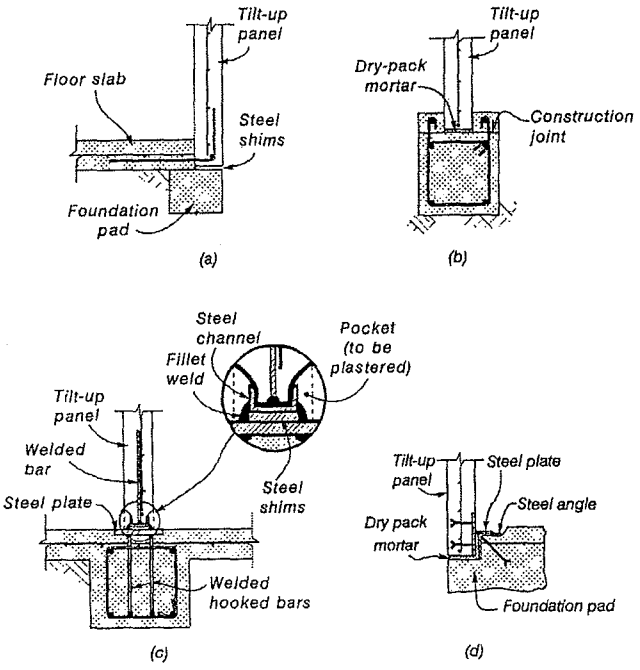

Figure 2.4: Wall-foundation connection designed as pinned connection [C1]

$$V_f = \mu_f C_c = \mu_f \left(N + \Sigma A_{si} f_{si}\right) \qquad [2\text{-}8]$$

where

μ_f = coefficient of friction

= 1.0 recommended for construction joint connection

C_c = internal compressive force within the wall carried by the concrete

N = gravity load acting in the horizontal joint

$A_{si}f_{si}$ = internal force in reinforcement undergoing tension

According to the experimental results [C1], the vertical reinforcement which located at the tension side of the wall, with area A_s, were assumed to be yielding.

$$V_f = \mu_f \left(N + A_s f_y\right) \qquad [2\text{-}9]$$

where

A_s = total area of tension reinforcement

f_y = yield strength of reinforcement

McMenamin [M1] performed experimental work in 1997. "Lateral-torsional buckling" or "Lateral buckling" was defined as a mode of failure that most often observed in flexural members with thin-walled sections, which are constructed out of high-strength steel. This mode of failure consists of simultaneous displacement out of the plane of loading and twisting about the longitudinal axis. These researches tested five 1:2.5 scale walls with different slenderness and reinforcement ratios. All test units had uniformly distributed reinforcement at the cast-in-place wall-foundation connection. None of the test units failed due to lateral buckling, despite a lateral displacement of more than half the wall thickness was observed to occur.

A test unit, which had a longitudinal reinforcement ratio of 1.1% and aspect ratio (h_w/l_w) of 1.25, failed at a displacement ductility factor of 1.25, due to out-of-plane flexure-shear failure at the base of the compression edge of the wall and laterally buckled on reloading when the boundary conditions altered. However, the

out-of-plane shear forces which resulted in the out-of-plane flexure-shear failure were not quantifiable during the test.

Three test units with a longitudinal reinforcement ratio of 0.6% and aspect ratios from 1.25 to 2.5, failed by fracturing of longitudinal reinforcement, with severe in-plane flexural strength degradation at large displacement ductility factors.

One test unit with a longitudinal reinforcement ratio of 1.1% and aspect ratio of 2.5, failed corresponding to an interstorey drift equal to 1.0%, due to spalling of the cover concrete which led to buckling of longitudinal reinforcement and an accompanying significant reduction of in-plane flexural strength.

The out-of-plane restraint forces at the top of the wall was measured but showed no correlation with the test applied in-plane forces. It was ranged approximately between 1.25% to 5.0% of the in-plane lateral strength.

A design solution was derived by McMenamin [M1] of limited application, as stated by these researchers. This solution applied to a linear, elastic, homogeneous, isotropic cantilever loaded at the top and restrained there against out-of-plane displacement, and used to assess the buckling load of thin precast concrete walls is expressed in Equation 2-10. However, there are three conditions that must be met in order to calculate the critical buckling in-plane lateral load, P_{crit}, based on gross sectional properties;

1. the extent of cracking is limited
2. the reinforcing does not yield
3. the concrete stress at the extreme compression fibre is less than $0.5f'_c$.

$$P_{crit} = \frac{0.598E_c b_w^3 l_w}{h_w^2} \qquad [2\text{-}10]$$

where

E_c = modulus of elasticity of concrete given by Equation 3-7 [N1]

f'_c = specified compressive concrete strength at 28 days

b_w = width of wall

l_w = length of wall

h_w = height of wall

As highlighted by McMenamin [M1], this method should also be employed when the wall elements that respond in an elastic or nominally elastic manner.

2.4 COMPARISON OF ANALYSIS, DESIGN AND DETAILING METHODS FOR TYPICAL PRECAST CONCRETE WALL PANELS BETWEEN NEW ZEALAND AND UNITED STATES STANDARDS

New Zealand

The "Guidelines For The Use of Structural Precast Concrete In Buildings" [G1] suggests that the method of analysis and design, which commonly used for monolithic or cast-in-place structural walls, are usually not suitable for jointed precast concrete wall construction. The strength design method, in which member strengths are assigned according to the relative elastic stiffness of undamaged structure, relies on inelastic load redistribution to adjust for differences between actual and computed load paths. Jointed precast concrete structures rely on discrete connectors. The changes in the relative wall stiffness of jointed wall systems that occur as joints open and close during a major earthquake are often neglected.

The seismic design of the precast concrete wall panels is not covered in the New Zealand Concrete Structures Standard [N1]. A design approach mostly based on both experimental test data verifying the seismic behaviour and detailed theoretical analysis. The most commonly used connection details in precast concrete construction can be found in Crisafulli et al. [C1].

United States [T2]

Slender precast concrete walls are commonly analysed as beam-columns. The Building Code Requirements for Reinforced Concrete provisions, ACI 318-89 [A3] was believed to be applicable to walls where the height-to-thickness ratio, h_w/t_w, of 30. Precast concrete walls will often exceed this limitation with h_w/t_w ratios of 40 to 50 or

more. These are permitted by ACI 318-89, but only where a detailed structural analysis, including long term effects, shows adequate strength and stability. The Building Code Requirements for Reinforced Concrete provisions, ACI 318-89 [A3] proposed several methods for computing the load carrying capacity of these wall panels.

In 1974, the Portland Cement Association published a design aid for precast concrete load bearing walls. A series of design charts were produced based on detailed computer analysis. Coefficients to determine the maximum axial loadings were given for several combinations of section thickness, reinforcing steel areas, in-plane lateral loading, panel height and concrete strength. Other variations of the design charts were produced which made it easier to consider special loading conditions or variations in section properties.

Most designers prefer a simplified analysis method that gives reasonably accurate but conservative results. Such a method is provided by the Structural Engineers Association of Southern California (SEAOSC) in the "Yellow Book" [R1] and the "Green Book" [T3]. These and other methods of approximate analysis are used to compute the in-plane flexural stiffness of the concrete section from which maximum panel in-plane deflection and thus *P*-delta moments (out-of-plane direction) can be obtained.

CHAPTER 3
WALL DESIGN

3.1 GENERAL

Precast concrete walls are one of the most efficient earthquake resisting systems for low to mid-rise buildings. They are sometimes also utilised as the gravity load carrying system. A special characteristic of such walls is their relatively large slenderness in order to minimise lifting weights and, hence, construction costs.

The structure shown in Figure 3.1 was modified from the example in "Examples of Concrete Structural Design to New Zealand Standard 3101" [E1] and used as prototype for this investigation. A typical industrial building in New Zealand with precast panels are usually designed as a lateral and gravity load resisting system.

The selected precast concrete wall panels for this investigation has a slenderness or height-to-thickness ratio, h_w/t_w, of 75. The design level was chosen to be "limited ductility" which equals to $\mu = 3$ where μ is the system ductility. All test specimens were designed according to New Zealand Concrete Structures Standard [N1] to satisfy both the general and the additional seismic design requirements.

3.2 DESIGN PHILOSOPHY OF TEST UNITS

A "Capacity Design" approach was applied in the design of the panels and connections. All flexural reinforcement was detailed to the ductility level for the design earthquake. Other elements were also designed to protect against undesirable failure modes and to maintain the chosen failure mechanism.

The panels themselves were designed to crack when subjected to the applied in-plane lateral load. That was to ensure that the panels might show increased susceptibility to fail in bucking mode.

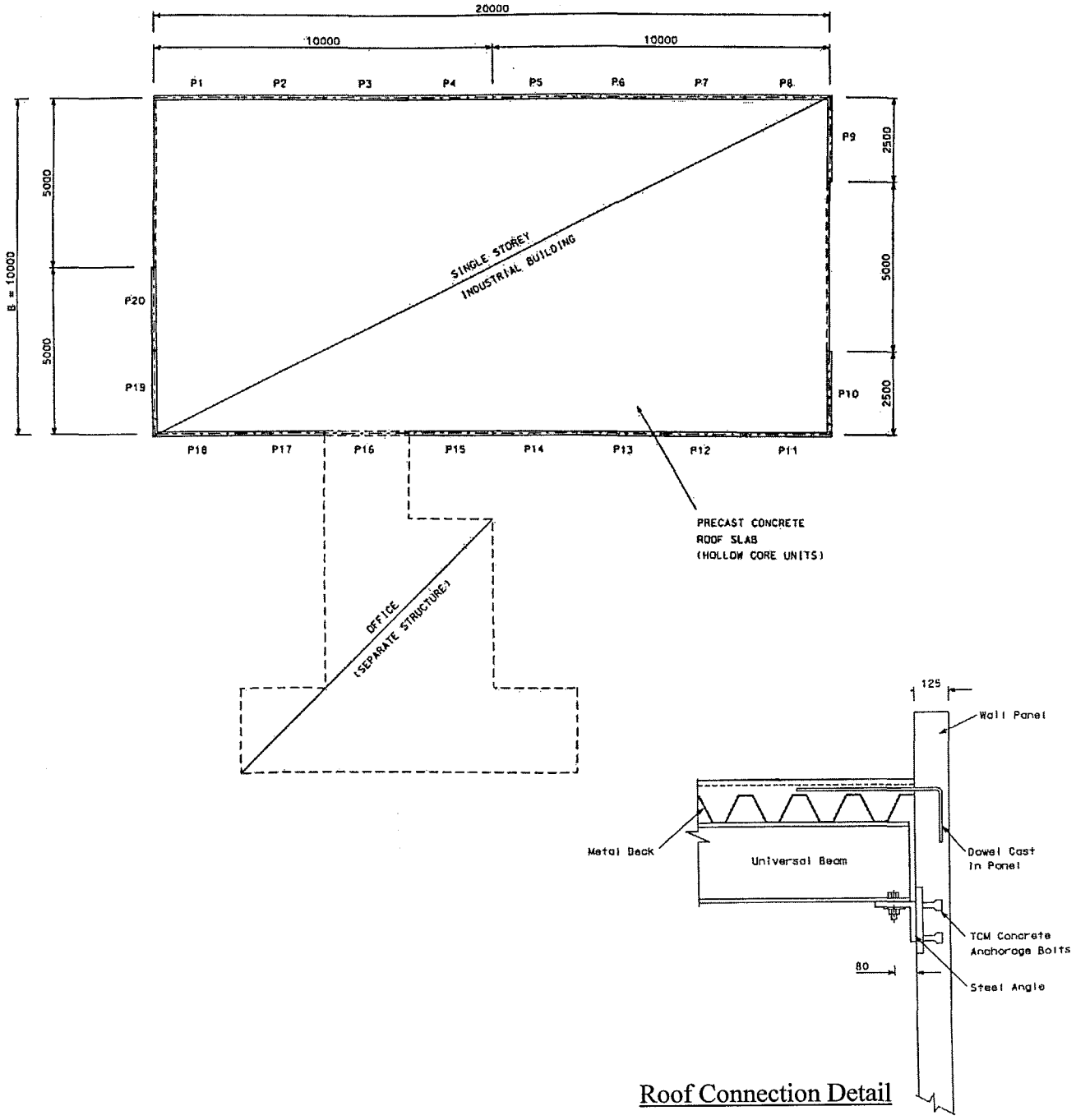

Figure 3.1: Idealised precast concrete structure modified for this investigation [E1]

3.3 WALL DESIGN AND ANALYSIS FOR FLEXURAL STRENGTH

This section outlines flexural strength design and analysis for walls. It was used in the design of connections and wall panels for this investigation.

3.3.1 Elastic Analysis

A strain compatibility method is required in determining the first yield curvature (ϕ'_y) of wall sections. When the first yield curvature is reached, the actual concrete compression stress block in walls will typically be approximately linear with a strain distribution as shown in Figures 3.2 (c) and (d).

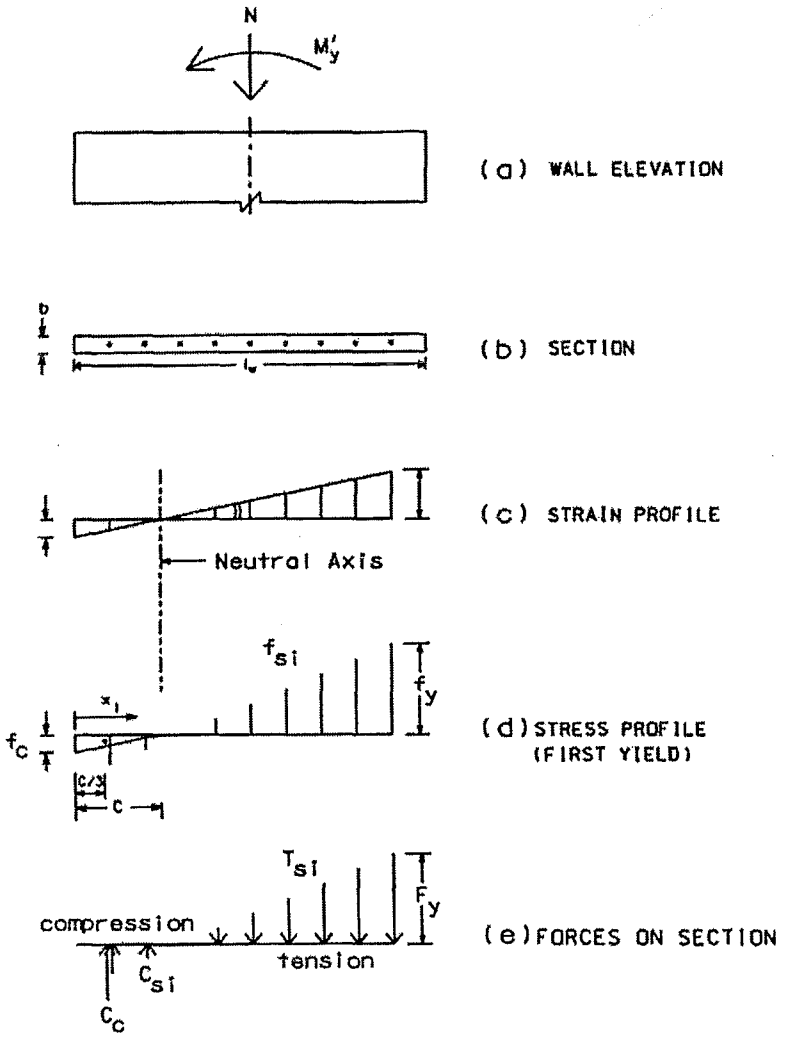

Figure 3.2: Stress-strain profile at the first yield curvature

Stress-Strain Compatibility

$$\varepsilon_{si} = \varepsilon_{cc}\frac{(c - x_i)}{c} \qquad [3\text{-}1]$$

and $$f_y \geq f_{si} = E_s\varepsilon_{si} \geq -f_y \qquad [3\text{-}2]$$

Internal forces in concrete and reinforcement are calculated using Equations 3-3, 3-4 and 3-5.

$$C_c = 0.5 f_c bc \qquad [3\text{-}3]$$

and $$C_{si} = A_{si} f_{si} \qquad [3\text{-}4]$$

and $$T_{si} = A_{si} f_{si} \qquad [3\text{-}5]$$

where

ε_{si} = strain of non-prestressed reinforcement

ε_{cc} = strain of the extreme fibre in compression

x_i = distance from the extreme compression fibre of the section

c = neutral axis depth of the section

f_y = lower characteristic yield strength of non-prestressed reinforcement

f_{si} = stress of non-prestressed reinforcement

E_s = modulus of elasticity of non-prestressed reinforcement

C_c = internal compressive force of concrete

f_c = compressive concrete stress in the outermost fibre in compression

b = wall thickness

C_{si} = internal compressive force of non-prestressed reinforcement

T_{si} = internal tensile force of non-prestressed reinforcement

A_{si} = cross section area of non-prestressed reinforcement

Assuming that the stress and strain in the concrete has a linear relationship. Therefore,

$$\frac{f_c}{\varepsilon_{cc}} = E_c \qquad [3\text{-}6]$$

where

E_c = modulus of elasticity of concrete

Modulus of elasticity of concrete (E_c) varies with concrete density (ρ). It should be taken as

$$E_c = \left(3320\sqrt{f'_c} + 6900\right)\left(\frac{\rho}{2300}\right)^{1.5} \qquad [3\text{-}7]$$

where

f'_c = specified compressive concrete strength at 28 days

ρ = concrete density

The assumption was made that concrete has no tensile capacity.

Equilibrium Conditions

Axial force: -

$$N = \left(C_c + \sum C_{si}\right) - \sum T_{si} \qquad [3\text{-}8]$$

Moment Equilibrium (about neutral-axis): -

$$M'_y = C_c\left(c - \frac{c}{3}\right) + \sum_1^m C_{si}(c - x_i) + \sum_1^n T_{si}(x_i - c) + N\left(\frac{l_w}{2} - c\right) \qquad [3\text{-}9]$$

where

N = applied axial force

M'_y = bending moment at first yield

l_w = length of the wall

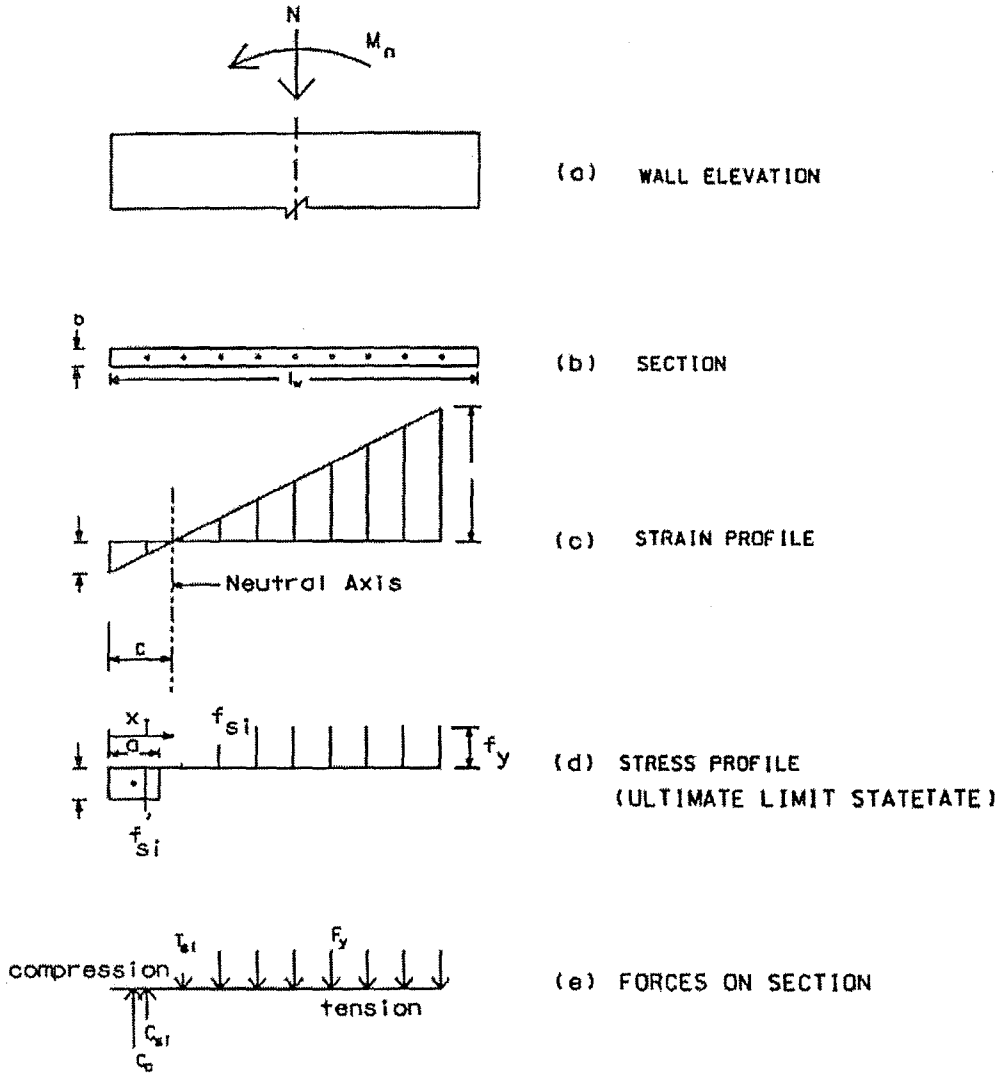

Figure 3.3: Stress-strain profile at ultimate limit state.

3.3.2 Ultimate Limit State Analysis

In ultimate limit state analysis, the Whitney equivalent rectangular stress block [W2] for the concrete is assumed to be $0.85f'_cab$ to represent the non-linear stress profile (Figure 3.3).

The ultimate strain of unconfined concrete, is taken approximately as $\varepsilon_{cu} = 0.004$. Stress-strain compatibility needs to be satisfied using Equation 3-1.

Both forces equilibrium and moment equilibrium are also needed to be satisfied to give nominal flexural strength, M_n and ultimate curvature, ϕ_u of the wall section.

$$\phi_u = \frac{\varepsilon_{cu}}{c} \qquad [3\text{-}10]$$

The reference yield curvature (ϕ_y) can be extrapolated from the first yield curvature using Equations 3-11 and 3-12. Figure 3.4 illustrates the relationships between the first yield curvature (at $0.75S_i$) and reference yield curvature (at S_i).

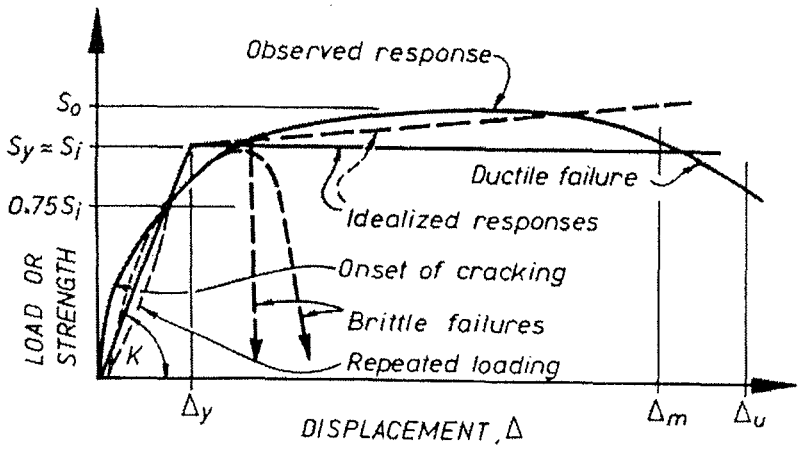

Figure 3.4: Typical in-plane load-displacement relationship for a reinforced concrete element [P1]

$$\phi'_y = \frac{\varepsilon_{cc}}{c} \qquad [3\text{-}11]$$

$$\phi_y = \frac{M_n}{M'_y}\phi'_y \qquad [3\text{-}12]$$

where M_n is the nominal flexural strength of the section

3.3.3 NZS 3101:1995 Code Limitations

The following limitations are taken from NZS 3101:1995 [N1].

Tensile Steel Ratio

The area of the longitudinal reinforcement of the section has to satisfy the following requirements.

$$p_{\min} \le p_l \le p_{\max} \qquad [3\text{-}13]$$

$$p_l = \frac{A_s}{bs_v} \qquad [3\text{-}14]$$

$$p_{\min} = \frac{0.7}{f_y} \qquad [3\text{-}15]$$

$$p_{\max} = \frac{16}{f_y} \qquad [3\text{-}16]$$

where

p_l = tensile steel ratio of the section

A_s = area of longitudinal non-prestressed reinforcement

f_y = lower characteristic yield strength of non-prestressed reinforcement

s_v = horizontal spacing of vertical reinforcement along the length of the section

Horizontal Spacing (s_v)

The horizontal spacing of the longitudinal reinforcement is chosen to be the least of the following criteria.

$$s_v \leq {}^{l_w}\!/_{3} \quad or \quad 3t_w \quad or \quad 450mm \qquad [3\text{-}17]$$

where

l_w = length of the section

t_w = thickness of the section

3.4 WALL DESIGN AND ANALYSIS FOR SHEAR STRENGTH

The in-plane shear force acting on the wall is determined using the capacity design. Allowance needs to be made for flexural overstrength of the wall and for the influence from higher mode effects of seismic lateral forces given in the New Zealand Loading Standard [N3]. The total design shear force shall be calculated using Equation 3-18 [P1].

The test specimens were designed to represent the wall panels used for factory buildings, which have a single-storey height. Hence, the number of stories (n) was chosen to be equal to 1.0. After substituting this value into Equation 3-19, dynamic shear magnification factor (ω_v) became 1.0.

$$V_u = V_{wall} = \omega_v \phi_{o,w} V_E \qquad [3\text{-}18]$$

where

ω_v = dynamic shear magnification factor, which shall be determined from Equations 3-19 and 3-20.

$\phi_{o,w}$ = overstrength factor

V_E = horizontal shear demand derived from code-specified lateral static force

For buildings up to six stories [P1],

$$\omega_v = 0.9 + n/10 \qquad [3\text{-}19]$$

For buildings over six stories [P1],

$$\omega_v = 1.3 + n/30 \quad \leq 1.8 \qquad [3\text{-}20]$$

where

n = number of stories which cannot be taken larger than 15

The nominal shear stress (v_n) can be defined using Equation 3-21. The New Zealand Concrete Structures Standard [N1] limits the nominal shear stress to prevent diagonal compression failure of the wall, in "General principles and requirements", with the following criterions in Equation 3-22.

$$v_n = \frac{V_{wall}}{\phi bd} \qquad [3\text{-}21]$$

$$v_n \leq 1.1\sqrt{f'_c} \quad or \quad 0.2f'_c \quad or \quad 9\,MPa \qquad [3\text{-}22]$$

where

V_{wall} = design shear force from Equation 3-18

ϕ = strength reduction factor when the shear results from overstrength flexural action

= 1.0

d = effective depth of the section

= $0.8l_w$

b = thickness of the wall

In the potential plastic hinge regions, concrete contributes some shear strength to the wall depending on the level of the axial force in compression and level of ductility. This is taken from "Additional design requirements for earthquake effects [N1]" provisions and shown in Equations 3-23 (a) and 3-23 (b). There is no concrete shear contribution when the wall is subjected to tensile axial force as in Equation 3-23 (c).

$$v_c = 0.6\sqrt{\frac{N^*}{A_g}} \qquad \text{when } N^* \text{ is compression} \qquad [3\text{-}23\ (a)]$$

and

$$v_{c,\max} = \left(\frac{\phi_{ow}}{\mu_\Delta} + 0.15\right)\sqrt{f_c'} \qquad [3\text{-}23\ (b)]$$

$$v_c = 0 \qquad \text{when } N^* \text{ is tension} \qquad [3\text{-}23\ (c)]$$

For the region outside the potential plastic hinge, which is taken from "Additional Design Requirements for Earthquake Effects [N1]", the maximum concrete shear contribution for walls with either net compression or net tension axial forces is shown in Equation 3-24. In which case N^* is negative in Equation 3-24 (b).

$$v_{c,\max} = 0.2\sqrt{f'_c} \qquad \text{when } N^* \text{ is compression} \qquad [3\text{-}24\ (a)]$$

$$v_{c,\max} = 0.2\left[\sqrt{f_c'} + \frac{N^*}{A_g}\right] \qquad \text{when } N^* \text{ is tension} \qquad [3\text{-}24\ (b)]$$

where

v_c = concrete shear contribution

N^* = axial force associated with the shear being considered (taken as negative for tension)

A_g = gross section area of the section

ϕ_{ow} = ratio of overstrength moment of resistance to moment resulting from specified loading, where both moments refer to the base section of a wall [N1].

μ_Δ = ductility factor

Once the nominal shear stress, v_n, and concrete shear contribution, v_c, are determined, the amount of shear reinforcement can be calculated from Equations 3-25 and 3-26 [N1].

$$A_v = \frac{(v_n - v_c)bs_h}{f_{yt}} \qquad [3\text{-}25]$$

and

$$A_v \geq \frac{0.7bs_v}{f_{yt}} \qquad [3\text{-}26]$$

where

A_v = area of shear reinforcement

f_{yt} = lower characteristic yield strength of non-prestressed shear reinforcement

s_h = vertical spacing of the shear reinforcement, to be found from Equation 3-27

$$s_h \leq {}^{l_w}\!/_5 \quad or \quad 3t_w \quad or \quad 450mm \qquad [3\text{-}27]$$

where

t_w = overall thickness of the section

3.5 DESIGN OF THE TEST UNITS

Four single wall units were designed similarly in accordance with the provisions given by the New Zealand Concrete Structures Standard [N1]. In order to maintain a wall thickness of 50 mm, the wall height had to be 3.75 m which resulted in a higher slenderness ratio ($h_w/t_w = 75$). These scaled models were 1:2.5 of the prototype structure.

3.5.1 Description of the Prototype Building

A prototype building chosen for the design of the specimens is shown here in Figure 3.1. The building is a single storey factory with a one-way reinforced concrete roof slab on metal decks running between steel beams. The building is 10 m wide by 30 m long. The wall panels are 9.375 m high and 125 mm thick. The steel beams are supported by steel cleats which are bolted into the concrete at the top of the precast concrete wall panels. The maximum eccentricity of the centre of the steel beam supports is 80 mm to the wall face. The thickness of the reinforced concrete slab is 160 mm. The design gravity load calculations are shown in Appendix A.

3.5.2 Design and Analysis of Wall-Foundation Connections

The starter bars were used as the connection between wall panels and foundation beams. They were initially designed to be 6 mm diameter Grade 430 deformed bars (HD6) and grouped at both ends of the wall. However the design had to be changed due to the recent unavailability of 6 mm diameter deformed bars in New Zealand. Hence, 10 mm diameter Grade 300 deformed bars (D10) were used for all test specimens.

These starter bars were designed to yield after the cracking of panel occurs so that softening of concrete could take place, which might increase an instability of the panel. The flexural strength of the panel at cracking was estimated using the modulus of rupture (f_r) calculated from Equation 3-28.

$$f_r = 1.0\sqrt{f'_{c,eff}} \qquad [3\text{-}28]$$

where

$f'_{c,eff}$ = effective specified concrete compressive strength at 28 days

The specified 28 days compressive strength of concrete (f'_c) was 30 MPa. Therefore the effective compressive strength of concrete ($f'_{c,eff}$) had to be increased up to 45 MPa to allow for: -

a) Target compressive strength of concrete being higher than the characteristic compressive strength, f'_c.
b) Ageing of concrete with time

In order to perform the flexural design of the starter bars, the flexural strength of the panel at cracking had to be increased by 30% to allow for overstrength action because: -

a) Actual strength of the reinforcing bars could be higher than the specified characteristic strength.
b) Strain hardening of the reinforcing bars.

3.5.2.1 Unit 1

Unit 1 was designed following the work performed by Crisafulli et al. [C1] and McMenamin [M1]. In McMenamin test units, the walls and foundation beam were built monolithically.

Cast-in-place horizontal connections between wall panels and the foundation have been tested by McMenamin [M1]. The reinforcement at the wall-foundation connection was evenly distributed along the joint to represent the cast-in-place panel. The test specimens were subjected to cyclic in-plane shear force and overturning moment at the connection.

Crisafulli et al. [C1] carried out a test on a precast concrete panel with a construction joint as the horizontal connection (non-monolithic). The unit showed ductile response. Plastic deformations took place in the connection joint between the panel and foundation beams and no cracking on the panels occurred.

Unit 1 was designed to have four 10 mm Grade 300 deformed bars (D10) as the starter bars and grouped at both ends of the wall-foundation connection. The first starter bar was located at 65 mm from the edge of the wall. The rest of the starter bars were located at 50 mm centres, next to the previous bars. All the starter bars were protruded from foundation beams and grouted into ducts cast in the base of the wall panels. These starter bars were designed to yield. The flexural reinforcement ratio in this unit was p = 1.26%. This value seemed to be relatively high when compared to current New Zealand practice due to the replacement of the 6 mm Grade 430 deformed bars (HD6) with 10 mm Grade 300 deformed bars (D10) in the test specimens.

The development length of these starter bars as the lap length for the splices between the starter bars and the wall longitudinal reinforcement was designed using Equation 3-29 [N1]. Consequently, the starter bars with 300 mm length penetrated into the foundation beam and the other 300mm was lapped with the wall longitudinal reinforcement. The method for connecting the walls to the foundation beam is described in Section 4.3.1. General details of Unit 1 are shown in Figure 3.6.

$$L_{db} = \frac{\left(0.5\alpha_a f_y\right)}{\sqrt{f'_c}} d_b \quad \geq \quad 300\text{mm} \qquad [3\text{-}29]$$

where

α_a = 1.3 for top reinforcement where more than 300 mm of fresh concrete is cast in the member below the bar, or 1.0 for all other cases [N1].

f_y = yield stress of steel

f'_c = specified concrete strength, MPa

d_b = diameter of reinforcing bars, mm

$$L_{db} = \frac{0.5 \times 1.0 \times 300}{\sqrt{30}} d_b$$

$$= 27.4 d_b$$

$$= 274mm$$

Therefore, lap length for D10 bars was taken as 300 mm.

3.5.2.2 Unit 2

Unit 2 was designed to be able to support an additional gravity load from the roof as the proposed idealised building. These types of building construction usually have some roofing connected at the top of the wall panels. There is a large variation of gravity load depending on the functional purposes of the buildings. In common practice, the gravity load level is ranged from 0.3 kPa to 4.0 kPa which is represented by light steel trusses to reinforced concrete slabs respectively.

In the New Zealand Loading Standard [N3], the combination of the gravity and earthquake loads must be used for the design purpose. Gravity load only includes the dead load (G) of the roofing materials while the reduced live load (Q_u) is equal to zero during an earthquake event. The concurrency of the earthquake and snow loads to take place simultaneously is normally neglected.

Hence, the reinforced concrete slab roof was assumed to be the worst case scenario for the design of Unit 2. Eventually, the reinforcing details for Unit 2 were exactly identical to Unit 1 with the same lap-splice length as Figure 3.6 shows.

3.5.2.3 Unit 3

Unit 3 was designed to verify any effects, which might arise as the result of the difference in the lap length, and hence softening of the wall, can occur above the lap can lead to local buckling failure. It represented an identical precast concrete wall panel with smaller reinforcing bar diameter, hence smaller lap-splice length. However, the 6 mm

diameter Grade 430 deformed bars (HD6) was not commercially available. The 10 mm Grade 300 deformed bars (D10) had to be used instead. Unit 3 was designed similarly to Unit 1 which there were four 10 mm Grade 300 deformed bars (D10) grouped at both ends at the wall-foundation connection. The first starter bar was located at 60 mm from the edge of the wall. The rest of the starter bars were placed at 50 mm centres next to the previous one.

In order to simulate the required condition, lap-splice length between the starter bars and the wall longitudinal reinforcement were designed according to Equation 3-29 but with 6 mm diameter. Hence, the lap-splice length was 180 mm. This value was only suitable for the experiment, but not applicable in practice. The starter bars and the wall longitudinal reinforcement were welded together to ensure the failure of lap-splice would not occur. Reinforcement detail of Unit 3 is shown in Figure 3.7.

3.5.2.4 Unit 4

Unit 4 with the same artificial lap-splice as Unit 3 representing the smaller size of reinforcement was designed to resist both in-plane lateral and eccentric vertical loadings. The reinforcement detail was exactly the same as Unit 3, which is illustrated in Figure 3.7.

3.5.3 Design of Wall Panels

Fundamentally, the amount of longitudinal reinforcement in the wall was restricted by number of starter bars and minimum spacing requirement for the longitudinal reinforcement as in Equation 3-17. The number of the starter bars governed the wall longitudinal reinforcement at both ends and the minimum spacing requirement was occupied in the middle region.

It was important that the longitudinal reinforcement from the wall being placed against the starter bars at both ends. The applied load at the top of the wall would induce tension and compression forces due to an overturning moment of the wall. The load path

would be maintained by transferring of tension and compression forces from the wall reinforcement to the starter bars and eventually to the foundation.

In this type of walls, the longitudinal reinforcement in the wall would not be able to be placed right next to the starter bars. There must be gaps which will be filled with grout during construction. However, some allowance had been made in "Guidelines for the Use of Precast Concrete in Buildings" [G1] for the maximum clearance between lapped bars. According to New Zealand Concrete Structures Standard [N1], the maximum longitudinal reinforcement vertical spacing (s_v) is specified in Equation 3-17 for the middle region of the wall.

The diameter of the 10 mm diameter starter bars was 1/5 of the wall thickness and thus did not comply with New Zealand Concrete Structures Standard [N1], which states that: -

For a limited ductile wall (*Cl.* 17.3.6.3): -

"The diameter of longitudinal bars used in any part of a wall shall not exceed 1/8 of the wall thickness. In all other respects the requirements of 12.4.3 shall apply."

For fully ductile wall (*Cl.* 12.4.3.3): -

"The diameter of the bars used in any part of a ductile wall shall not exceed one tenth of the thickness of the wall."

The effect of the bar diameter –to-wall thickness ratio used in this project is to be observed.

Transverse reinforcement in the wall was designed to avoid shear failure. Capacity design approach was employed to take into account of the flexural overstrength action. Nominal flexural strength was increased by 25% to incorporate strain hardening and the 5th percentile characteristic strength effects. Consequently, shear force on the wall was increased by 25% with the additional dynamic magnification factor (ω_v) taken

from Equations 3-19 and 3-20, which set equal to 1.0. Finally, the minimum transverse reinforcement, calculated from Equation 3-26, was sufficient.

The amount of the transverse reinforcement in the wall was designed using Equations 3-25, 3-26 and 3-27. Consequently, 6 mm diameter Grade 300 round bar (R6) with spacing of 150 mm were used for the horizontal reinforcement above the starter bars up to the top of the wall. Standard 90° hooks were used at the both ends of the horizontal reinforcement. In the lap-splice region, a series of hoops of 6 mm diameter Grade 300 round bars with 75 mm and 60 mm spacing, with standard 180° hooks, were used for Units 1 & 2 and Units 3 & 4 respectively (see Figures 3.6 and 3.7). This was to protect the wall from splitting of the concrete across the width of the wall which can be shown in Figure 3.5.

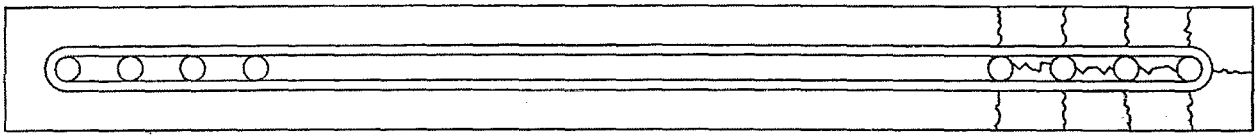

Figure 3.5: Splitting failure of concrete across the wall thickness

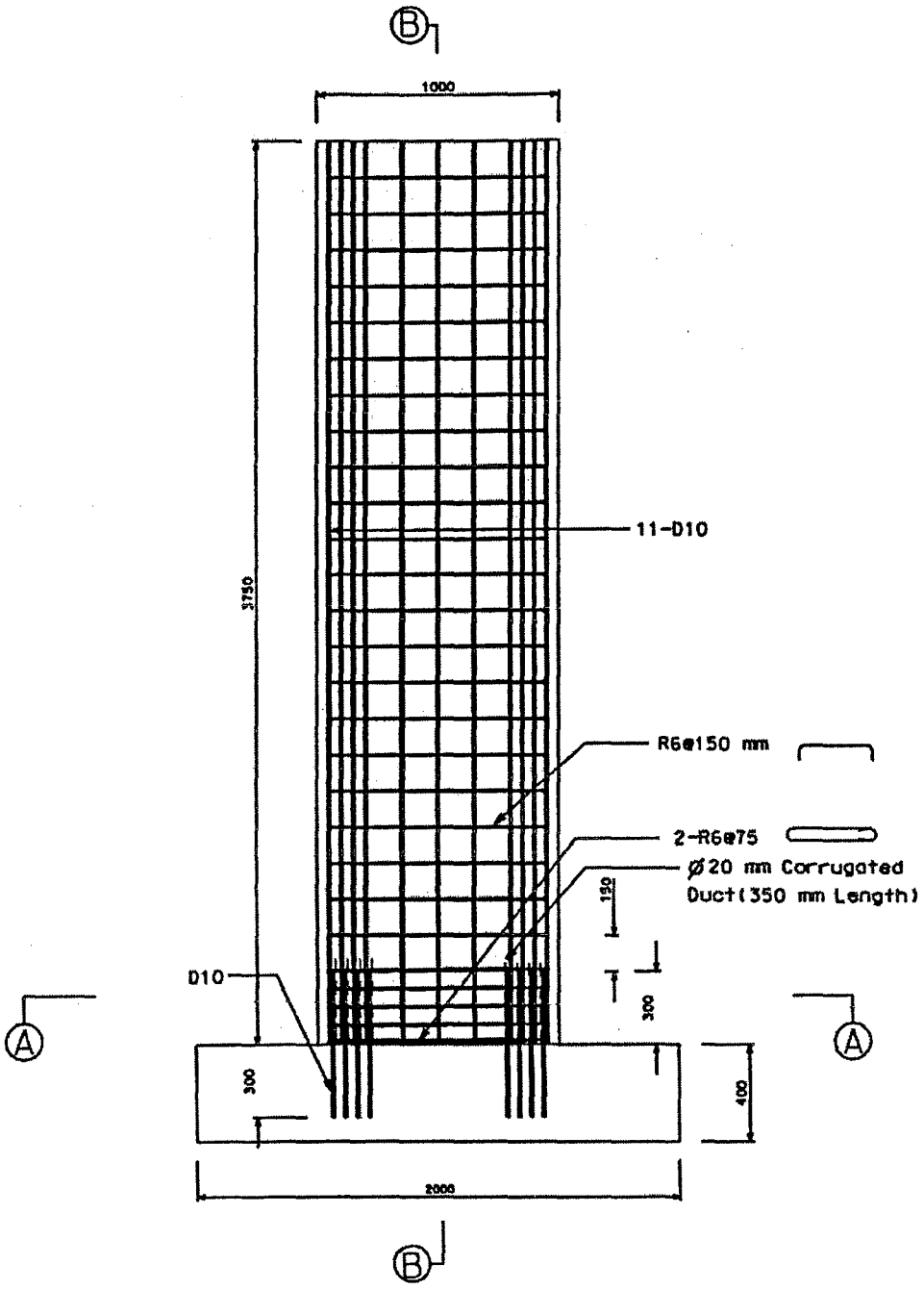

Figure 3.6: Wall reinforcement details for Units 1 and 2

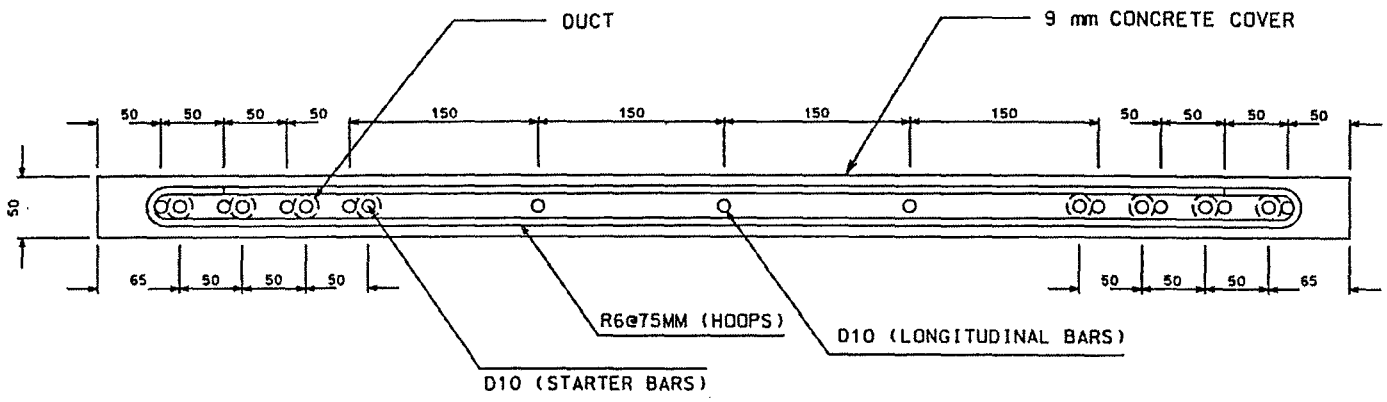

SECTION A–A

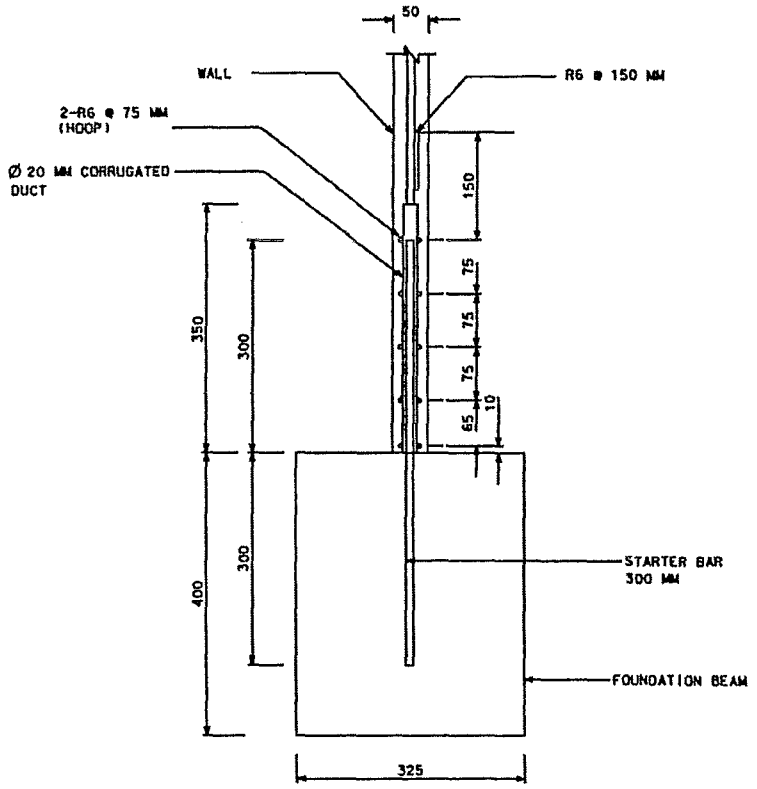

SECTION B–B

Figure 3.6 (cont.): Wall reinforcement details for Units 1 and 2

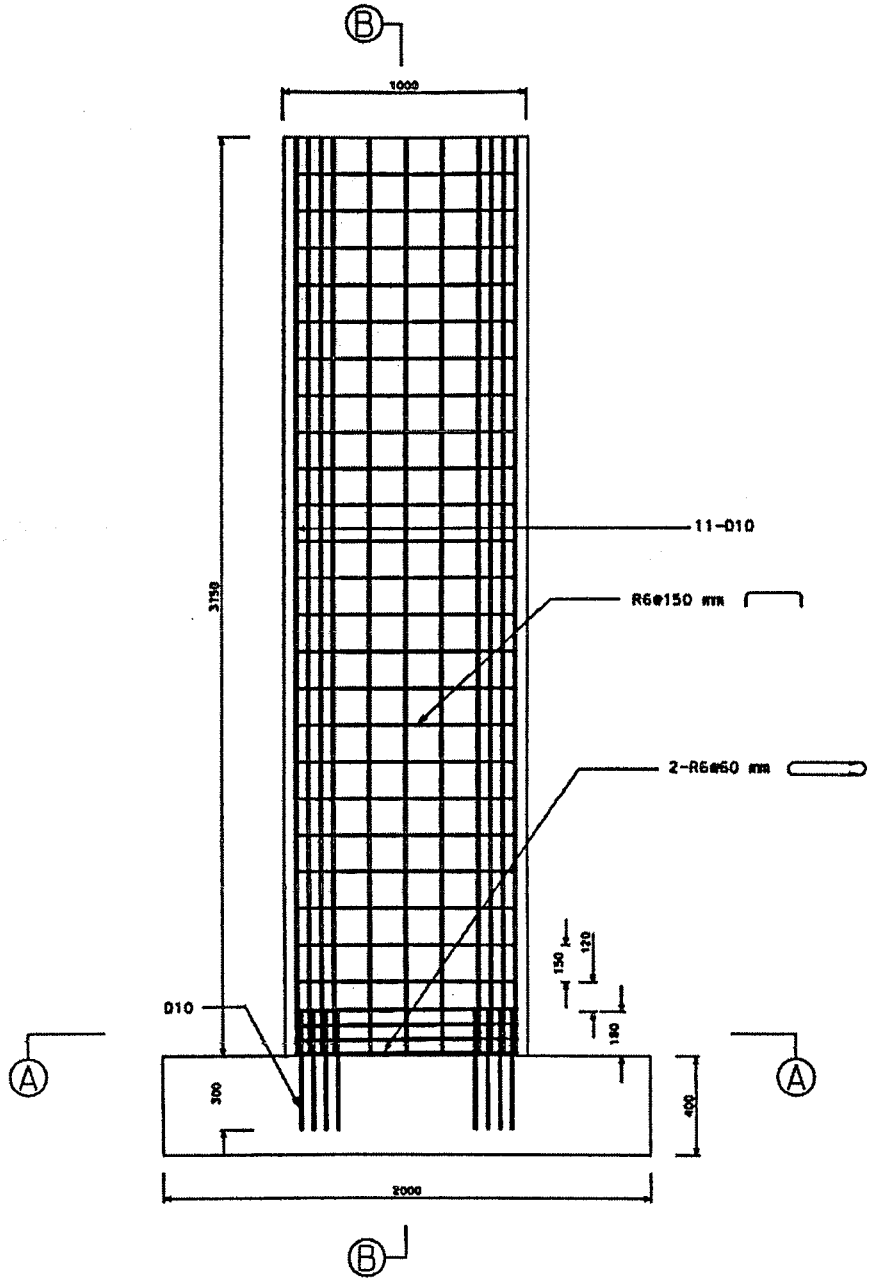

Figure 3.7: Wall reinforcement details for Units 3 and 4

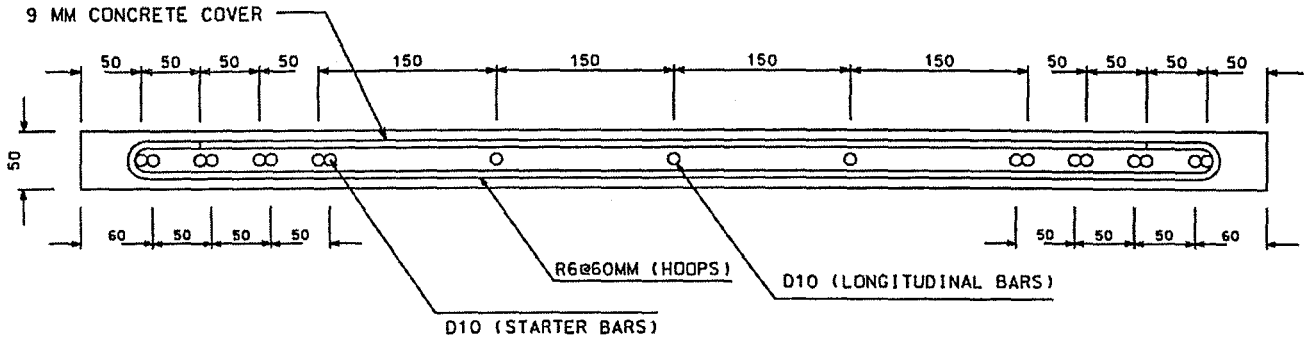

SECTION A-A

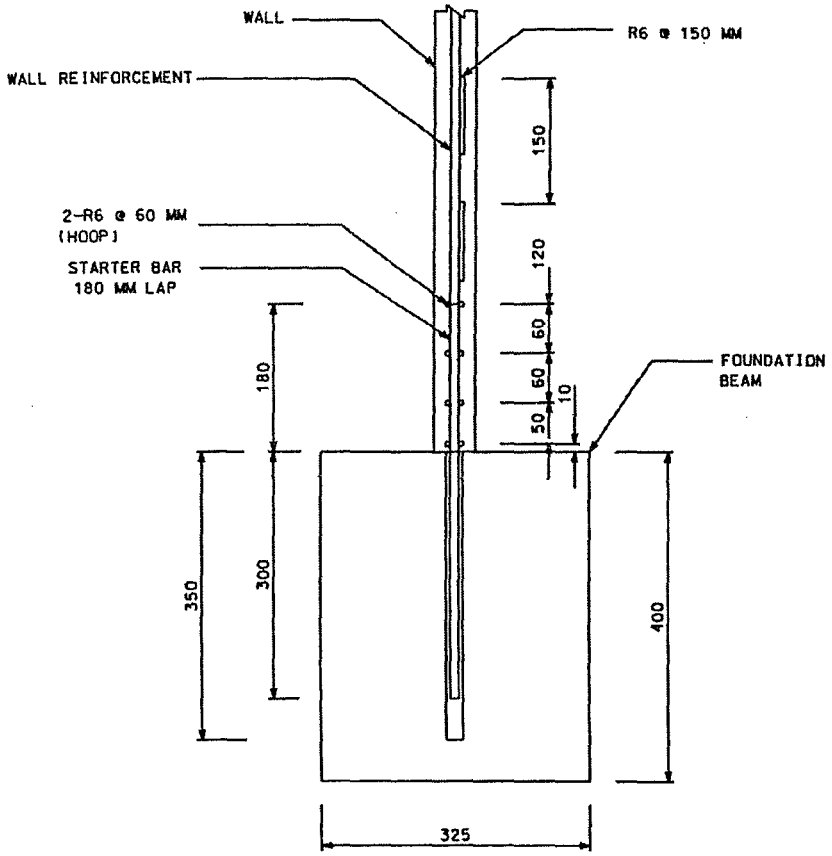

SECTION B-B

Figure 3.7 (cont.): Wall reinforcement details for Units 3 and 4

CHAPTER 4
EXPERIMENTAL PREPARATION

4.1 INTRODUCTION

This chapter gives full descriptions of the mould and strong-back, loading frame, test preparation, including construction methods and instrumentation.

4.2 DESIGN AND MODIFICATION OF EXPERIMENTAL APPARATUS

4.2.1 Mould and Strong-Back Modification

Figure 4.1 shows an existing mould from the early research by McMenamin [M1], which was modified to suit this research. The mould has been extended from 2.4 m to 3.75 m using an identical steel channel section as a strong-back (see Figure 4.2).

At the early stage of this project, the mould was designed as a part of lifting and positioning process. This means the mould must be able to support the wall without having an excessive deflection which would crack the panel during the lifting process.

Concrete compressive strength during lifting process was assumed to be 80% of the specified compressive strength at 28 days. Conservatively, the modulus of rupture, f_r is taken to be approximately $0.4\sqrt{f_c'}$. Subsequently, the calculation for the same steel channel sections gave the factor of safety of 1.7.

The strong-back was made of layers of plywood placing on top of the steel channels. The plywood had been constructed with a circular curve profile that was equivalent to the out-of-plane imperfection which might happen in practice. This imperfection was made equal to the maximum tolerance that had been chosen from Table 4.1, according to NZS 3109:1997 Concrete Construction Standard [N2] and scaled to suit the actual size of the test units. Different sizes of metal shims are inserted between the plywood and the steel channels at different positions in order to achieve this out-of-plane curvature.

Table 4.1: Specified tolerances for precast units [N2]

Component	Dimension (m)	Tolerance (mm)
1 (e) Camber: Variation from average camber for units up to two months after manufacture.	L<3.0	±5
	3.0<L<6.0	±8
	6.0<L<12.0	±12
	12.0<L<24.0	±20
	L>24.0	±30

The strong-back had to be modified to suit the new mould, which was still in the same range of wall height as McMenamin's research [M1]. Therefore, the wall had the same tolerance of ±12 mm (see Table 4.1) which was scaled down to 4.8 mm at the mid-height of the wall. The circular profile was stretched out to cover the whole new length of the wall. New sheets of plywood were overlaid on top of the existing sheets for reutilising purposes of the further research. The profile of the modified strong-back is shown in Figure 4.3.

4.2.2 Loading Frame Modification

The loading frame from Crisafulli et al.'s research [C1] in 1993-96 was modified and used in this research. Calculations were undertaken to confirm that the existing

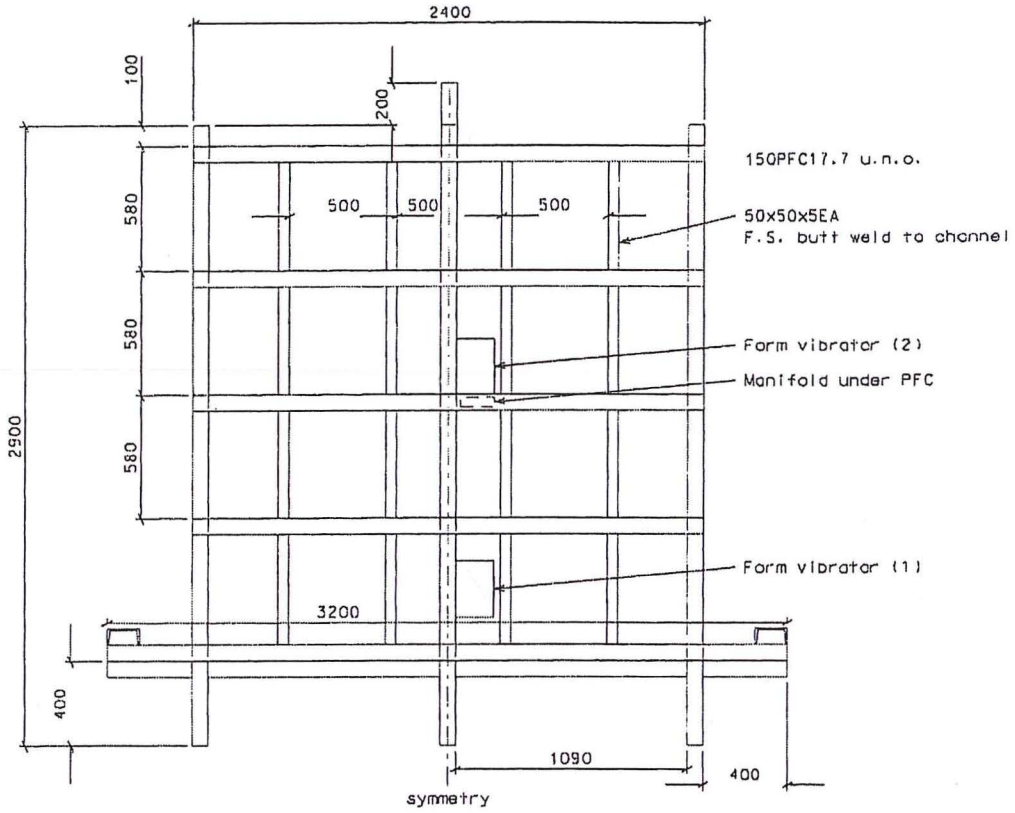

Figure 4.1: An existing mould from an early research [M1]

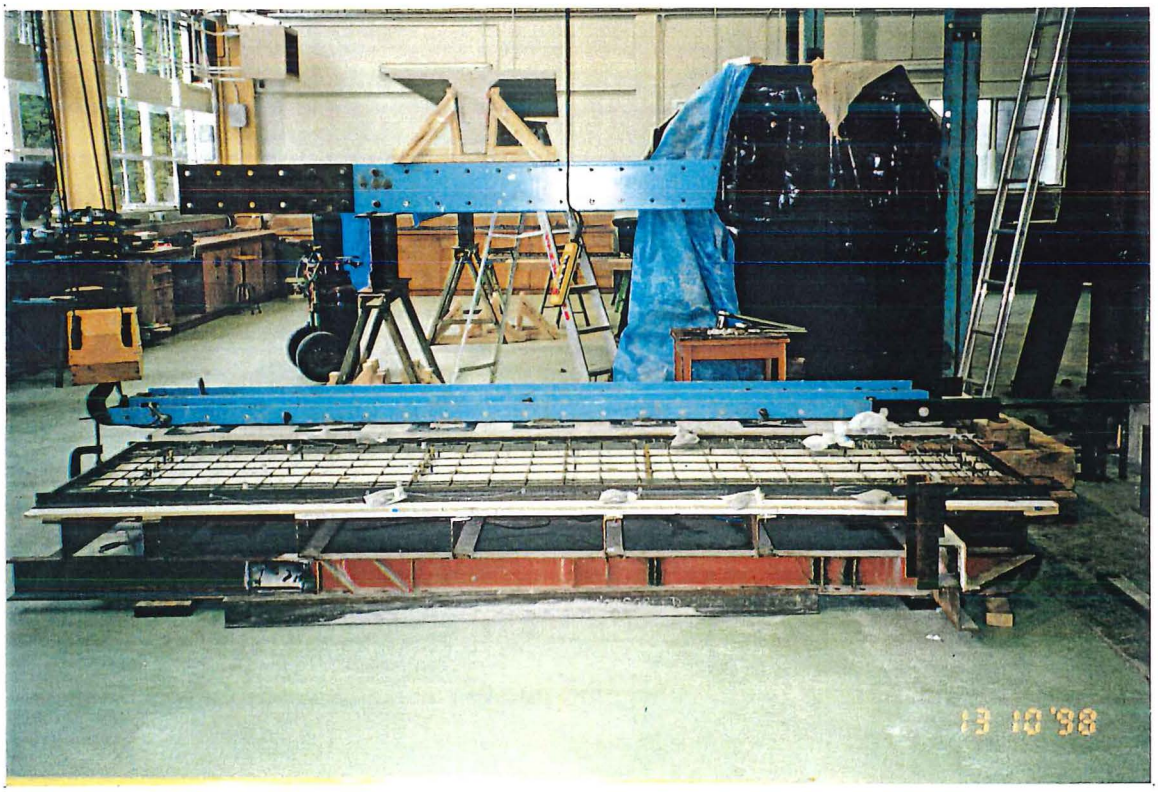

Figure 4.2: A modified mould for this research program

loading frame had an adequate strength. Member flexural capacity and shear capacity were checked using the procedure in Steel Designer's Handbook [S2].

The loading frame columns were made of double 250 parallel flanged channels (250 PFC) with welded plate lateral restraints at the position of diagonal braces. Both columns were welded on to 1 m by 1 m steel base plates which were bolted to the laboratory strong floor. There were two diagonal braces at 2.15 m above the floor on either side of the columns.

The existing loading frame did not required to be strengthened because of an anticipatal relatively small in-plane applied load. Diagonal braces also had sufficient capacity.

In out-of-plane loading direction, the deflection at the loading position near the top of the wall with 5% of ultimate load had been checked. As the result, out-of-plane bracing was required in order to prevent an excessive lateral movement of the loading frame. The modifications of the loading frame can be shown in Figures 4.4 and 4.5.

The position of the loading point had to be changed to the top of the wall. This represented the lateral load induced from the roof structures during a major earthquake event.

There were lateral restraint beams to prevent any out-of-plane movement at the top of the wall during the test. This component would initiate the boundary test condition as proposed in the previous chapter. They were made of 100 mm by 50 mm rectangular hollow section (100 RHS) placed on either face of the wall at 170 mm below the top of the wall as shown in Figure 4.6. Nylon circular strips were placed between the wall face and the lateral restrained beam at 130 mm from either end of the wall.

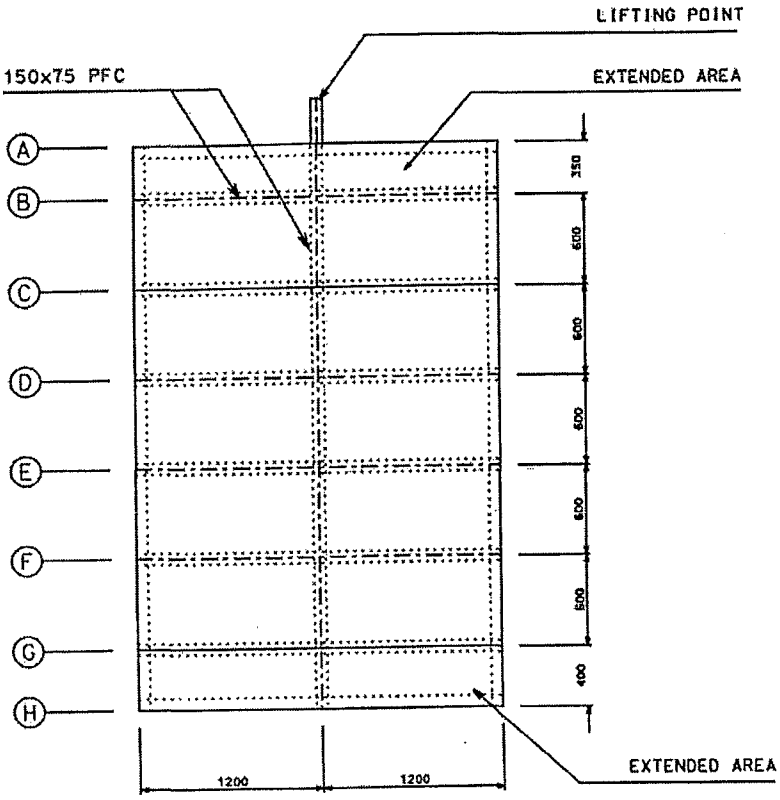

Note : 1. All extended members have the same size as the existing members.
2. All extended members are welded to the existing ones.
3. New plywood is on top of the existing one.
4. Lifting point is cut and rewelded to the extended member.
5. Strongback profile is attached.

Figure 4.3: Drawing of strong-back modification

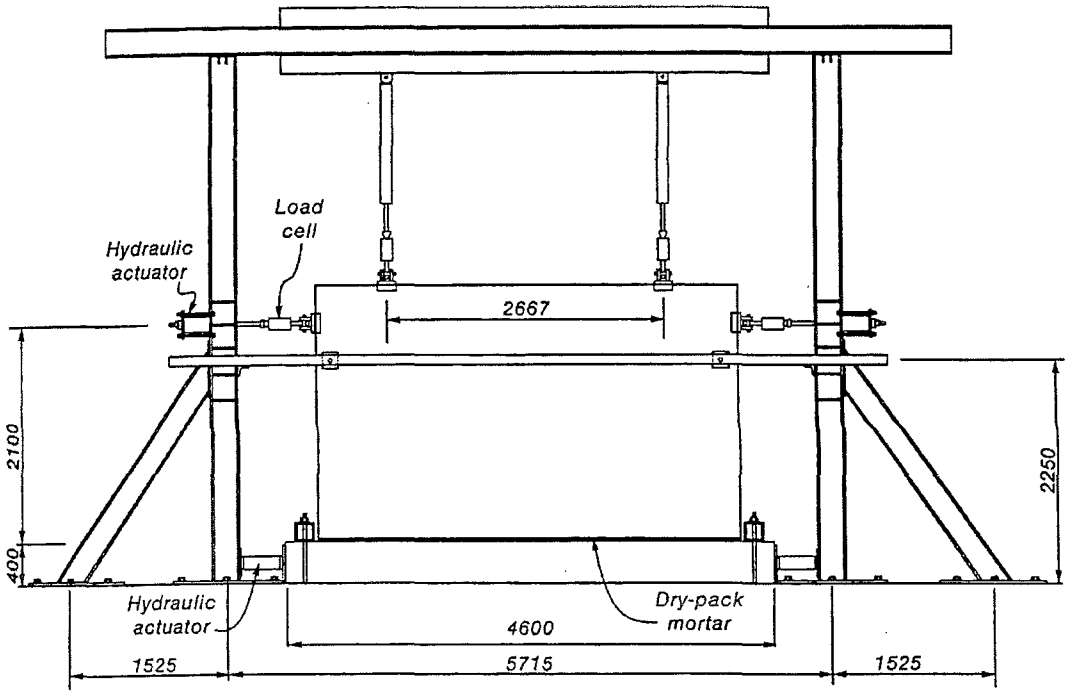

Figure 4.4: An existing loading frame from Crisafulli et al. research [C1]

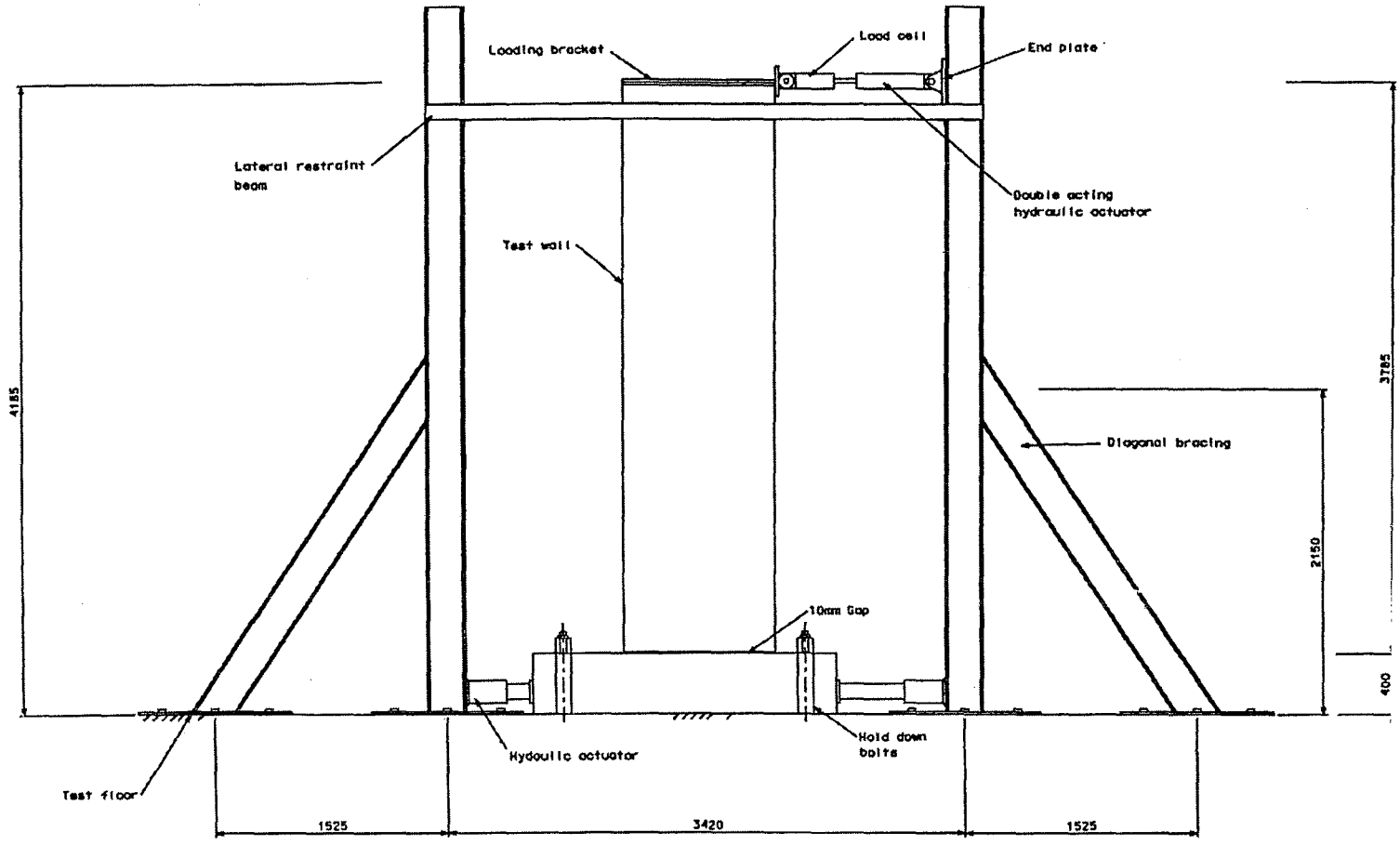

Figure 4.5: The modified loading frame for this research

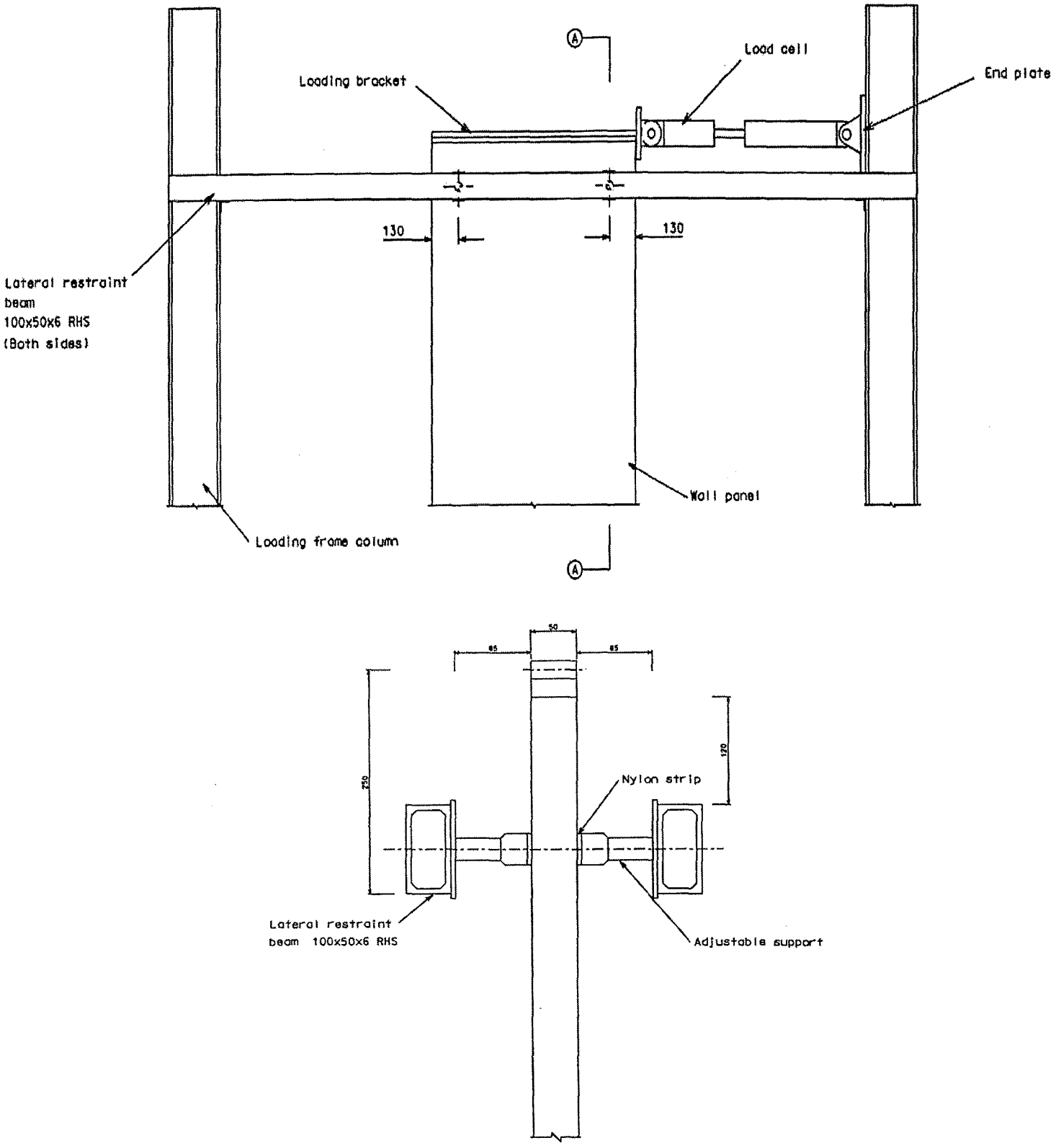

Figure 4.6: Lateral restraint beams at the top of the wall

4.2.3 Loading Bracket

Loading bracket was designed to fit on top of every test specimens. The sketch of the loading bracket is shown in Figure 4.7. There were two parts of the loading bracket. One was the bottom loading bracket which would permanently attached to the top of the wall. The second part would be sitting on top of the previous one which would be connected by four 12 mm diameter high strength friction grip bolts. These bolts were used to transfer the applied load to the wall by shear. End plate was welded at one end of the top loading bracket. It was designed to fit onto the hydraulic ram and the load cell.

The wall reinforcing steel was inserted through the bottom loading bracket, welded and grinded flush with the surface of the bracket. This would ensure that the applied load would be fully transferred from the loading brackets to the wall.

Small steel angles were welded to the bottom loading bracket to act as "shear keys". These angles are cast in to the concrete to make sure the load gets transferred uniformly along the top of the wall.

4.2.4 Loading Frame Column-Hydraulic Ram Connections

This connection was chosen to be able to sustain an overstrength action of the applied load without yielding. It was welded to a steel plate which was bolted to the loading frame column as shown in Figure 4.8. Capacity design was employed to protect any yielding including welding failure.

4.2.5 Container for Lead Ingots

The container to carry the weight of the lead ingots at the top of the wall was designed for ultimate limit state. It was to be supported by the laboratory crane during the test to prevent any falling of 26 kg lead ingots. The worst case scenario was expected if the wall buckled and dropped vertically leaving the crane to take the entire load. All lead ingots were placed inside this container in the certain way to make sure that the resultant vertical applied load acted eccentrically as shown in Appendix A. The container that carried the lead ingots is shown in Figures 4.9 and 4.10.

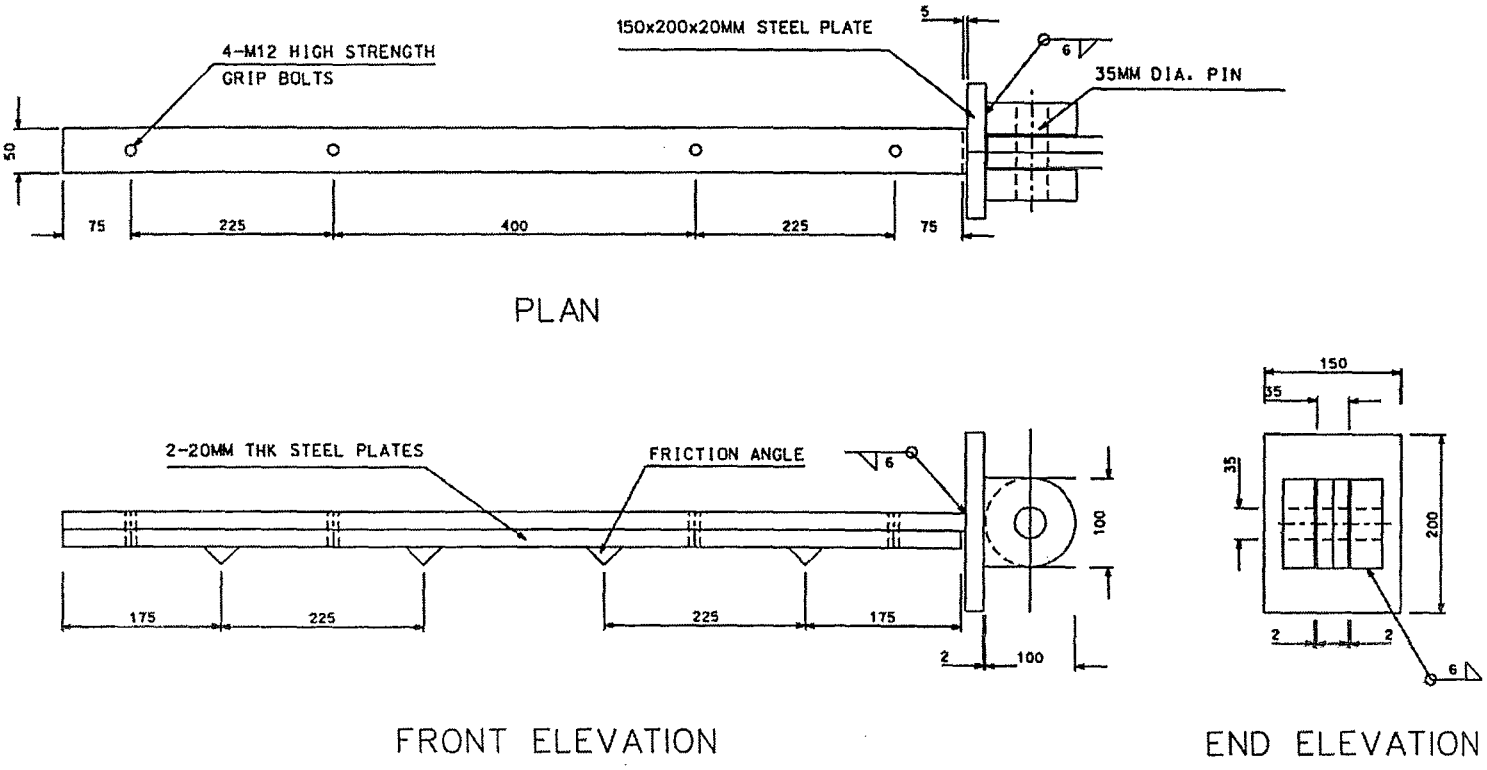

Figure 4.7: Loading bracket

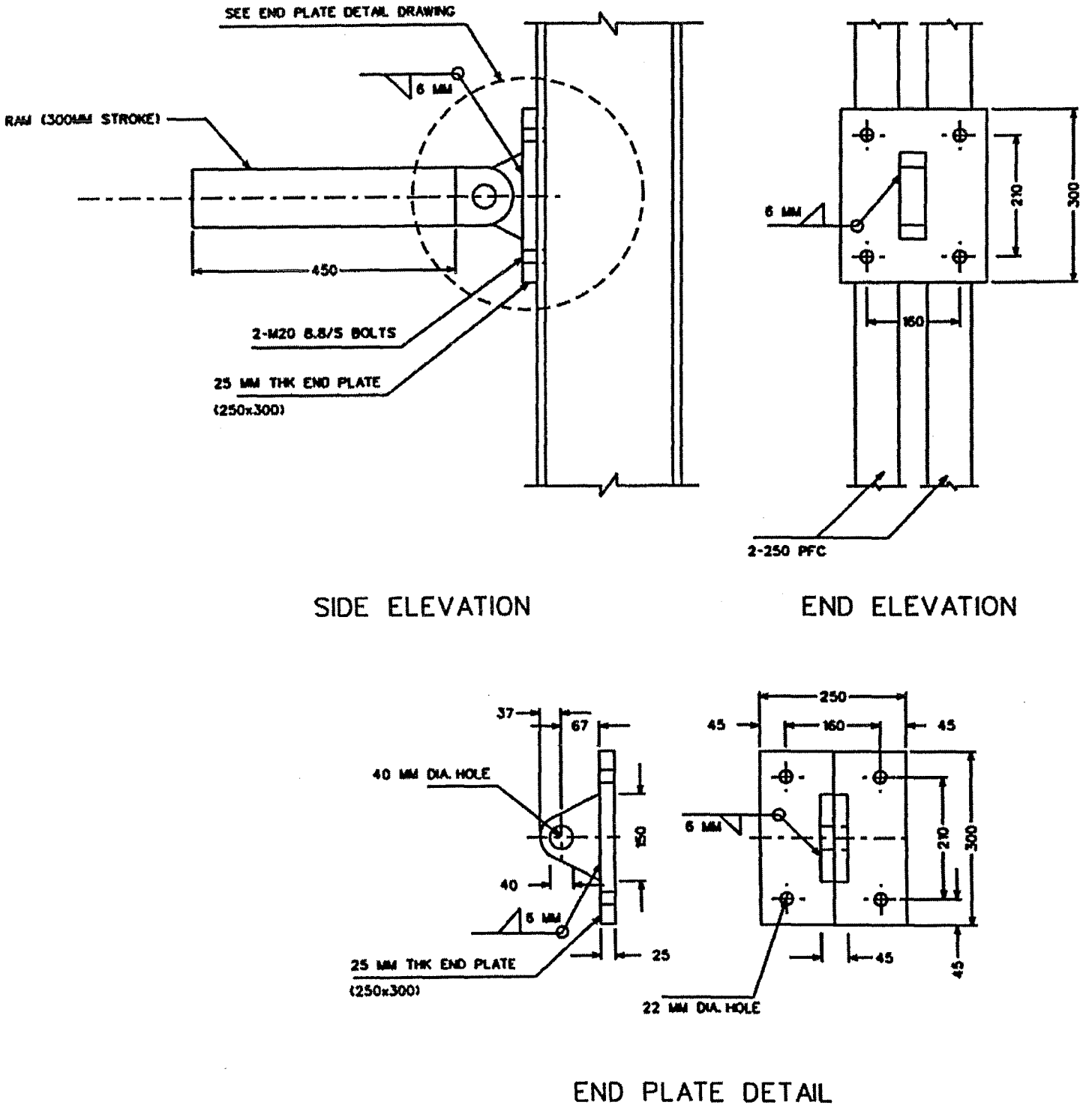

Figure 4.8: End plate connection

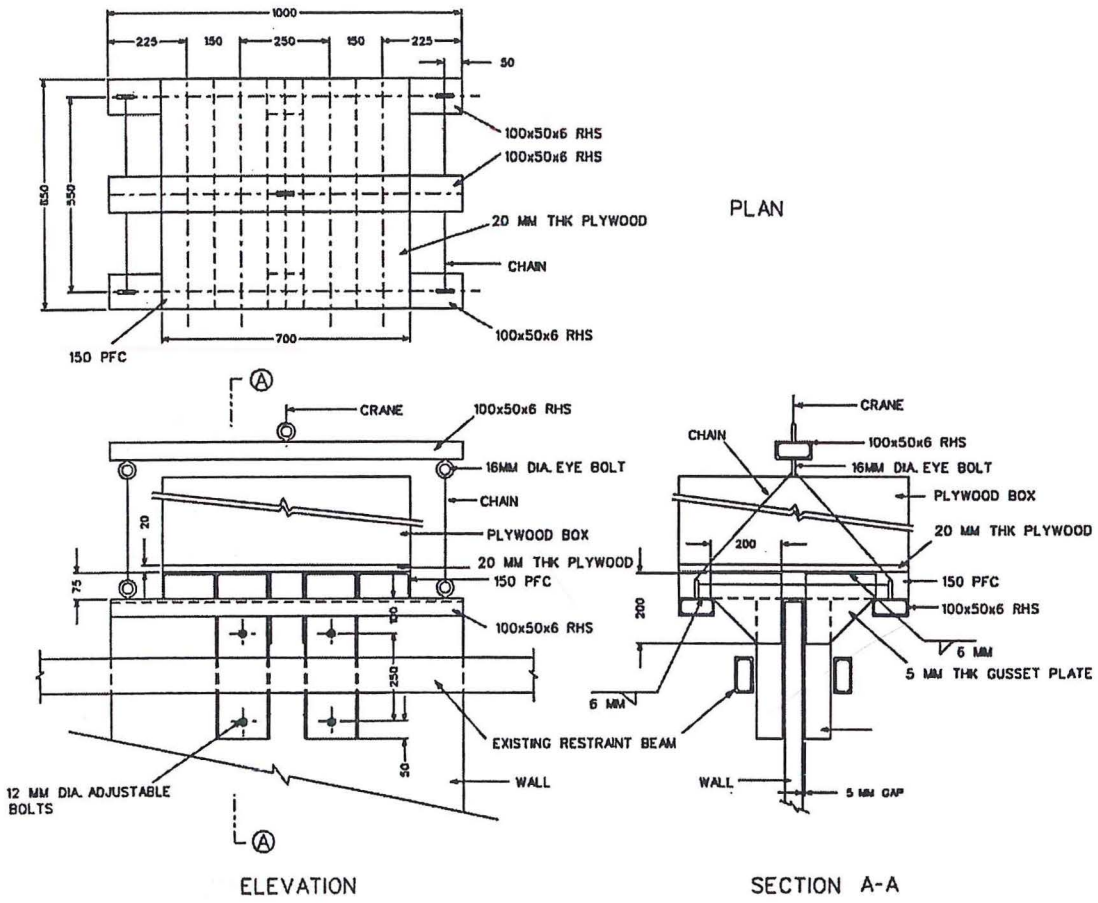

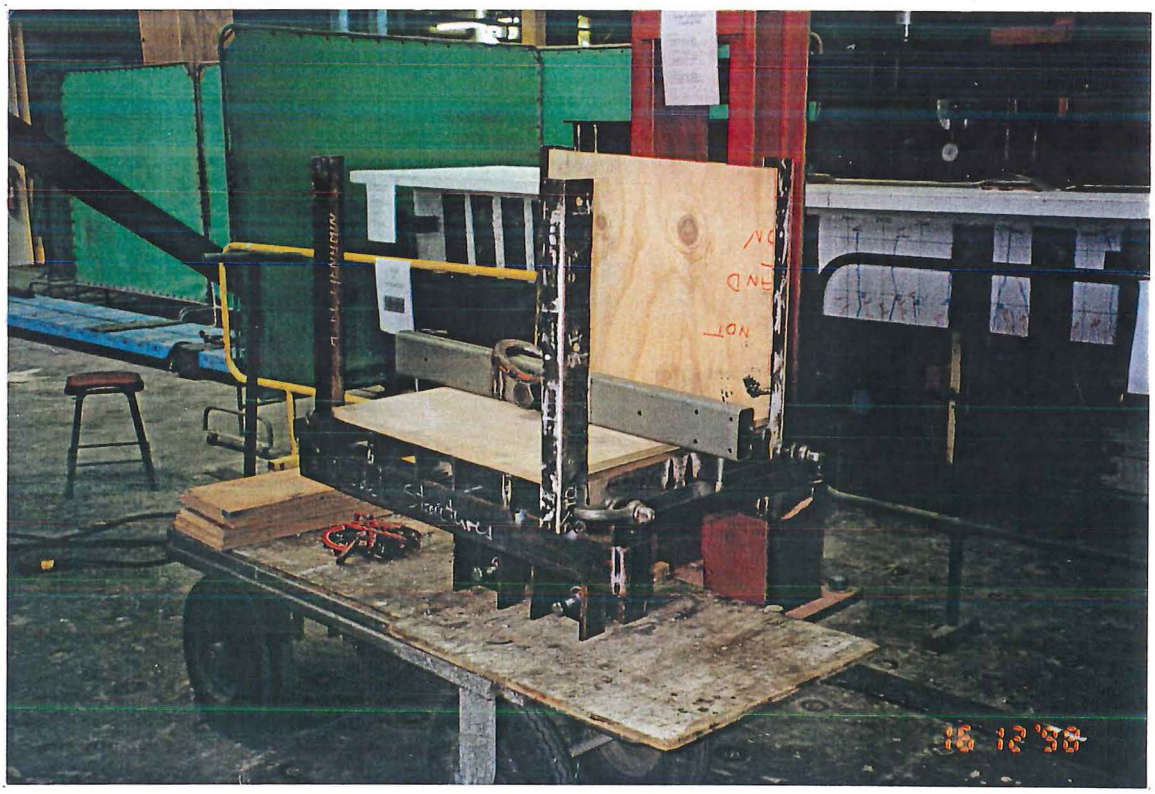

Figure 4.9: Detail drawing of the container used for Units 2 and 4

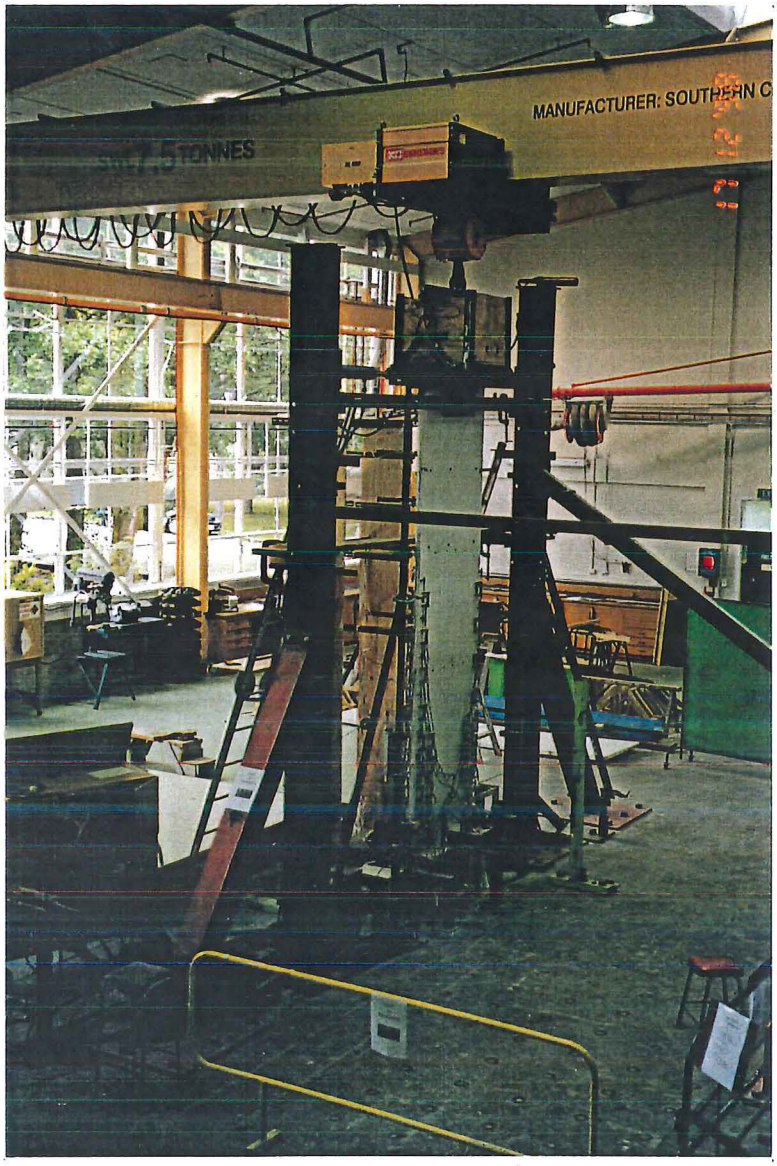

Figure 4.10: View of container carrying lead ingots at the top of the wall

The container was designed to carry an eccentric vertical load which represents an additional self-weight of the wall panel and the simply-supported roof structures. Hence, this container had to be eccentrically located on the top of the wall. The configuration of lead ingots inside the container is also shown in Figure 4.11. The calculations of the resultant eccentricity are shown at the end of Appendix A.

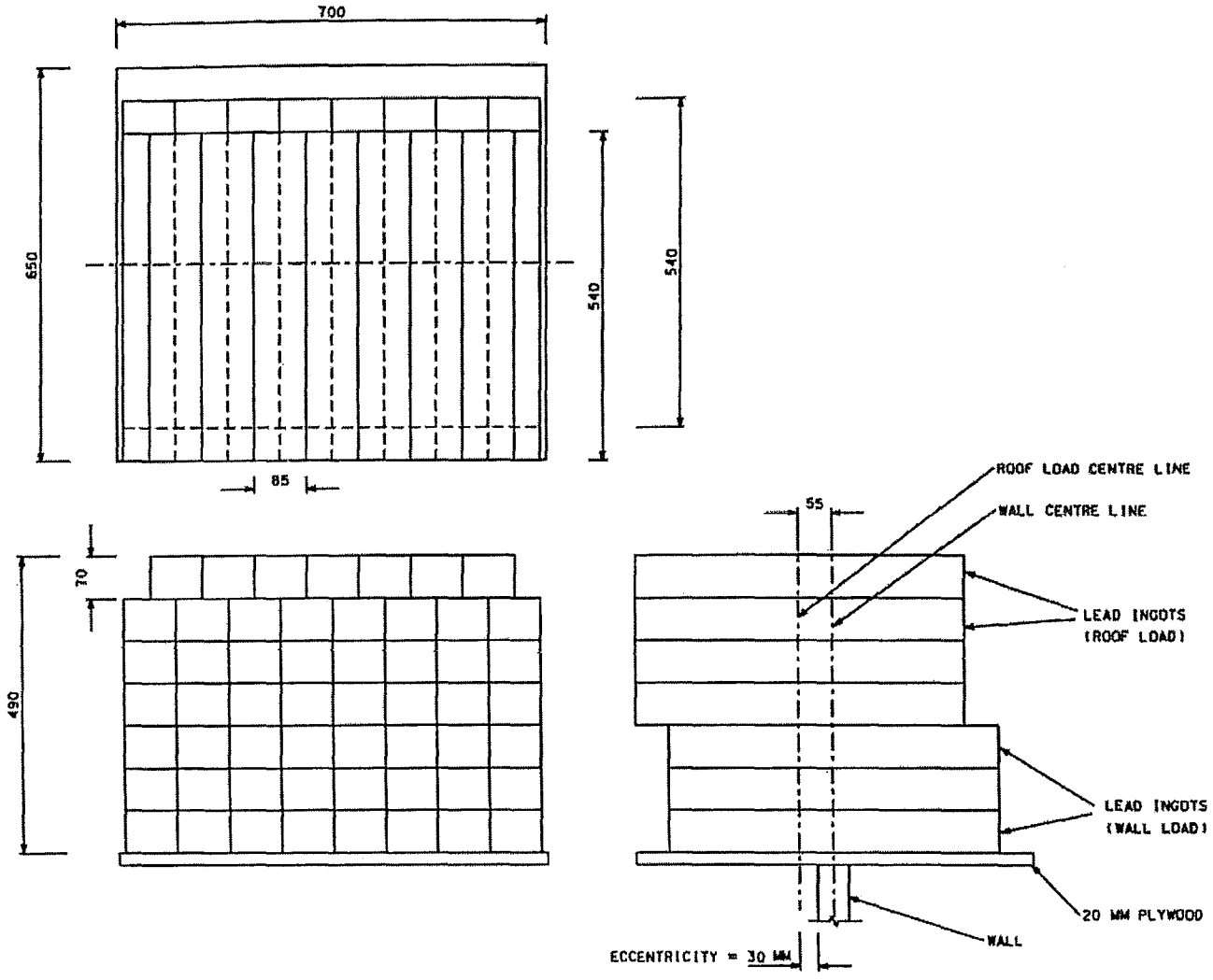

Figure 4.11: Container and lead Ingots configurations

4.3 CONSTRUCTION OF TEST UNITS

4.3.1 Unit 1

The panel was cast on plywood mould and steel strong-back which was placed flat on the laboratory floor. Fresh concrete with 100 mm slump was cast and mechanically vibrated. The wall panel was removed from the mould after a seven day of curing process (see Figure 4.14).

The foundation beam was cast two weeks prior to the concreting of the wall panel. Holes in the beam were constructed using rubber tubes with "Rugasol" which would slow down the hardening process of the concrete and allowed the holes to be brushed to expose some aggregate (instead of using corrugated ducts). This was expected to increase bond strength of the grout and concrete interface (see Figure 4.12).

The reinforced concrete foundation beam was placed and fixed to the floor of the laboratory. Gap between the beam and uneven floor was filled with cement-based grout. The top of the beam had been roughened when the concrete was in partial-hardened state. The bottom of the wall panel was also roughened before the erecting process. To ensure a uniform gap thickness between the wall panel and the foundation beam, 7.5 mm steel shims were placed at 350 mm from either ends of the wall. Plywood was used to seal the gap around the wall. Two restrained beams which attached to the loading frame were clamped to the wall to keep the wall panel in its vertical position. Each hole, receiving a starter bar, was filled with cement-based grout that was gravity fed into the hole through a small tube located at the bottom of the wall. An outlet tube placed at the top of the hole to allow air to escape (see Figure 4.15). Gap between the wall panel and the foundation beam was also separately filled with same type of cement-based grout.

4.3.2 Unit 2

The wall panel was cast on the plywood mould which was placed on the laboratory floor. Fresh concrete with 80 mm slump was poured and mechanically

vibrated. The wall was removed from the mould 21 days after the concrete had been poured.

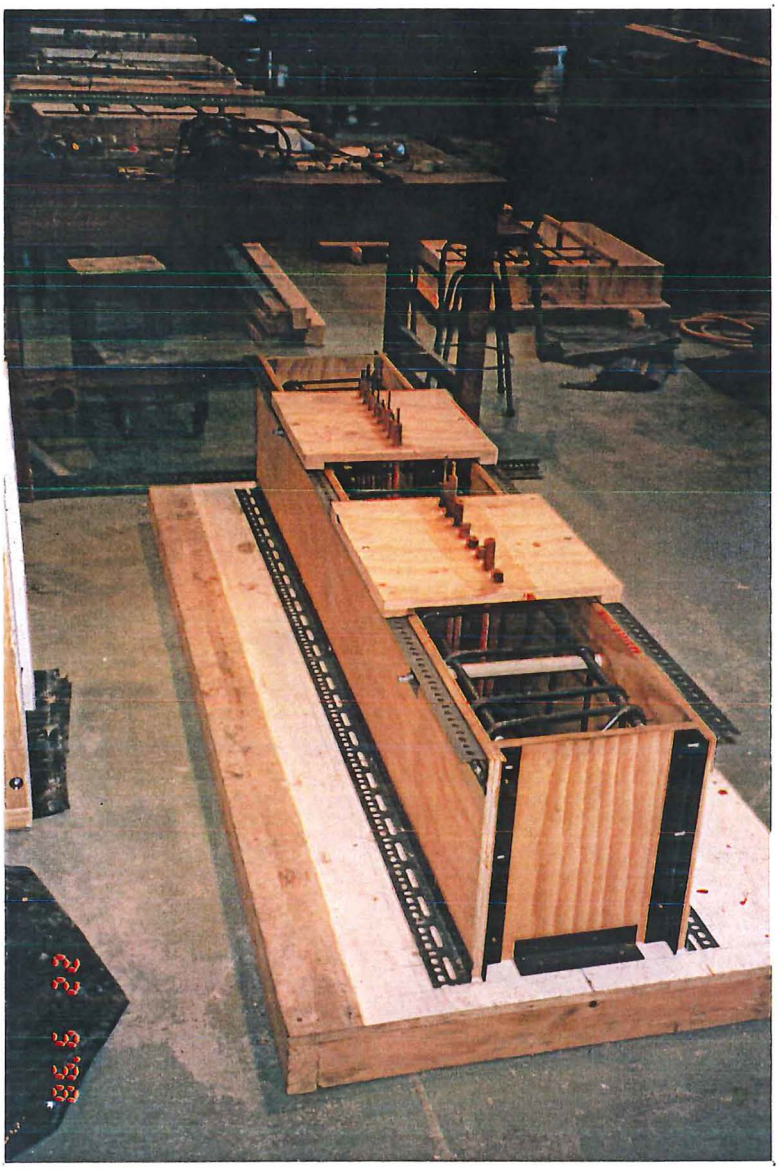

Figure 4.12: Construction of precast foundation beam in laboratory

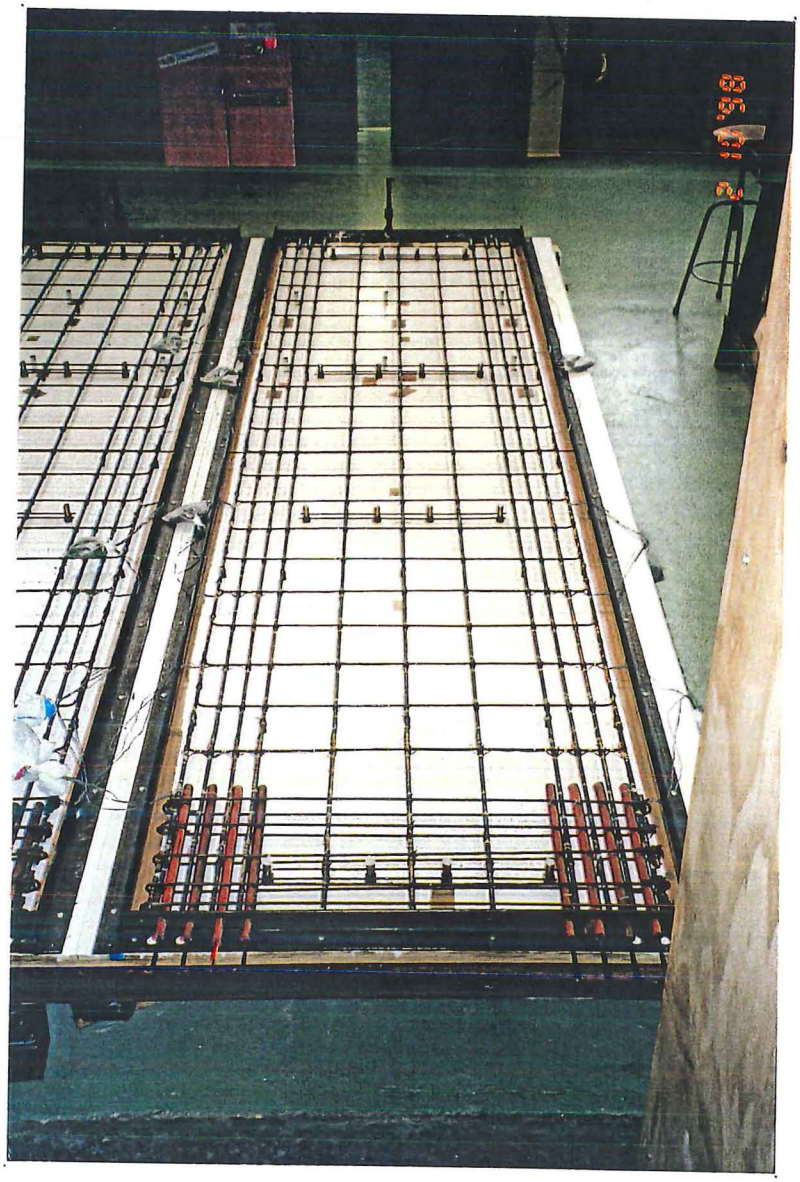

Figure 4.13: Reinforcing cage of wall panel prior to concrete casting for Units 1 and 2

The existing foundation beam which was used during the test of Unit 1 with provided starter bars had been utilised again. This reinforced concrete foundation beam was placed and fixed to the floor. The wall was lifted and placed on the foundation beam using exactly the same construction method as described in Section 4.3.1. In order to assure a uniform thickness of the gap between the wall panels and the foundation beam, 7.5 mm steel shims were placed on the foundation beam. Different type of cement-based grout was used to avoid some difficulty during grouting process due to the amount of course aggregates having to travel through the limited size of gaps. The viscosity of grout was measured before grouting by "Flow-Cone Test" described in reference [A1]. The flowing time of mixed grout was approximately 1 minute. The wall panel was kept in the vertical position by two steel beams bolted to the loading frame. Grout was gravity fed into the holes through the bottom and an outlet tube placed at the top allowed the air to push out from the holes.

4.3.3 Units 3 and 4

The panels for Units 3 and 4 were cast on plywood mould placed on the laboratory floor. Starter bars were protruding from the bottom of the wall while concrete was cast. The measured concrete slump was 90 mm. The wall was removed from the mould after a seven day curing process.

The foundation beam was cast one week before concreting of the wall panel. There were 8 predrilled vertical holes for the starter bars to locate. Eight additional horizontal holes were drilled from the side of the beam and stopped where they intercepted the vertical holes. The foundation beam was placed on the laboratory floor sitting on 10 mm steel shims. The gap around the base was sealed with the sealant after the beam was leveled. Cement-based grout was fed from one end of the beam with an outlet at the other end until the gap underneath the foundation beam was filled.

The top of the beam and the bottom surface of the wall panel were roughened prior to the lifting process. Steel shims of 10 mm thick were placed between the wall

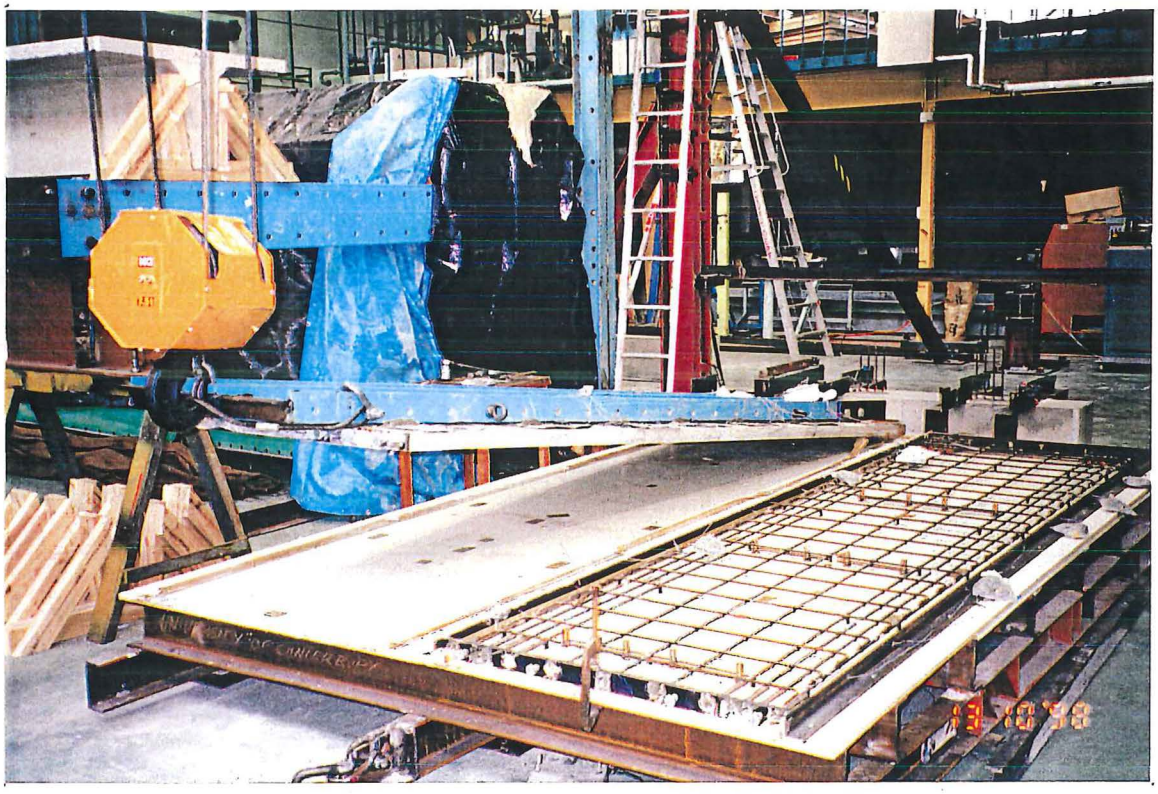

Figure 4.14: Lifting of Unit 1 panel from the mould

Figure 4.15: Grouting of starter bars at the horizontal connection

panel and the foundation beam at 350 mm from both ends of the wall. Cement-base sealant was used around the base of the wall. The wall panel was laterally supported by two restrained beams placed at mid-height and near the bottom of the panel. Both restrained beams were attached to the loading frame to keep the wall panel in its vertical position.

Cement-based grout was initially gravity fed into each inlet hole from the side of the foundation beam. Each hole was grouted individually until every hole was filled with grout. Subsequently, the gap between the wall panel and the foundation beam was filled with the same type of grout.

4.4 MATERIAL PROPERTIES

4.4.1 Concrete Placed in Laboratory

The concrete used in the construction of test specimens was supplied by Allied Concrete Ltd. The concrete mix design was specially made for testing which restricted by the maximum size of aggregate as shown in Table 4.2.

Table 4.2: The mix design specified for wall specimens

Precast Concrete Panel Specimen Concrete Mix Specification	
Specified Strength	30 MPa
Slump	100 mm
Max. Aggregate Size	6 mm
Quantities Per Nominal 1.5 m^3 Load:	
485 kg Ordinary Portland Cement	
1595 kg 5/6 mm Seal Chip	
1350 kg Mortar Sand	
w/c	0.62

A specified concrete strength of 30 MPa was required. Sixteen concrete samples of 100 mm diameter by 200 mm high cylinders were produced to determine the concrete compressive strength. The compressive strengths at the time of testing are also given in

Table 4.3. It can be seen that the compressive strength varied quite significantly. This indicates that additional water added into the concrete for Units 3 and 4 caused the strength reduction. Maximum of 10 litres of water was advised by Allied Concrete Ltd. to increase the slump of Units 2 to 4.

Table 4.3 : Strength of concrete used in all test specimens

Test Unit	Compressive Strength at test date (MPa)	Received Slump (mm)	Modulus of Rupture (MPa) ***	Compressive Strength at 28 days (MPa) ***
1	39.3 (49 Days)*	100	4.90	34.0
2	43.9 (48 Days)*	35 (80)**	4.60	40.9
3	23.0 (16 Days)*	70 (90)**	3.84	30.3
4	30.3 (35 Days)*	70 (90)**	4.40	30.3

* Number of days after pouring on the test date.

** Slump after additional water was added.

*** Average of three sample testing results.

4.4.2 Cement-Based Grout

Cement-based grout was used to fill between starter bars and holes and the gap underneath the wall panel. There were two different types of cement-based grout used in the experiment, SIKA 212 and Conbextra GP. SIKA 212 grout was only used in Unit 1, which generated some difficulties during the grouting process due to the large size of coarse aggregates having to travel through the narrow gap. Conbextra GP grout was introduced for Units 2 to 4. Table 4.4 summarises the compressive strength of both types of cement-based grouts. It can be seen that SIKA 212 yielded lower strength because of the additional amount of water added to reduce viscosity and to become more flowable.

4.4.3 Reinforcing Steel

There were two different types of reinforcement used in the experiment, deformed and plain round bars. The samples were randomly selected and tested using Avery Universal Tensile Testing Machine in Civil Engineering Department laboratory. The stress-strain curves of reinforcing steel can be illustrated in Figure 4.16. Table 4.5 also summarises the average properties of the reinforcement from three sample test results.

Table 4.4: Strength of cement-based grout used in all test specimens.

Test Unit	Compressive Strength (Holes in Wall) at the Test Date (MPa)***	Compressive Strength (Holes in Foundation Beam) at the Test Date (MPa)***	Compressive Strength (Gap) at the Test Date (MPa)***
1*	32.0 (30 Days)		32.0 (30 Days)
2**	50.0 (19 Days)		50.0 (19 Days)
3**		35.5 (8 Days)	40.0 (7 Days)
4**		43.6 (8 Days)	39.8 (7 Days)

* SIKA 212 grout

** Conbextra GP Grout

*** Average of three sample testing results.

Table 4.5: Tensile properties of the reinforcing steel

Steel Type	f_y (MPa)	f_u (MPa)	f_u/f_y
D10	318	438	1.38

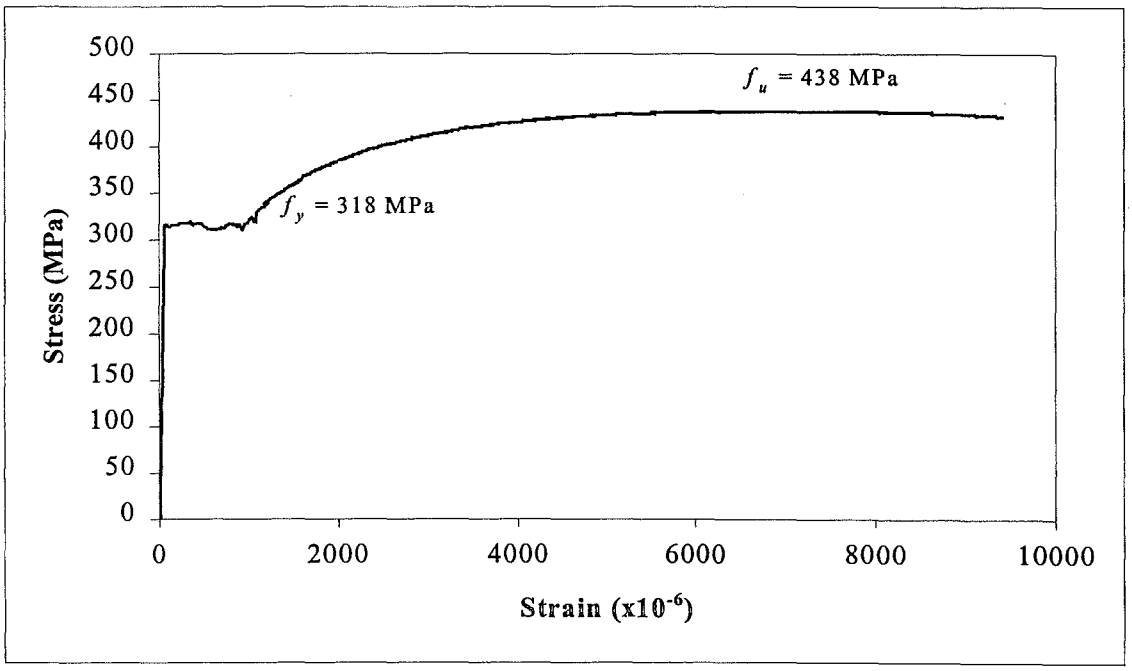

Figure 4.16: Stress-strain curve for a D10 bar

4.5 LOADING HISTORY

The wall specimens were subjected to reversed cyclic quasi-static in-plane lateral loading in two stages. The first stage involved four reversing load-controlled cycles in the elastic range at 0.50, 0.62, 0.75 and 0.88 times the theoretical nominal flexural strength. The second stage involved reversing displacement-controlled cycles of loading with increasing nominal displacement ductility factors until the load carrying capacity of the wall decreased substantially. Two consecutive cycles for each displacement level were repeated to incorporate the effect of potential strength degradation.

The reference yield displacement which represented the displacement ductility of 1.0 was extrapolated from the actual yield displacement from dividing the theoretical nominal capacity by an average wall stiffness when the applied force was equal to 75% of the theoretical nominal capacity (see Figure 3.4). The calculation of the reference yield displacement for all test specimens is shown in Appendix B.

$$k_{75} = \frac{P_{75}}{\Delta_{75}} \qquad [4\text{-}1]$$

$$\Delta'_y = \frac{P_n}{k_{75}}$$

where

k_{75} = secant stiffness at 75% of the theoretical nominal capacity

P_{75} = applied force at 75% of theoretical nominal capacity

Δ_{75} = average horizontal displacement at 75% of theoretical nominal capacity

P_n = theoretical nominal capacity

Δ'_y = reference yield displacement

Therefore, the displacement ductility factor (DF) was determined by the ratio of the horizontal displacement to the reference yield displacement. The measured

displacement ductility from the experiment was not represent the exactly values of the theoretical displacement ductility.

Load steps are referred by the direction of imposed in-plane load or displacement, magnitude and the cycle number to that step. For example

- "+0.75P_n×1" means the first cycle to a load of 75% of the theoretical nominal strength in the positive direction (push); and
- "μ_Δ = -2×2" (or "DF = -2×2" in photographs) means the second cycle to an estimated displacement ductility of two in the negative direction (pull).

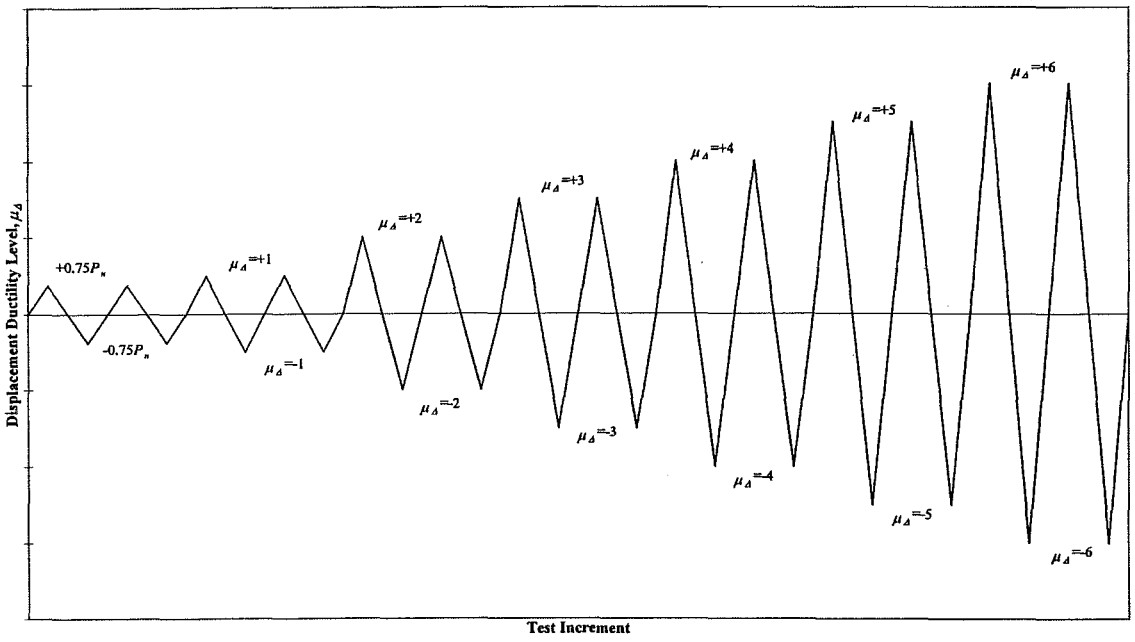

Figure 4.17: University of Canterbury typical loading history for test units

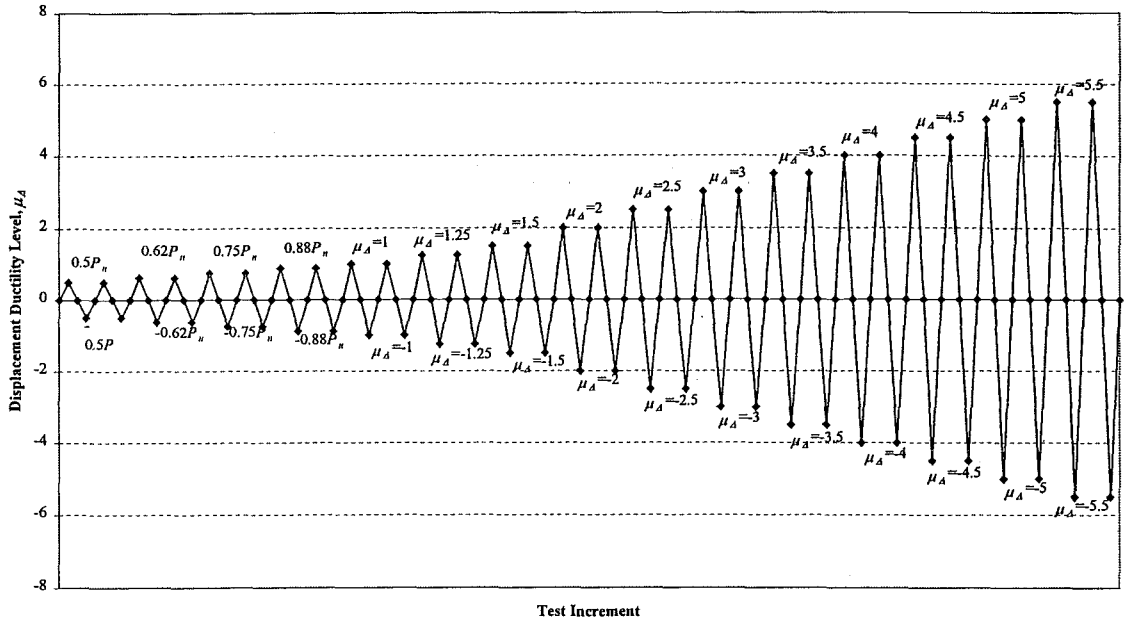

Figure 4.18: General loading history for test Units 1 to 4

Typical loading scheme for University of Canterbury is shown in Figure 4.17. The general loading history for all the test specimens is shown in Figure 4.18. The chosen loading scheme was refined to suit this experimental purpose in order to ensure the actual wall behaviour is fully covered from the collected data. Hence, the increments of the applied in-plane loads were made smaller before the first-yield was achieved during load-controlled stage and also the increment of the applied in-plane displacement was smaller during displacement-controlled stage. During testing, the load or displacement increments were numbered with a magnitude of the applied load in percentages to the theoretical nominal capacity and DF number (Ductility Factor) for the load-controlled and displacement-controlled cycles, respectively. These numbers appear in the photographs.

4.6 INSTRUMENTATION

4.6.1 Applied Load

The in-plane horizontal applied load was generated by a hydraulic actuator and measured by a 50 kN capacity load cell which was manufactured in the Civil Engineering Department. It was mounted between the actuators and a pinned-bracket which attached to the top loading bracket.

4.6.2 External Displacements

The in-plane horizontal displacements at the top of the wall were measured by two 200 mm travel linear potentiometers, P_1 and P_2. They were placed at both ends of the wall (see Figure 4.19).

Two 50 mm travel linear potentiometers, P_3 and P_4, measured the sliding of the wall base at the wall-foundation connection level.

The horizontal movement of the foundation beam was recorded by a 30 mm travel linear potentiometer, P_5, positioned at one end of the foundation beam (see Figure 4.19).

An additional 50 mm linear potentiometer, P_6, was placed to the out-of-plane lateral restraint beam to detect a lateral movement of this supported beam.

Out-of-plane displacements of the panel were measured using a number of different sizes of linear potentiometers which were assigned according to the amount of movements expected at different locations along the edges of the wall. Sixteen linear potentiometers, P_7 to P_{22} were used for this purpose. The target plates were attached directly to the concrete (see Figure 4.19).

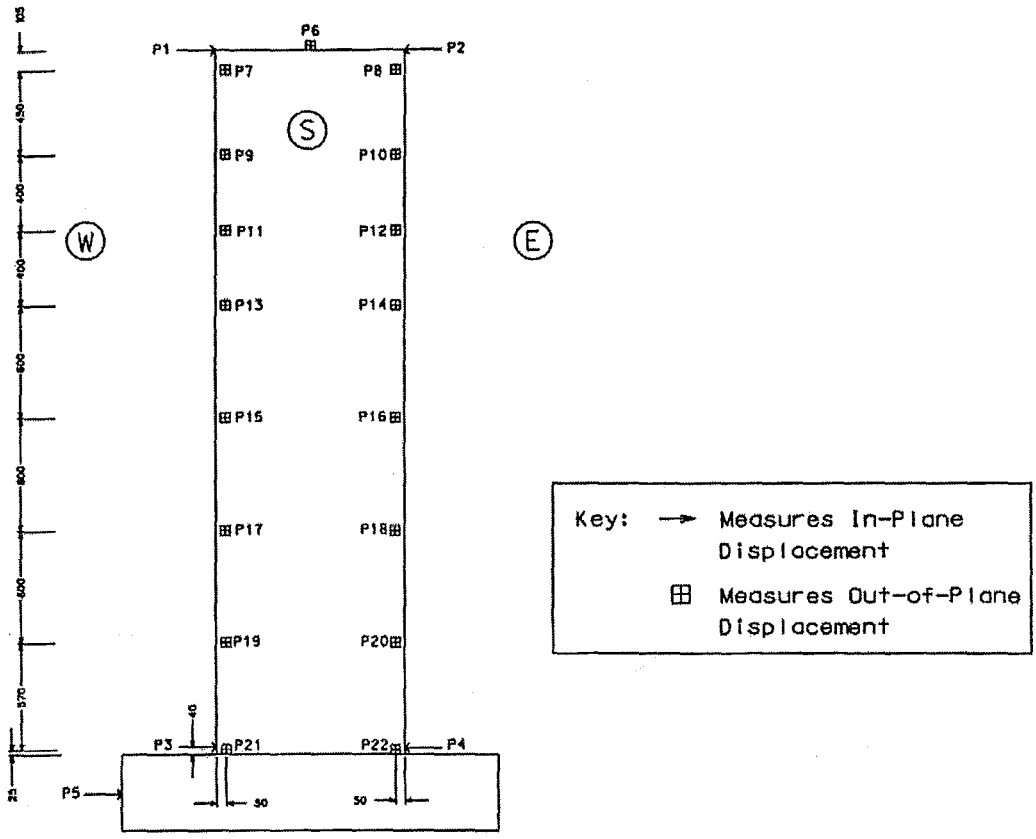

Figure 4.19: Location of linear potentiometers in Units 1 to 4

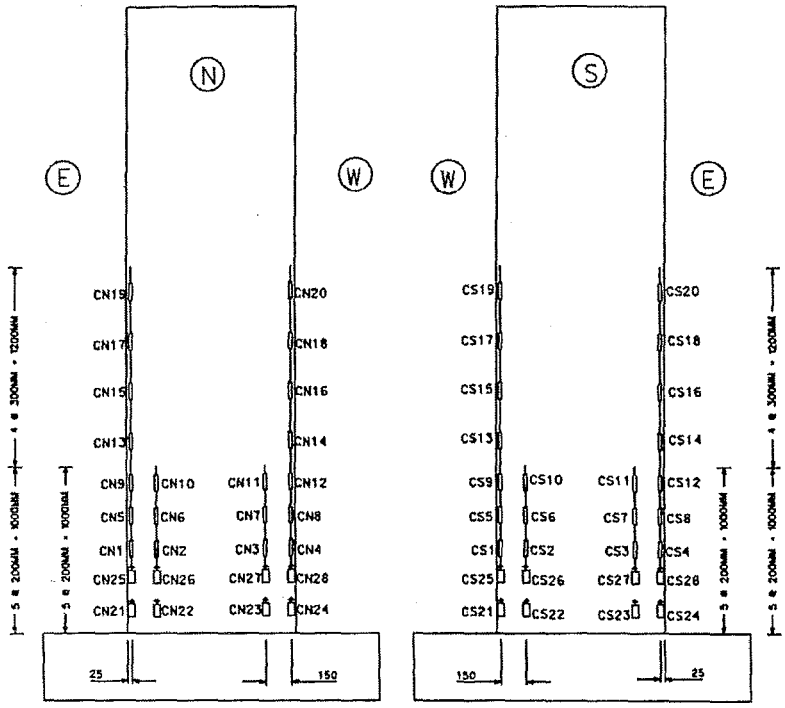

Figure 4.20: Location of clip gauges in Units 1 to 4

4.6.3 Reinforcement Strains

Local strains generated in the reinforcement during the testing were measured using electric resistance foil strain gauges with 2 mm gauge length and 120.1Ω resistance. They were attached to the reinforcing bars with Cyanoacrylate strain gauge adhesive and coated with water proofing strain gauge cement. Furthermore, on top of that, they were covered with a vinyl mastic tape for insulation, moisture sealing and further protection.

These strain gauges were employed at the regions where high strains were expected to develop. For instance, the wall-foundation connection and the top of lap-splice (see Figures 4.21 and 4.22).

4.6.4 Concrete Strains

Clip-gauges were used to measure the strains generated at the concrete surface of the wall. They were mounted within the lower halves on both wall faces. On each wall face, two columns of clip gauges were used on both edges of the wall. The outer columns (outermost) were located at 25 mm from the edge with 200 mm gauge length in the lower 1 m height and 300 mm gauge length continued to the height of 2.4 m above the foundation beam. The inner columns (innermost) were located at 150 mm from the outer columns with 200 mm gauge length to the height of 1 m above the foundation beam. Sixteen 50 mm travel linear potentiometers were used to replace the bottom two rows of clip gauges due to the unavailability of clip gauges in the laboratory (see Figure 4.20).

4.6.5 Data Acquisition System

Data measured from load cell, linear potentiometers, strain gauges and clip gauges were connected to P.C. Lab data acquisition unit. The data were read and stored by a computer using a data logger unit with analogue-to-digital converter cards. The existing computer software read in real time forces, displacements and strains during the test.

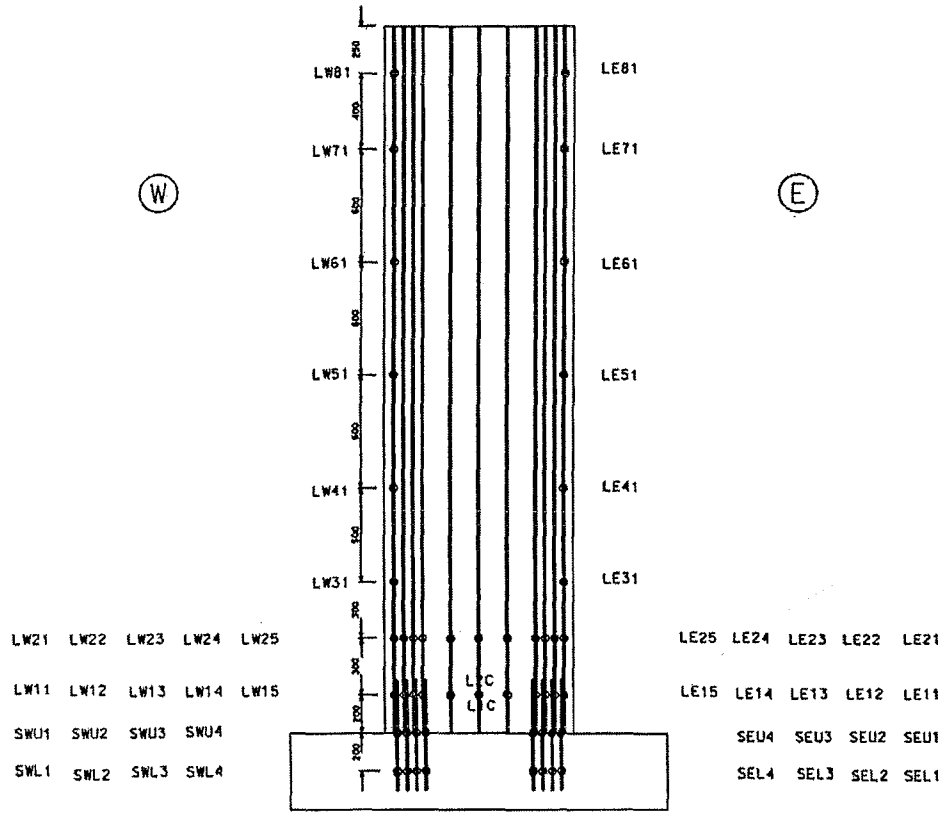

Figure 4.21: Location of strain gauges in Units 1 and 2

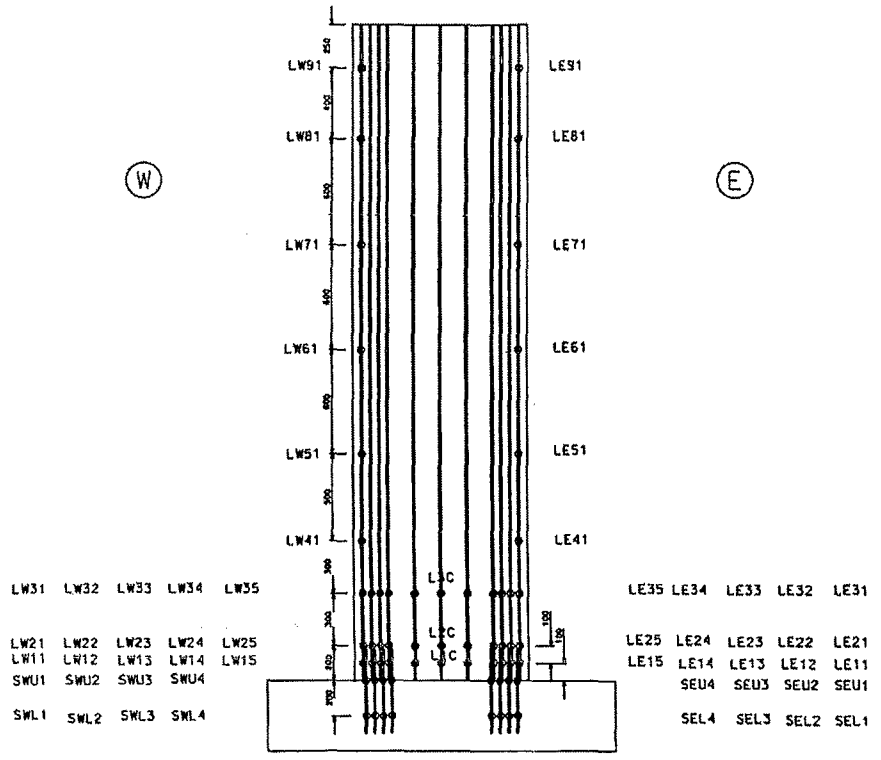

Figure 4.22: Location of strain gauges in Units 3 and 4

In additional, the tests were monitored with the load-displacement curve recorded in a x-y plotter with the data from the load cell and from a linear potentiometer that measured the in-plane horizontal displacements. This provided a real time visual aid while the tests were conducted.

The total number of instrumentation used for all test specimens is shown in Table 4.6.

Table 4.6: Summary of instrumentation

Test Unit	Load Cell	Linear Potentiometers	Strain Gauges	Clip Gauges
1	1	38	50	40
2	1	38	50	40
3	1	38	61*	40
4	1	38	61*	40

* Additional strain gauges used in Units 3 and 4 due to the short length of lap-splice.

4.7 TEST ARRANGEMENT

The loading frame made of two steel columns and diagonal braces, which bolted to the laboratory floor as described in Section 4.2.2. The foundation beam was anchored to the floor using several steel beams and steel rods (see Figure 4.5). Both ends of the beam were compressed with two hydraulic actuators to avoid the horizontal movement of the base. Two lateral restrained beams were located on either side of the wall to stop the out-of-plane movement. They were made of the nylon strips on the restrained beams and Teflon strips attached on the panel at the contact points.

The in-plane lateral forces were applied using a hydraulic actuators connected to the specimen at 3.75 m from the top of the foundation beam. Hydraulic actuator was used to applied compression force (push) and tension force (pull) depending on the direction of the applied force and displacement.

In the case of applying constant vertical load for Units 2 and 4, the empty lead ingot container was initially lifted and carefully placed on the wall. The adjustable bolts

were used to clamp the container to the wall in order to transfer the eccentric load to the top of the wall. Lead ingots were loaded individually to ensure an accurate required eccentricity was achieved. Four pieces of 14 mm thick plywood were vertically placed around the container to protect any accidentally fallen ingots during and after the test. Eventually, it was chained to the crane before commencing the test. Photographs of test set-up prior to the starting of the test for all the specimens illustrate in Figure 4.24.

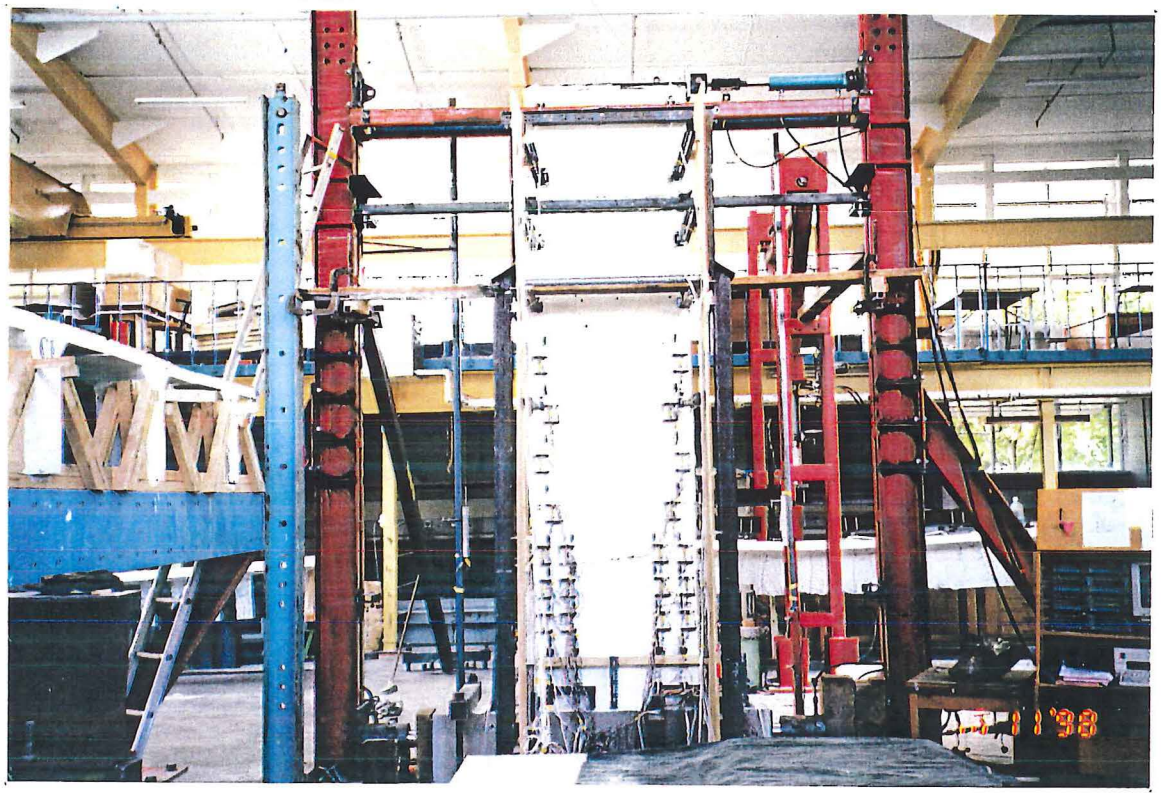

Figure 4.23: Test arrangement of Units 1 and 3

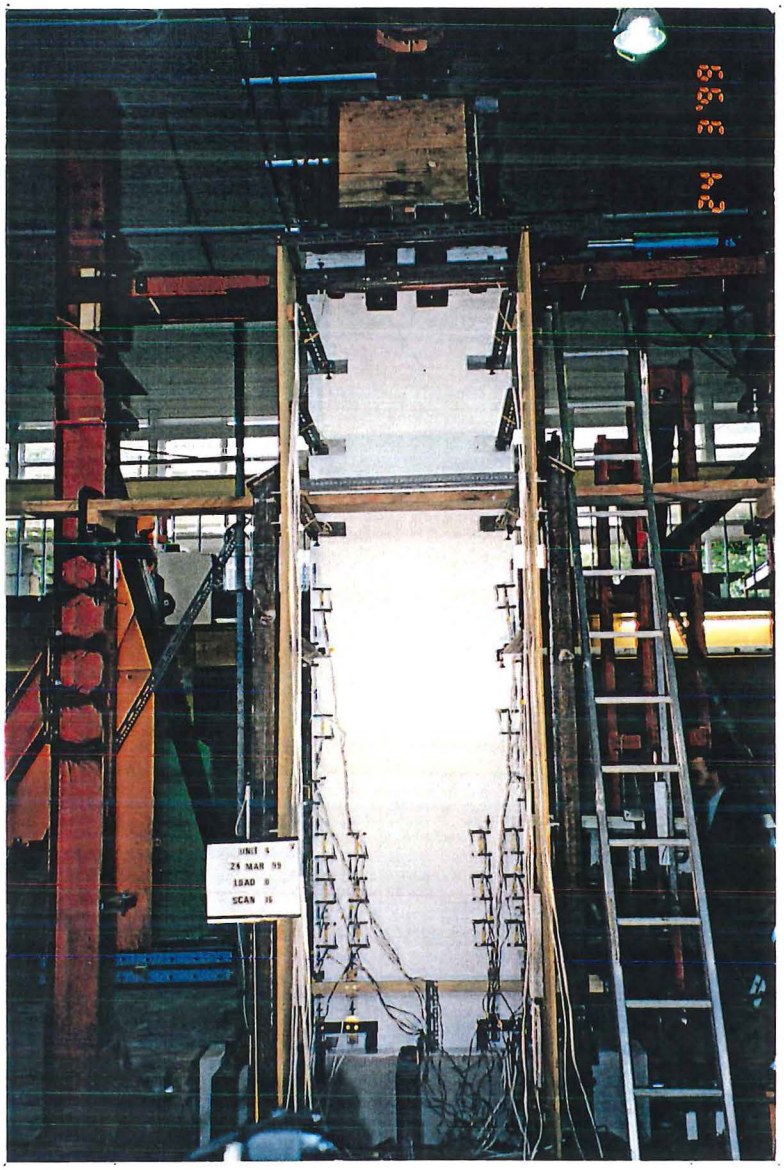

Figure 4.24: Test arrangement of Units 2 and 4

CHAPTER 5

EXPERIMENTAL RESULTS AND OBSERVATIONS

5.1 Unit 1

5.1.1 Unit 1 Properties

The properties of Unit 1 are illustrated in Table 5.1. All measured values were calculated with the material properties measured on the day of test, and the nominal values were calculated using the nominal material properties.

Table 5.1: Measured properties of Unit 1

Property			Nominal value	Measured value
Reinforcing ratio	p	%	1.26	N/A
Longitudinal reinforcing yield strength	f_y	MPa	300	318
Concrete compressive strength*	f'_c	MPa	30	39.3
Modulus of rupture*	f_r	MPa	4.38	4.90
Axial load level	$N^*/A_g f'_c$		0.0031	0.0024
Cracking load	P_{crack}	kN	9.73	10.9
First yield strength	P_{yield}	kN	17.5	18.7
Nominal strength	P_n	kN	22.7	24.4

* At the day of testing

The secant stiffness measured at $0.75P_n$ was k_{75} = 1.41 kN/mm and the estimated reference yield displacement was Δ_y = 17.32 mm (see Appendix B).

5.1.2 General Behaviour and Observations : Unit 1

Flexural cracks started to develop on the concave side of the wall in the region of lap-splice and appeared on both sides at cracking strength (see Figure 5.1). Extended horizontal cracks slowly propagated upwards when the applied forces increased.

Once the applied force reached $0.62P_n$, cracks commenced to propagate diagonally rather than horizontally (see Figure 5.2). Cracks at the horizontal joint became wider to approximately 0.5 mm along the wall-foundation interface at one end of the wall.

At the applied force of $0.75P_n$, horizontal cracks in lap splice region on the tension edge started to develop vertically towards the horizontal joint. They appeared to coincide with the location of the starter bars, see Figure 5.3. At this stage, the starter bars at the wall-foundation interface, which were subjected to tension, started to yield. The horizontal cracks on the panel extent up to the height of 2.5 m. After completed the two cycles of $0.75P_n$, cracks at the horizontal joint opened up to approximately 1 mm at the edges of the wall panel. Sliding shear at the horizontal joint was not significant at this stage (see Figure D-1).

More vertical cracks became visible near the locations of the starter bars in the first cycle of $\mu_\Delta = +1.25$. Out-of-plane movement became barely noticeable. Cracks at the horizontal construction joint opened up to 3 mm along the entire length.

In the first cycle of $\mu_\Delta = +1.5$, cracks at the horizontal construction joint widen to approximately 5 mm along the entire length of the panel. As a result the panel started to slide significantly at the base (see Figure 5.4). More vertical cracks appeared near the locations of starter bars.

When $\mu_\Delta = -2\times1$ was reached, a few diagonal cracks initiated within the region of lap splice and propagated towards the horizontal construction joint. This was an indication of horizontal splitting of concrete across the wall thickness at the location of the starter bars. At this stage of concrete cover started to spall off the panel (see Figures 5.5 and 5.6). This illustrated the compression failure in the concrete compression zone which was not adequately confined. At this stage, most of the starter bars at the horizontal joint were yielding.

The panel started to twist about the vertical axis at the horizontal joint when subjected to the load that corresponding to $\mu_\Delta = 2.5$ as illustrated in Figures 5.7 to 5.9.

Once the panel was subjected to the reverse loading, the bars that had yielded extensively in tension were subjected to compression and started to buckle, pushing the panel sideways which induced twisting. When the wall was subjected to the next loading cycle, the compression edge rotated back to the original position due to the stretching under tension of the buckled starter bars. Then the compression edge started to behave in the same fashion as the previous cycle.

During the last cycle where the test was terminated, the wall had been pushed until it reached $\mu_\Delta = +5\times1$. Sliding shear and twisting of the panel had the most contribution at this stage (see Figures 5.10 and 5.11).

Interestingly, cracks did not concentrate at the base of the wall but they were uniformly spread up the height of the wall. This implied that the high steel content had a major effect on cracking development. It was also important to note that crack patterns completely changed from horizontal cracks to uniform diagonal crack pattern at the end of the test (see Figure 5.13). The cracking pattern taken from concave side and East edge of the wall is also shown in Figures 5.12 and 5.14.

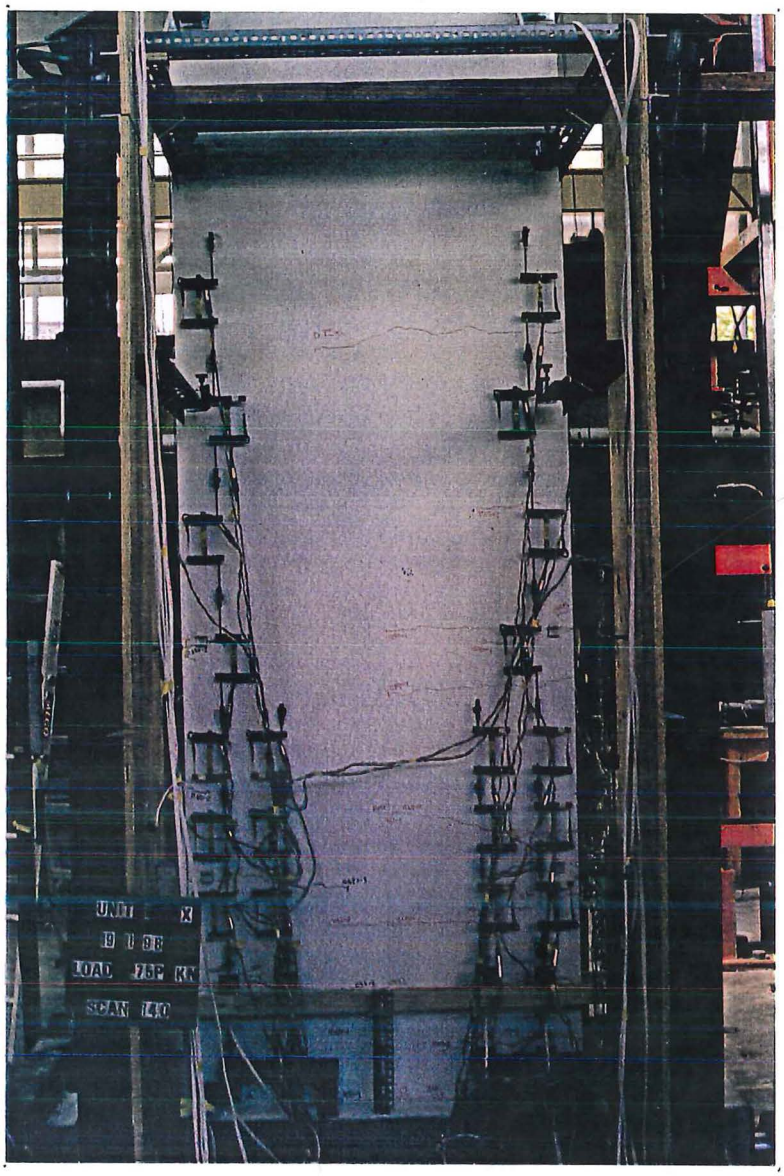

Figure 5.1: View of Unit 1: At cracking strength (South/Concave)

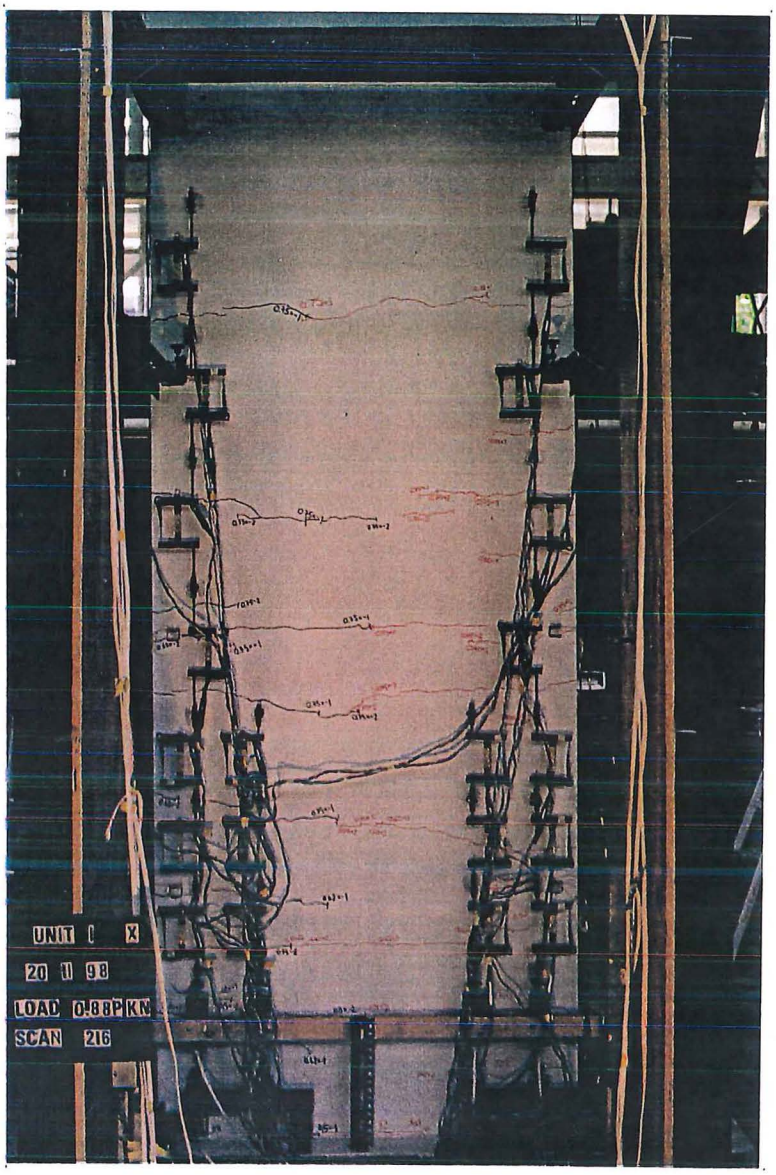

Figure 5.2: View of Unit 1 at 62% of the theoretical lateral load (South/Concave)

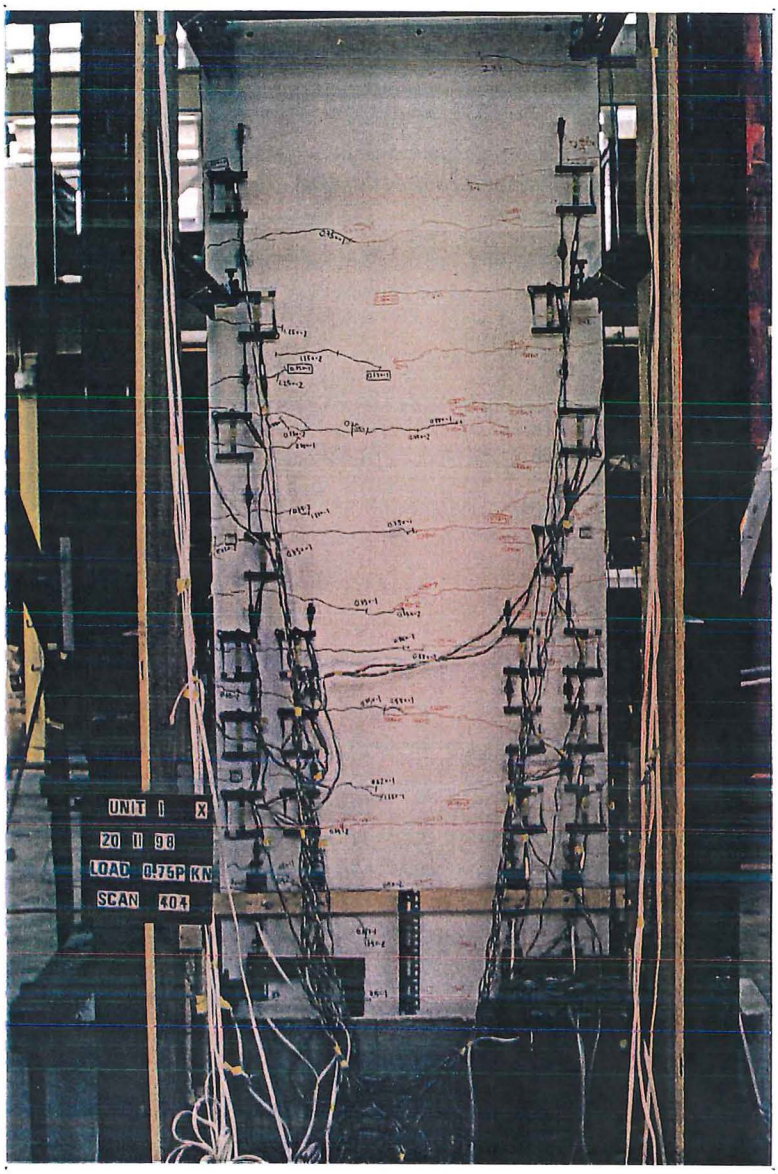

Figure 5.3: View of Unit 1: first yield at the positive direction loading (South/Concave)

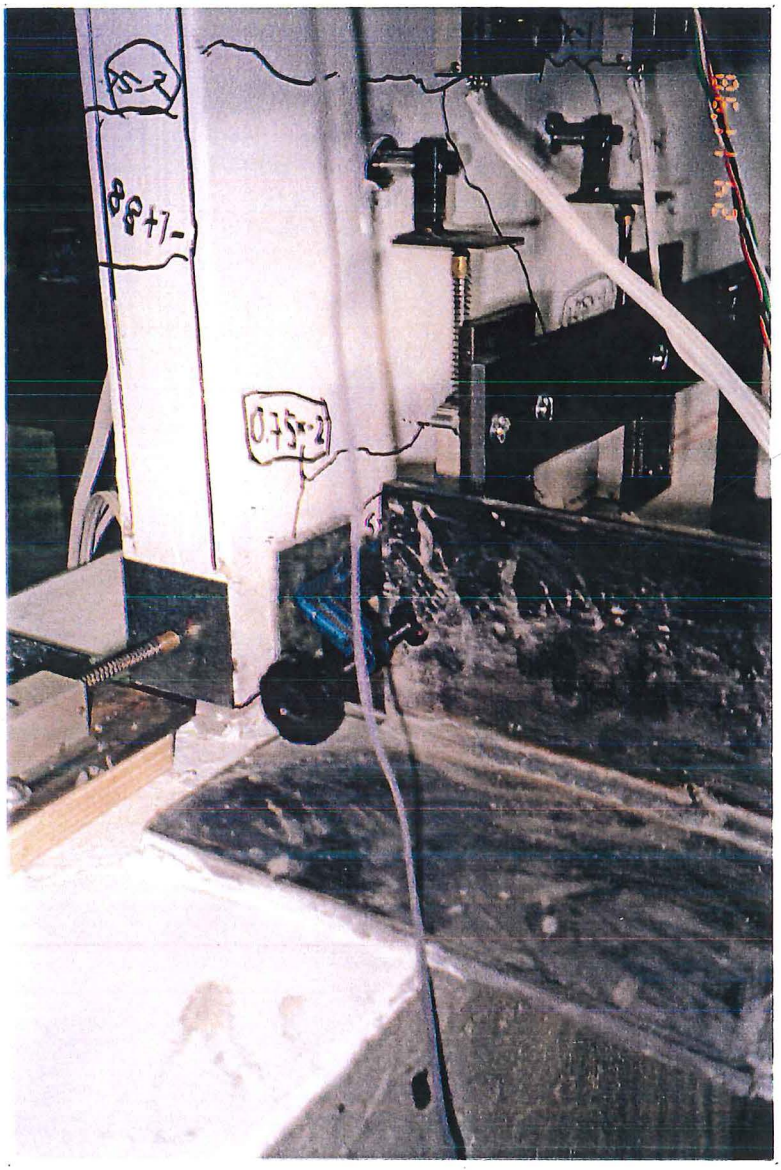

Figure 5.4: Unit 1: Cracking and sliding along the horizontal joint at μ_Δ = +1.5×1 (West edge)

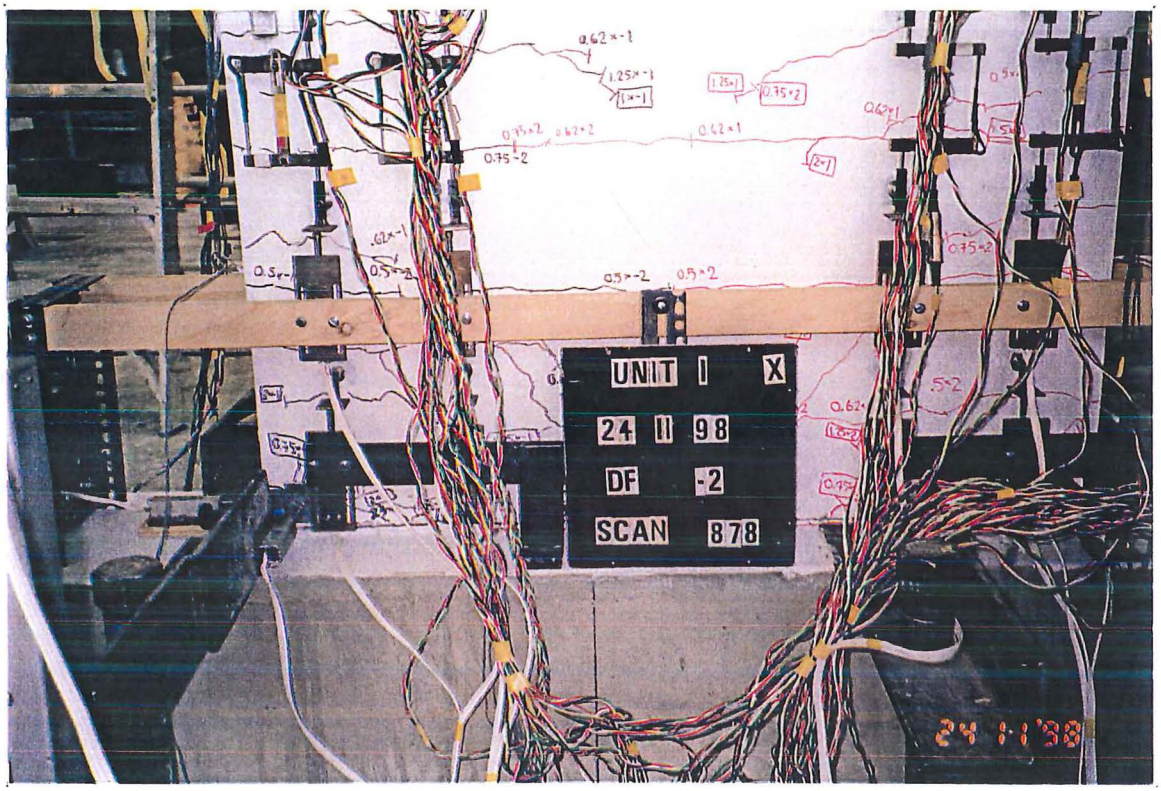

Figure 5.5: Unit 1: Crushing and spalling of concrete at μ_Δ = -2×1 (South/Concave)

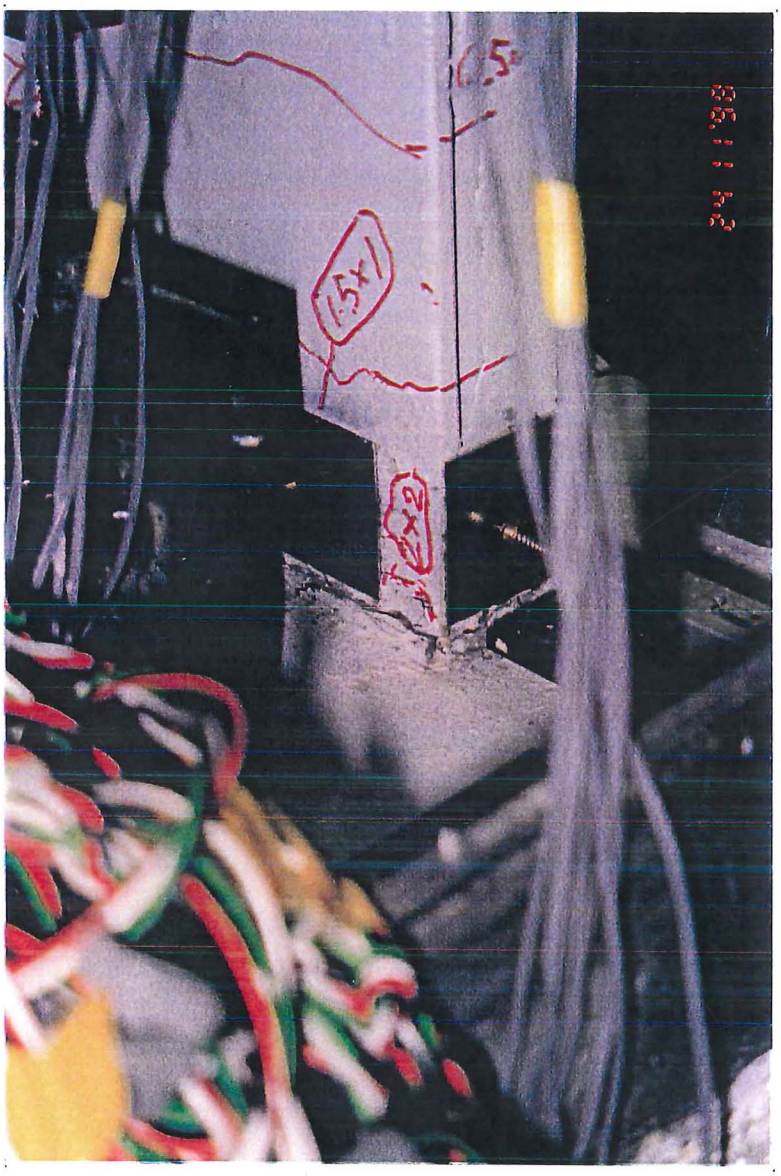

Figure 5.6: Unit 1: Crushing and spalling of concrete at $\mu_\Delta = +2\times2$ (East edge)

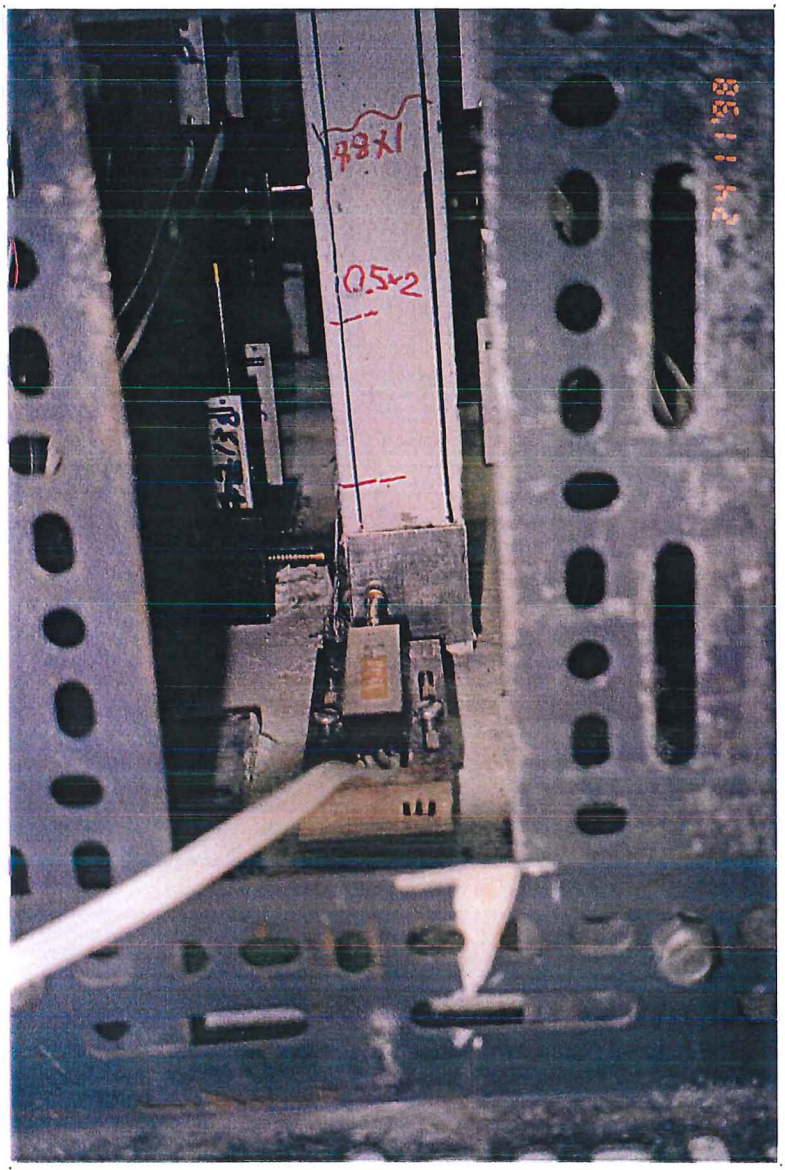

Figure 5.7: Unit 1: Twisting at the base of the wall on the compression edge at μ_Δ= -2.5×1 (East edge)

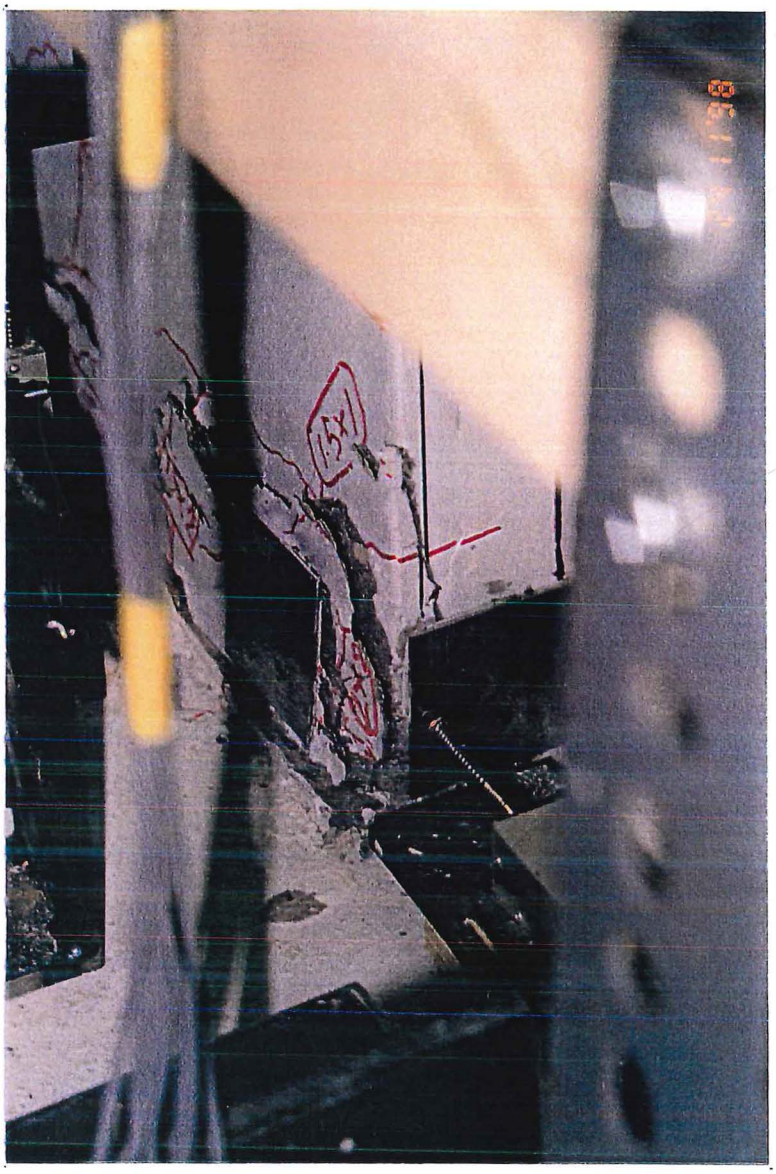

Figure 5.8: Unit 1: Spalling and twisting of the base of the wall on the compression edge (East edge) at μ_Δ = -2.5×1

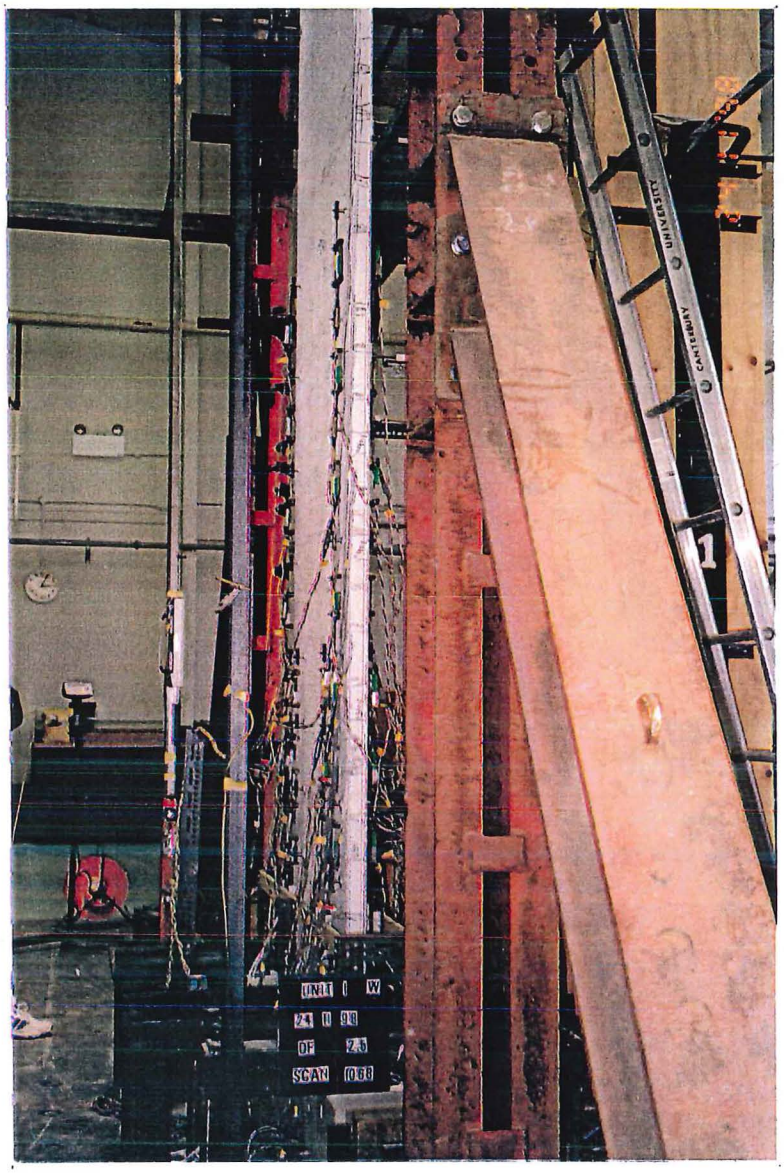

Figure 5.9: Unit 1: Wall still remains vertically during twisting at the base at μ_Δ= -2.5×1 (West edge)

Figure 5.10: Unit 1: View of West edge of the wall at μ_Δ= +5×1

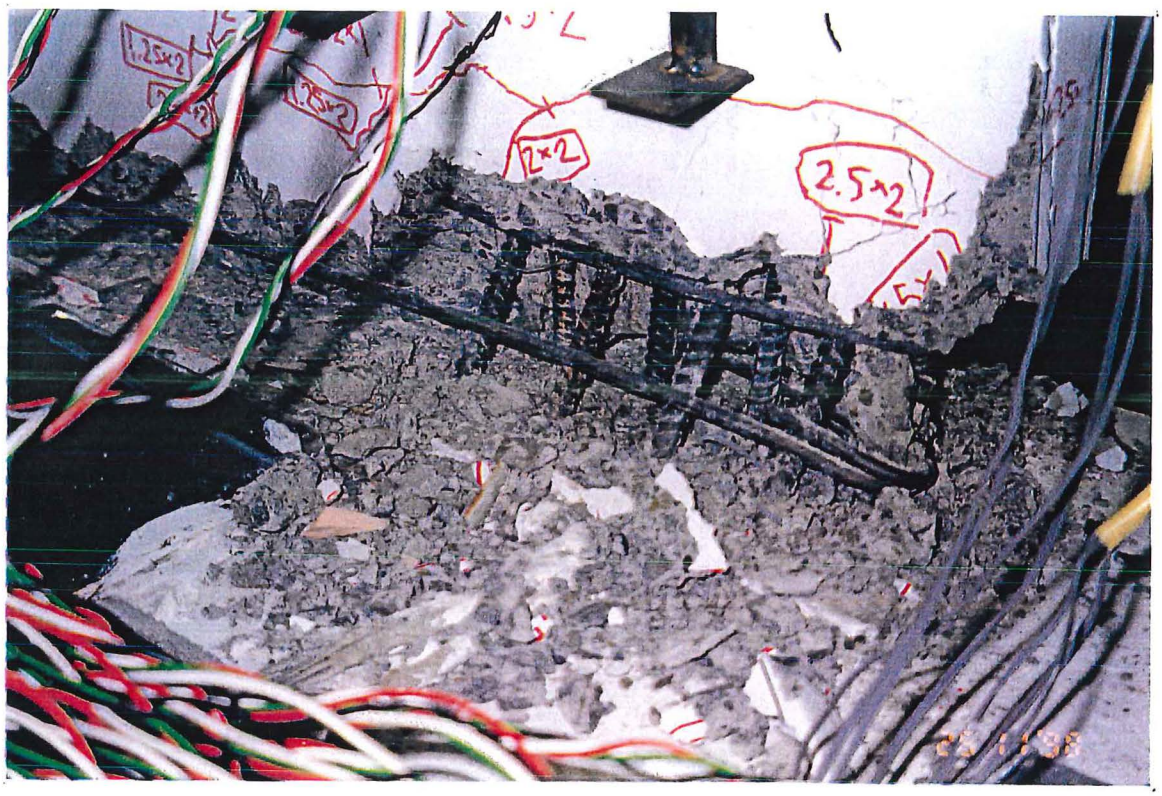

Figure 5.11: Unit 1: Buckling of compression starter bars at μ_Δ= -5×1 (South/Concave)

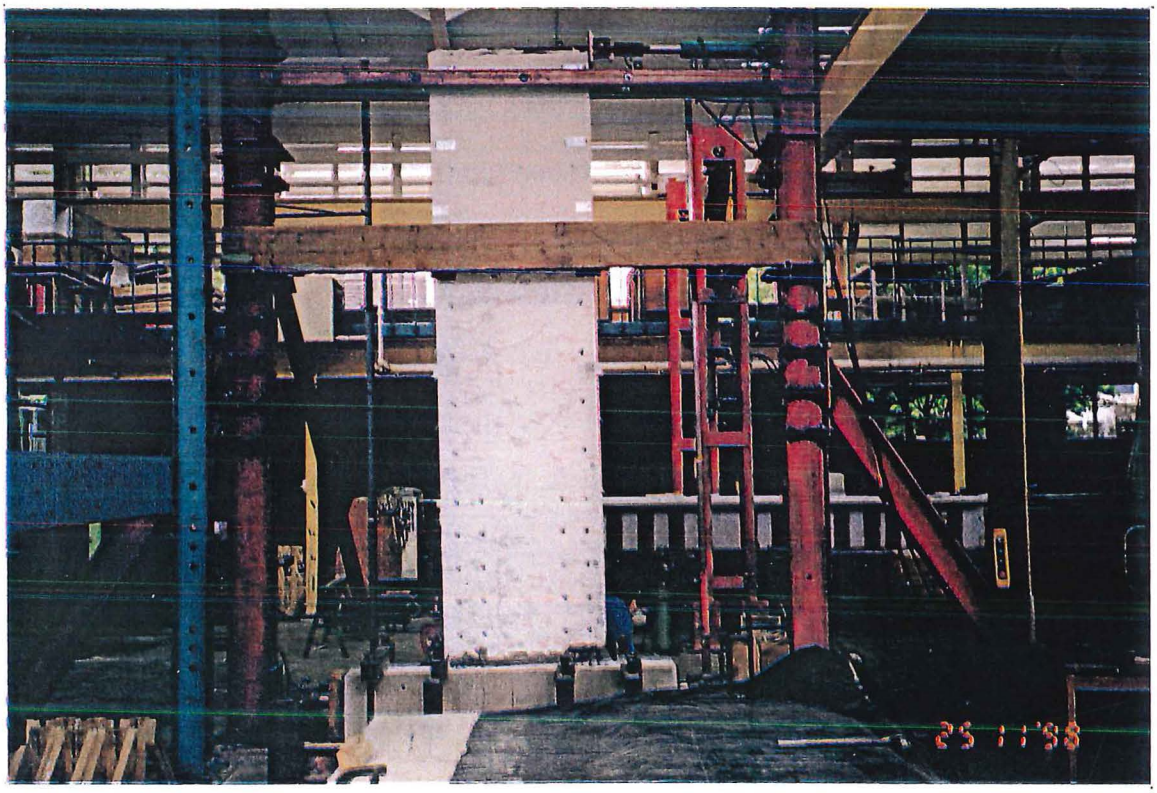

Figure 5.12: View of Unit 1 taken from South/Concave edge of the wall at the end of test

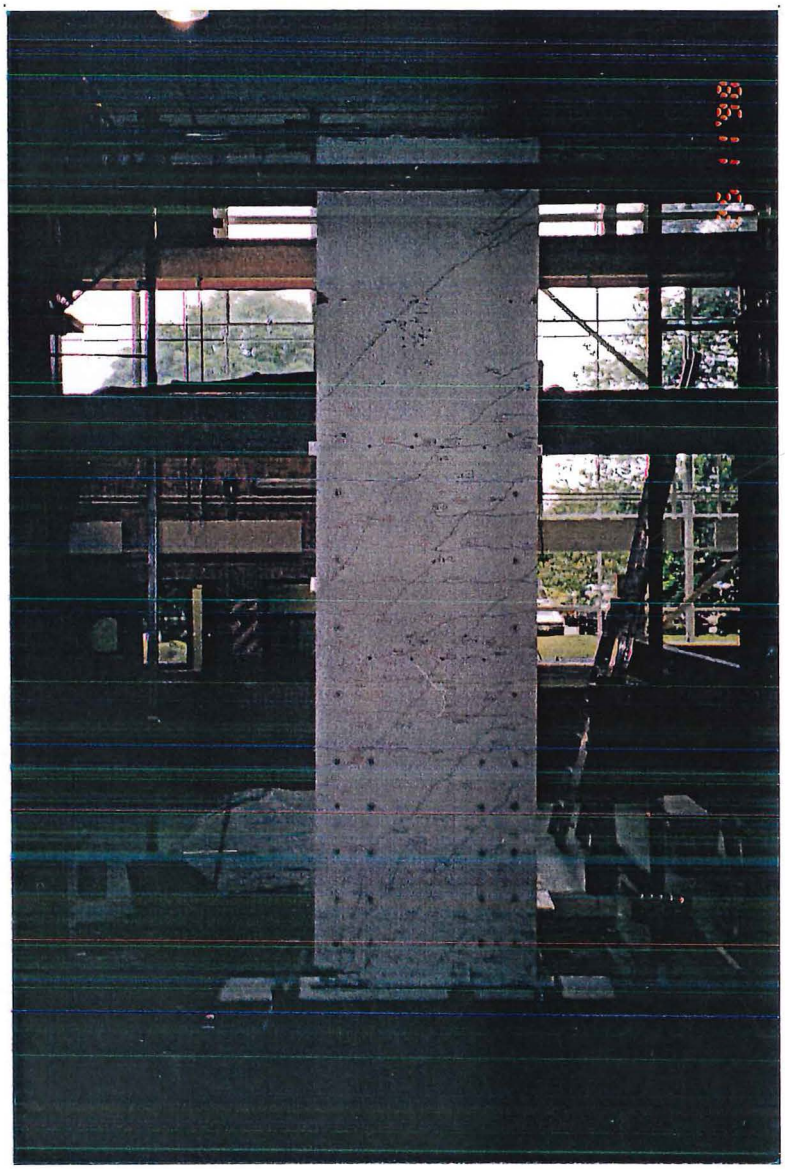

Figure 5.13: View of Unit 1 showing the diagonal crack pattern that formed at the end of test (North/Convex)

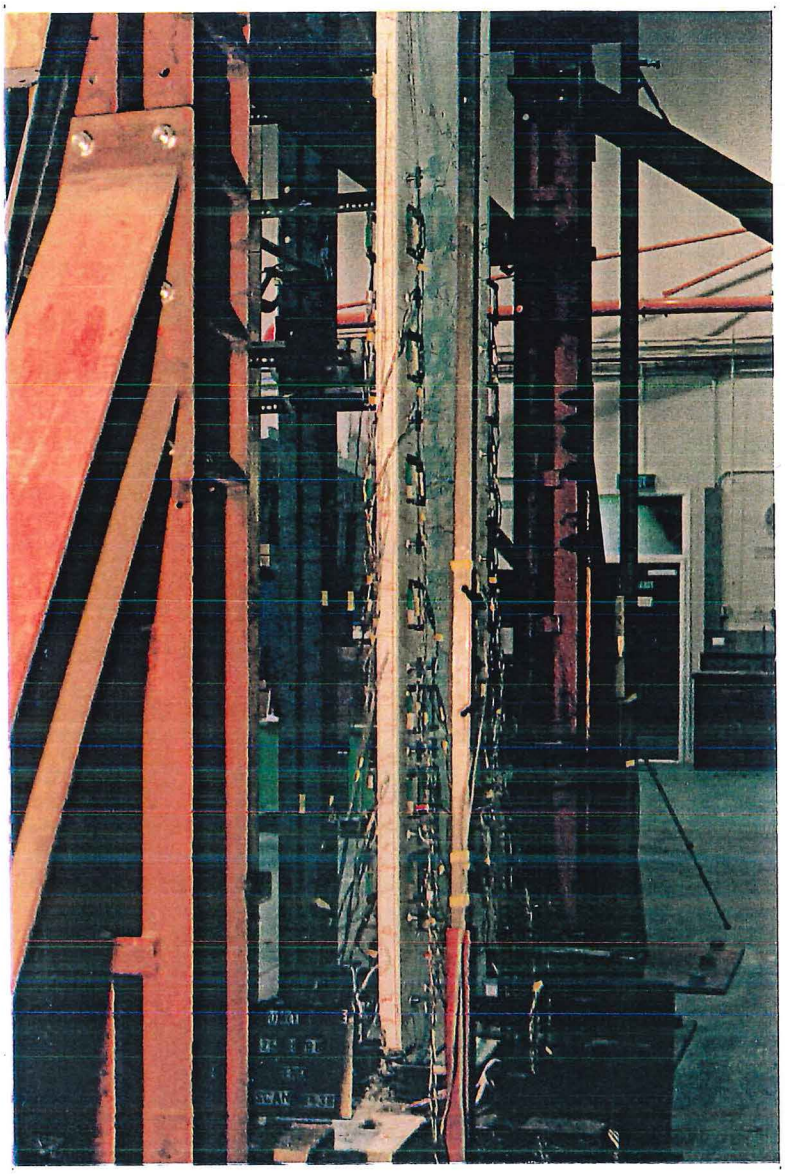

Figure 5.14: Unit 1: East edge of the wall at the end of test

5.1.3 Analysis of Experimental Results : Unit 1

5.1.3.1 Lateral Force-Lateral Displacement Response : Unit 1

During "elastic cycles" i.e. the initial cycles prior to $\mu_\Delta = 1$ was achieved, the hysteresis loops tended to be symmetrical in both positive and negative loading directions. The displacements of the initial cycles were contributed by the formation of cracks at the horizontal joint and sliding shear at the base. The overall response of Unit 1 is illustrated in Figure 5.15. The theoretical moment-curvature curves, plotted in Figure 5.16, represent the behaviour estimated assuming a monotonic loading in each direction. This was derived using the first outermost set of potentiometers which located at the level of the horizontal connection. This procedure was repeated for all other test units.

In the post-elastic cycles, the hysteresis loops shows an adequate energy dissipation capacity up to $\mu_\Delta = +2.5\times1$. It must be noted that the applied load dropped once the maximum capacity of 24.2 kN was reached at $\mu_\Delta = +2.5\times1$, which coincided with the change of the position of the neutral axis. A skewness of the neutral axis developed, reducing the internal lever arm and caused the reduction of capacity. When reloading in the opposite direction, the wall lost the ability to maintain its full capacity due to the buckling of the compression reinforcement. The wall started to twist about the vertical axis due to the buckled compression reinforcement which pushed the wall sideways, inducing a twisting action at the horizontal joint. Straighten and retensioning of the starter bars, on reverse loading, resulted in an increase in in-plane lateral load as can be seen at the large displacement ductilities. The displacement ductility of $\mu_\Delta = 4.9$ was reached before the end of the test with very little residual stiffness.

The repetition of the same displacement ductility was accompanied by the reduction in strength with significant amount of stiffness degradation during reloading cycles.

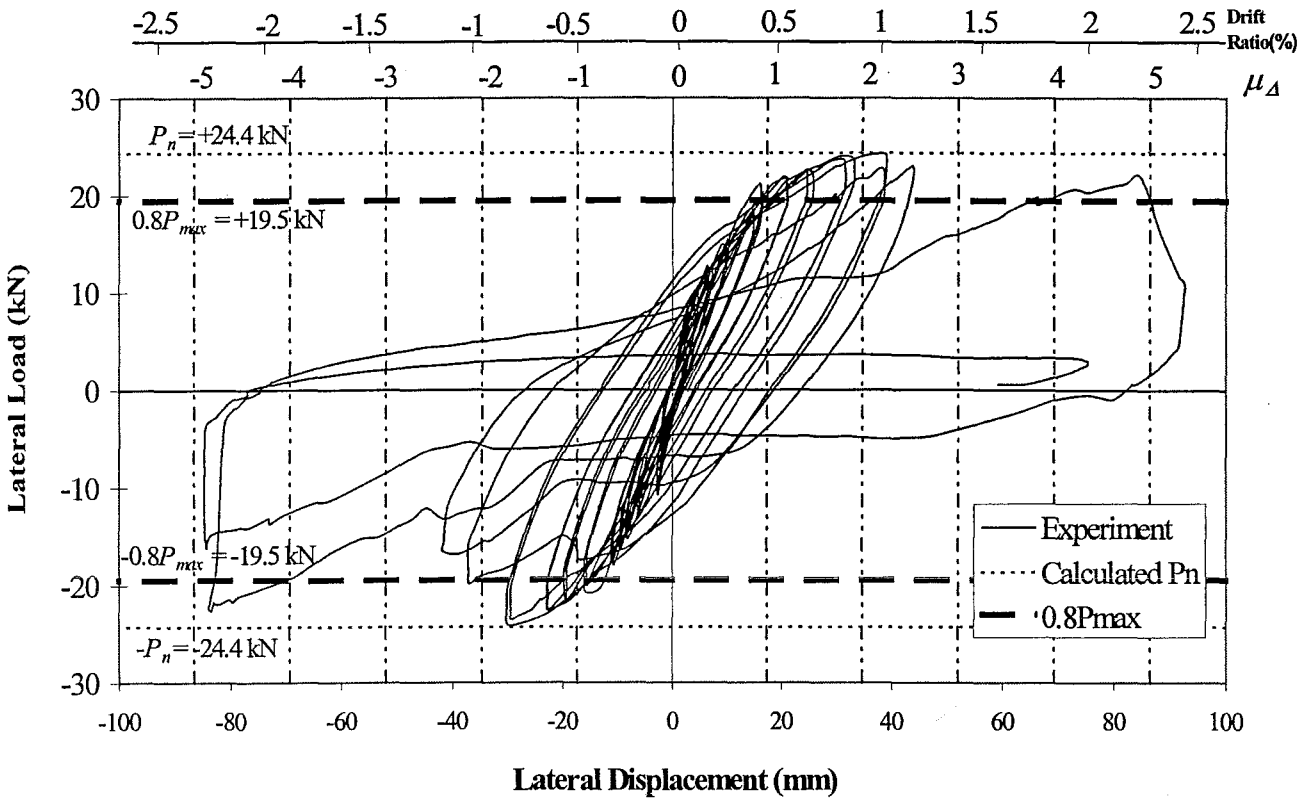

Figure 5.15: In-plane lateral load-lateral displacement response of Unit 1

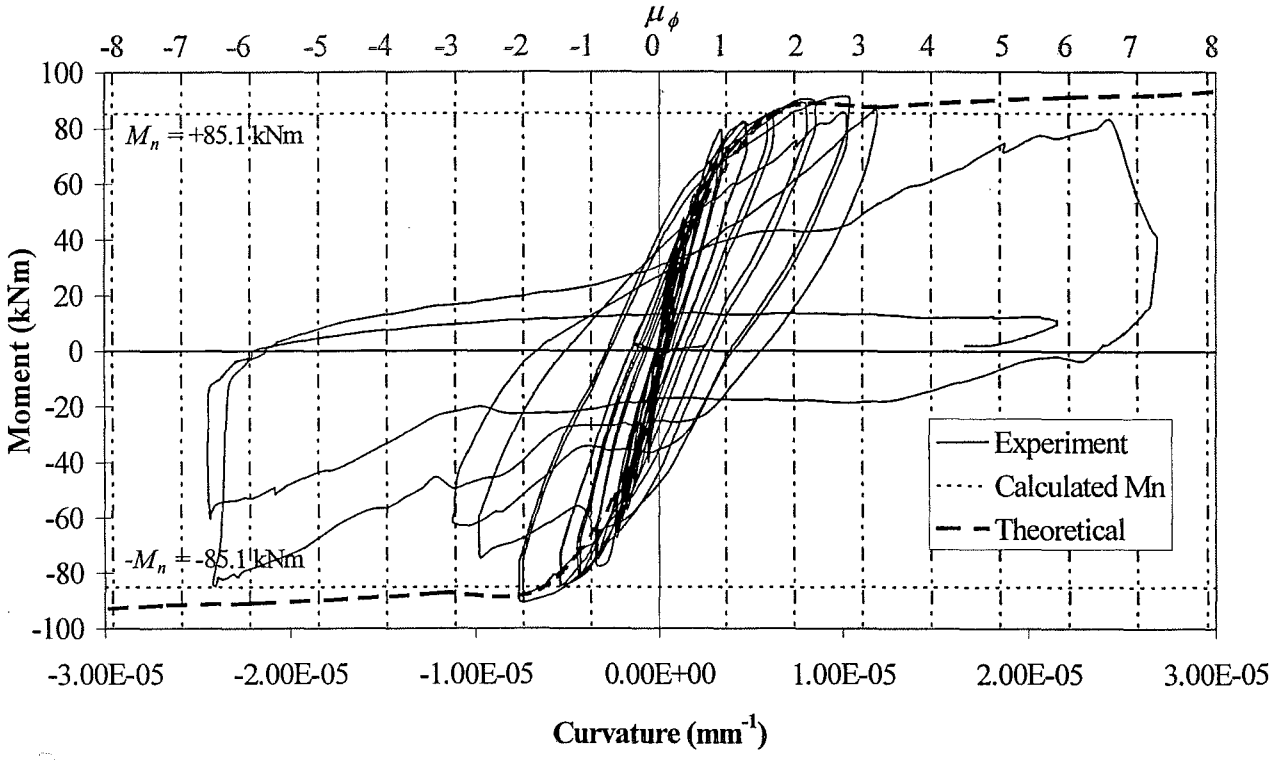

Figure 5.16: Moment-curvature response of Unit 1

5.1.3.2 Out-of-Plane Displacements : Unit 1

The out-of-plane movements were measured using linear potentiometers located at 50 mm from the edges of the wall (see Figure 4.19). All the out-of-plane displacement plots represent "North face" on the right and "South face" on the left. The initial wall profiles were taken from both edges prior to the test. It was found that the wall changed shape during the curing and instrumentation period and the initial out-of-plane displacement of 4.8 mm had been reduced to 3 mm.

Figure 5.17 shows the out-of-plane displacements at the positive peak cycles on the East edge (tension edge) only. During the initial loading cycles, the first few cracks developed on the concave side as the wall tended to straighten. More cracks appeared and extended as the applied force increased. The wall profiles changed from a single curvature to a double curvature when starting the post-elastic loading cycles. At $\mu_\Delta = 2.5$, the maximum out-of-plane displacement was less than 4 mm, which was equivalent to 0.11% out-of-plane storey drift.

The West edge (compression edge) of the wall behaved similarly to the tension edge, see Figure 5.18 (out-of-plane deflection of the peak of each positive cycle). The wall tended to deflect outwards at the low applied load level resulting in the crack formation on the concave side. The wall profile showed double curvature when it reached $\mu_\Delta = +1$. The only difference was that the point of inflection was higher compared to the tension edge at the same magnitude of positive cycle.

In Figure 5.18, it must be noted that the out-of-plane displacement at the base of the wall was reasonably large at $\mu_\Delta = +2.5\times1$. This was due to the large movement that occurred when the base of the wall started to twist in clockwise direction. This movement was induced by the buckling of the starter bars. When the wall was subjected to the positive peak load, the tension edge moved back to the original position. Hence this type of movement was not noticeable in Figures 5.17 and 5.20. Figure 5.20 illustrated similar behaviour of the wall on the West edge when subjected to the negative cycle.

The maximum out-of-plane displacement was less than 3 mm or 0.08% out-of-plane storey drift.

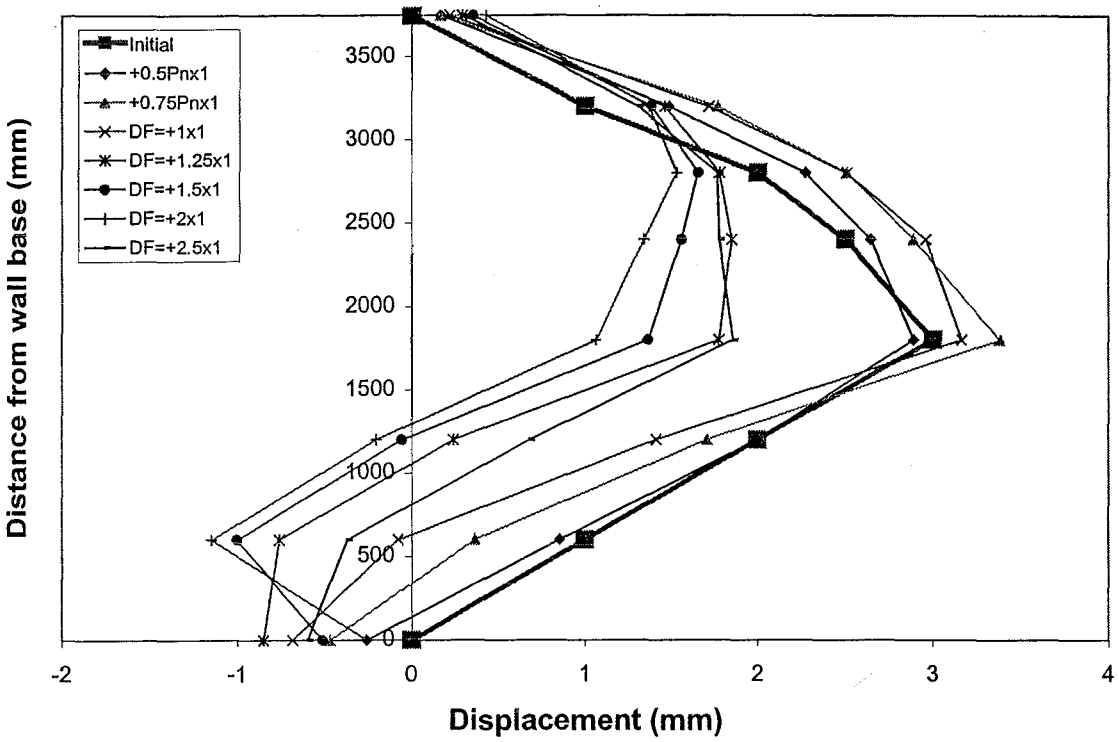

Figure 5.17: Unit 1: Out-of-plane movement on East edge of the wall at positive peak cycles (Tension edge)

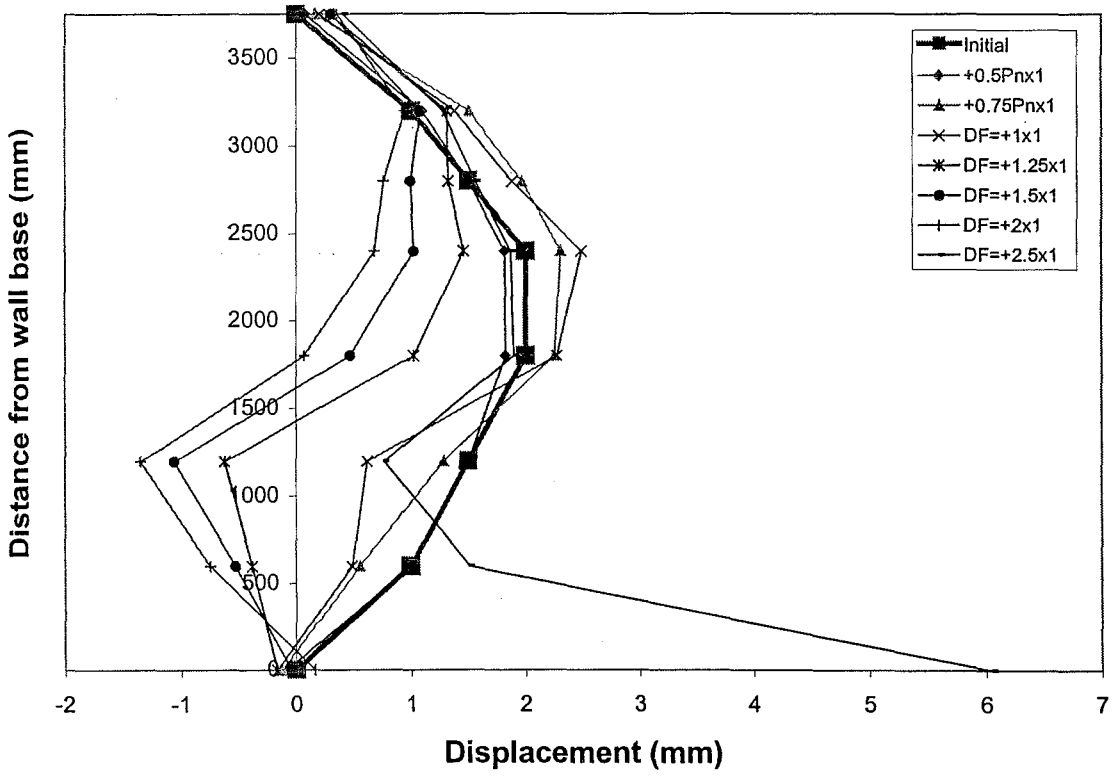

Figure 5.18: Unit 1: Out-of-plane movement on West edge of the wall at positive peak cycle (Compression edge)

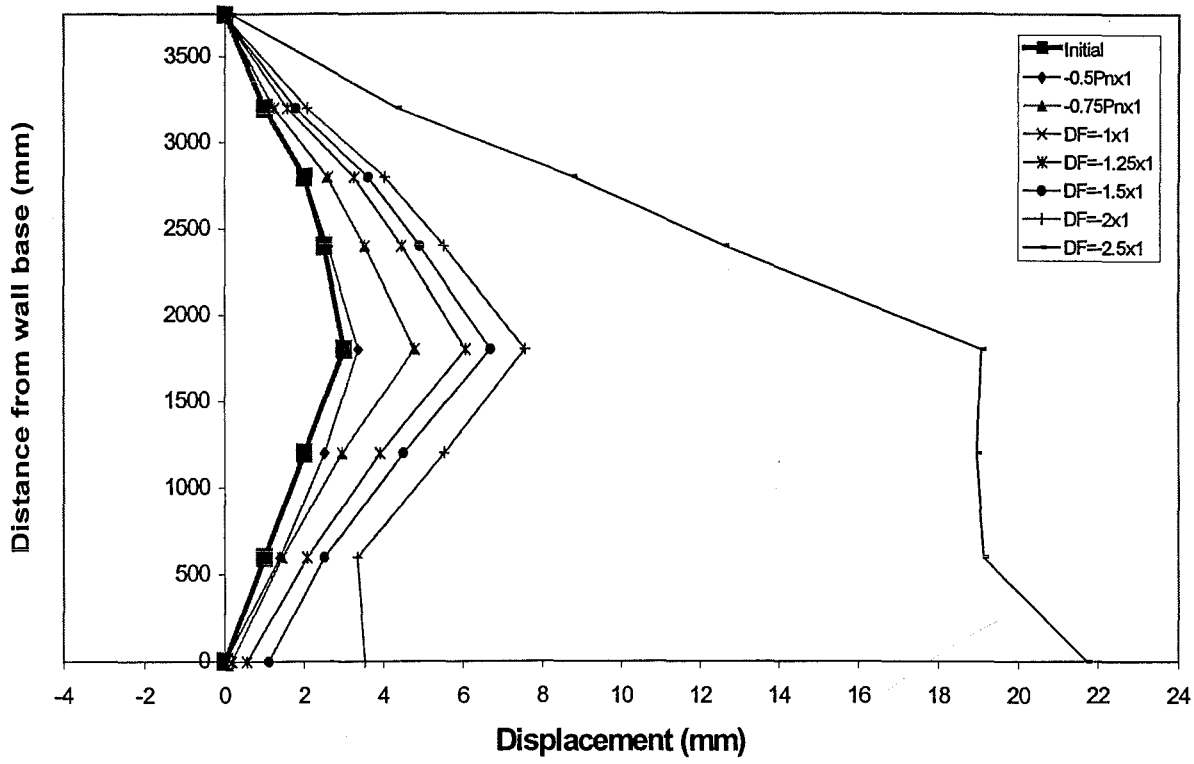

Figure 5.19: Unit 1: Out-of-plane movement on East edge of the wall at negative peak cycles (Compression edge)

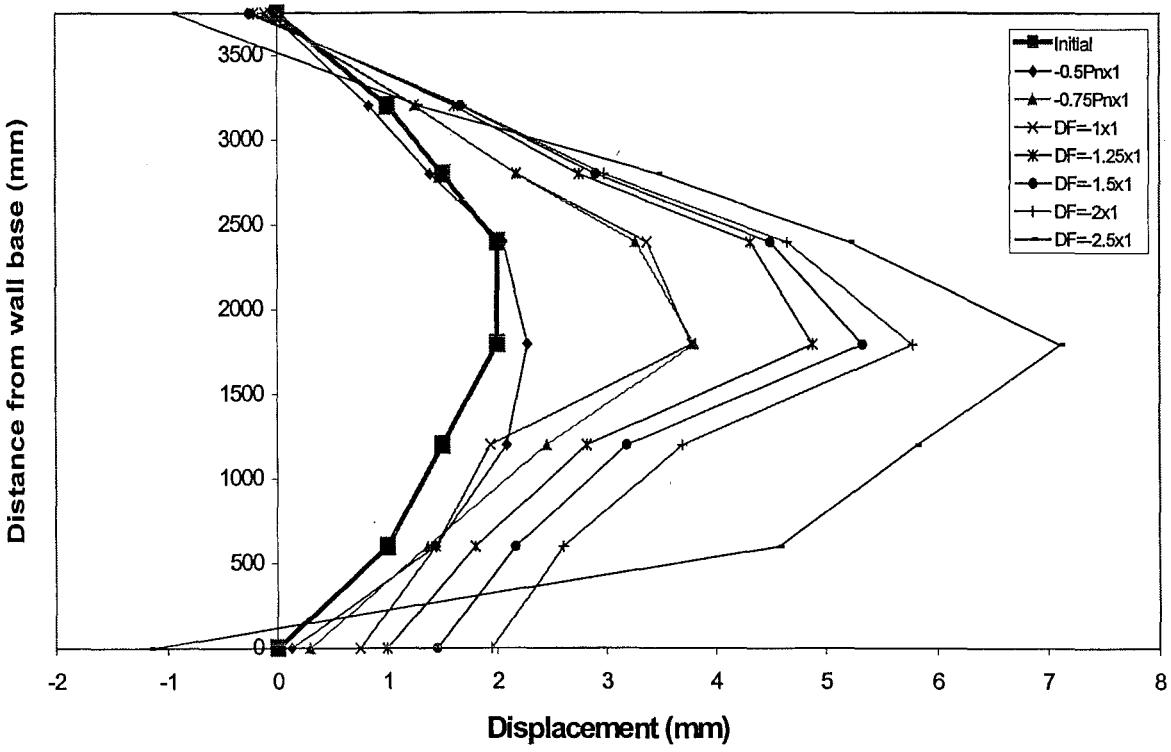

Figure 5.20: Unit 1: Out-of-plane movement on West edge of the wall at negative peak cycles (Tension edge)

5.1.3.3 Local Bar Strains : Unit 1

The local strains measured from the outermost starter bar on East edge of the panel during the test at peaks of cycles of loading are shown in Figure 5.21. The strain gauge was located at the wall-foundation interface. Yielding in tension started at the applied force level of $0.75P_n$. Once the bars yielded in tension, there was a permanent elongation in the bars (see Figure 5.21).

Strains profiles measured along the outermost longitudinal reinforcement in the wall at the positive peak cycles are illustrated in Figures 5.22 and 5.23. It must be noted that no yielding occurred within the region of lap-splice at any stage during the test. Nor anywhere above 800 mm measured from the top of the foundation beam.

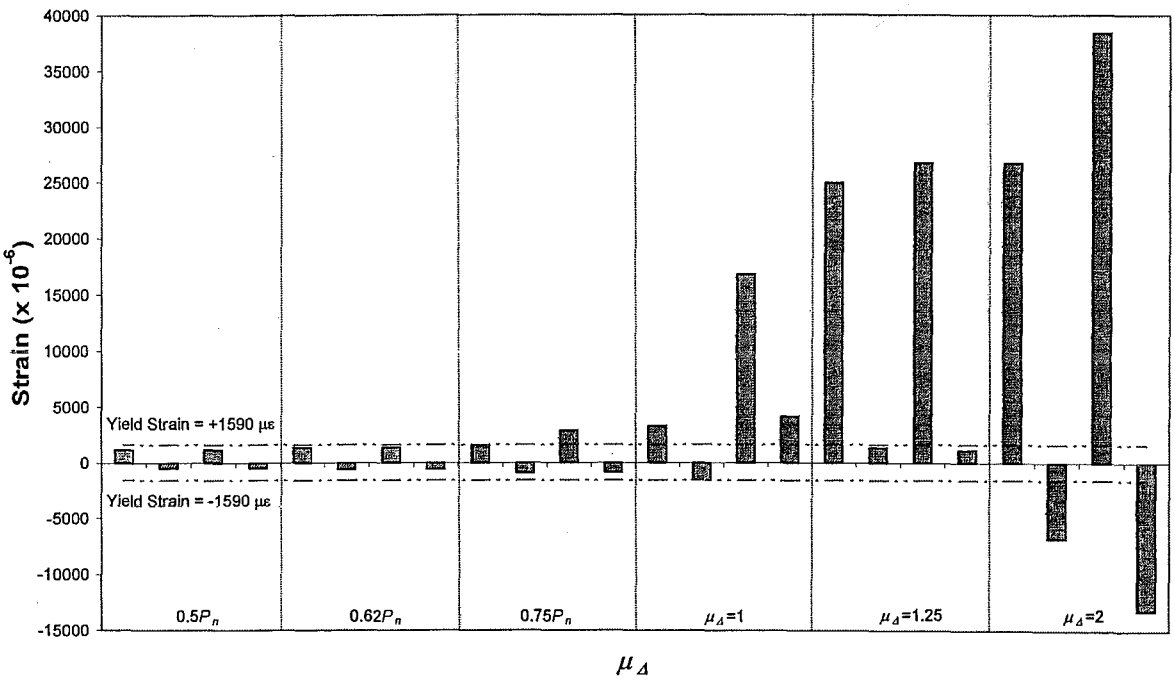

Figure 5.21: Unit 1: Strains of the outermost East edge starter bar measured at the wall-foundation interface during the test

Considering the East edge (tension edge) of the wall in Figure 5.22, the first yielding occurred in the starter bars at the wall-foundation interface and in the region above the lap splice when 75% of the nominal capacity was reached. Spreading of yielding on the starter bars was more extensive than in other locations. More cracks developed above the lap splice and most of them remained horizontal. There was no

yielding taken place within lap splice region because of the high capacity provided over the lap zone. Most of yielding occurred at the wall-foundation interface as expected. Again, similar behaviour took place in the negative direction loading (see Figure 5.24).

The strain distribution of the outermost longitudinal reinforcement in the wall is shown in Figures 5.23 and 5.25. When the wall was subjected to the positive peak cycles, the reinforcement on this side underwent into compression. At 75% of the nominal capacity when tension steel started to yield, the strain in the compression steel stayed well below the yield level. Some compressive force was taken by concrete as well as these compression steel. When the wall reached $\mu_\Delta = 1.25$, these compression steel had the positive (tension) residual strains at the wall-foundation interface.

Figure 5.26 shows the development of strains in the each starter bar along the wall-foundation interface during the initial cycles up to when the wall reached $\mu_\Delta = 1.0$. During the peak cycle at $0.5P_n$, strains of tension starter bars remained under the yield stain. The neutral axis was approximately 198 mm from the extreme compression fibre. These starter bars began to yield when the applied force reached $0.75P_n$. The outermost starter bars yielded at this stage while all the compression starter bars remained well below the yield strain. The neutral axis reduced to approximately 183 mm from the extreme compression fibre. This measured value was relatively identical to the predicted neutral axis depth of 202 mm at yield capacity. At $\mu_\Delta = +1\times1$, most strain gauges in this region was damaged and the available data became unusable.

Figure 5.27 shows the strains of the wall reinforcement measured at 200 mm above the foundation beam during elastic cycles, i.e. $0.5P_n$, $0.75P_n$ and $\mu_\Delta = 1$. Within the elastic range, none of the wall reinforcement reached yield strain within the lap splice region. In both directions of loading, strain profiles were relative symmetrical to the centre line of the wall. The repetition of the same direction loading had the greater effects on the larger applied load level. The neutral axis depth did not change very significantly.

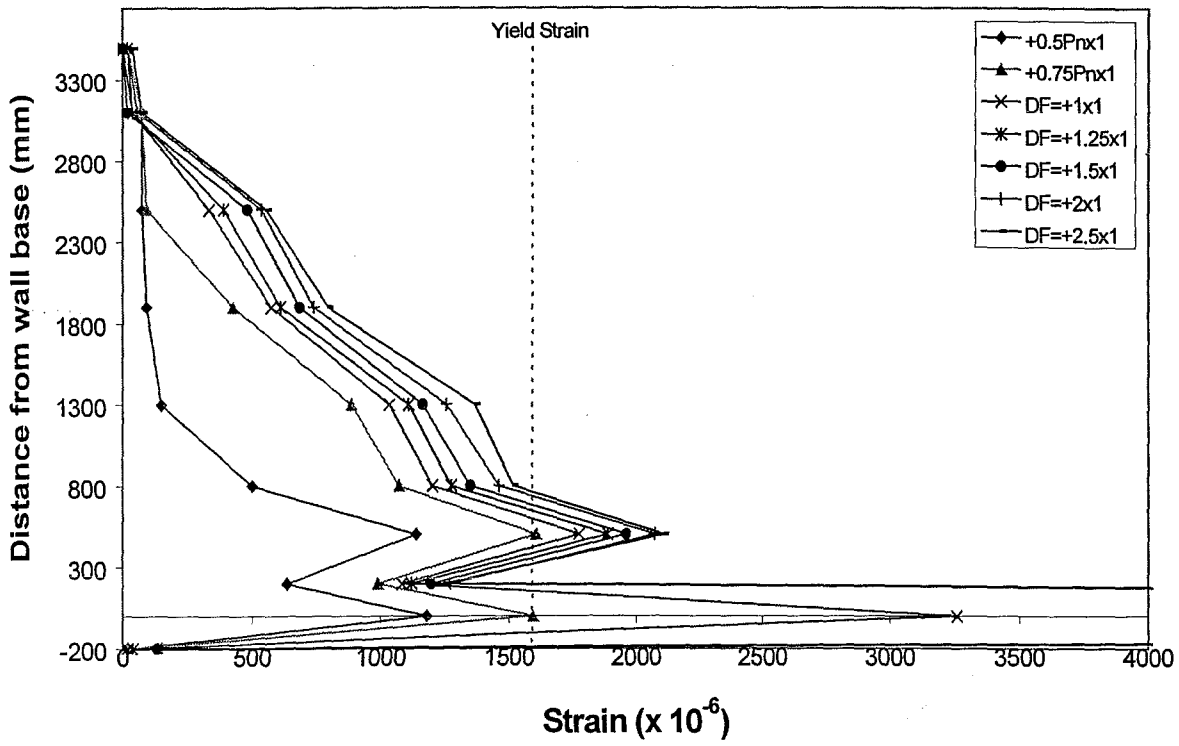

Figure 5.22: Unit 1: Outermost East edge longitudinal reinforcement strains measured at positive peak cycles (tension edge)

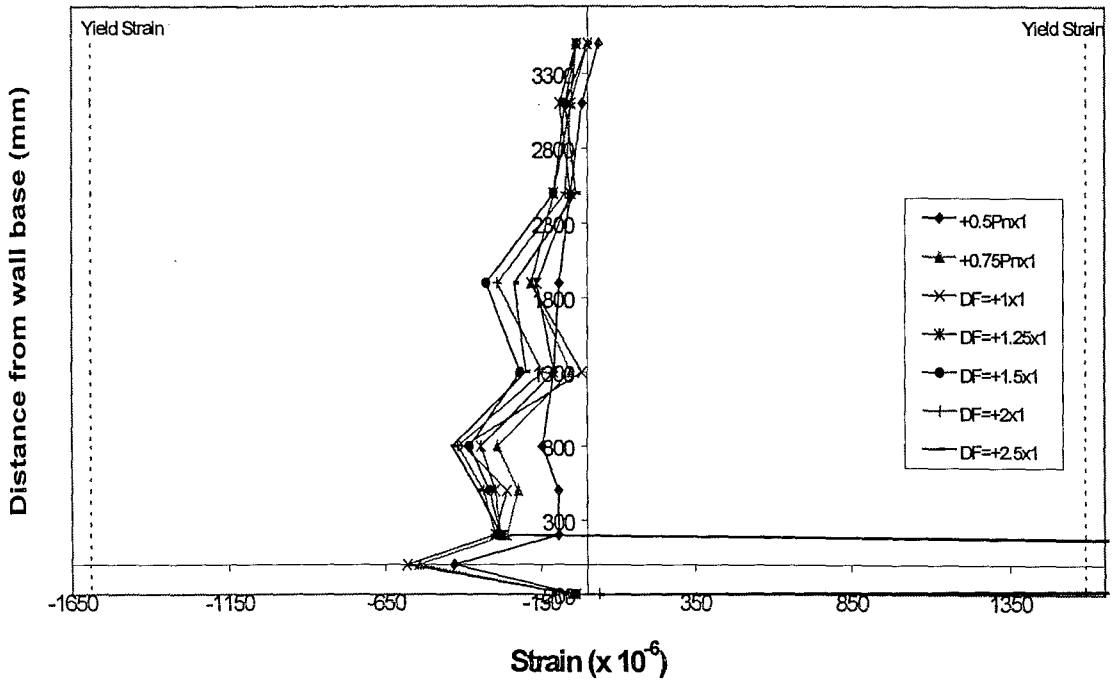

Figure 5.23: Unit 1: Outermost West edge longitudinal reinforcement strains measured at positive peak cycles (compression edge)

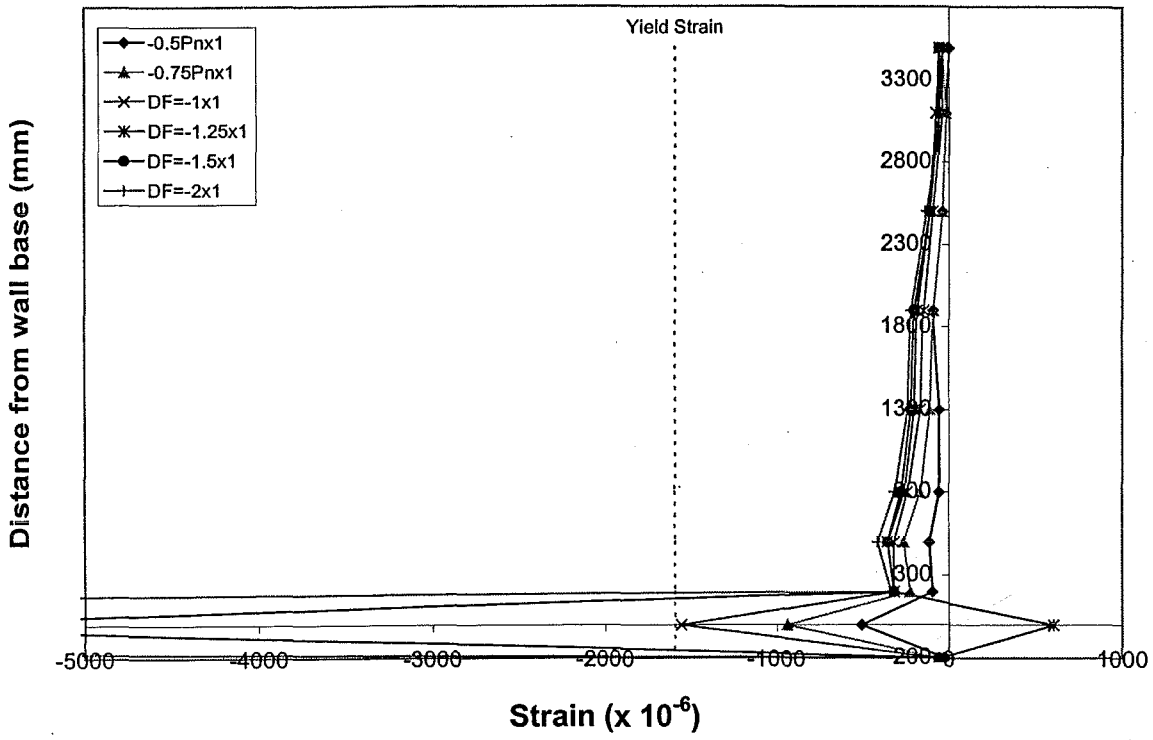

Figure 5.24: Unit 1: Outermost East edge longitudinal reinforcement strains measured at negative peak cycles (compression edge)

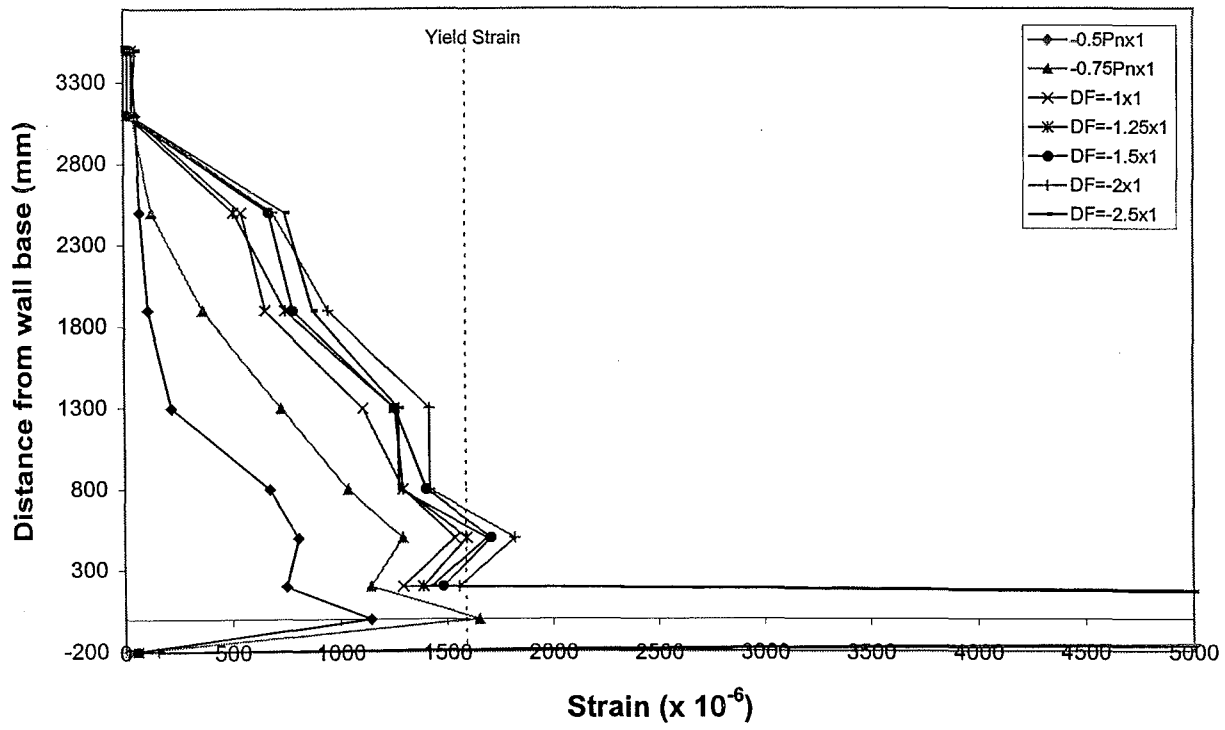

Figure 5.25: Unit 1: Outermost West edge longitudinal reinforcement strains measured at negative peak cycles (tension edge)

The wall reinforcement yielded in the region immediately above lap splice when the wall was subjected to $0.75P_n$. The strains of the wall reinforcement were measured at 500 mm above the foundation beam (see Figure 5.28). The strain profiles remained approximately symmetrical to the centre line of the wall. Similar types of behavior to that of the lap splice region took place in this location. The local bar strains at the higher level of ductility were not shown because the strain gauges were damaged.

Another prediction had been made was that the wall would develop a large number of cracks within this region. Some yield penetration was expected to take place and spread upwards. This type of behaviour would induce the instability to the wall. In the opposite direction loading, the yielded reinforcement would have to take compression forces and out-of-plane buckling would be more likely to occur. The chance of the wall failing in buckling mode is higher for a singly reinforced wall [G2].

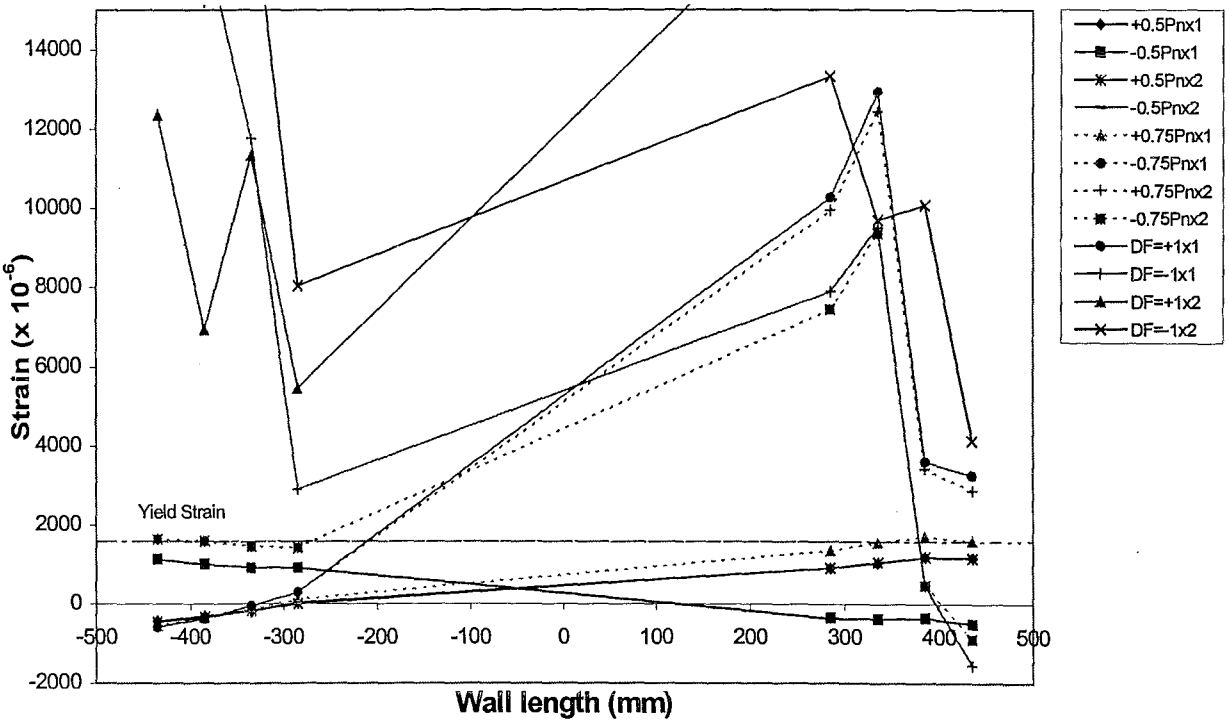

Figure 5.26: Unit 1: Strains of starter bars across the wall-foundation interface during the test

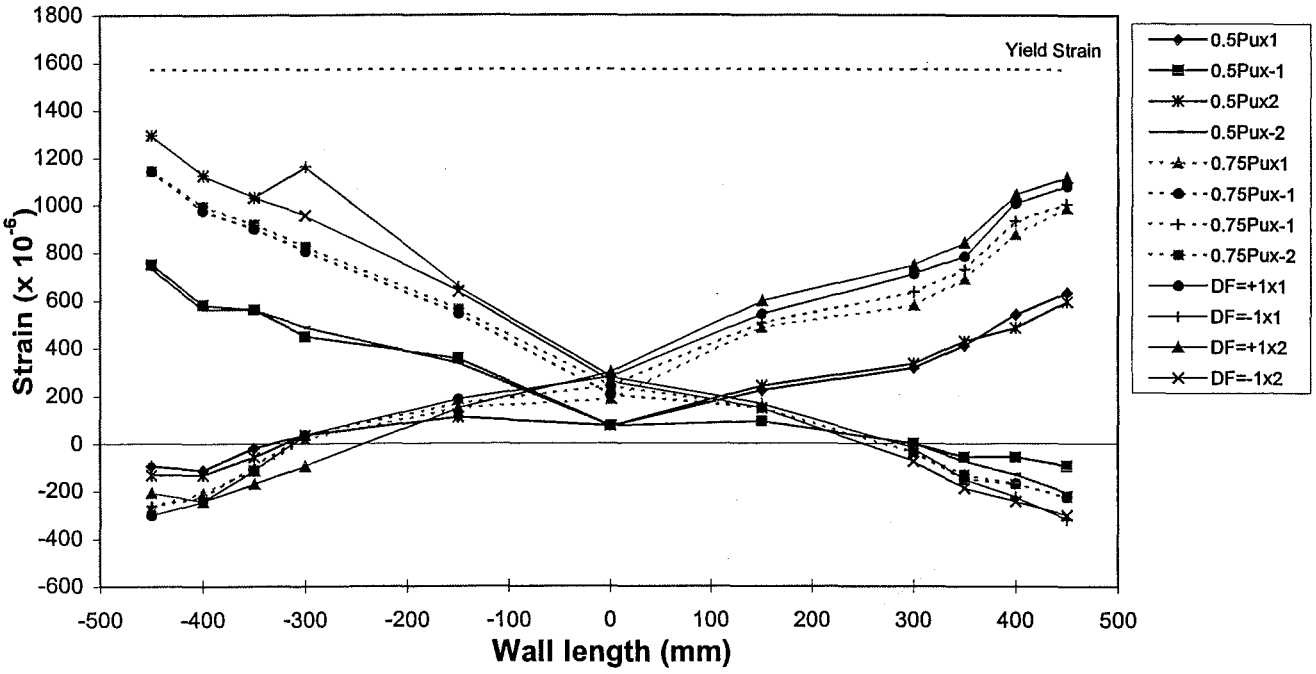

Figure 5.27: Unit 1: Strains of wall reinforcement within lap splice region (200 mm above the foundation beam) during the peak elastic cycles

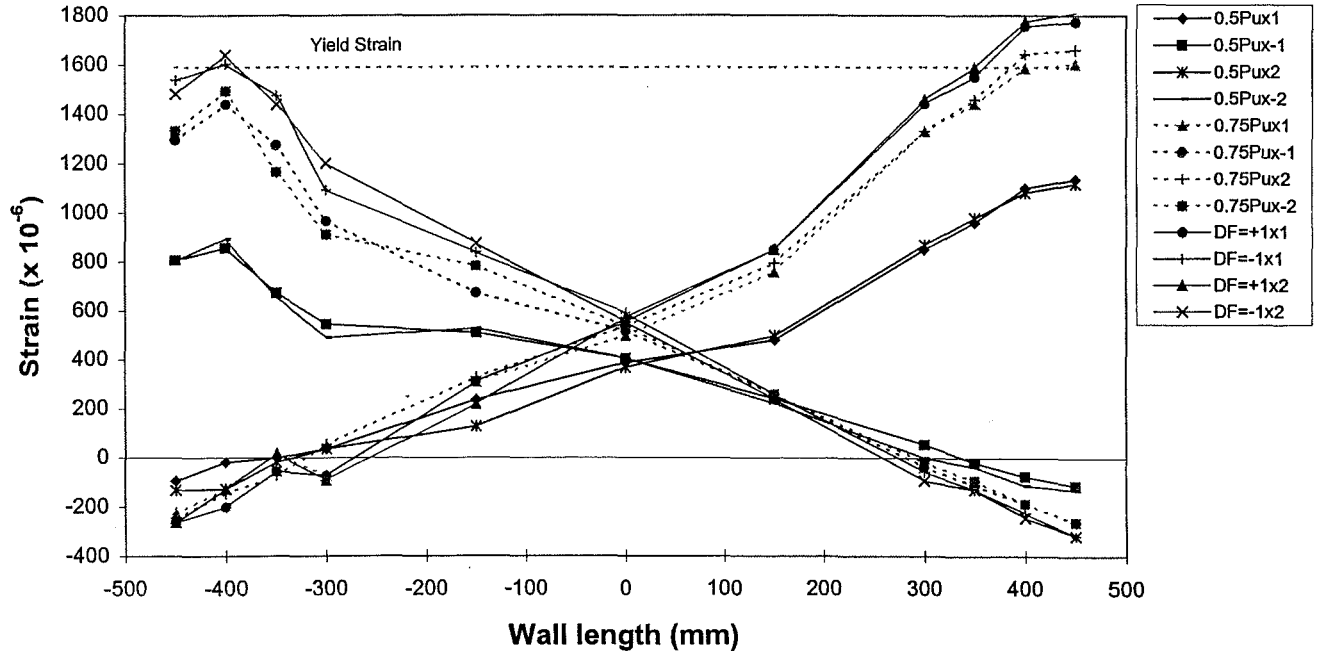

Figure 5.28: Unit 1: Strains of wall reinforcement above the region of lap splice (500 mm above the foundation beam) during the peak elastic cycles

5.1.3.4 Concrete Strains : Unit 1

Figures 5.29, 5.30, 5.33 and 5.34 show the concrete strains at the wall base at different stages during the test. When the peak to $\mu_\Delta = +1.25$ was reached, the entire base of the wall started to lifted and induced tensile strains everywhere along the horizontal joint. The compression edge of the wall became in contact with the foundation beam again at $\mu_\Delta = -2.5\times1$ and caused the concrete to spall. The spalling strain was approximately -0.004 (see Figure 5.33).

By comparing the difference in concrete strains in the opposite side of the West edge, see Figure 5.29, it becomes an evident that the neutral axis depth became skewed for the cycles to $\mu_\Delta = 1.25$. At $\mu_\Delta = 2.5$, concrete strains dropped rapidly because of the presence of the twisting at the wall base (see Figures 5.31 and 5.35).

Longitudinal concrete strains measured along the wall base when subjected to compression were significantly greater than the ones at the region immediately above lap splice (see Figures 5.31 and 5.35). Only a single line of data is shown in Figures 5.31(b) due to the occurrence of potentiometer failure prior to the experiment. Similarly, the longitudinal concrete strains at the wall base when subjected to tension was much greater than the longitudinal concrete strain at the region immediately above lap splice (see Figures 5.32 and 5.36). Figure 5.33 displays the longitudinal concrete strains on the East edge when subjected to compression. Similar results were observed as in Figure 5.29 apart from both gauges underwent into tension and compression when subjected to the first cycle of $0.5P_n$. The East edge started to go into tension when subjected to $\mu_\Delta = -1.25\times2$ (see Figure 5.35) along the wall base and in the region immediately above lap splice. Similar behaviour occurred when East edge subjected to tension (see Figure 5.34).

In-plane curvature distribution at 200 mm above the foundation beam was measured by taking an average of a pair of clip gauges at both edges of the wall, i.e. CS21, CN24 and CS24 and CN21 respectively (see Figure 4.20). Figure 5.37 illustrates the in-plane curvature which measured at the peak cycle during the test. It shows a direct correlation between the in-plane curvature and the applied loading pattern.

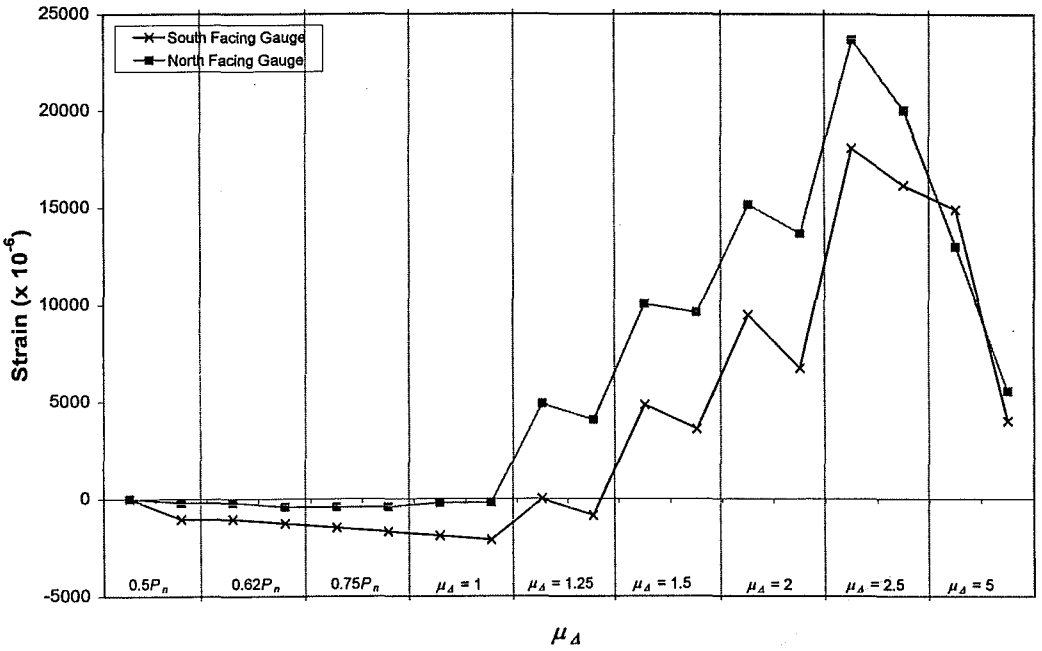

Figure 5.29: Unit 1: Concrete longitudinal strains of West edge when subjected to compression obtained from outermost clip gauges (base of wall)

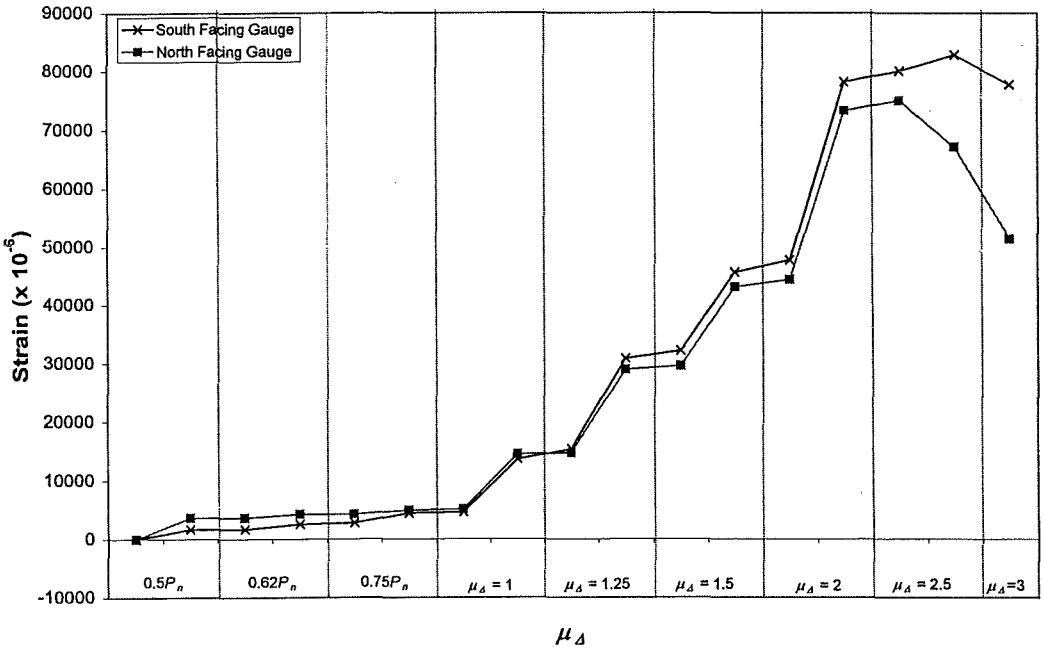

Figure 5.30: Unit 1: Concrete longitudinal strains of West edge when subjected to tension obtained from outermost clip gauges (base of wall)

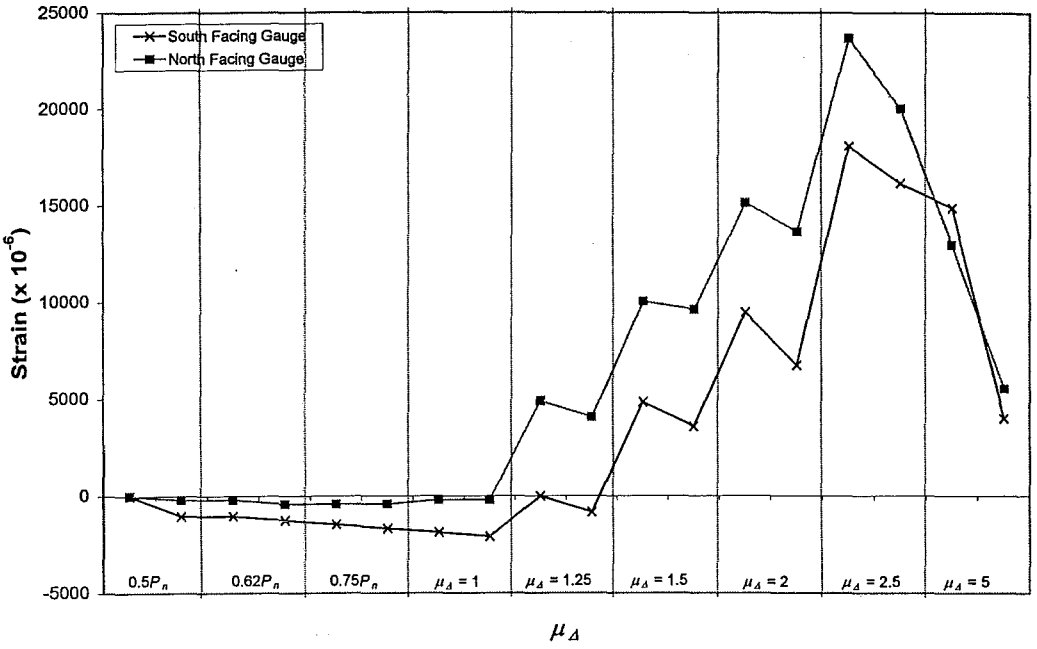

(a) Wall base

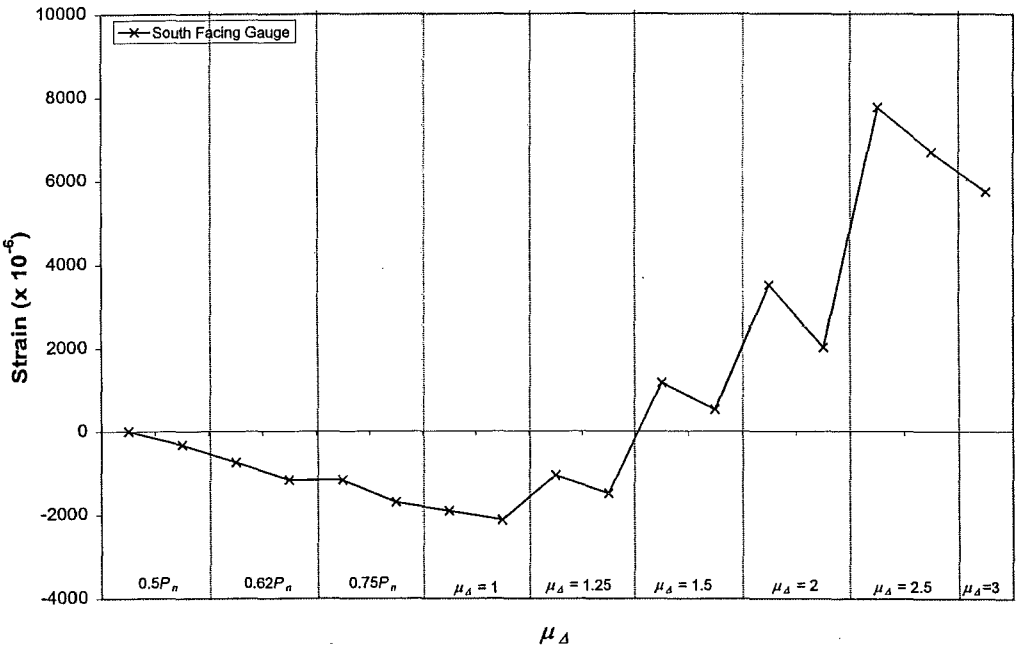

(b) Immediately above lap splice

Figure 5.31: Unit 1: Difference in longitudinal concrete strains in West edge when subjected to compression obtained from the outermost clip gauges

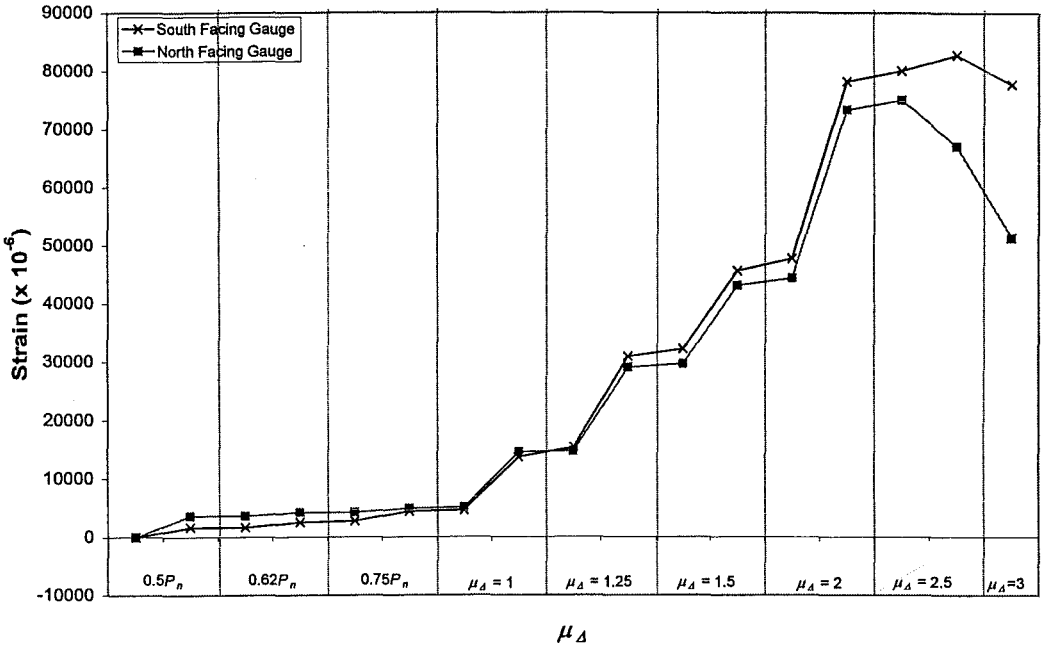

(a) Wall base

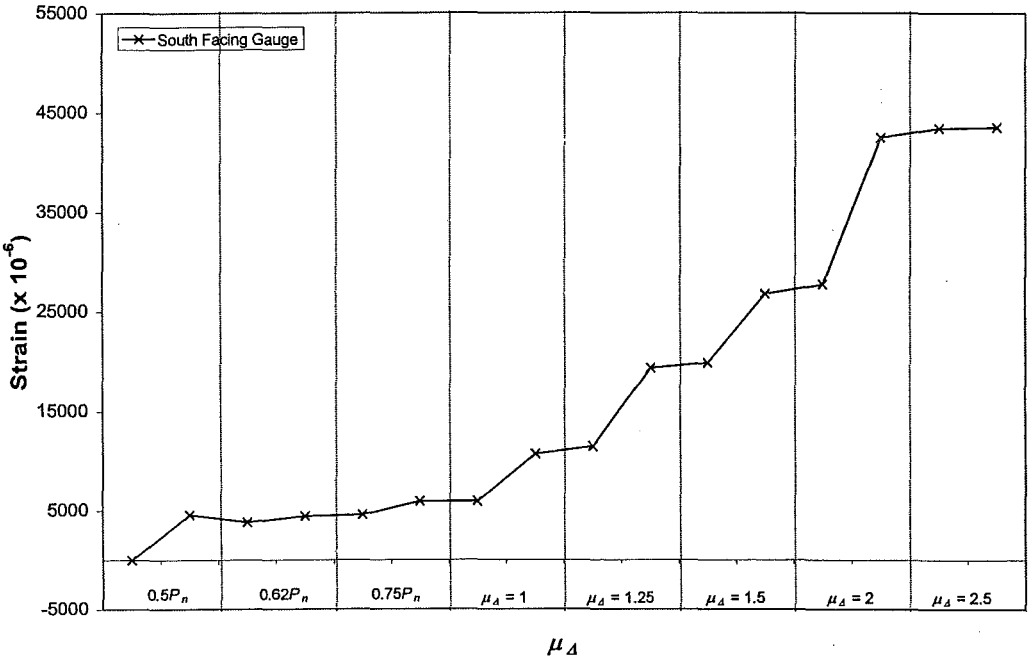

(b) Immediately above lap splice

Figure 5.32: Unit 1: Difference in longitudinal concrete strains in West edge when subjected to tension obtained from the outermost clip gauges

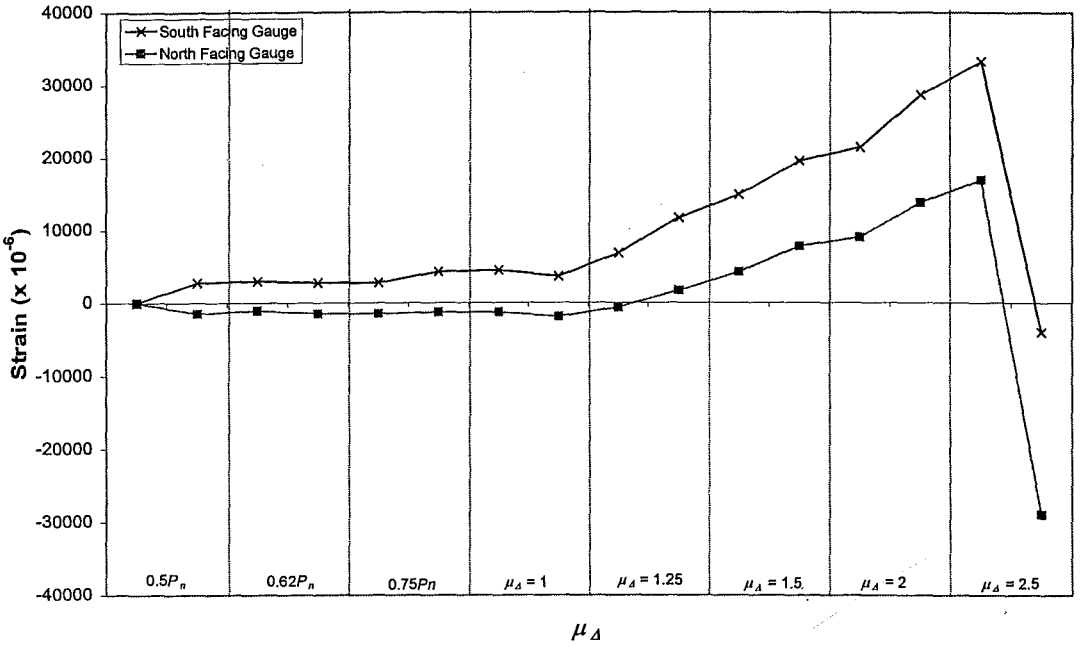

Figure 5.33: Unit 1: Concrete longitudinal strains of East edge when subjected to compression obtained from outermost clip gauges (base of wall)

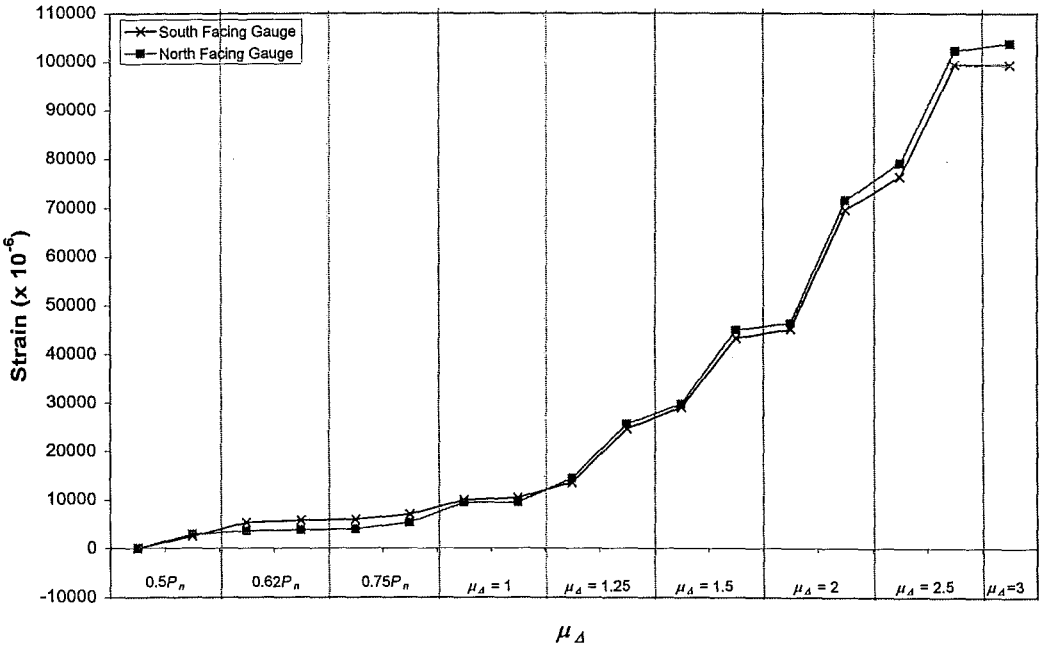

Figure 5.34: Unit 1: Concrete longitudinal strains of East edge when subjected to tension obtained from outermost clip gauges (base of wall)

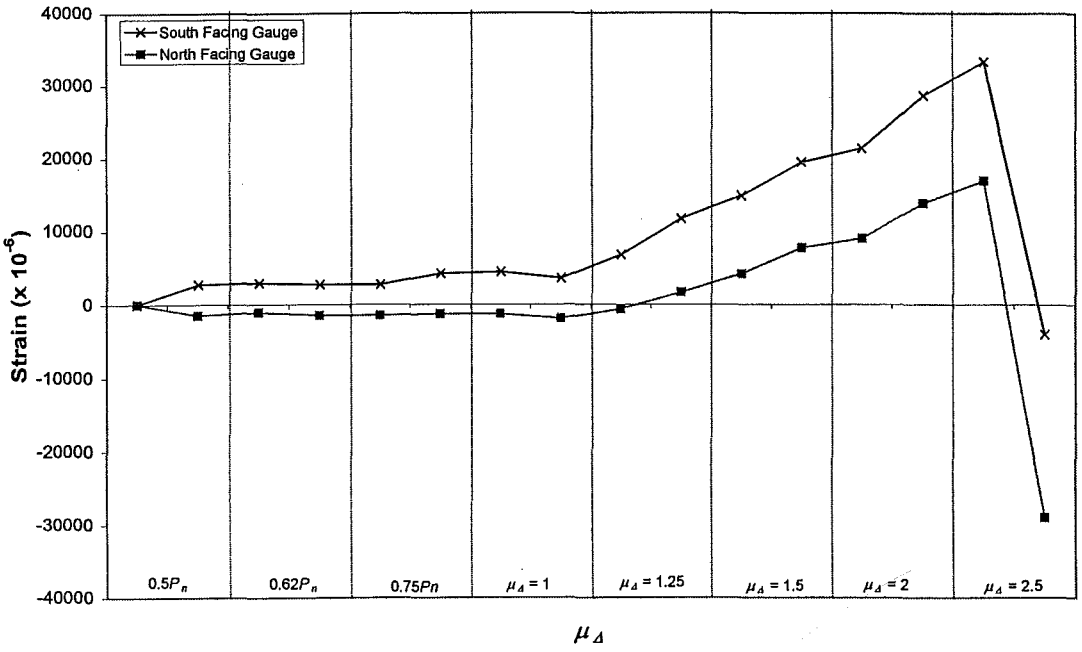

(a) Wall base

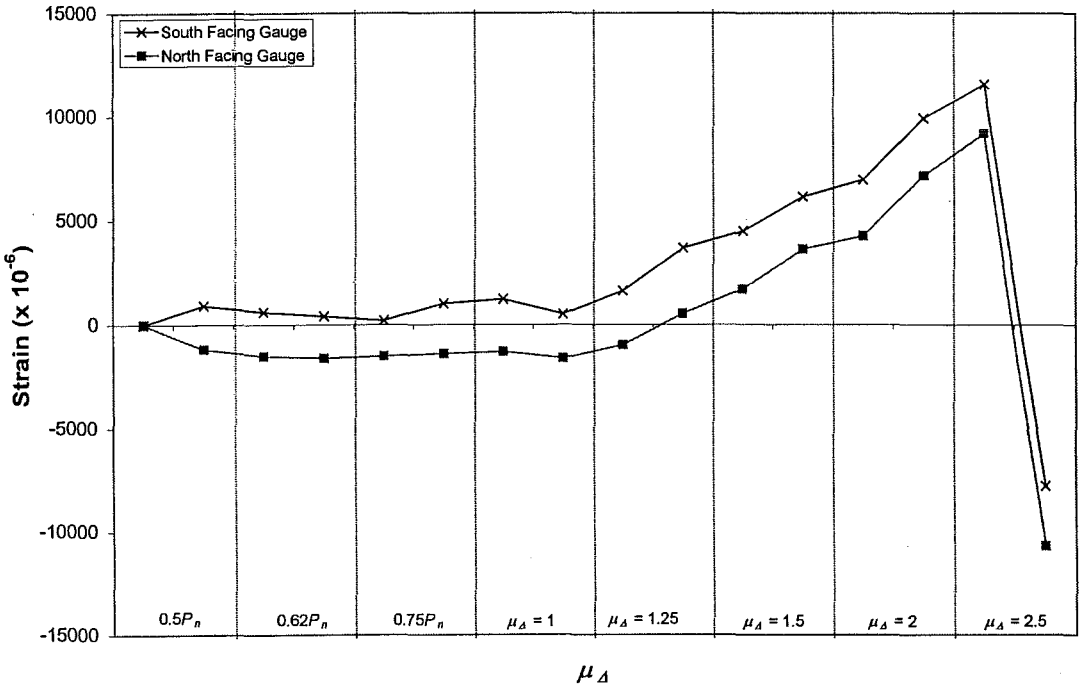

(b) Immediately above lap splice

Figure 5.35: Unit 1: Difference in concrete strains in East edge when subjected to compression obtained from the outermost clip gauges

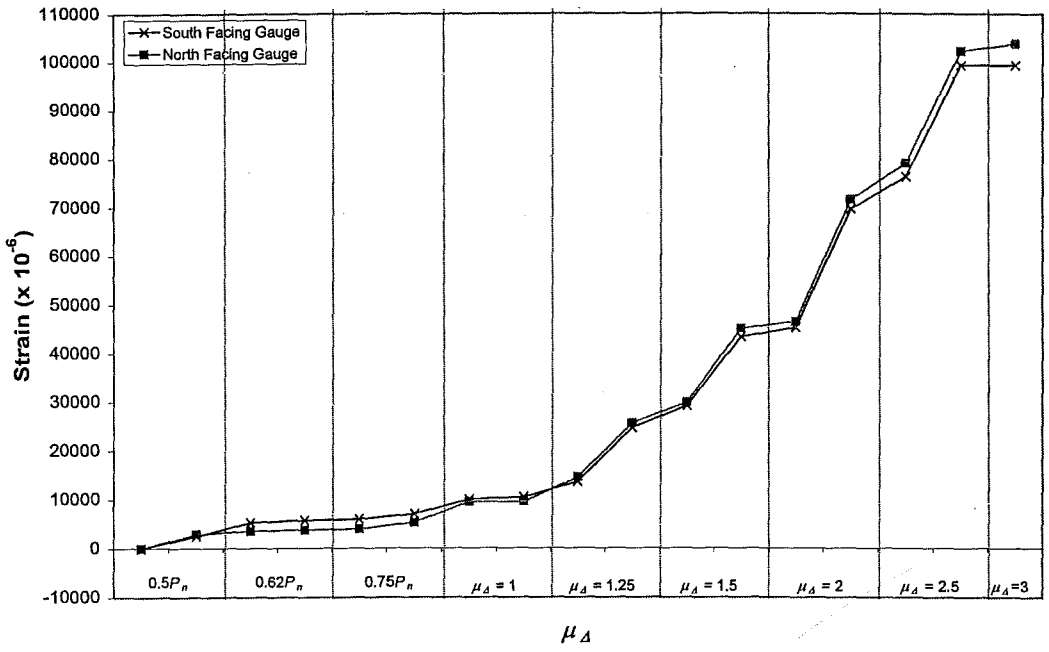

(a) Wall base

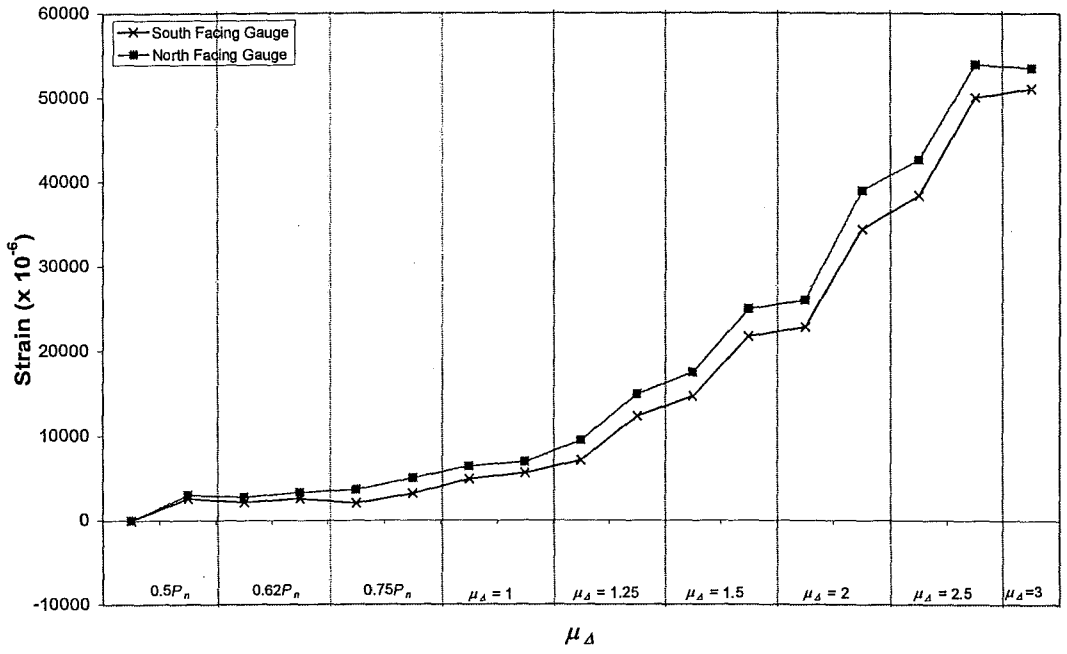

(b) Immediately above lap splice

Figure 5.36: Unit 1: Difference in concrete strains in East edge when subjected to tension obtained from the outermost clip gauges

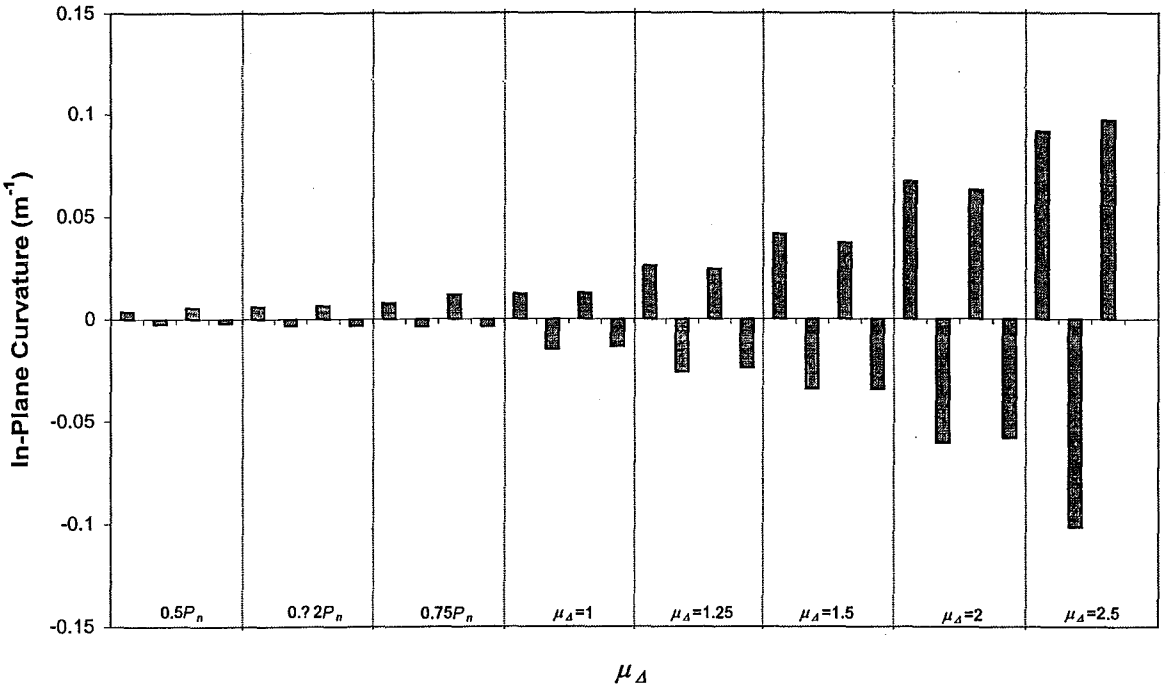

Figure 5.37: Unit 1: In-plane curvature distribution measured at 200 mm above the foundation beam

Out-of-plane curvatures were also measured at different heights using clip gauges. Figures 5.38 and 5.39 show the out-of-plane curvature along the outermost column of clip gauges on the wall (see Figure 4.20). All plots of values are presented as through viewed from the East edge of the wall. The results became extremely large when $\mu_\Delta = 2.5$ was reached.

At 200 mm above the foundation beam, the wall tended to bow in the out-of-plane direction. Additionally, as the height increases, the out-of-plane curvature decreases rapidly.

Figures 5.40 and 5.41 show the value of average concrete strains measured by the outermost and innermost clip gauges (see Figure 4.20) on the West edge when subjected to compression and tension, respectively. The data were taken from three different levels, i.e. 200 mm, 600 mm and 1000 mm consecutively.

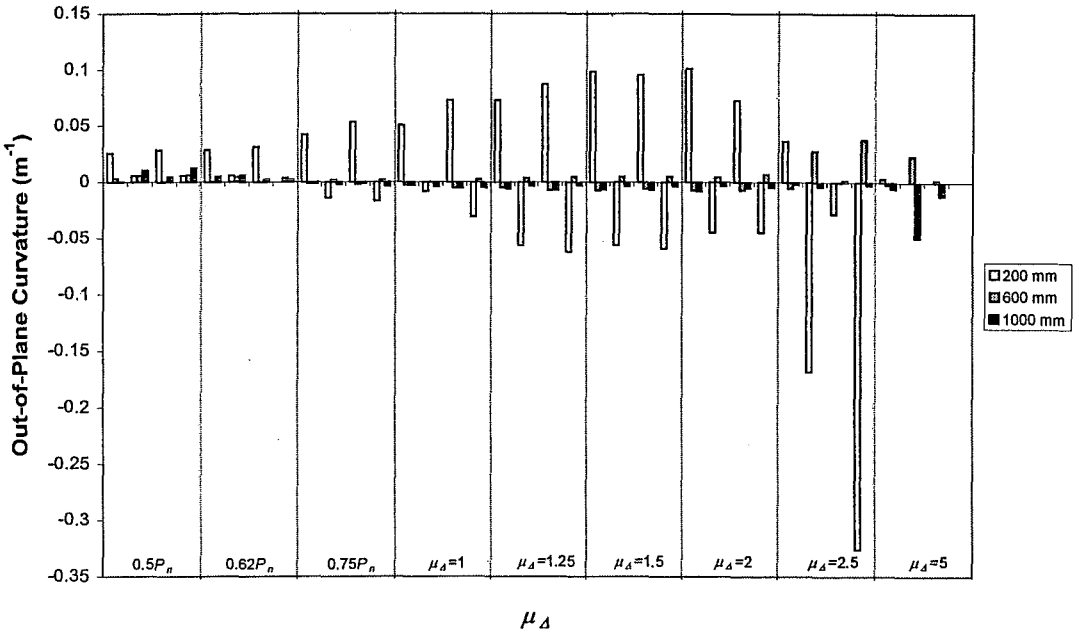

Figure 5.38: Unit 1: Out-of-plane curvature distribution obtained from outermost clip gauges on the West edge during the test

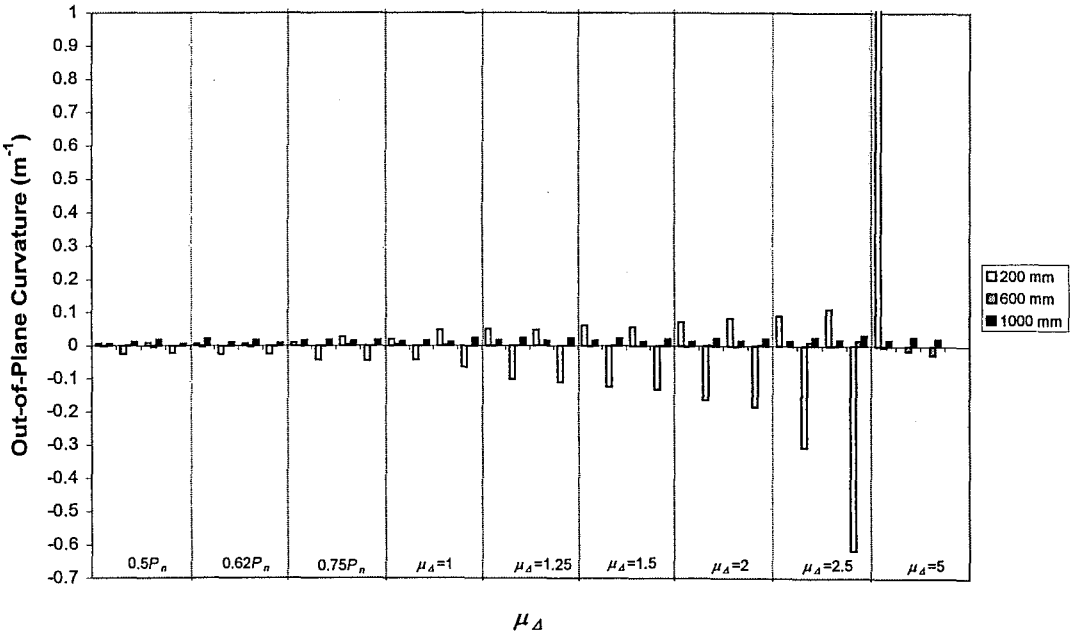

Figure 5.39: Unit 1: Out-of-plane curvature distribution obtained from outermost clip gauges on the East edge during the test

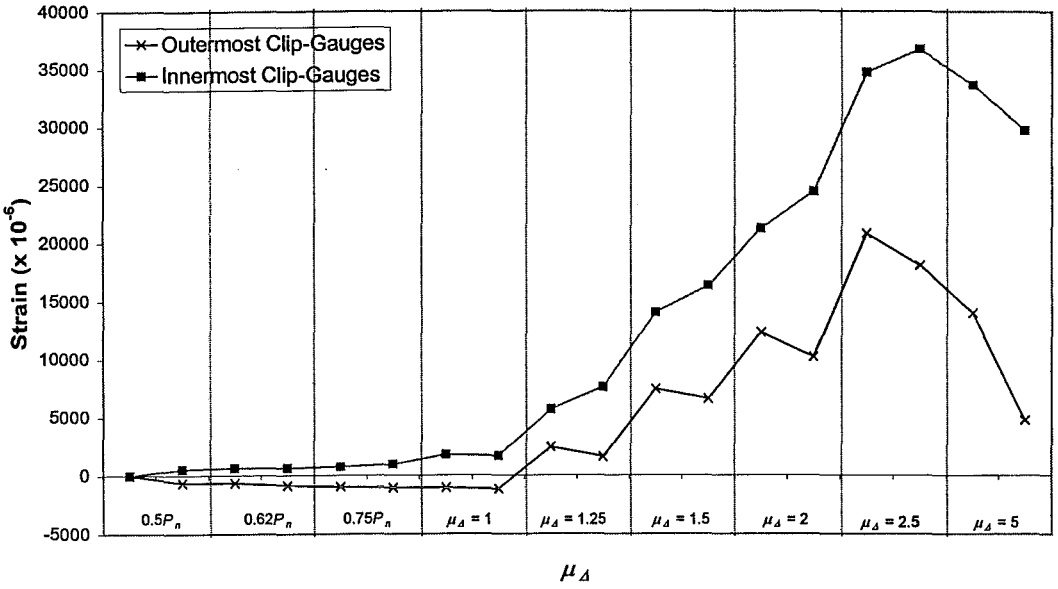

(a) 200 mm

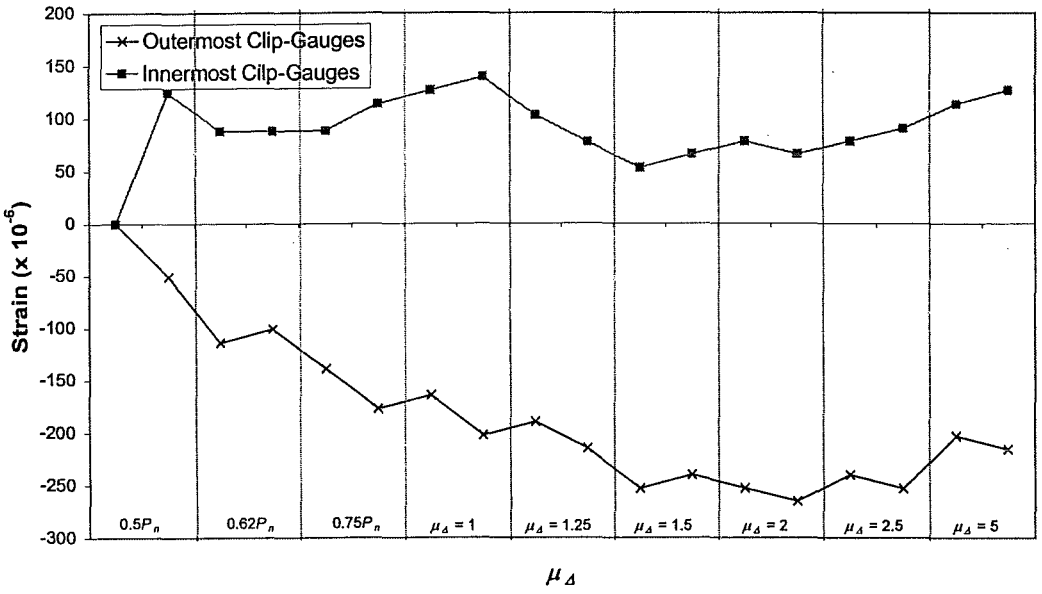

(b) 600 mm

Figure 5.40: Unit 1: Difference in concrete strains in West edge when subjected to compression obtained from the outermost clip gauges at different heights

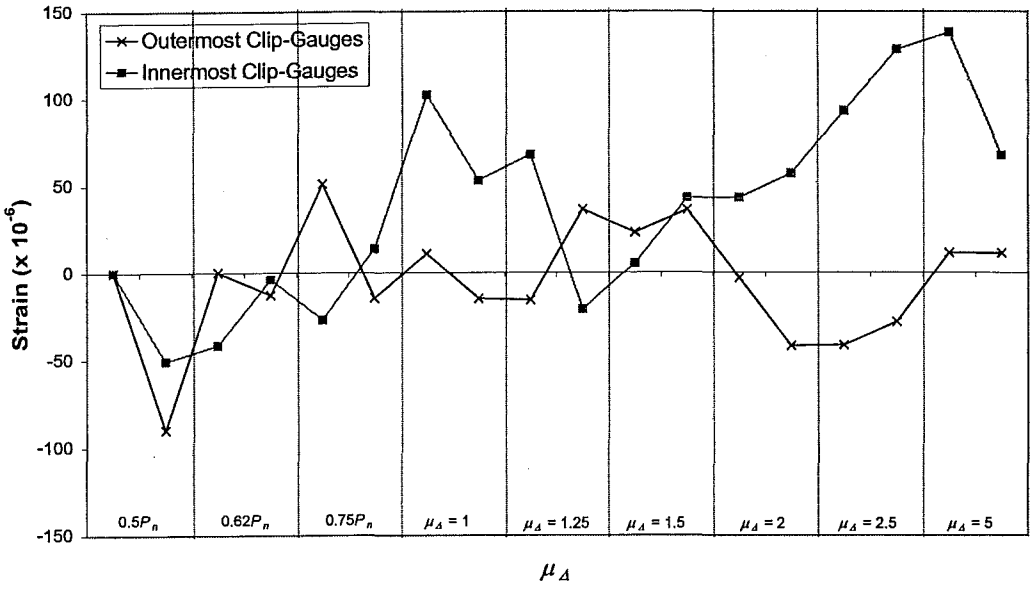

(c) 1000 mm

Figure 5.40 (cont.): Unit 1: Difference in concrete strains in West edge when subjected to compression obtained from the outermost clip gauges at different heights

Figures 5.40 and 5.41 illustrate that longitudinal strain in tension due to yielding of reinforcement had a much greater magnitude compared to the longitudinal strain in compression. More or less, the wall tended to be elongated along the horizontal joint in the post-elastic cycles (see Figure 5.40 (a)) while neutral axis depth moves towards the West edge (extreme compression fibre) when subjected to the positive direction loading (compression). Longitudinal strains also became smaller as the height increases due to the reducing strains in the longitudinal reinforcement and concrete.

Figure 5.41 shows that the tensile concrete strains for both outermost and innermost clip gauges have an identical trend. The innermost clip gauges tended to be smaller due to the larger distance from the extreme tension fibre.

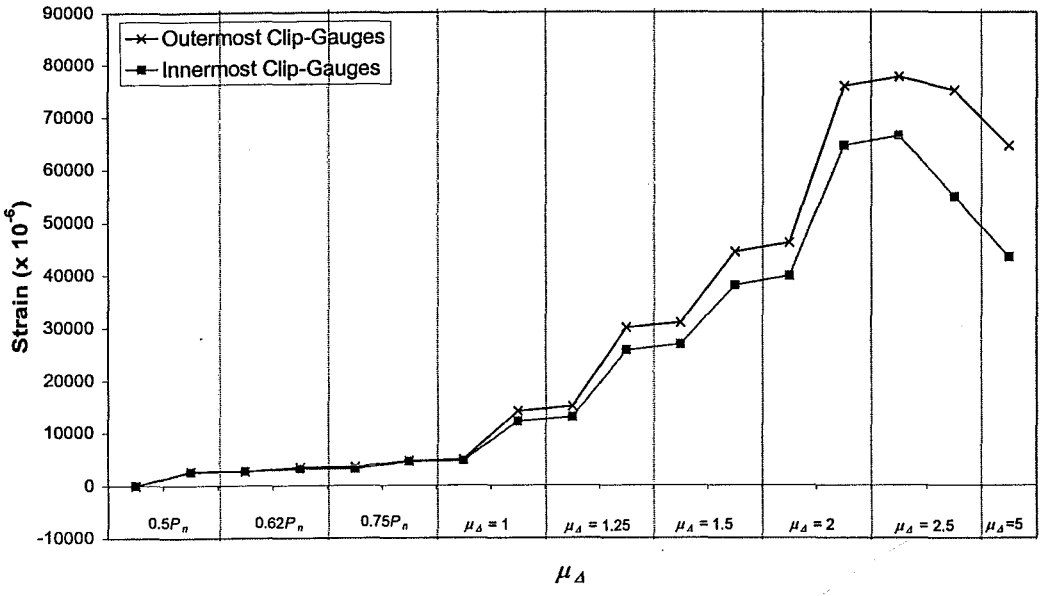

(a) 200 mm

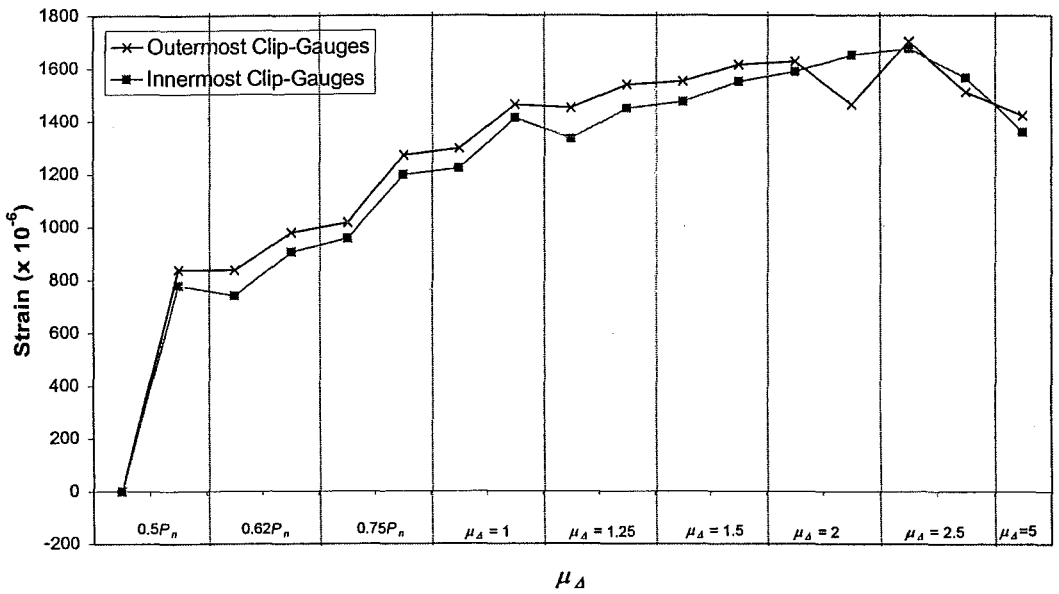

(b) 600 mm

Figure 5.41: Unit 1: Difference in concrete strains in West edge when subjected to tension obtained from the outermost clip gauges at different heights

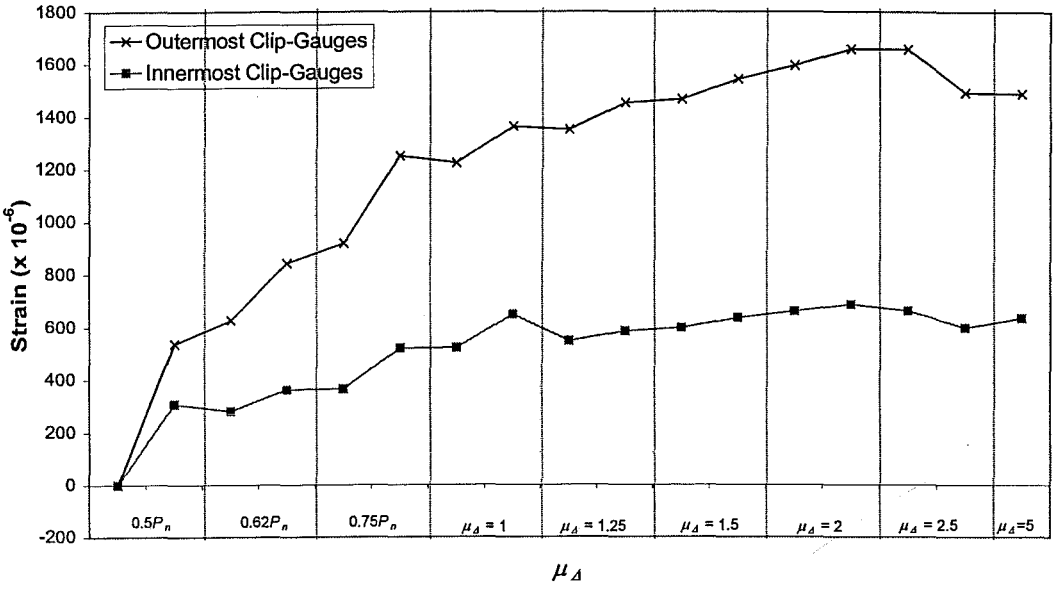

(c) 1000 mm

Figure 5.41 (cont.): Unit 1: Difference in concrete strains in West edge when subjected to tension obtained from the outermost clip gauges at different heights

5.1.3.5 Sectional Neutral Axis : Unit 1

The locations of neutral axis at different heights were calculated using concrete strains measured at the concrete surface by clip-gauges as mentioned in the previous section. At the wall-foundation connection, the neutral axis was initially lying perpendicular to the length of the wall.

The neutral axis depth at first yield capacity was approximately 200 mm from extreme compression fibre (see Figure 5.26) which was relatively similar to the predicted neutral axis depth at the theoretical first yield capacity. At this stage, the orientation of the neutral axis was not at the right angle to the longitudinal direction of the wall but lying in an inclined angle to the wall section, i.e. skewed neutral (see Figures 5.29 and 5.33). The actual centroid of an internal concrete compressive force was closer to the centroid of the internal tensile force of the steel. Therefore the

internal lever arm decreased. Hence, the actual first yield capacity was less than the theoretical first yield capacity.

When the West edge was subjected to compression, the neutral axis depth at 200 mm above the foundation beam appeared to be at the position between the outermost and innermost clip gauges until μ_Δ = +1.25×1 was reached (see Figure 5.40 (a)). At the height of 600 mm (see Figure 5.40 (b)), the neutral axis lay between the outermost and innermost clip gauges through out the test with smaller magnitude of the out-of-plane curvature (see Figure 5.38). At 1 m above the foundation beam (see Figure 5.40 (c)), the position of the neutral axis depth was inside of the innermost clip gauges until first yield was reached. It moved towards the extreme compression fibre and passed the outermost clip gauge when μ_Δ = 1.5 was achieved.

When μ_Δ = +2.5×1 was reached, the capacity suddenly commenced to drop because of the shifting of the neutral axis in the opposite direction. The skewness level increased when the wall twisted until the wall capacity approached zero.

Concrete strain along the tension edge tended to have the same trend. At a specific height, the measurement taken from both outermost and innermost clip gauges underwent into tension with similar order of magnitude except at 1 m above the foundation beam (see Figure 5.41). The measured concrete strain decreased as the height increased.

5.2 Unit 2

5.2.1 Unit 2 Properties

The properties of Unit 2 are illustrated in Table 5.2. All measured values were calculated with the material properties measured on the day of test, and the nominal values were calculated using the nominal material properties.

Table 5.2: Measured properties of Unit 2

Property			Nominal value	Measured value
Reinforcing ratio	p	%	1.26	N/A
Longitudinal reinforcing yield strength*	f_y	MPa	300	318
Concrete compressive strength*	f'_c	MPa	30	43.9
Modulus of rupture	f_r	MPa	4.38	4.60
Axial load level	$N^*/A_g f'_c$		0.0127	0.0087
Cracking load	P_{crack}	kN	9.7	10.2
First yield strength	P_{yield}	kN	18.9	20.1
Nominal strength	P_n	kN	24.1	26.1

* At the day of testing

The secant stiffness measured at $0.75P_n$ was k_{75} = 1.99 kN/mm and the estimated reference yield displacement was Δ_y = 13.1 mm (see Appendix B).

5.2.2 General Behaviour and Observations : Unit 2

The first cracks appeared horizontally initiating from the most extreme tension fibre during the first cycle of loading. They propagated across the panel at 300 mm above the foundation beam where the starter bars were terminated (see Figure 5.42). A few fine cracks developed on both sides and extent to the height of 1.8 m. As the applied force increased, the horizontal cracks within lap splice region started to decline in angle towards the horizontal joint.

When the applied force of $0.75P_n$ was reached, the horizontal cracks extended approximately 2.3 m from the base of the wall (see Figure 5.43). In the region above the lap splice where buckling was expected to occur, the existing cracks were widen

up to about 0.5 mm. At this stage, the wall was still in a good shape with an insignificant out-of-plane displacements. Starter bars at the wall-foundation interface that subjected to tension started to yield. Sliding at the base was not detected at any stage during the load controlled cycles.

Vertical cracks developed and coincided with the locations of the starter bars. The horizontal joint cracks started to open up wider along the base of the wall panel when $\mu_\Delta = +1\times1$ was reached. Out-of-plane displacement could be detected using theodolite (see Figure 5.44).

At $\mu_\Delta = +1.25\times1$, the horizontal joint cracks opened up approximately 1.5 mm. More vertical cracks at the location of the starter bars appeared during the second cycle. Maximum out-of-plane displacement was about 10 mm.

When $\mu_\Delta = -1.5\times1$ was achieved, the cracks which located immediately above lap splice region was widen up to about 0.5 mm (see Figure 5.45). At the same time, the horizontal cracks were approximately 3 mm.

Once $\mu_\Delta = -2\times1$ was reached, a large number of cracks developed on the convex side of the wall. Noticeably, there were more cracks occurred on the convex side than the concave side. The height of cracking on the convex side was greater than on the concave side. Cracks above lap-splice region extended and commenced to soften the whole region. The wall started to bow into one direction (see Figure 5.46). Sliding shear was not significantly noticeable (see Appendix D).

At $\mu_\Delta = +2.5\times1$, concrete at the extreme compression fibre started spalling but not significantly as shown in Figure 5.47. The crack along the horizontal joint was about 10 mm. Many crack patterns on the convex side changed from horizontal to diagonally sloping. At this stage, the out-of-plane displacement at mid-height was approximately 20 mm (see Figure 5.48).

Most linear potentiometers, which were used to measure the out-of-plane displacements, were out of range when the wall was subjected to the load at

$\mu_\Delta = +3.5\times1$. Small cracks tended to join up in the region where the maximum out-of-plane displacement occurred (see Figure 5.49). Horizontal joint crack on the concave side was wider compared to the convex side (see Figure 5.50).

Sign of compression failure was detected when concrete in the compression region spalled off at $\mu_\Delta = -4\times1$. The out-of-plane displacement became much more pronounced. Figures 5.51 and 5.52 show the profile of the wall at $\mu_\Delta = -4\times1$.

The measured maximum out-of-plane displacement on the compression edge was approximately 250 mm at the end of the test. Sliding shear was not very significant. Cracks tended to join up and concentrate in the region of lap splice on the concave side of the wall. Interestingly, cracks were more concentrated near the top on the convex side of the wall. It would presumably cause by the vertical load, which was placed eccentrically on the concave side. Many diagonal cracks developed near the end of the test. The end of test photographs are shown in Figures 5.53 to 5.57.

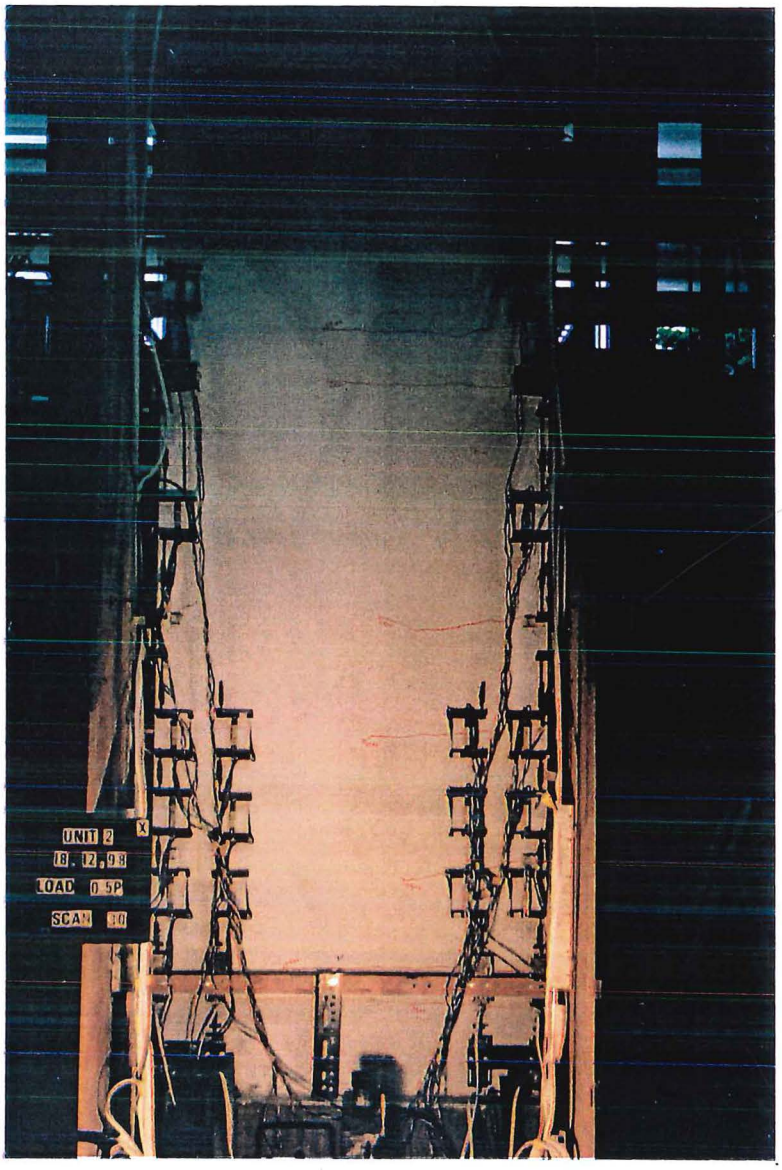

Figure 5.42: View of Unit 2 at cracking strength (South/Concave)

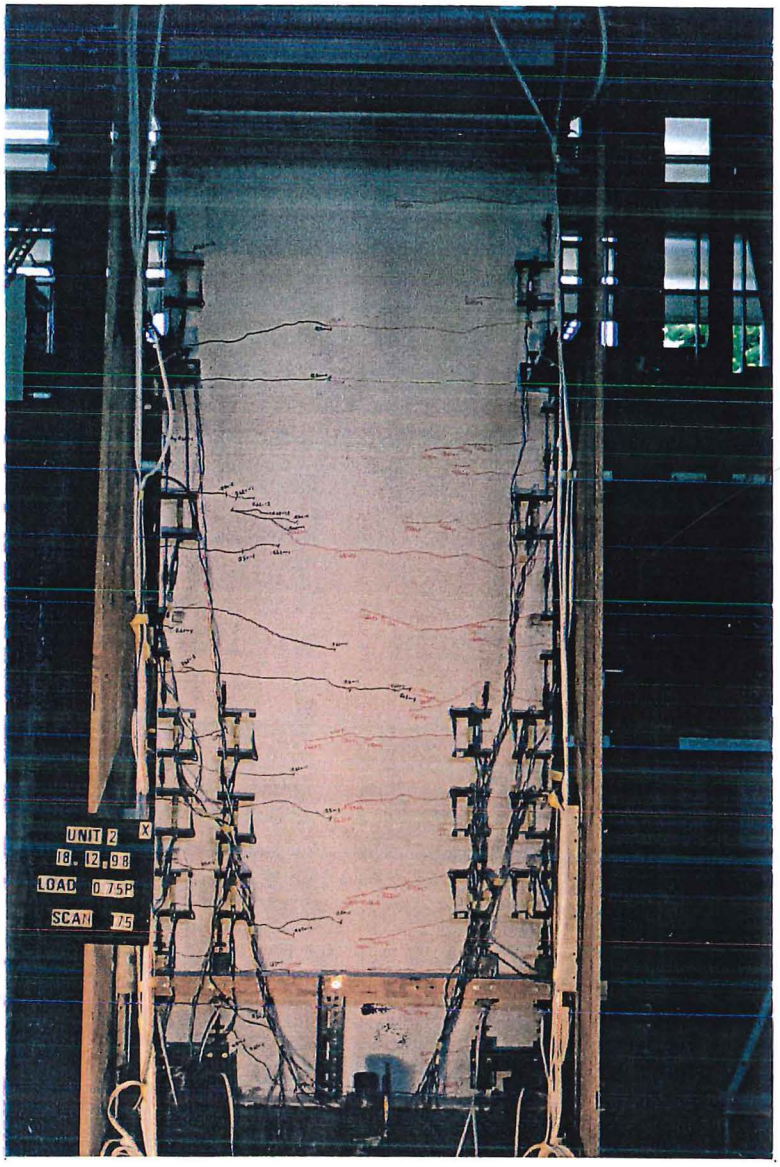

Figure 5.43: View of Unit 2: first yield at the positive direction loading (South/Concave)

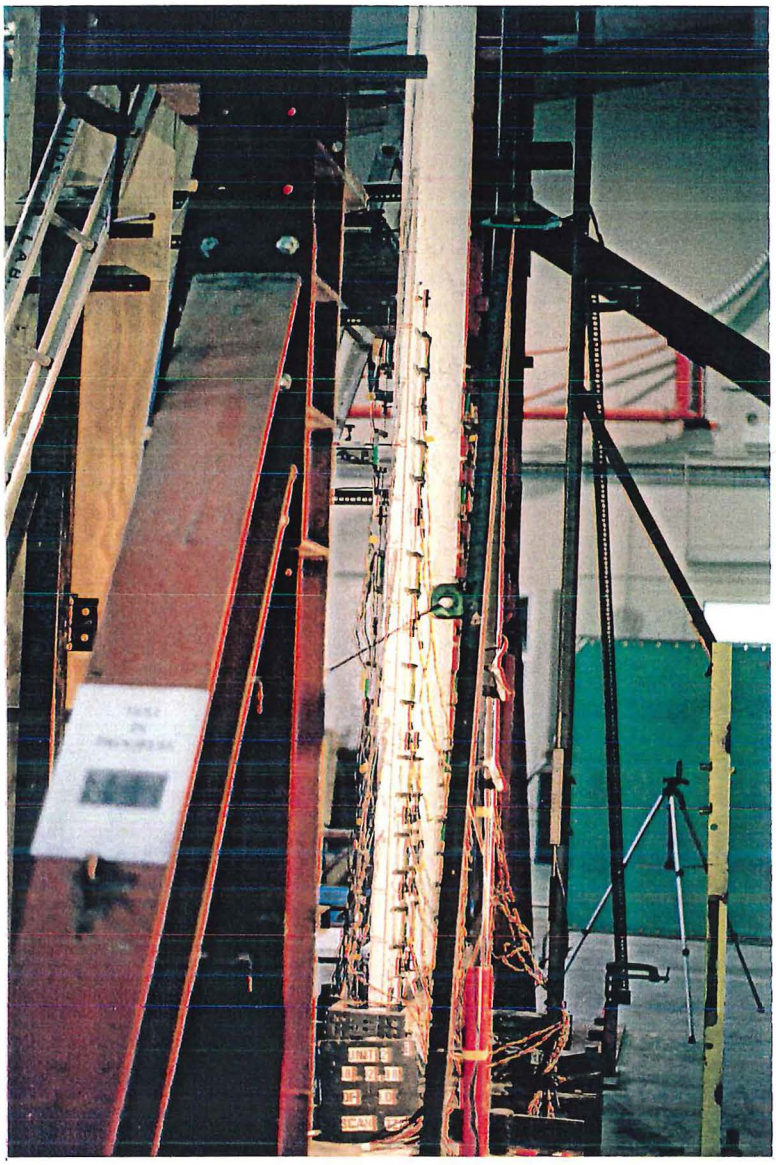

Figure 5.44: Unit 2: Out-of-plane displacement was observed at μ_{Δ}= +1×1 (East edge)

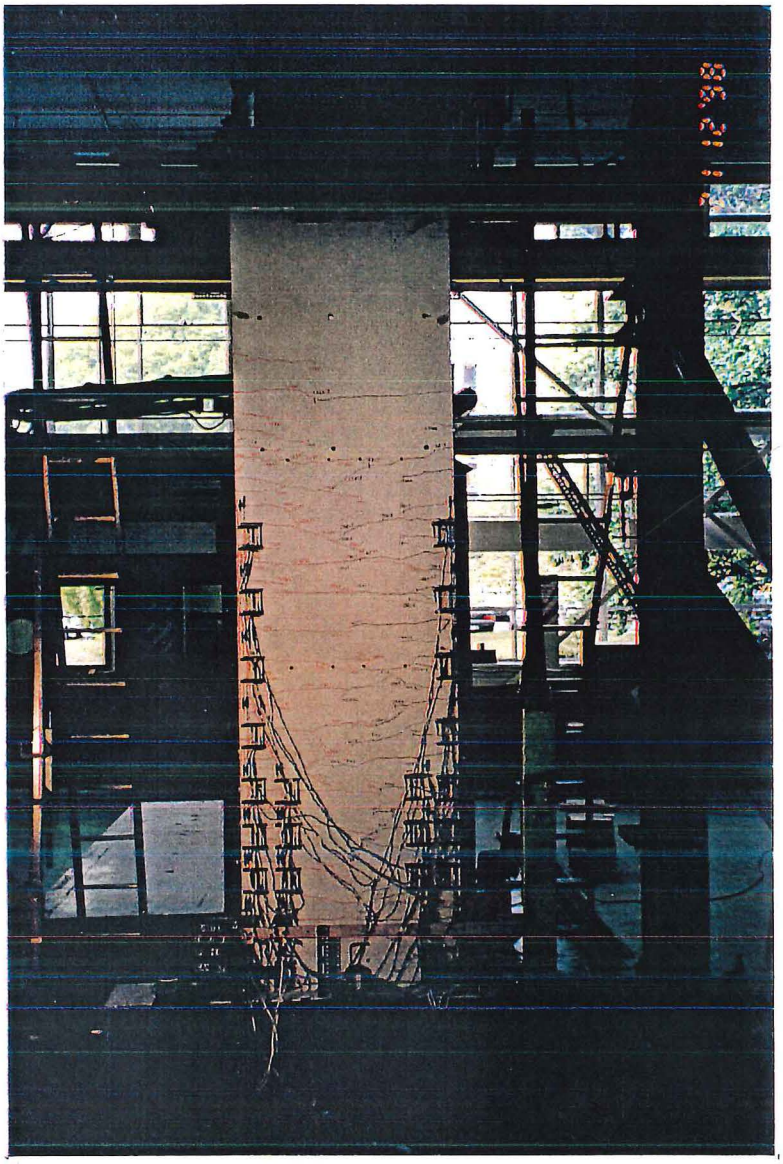

Figure 5.45: View of Unit 2 at μ_{Δ}= -1.5×1 (North/Convex)

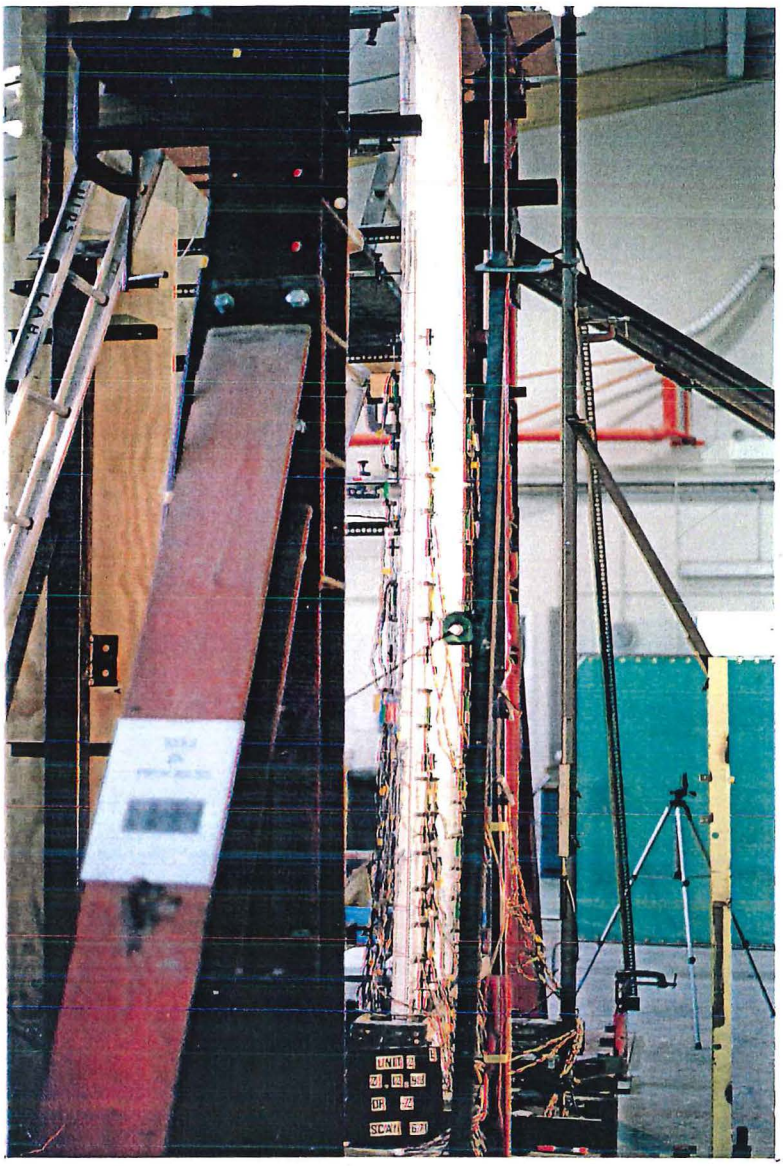

Figure 5.46: Unit 2: Out-of-plane displacement profile at μ_{Δ}= -2×1 (East edge)

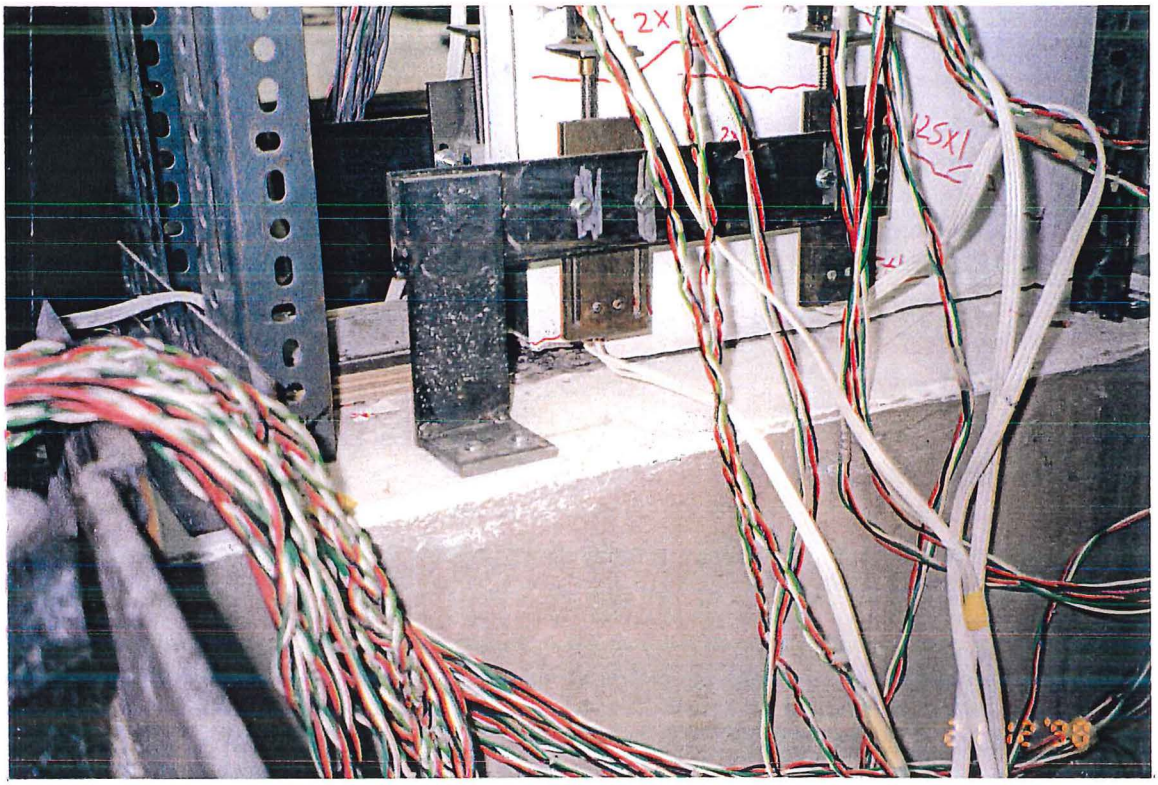

Figure 5.47: Unit 2: Crushing and spalling of compression concrete at $\mu_\Delta = +2.5 \times 1$ (East edge)

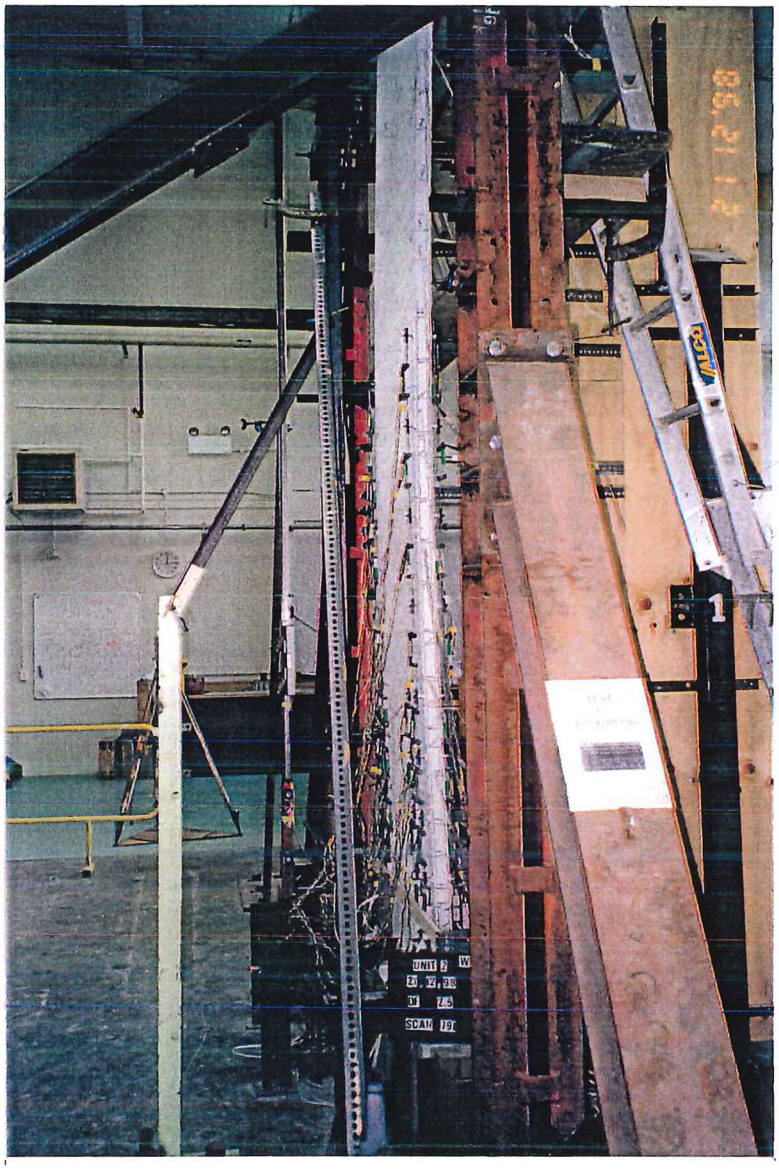

Figure 5.48: Unit 2: Out-of-plane displacement at μ_Δ= +2.5×1 (West edge)

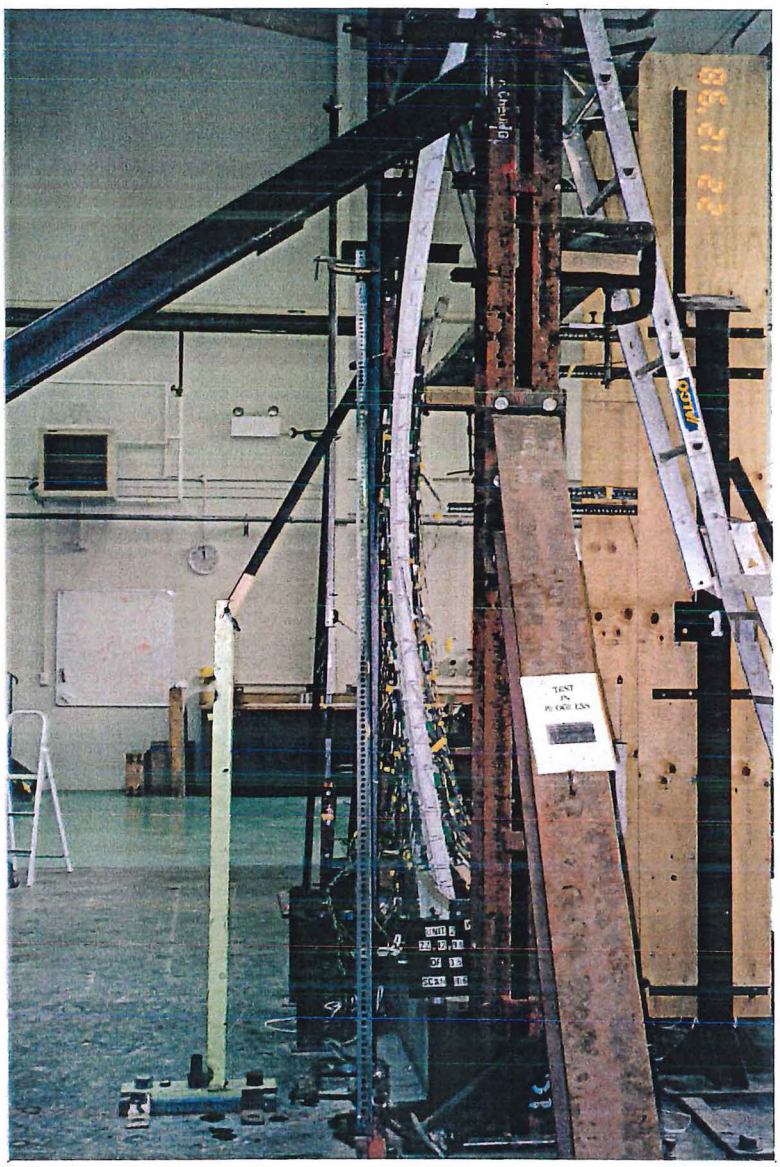

Figure 5.49: Unit 2: Out-of-plane displacement at μ_Δ = +3.5×1 (West edge)

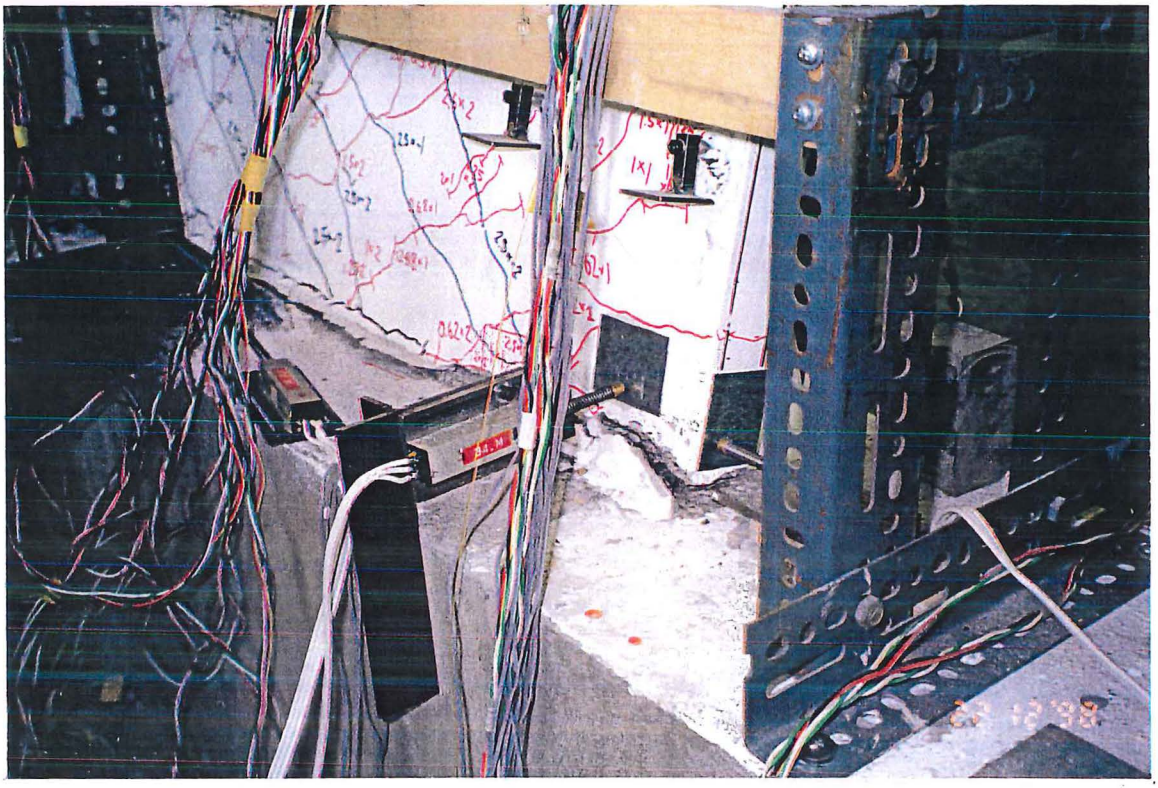

Figure 5.50: Unit 2: Change in boundary condition at the horizontal connection at μ_{Δ} = +4.5×1 (East edge)

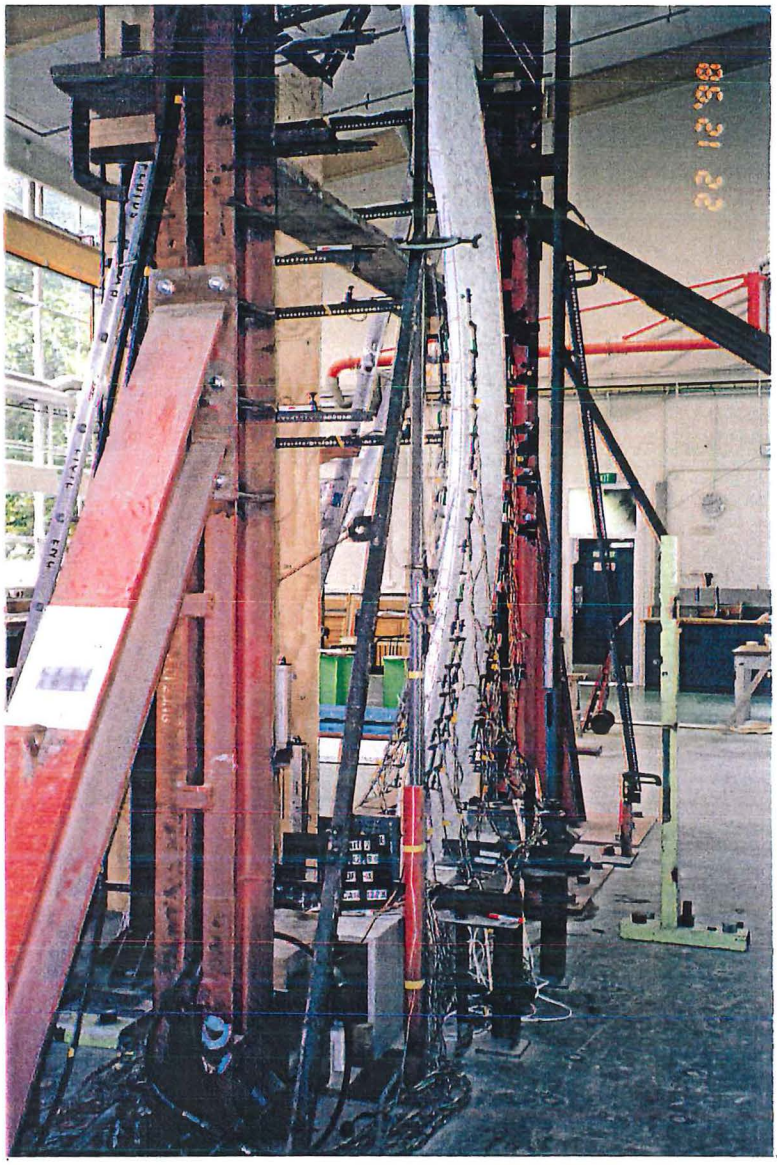

Figure 5.51: Unit 2: Out-of-plane displacement on the East edge at μ_Δ= -4×1

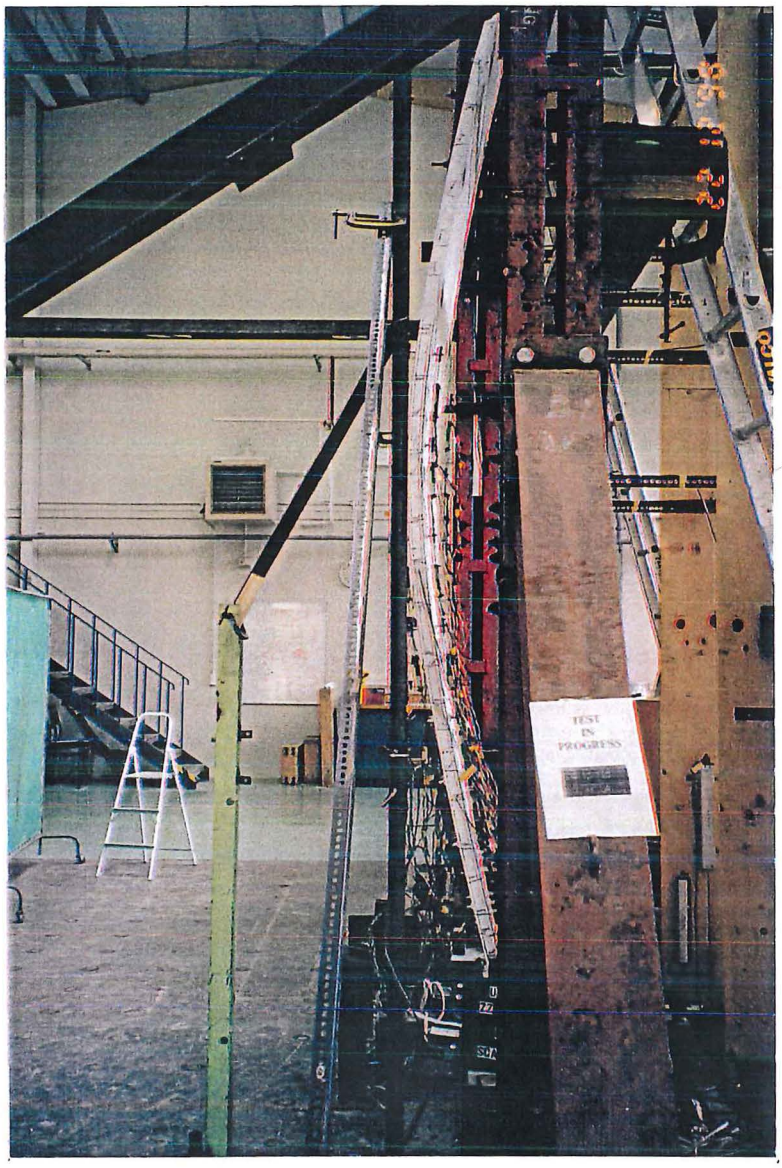

Figure 5.52: Unit 2: Out-of-plane displacement on the West edge at μ_Δ= -4.5×1

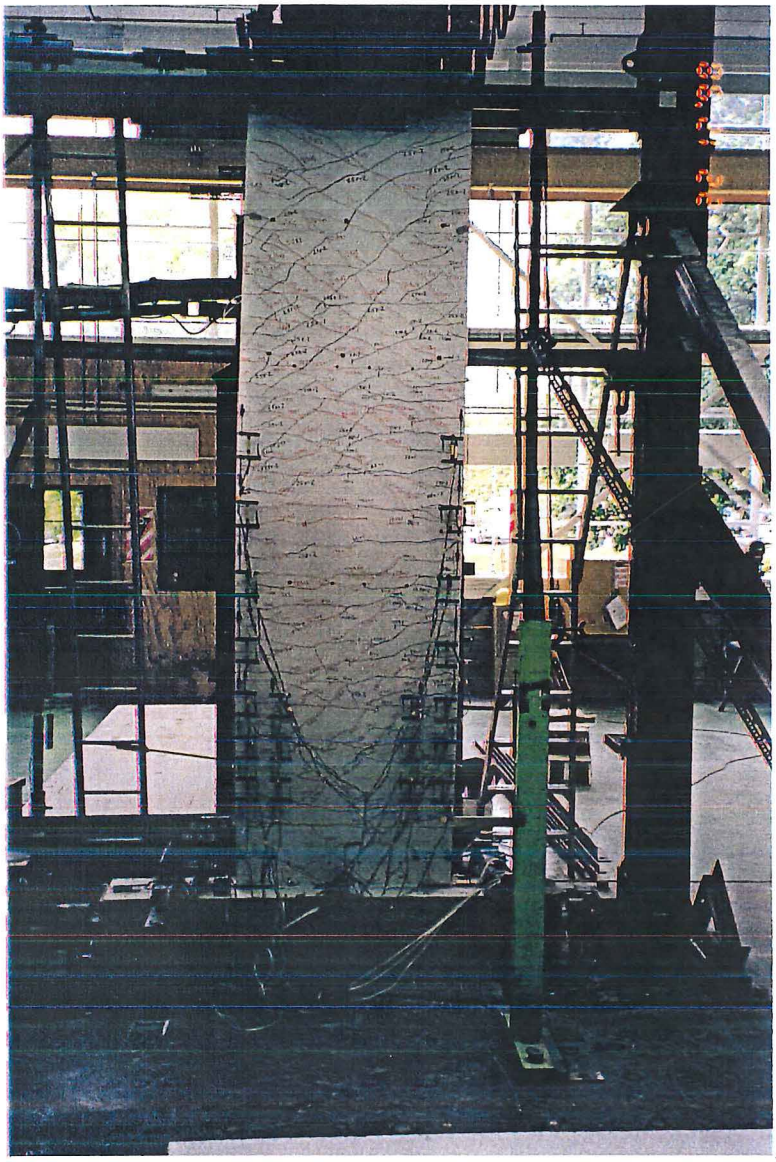

Figure 5.53: View of Unit 2 cracking pattern on the North/Convex side of the wall at the end of test

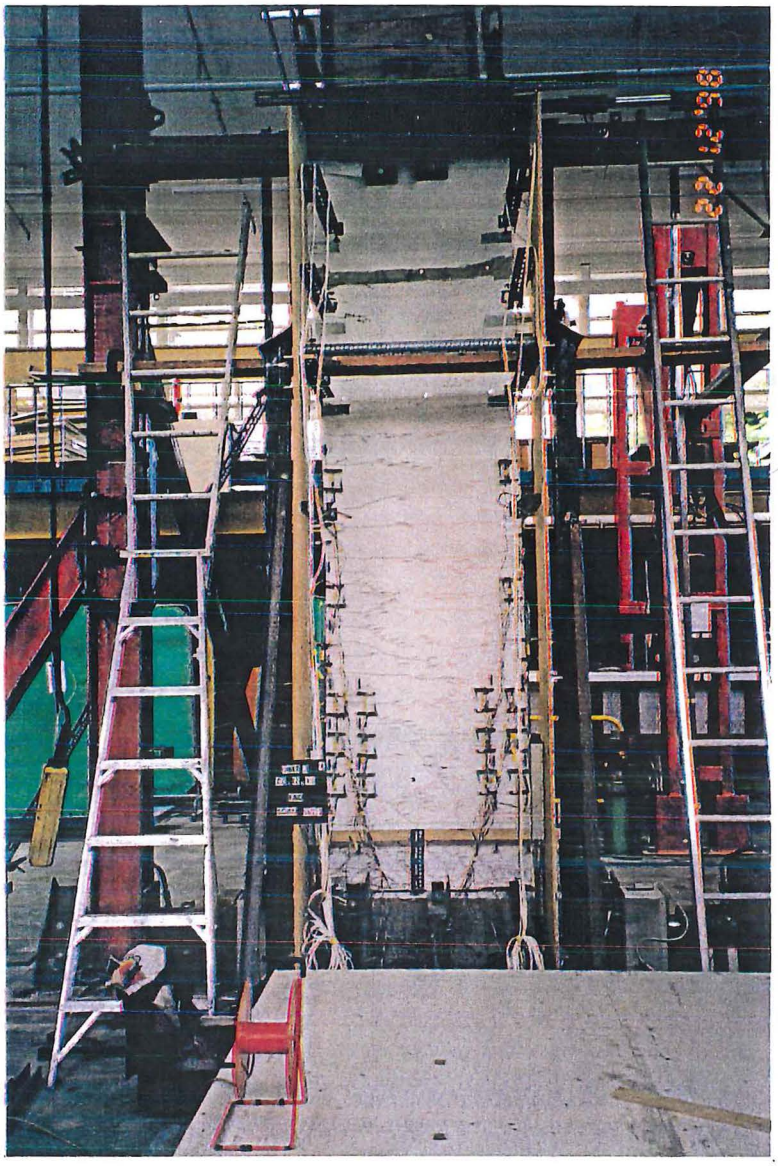

Figure 5.54: View of Unit 2: cracking pattern on the South/Concave side of the wall at the end of test

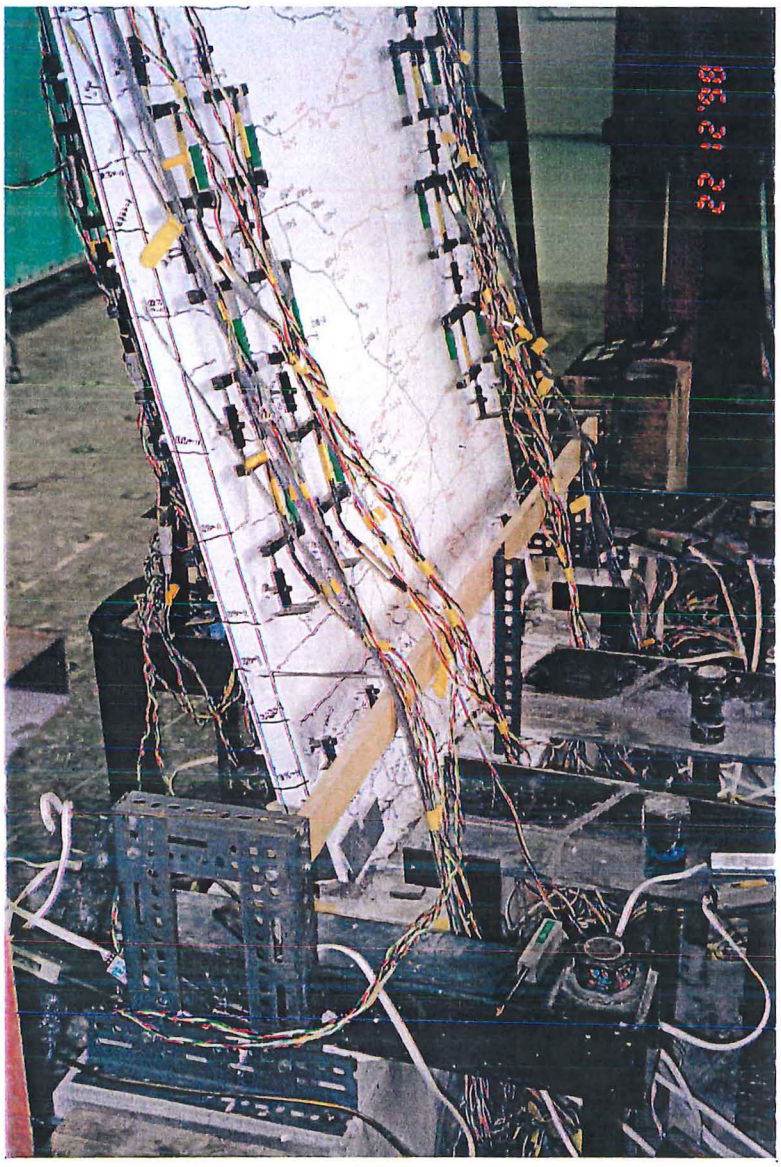

Figure 5.55: Unit 2: Boundary condition along the horizontal connection at the end of test (West edge)

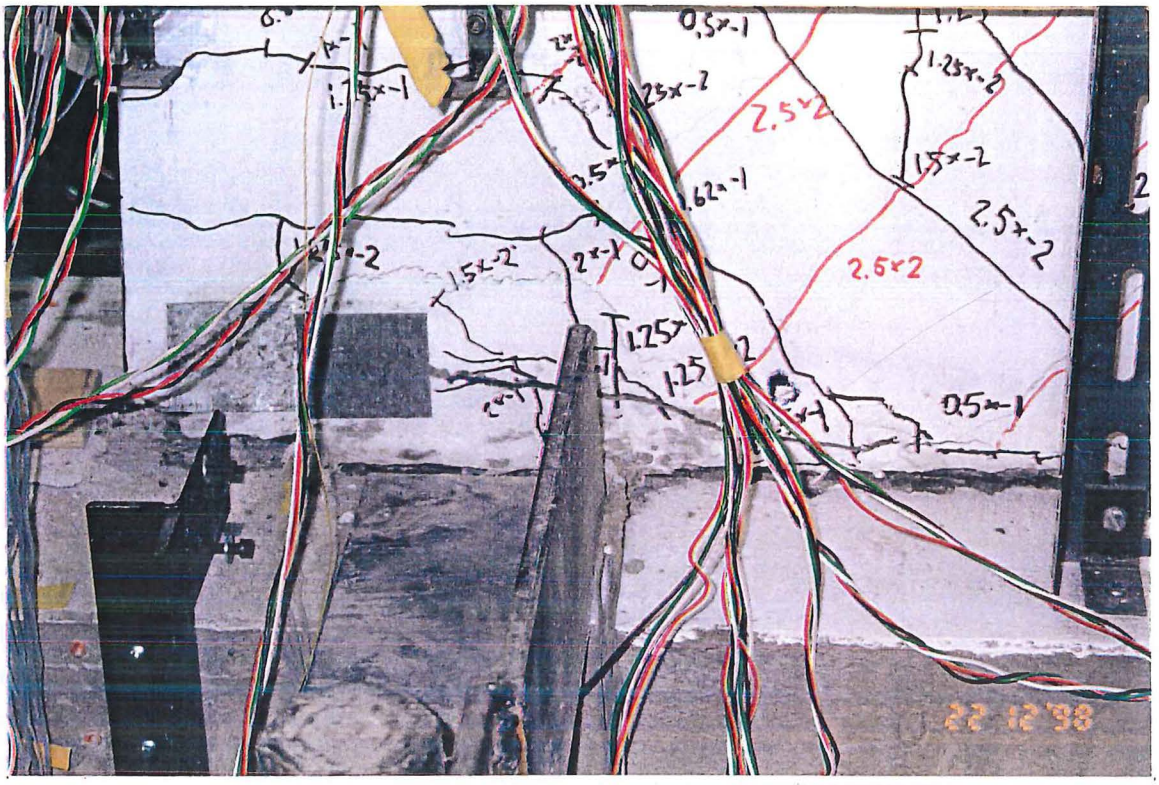

Figure 5.56: Unit 2: Cracking along the horizontal joint at the end of test (South/Concave)

Figure 5.57: Unit 2: Overall wall profile at the end of test (East edge)

5.2.3 Analysis of Experimental Results : Unit 2

5.2.3.1 Lateral Force-Lateral Displacement Response : Unit 2

The hysteresis loops of the test specimen is shown in Figure 5.58. The wall appeared to be reasonably strong during the load-controlled or elastic cycles. The lateral displacement at the top of the wall was relatively small at zero load. Sliding shear had no contribution during the "Elastic cycles" (see Figure D-2), hence flexure deformation dominated. The theoretical moment-curvature curves, plotted in Figure 5.59, represent the behaviour estimated assuming a monotonic loading in each direction.

The overall response of the test specimen was unsymmetrical. The hysteresis loops showed an adequate energy dissipation capacity. The actual maximum capacity was 26.8 kN which was reasonably accurate compared to the predicted nominal capacity of 26 kN. Overstrength action associated with strain-hardened did not develop as a result of the rapid change in the orientation of the neutral axis, as mentioned previously in Unit 1, resulting in reduction of internal lever arms not reduction of the apparent strength.

The capacity of the wall started to decrease at $\mu_\Delta = +2$. It gradually dropped off when the wall was imposed with the higher nominal displacement ductility. The repetition of the same displacement ductility gave a strength degradation during reloading cycles. The test was terminated when the wall achieved $\mu_\Delta = +4.5$.

5.2.3.2 Out-of-Plane Displacements : Unit 2

The initial wall profiles were taken before and after loading lead ingots. Another wall profile was taken after the test completion. During the test, all the measurements were recorded and stored using the data logger. All the out-of-plane displacement plots represent "North face" on the right and "South face" on the left.

Figure 5.60 (a) shows the out-of-plane displacements at the positive peak cycles on the East edge or tension edge of the wall. The initial profile was not a smooth circular profile as constructed. Shrinkage had been taken place during curing

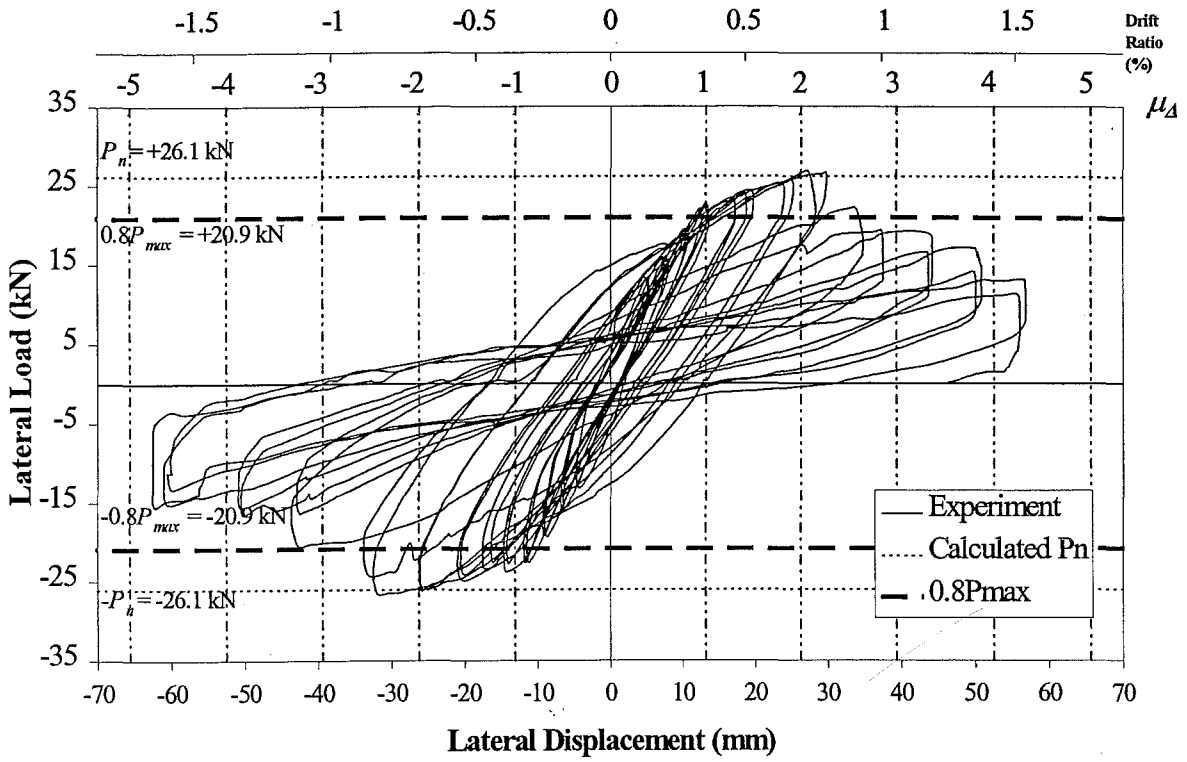

Figure 5.58: In-plane lateral load-lateral displacement response of Unit 2

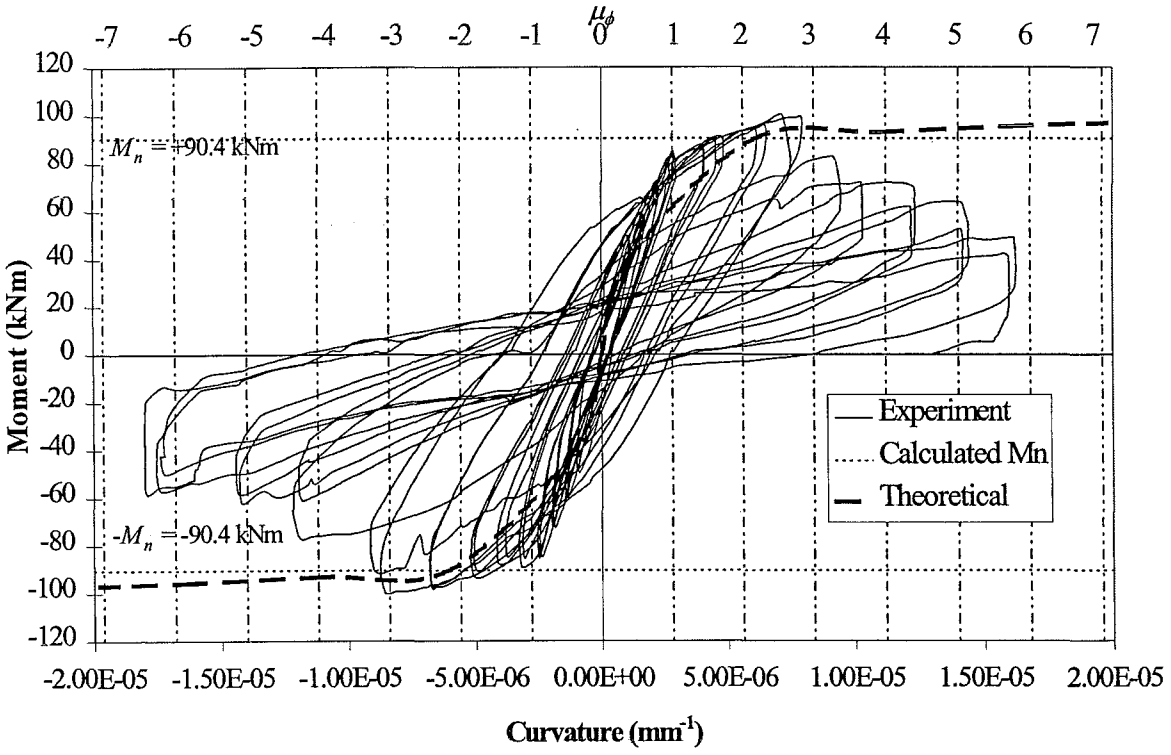

Figure 5.59: Moment-curvature response of Unit 2

period. The vertical load had a very little influence to the initial wall profile prior to the commencement of the test.

The out-of-plane displacement was not significant at $\mu_\Delta = 2$ for either direction of loading. However, the out-of-plane displacement increased rapidly from 9 mm to 17 mm at $\mu_\Delta = +2.5\times1$. At the end of the test ($\mu_\Delta = +4.5\times2$), the wall had a large out-of-plane displacement of 195 mm, see Figure 5.60 (b).

On the West edge (compression edge) of the wall when subjected to the positive cycles, the profile changed from a single curvature to double curvature when the first yield capacity was achieved. The out-of-plane displacements stayed in constant magnitude of 7 mm until $\mu_\Delta = +2\times1$ was reached. The out-of-plane displacements increased rapidly to 17 mm at the $\mu_\Delta = +2.5\times1$ as shown in Figure 5.61 (a).

During the negative cycles, East edge became the compression edge. The out-of-plane displacement was increased from 10 mm to 30 mm at $\mu_\Delta = -2.5\times1$ (see Figure 5.62 (a)). Similarly, West edge which was subjected to tension had the out-of-plane displacement of approximately 15 mm with a double curvature profile (see Figure 5.63 (a)).

At the end of the test, the maximum residual out-of-plane displacement was approximately 250 mm occurred at mid-height on the West edge of the wall (see Figure 5.61 (b)). This lateral deflection would be equivalent to 6.7% of the height of the wall. The overall wall profile of the compression edge can be seen in Figure 5.57.

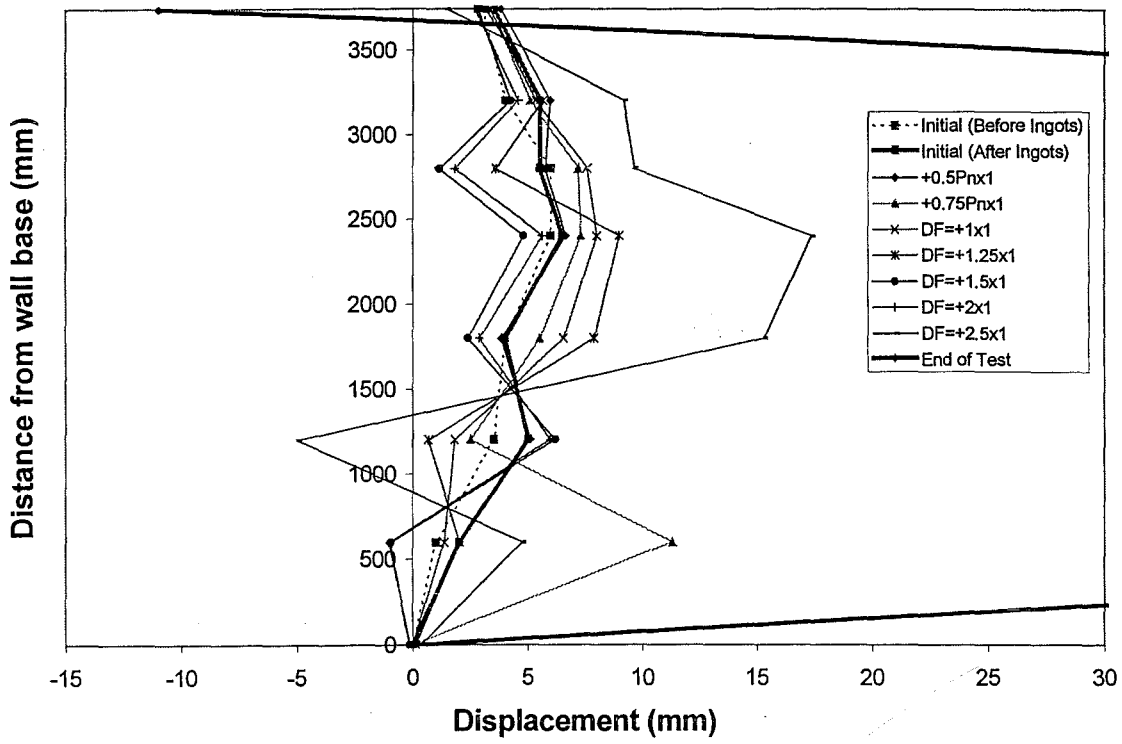

(a)

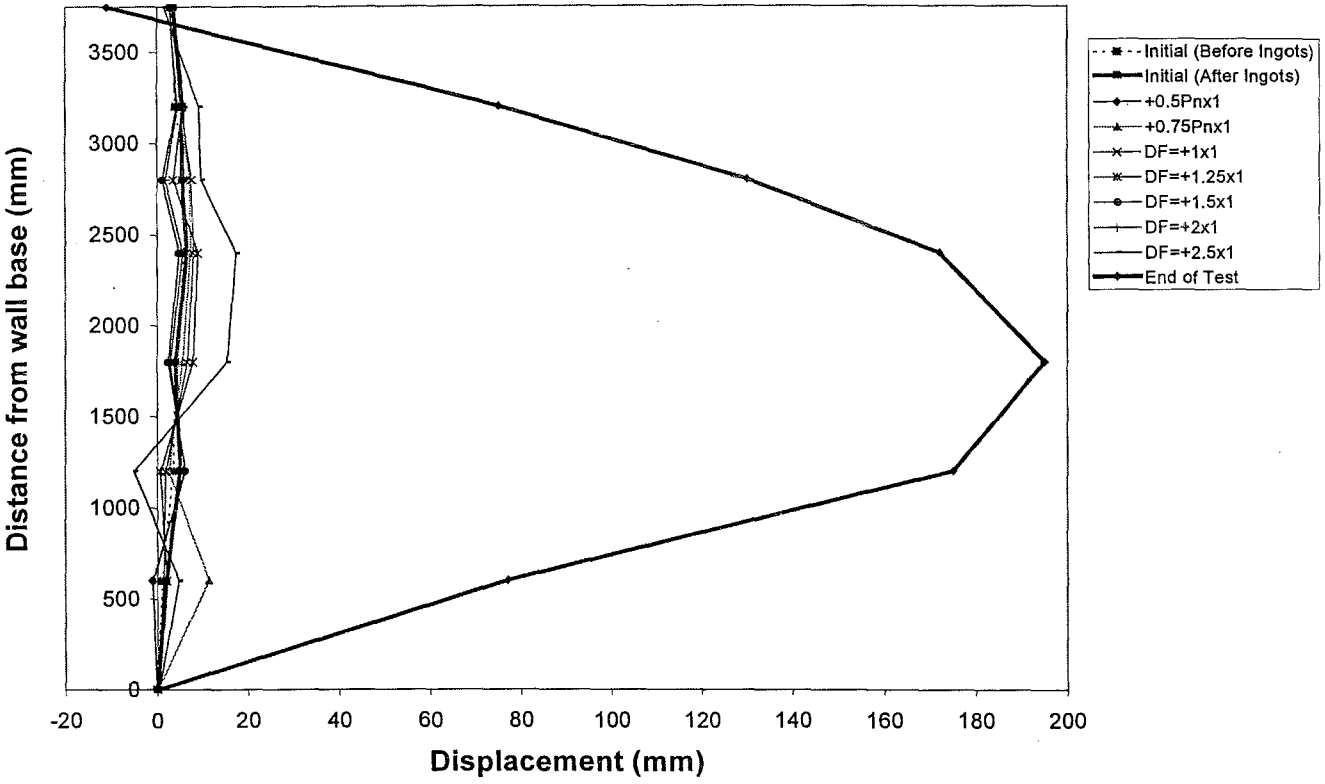

(b)

Figure 5.60(a): Unit 2: Out-of-plane movement on East edge of the wall at positive peak cycles (Tension edge)

Figure 5.60(b): Unit 2: Out-of-plane movement on East edge of the wall at positive peak cycles (Tension edge) at the end of test (alternative scale)

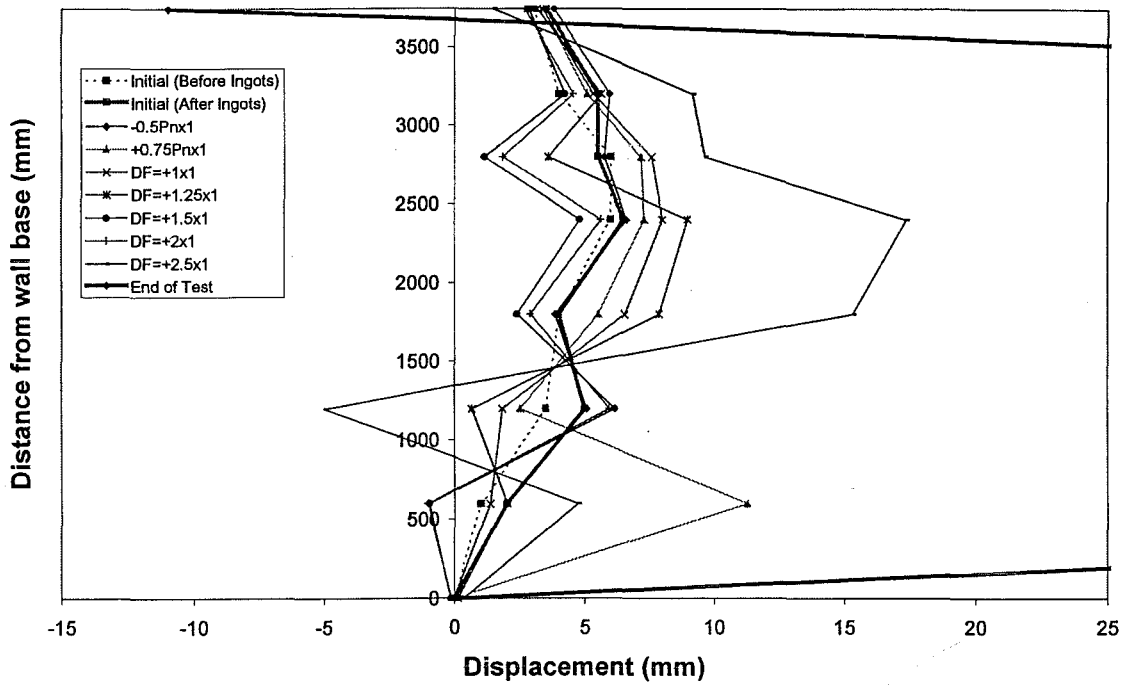

(a)

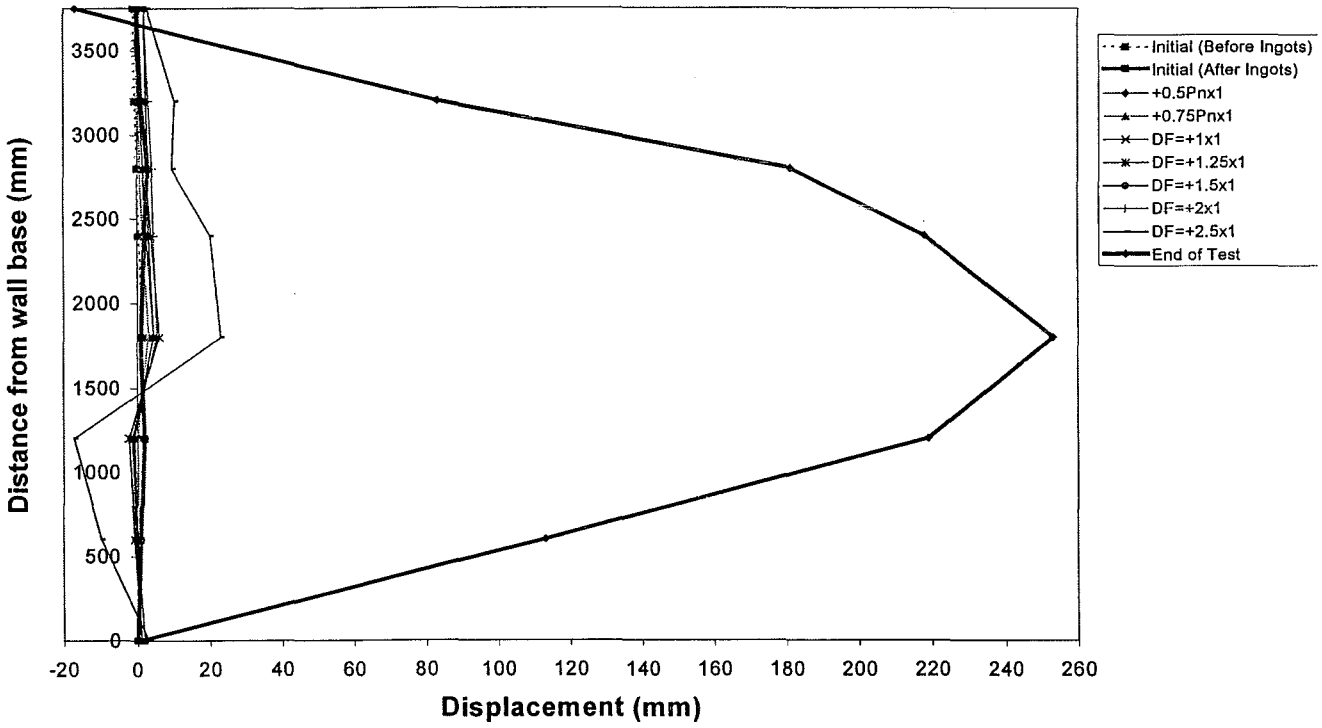

(b)

Figure 5.61(a): Unit 2: Out-of-plane movement on West edge of the wall at positive peak cycles (Compression edge)

Figure 5.61(b): Unit 2: Out-of-plane movement on West edge of the wall at positive peak cycles (Compression edge) at the end of test (alternative scale)

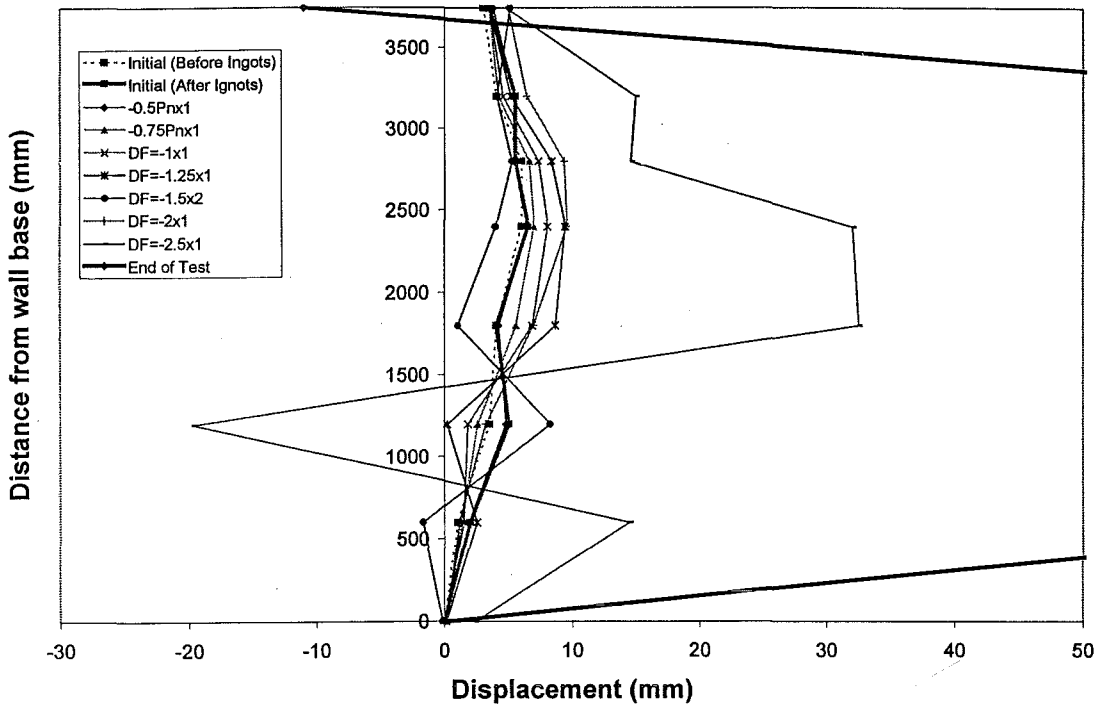

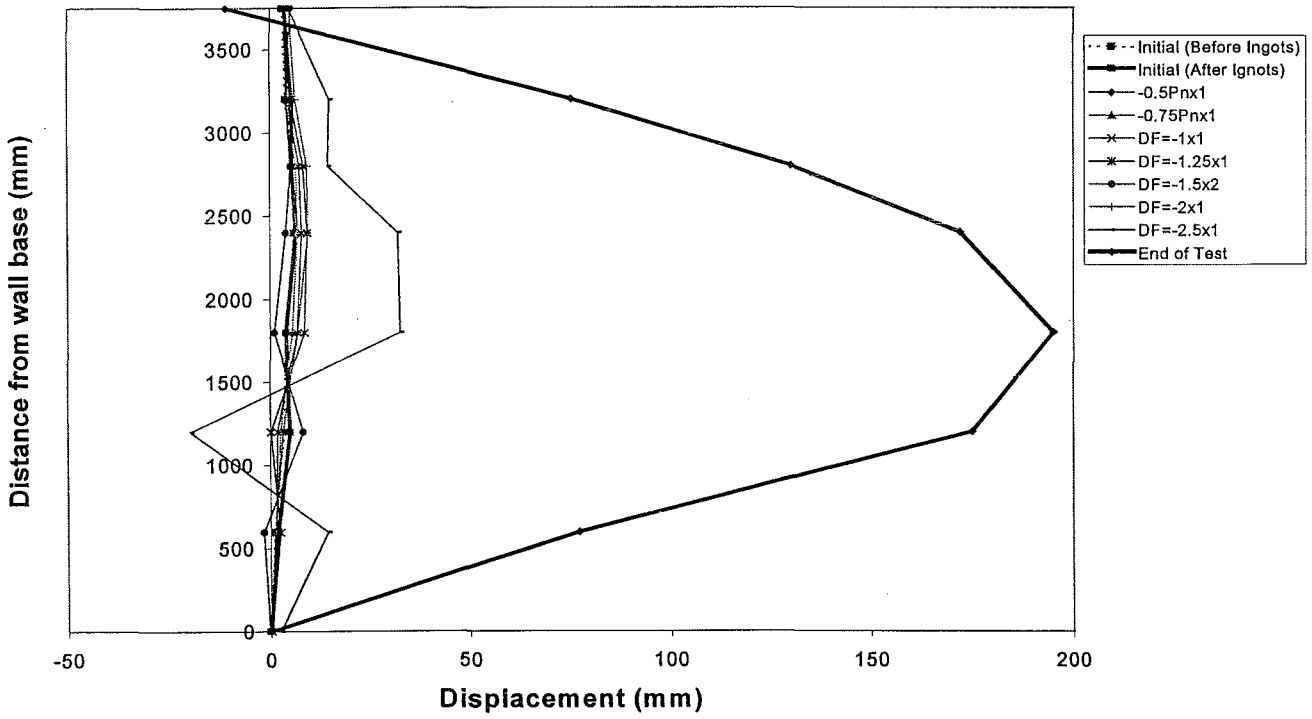

(a)

(b)

Figure 5.62(a): Unit 2: Out-of-plane movement on East edge of the wall at negative peak cycles (Compression edge)

Figure 5.62(b): Unit 2: Out-of-plane movement on East edge of the wall at negative peak cycles (Compression edge) at the end of test (alternative scale)

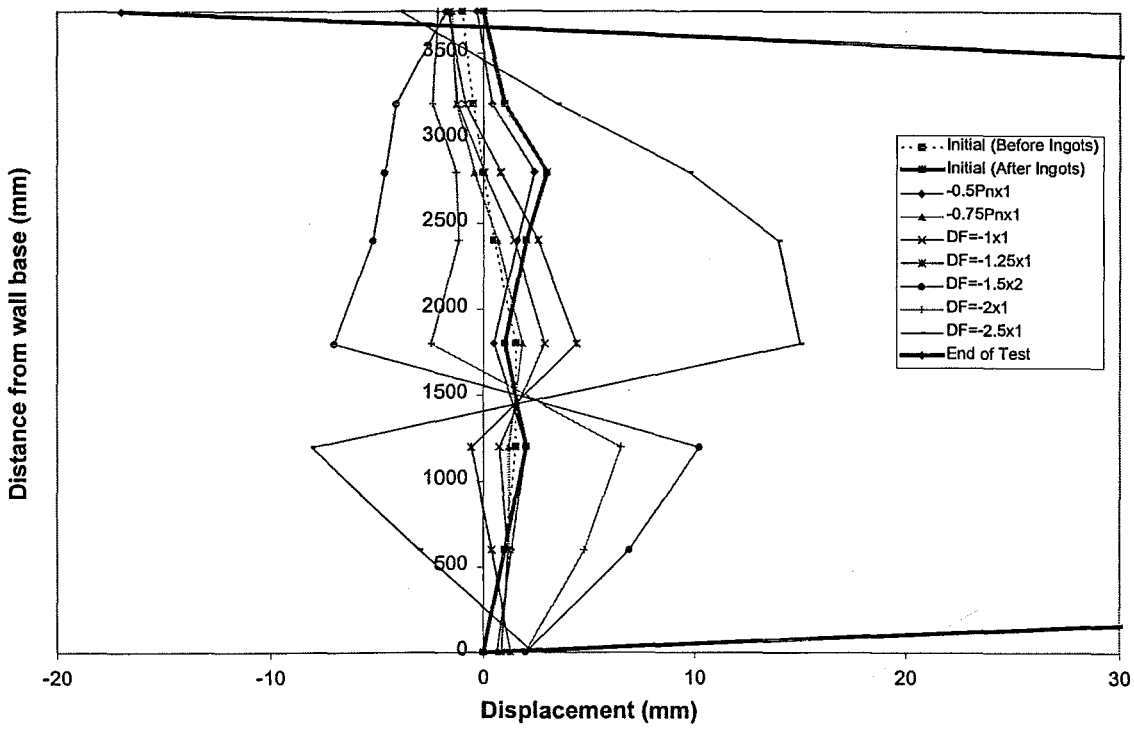

(a)

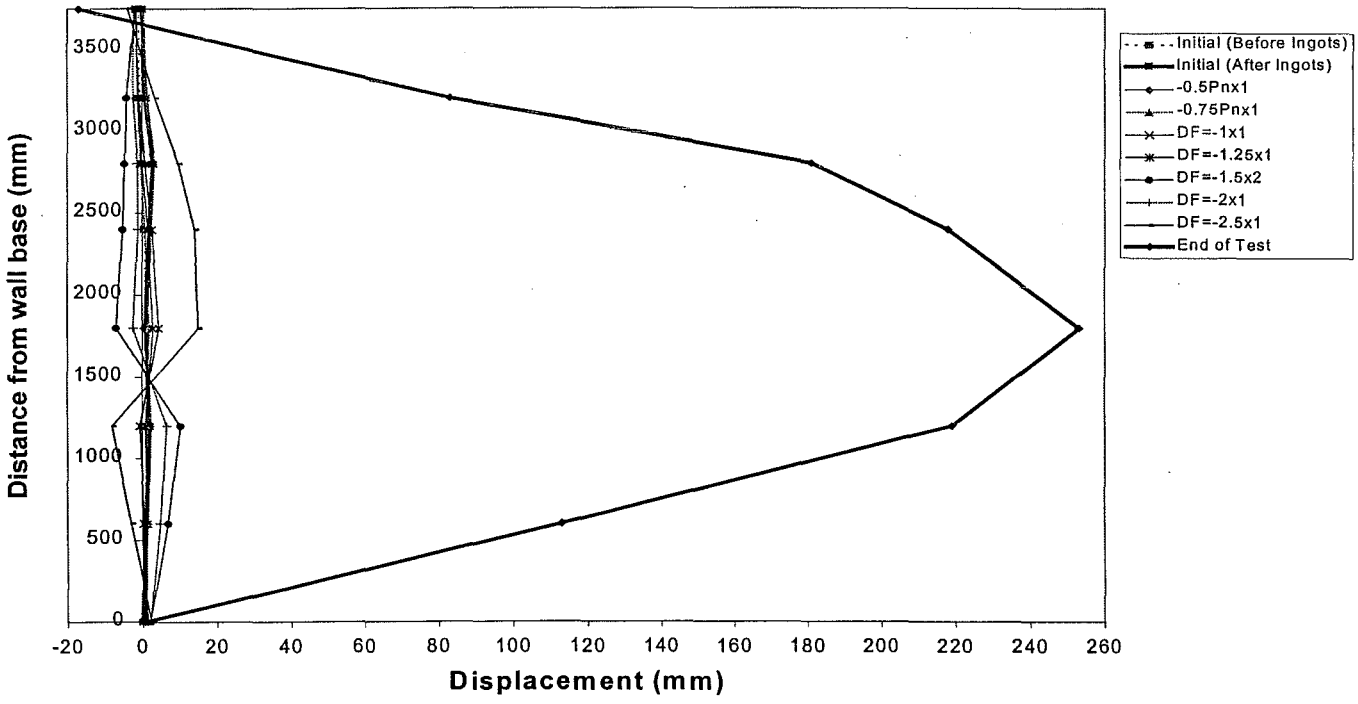

(b)

Figure 5.63(a): Unit 2: Out-of-plane movement on West edge of the wall at positive peak cycles (Tension edge)

Figure 5.63(b): Unit 2: Out-of-plane movement on West edge of the wall at positive peak cycles (Tension edge) at the end of test (alternative scale)

5.2.3.3 Local Bar Strains : Unit 2

Figure 5.64 shows the local bar strains at the wall-foundation interface during the test. The data were taken from the most extreme starter bar on the East edge of the wall. The two horizontal lines represented the actual yield strain of the reinforcement.

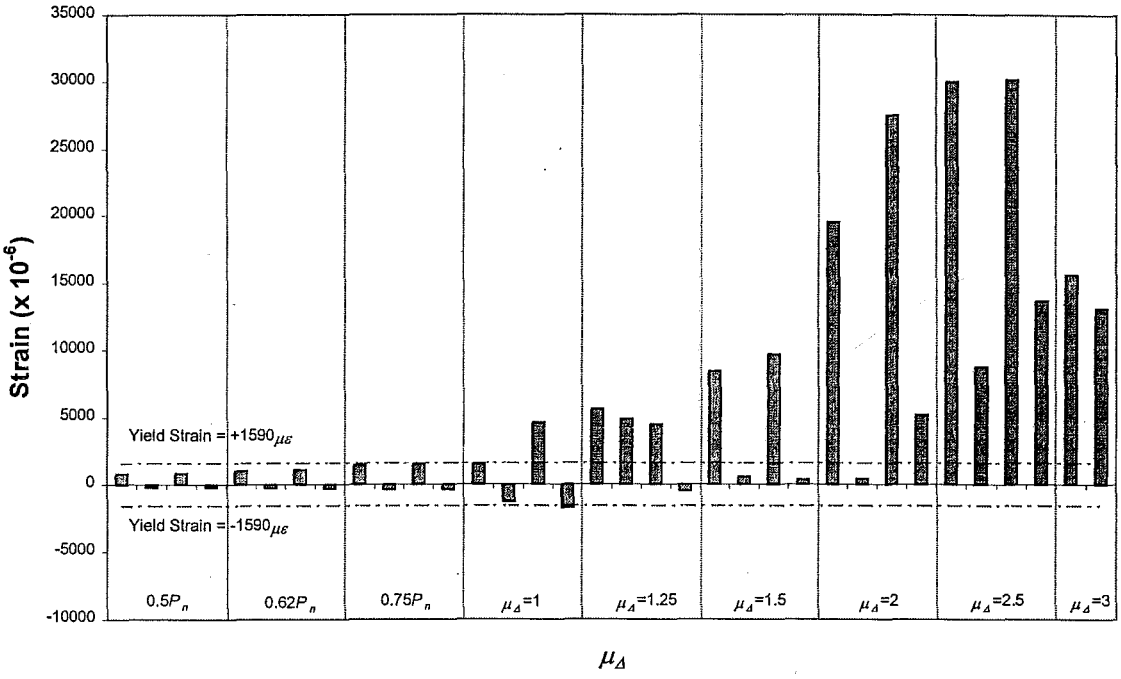

Figure 5.64: Unit 2: Strains of the outermost East edge starter bar measured at the wall-foundation interface during the test

The first yielding of the starter bar occurred on the most extreme tension bar when the wall was subjected to $0.75P_n$ (see Figure 5.64). At the same time, the extreme compression bar still remained well below the yield strain. Once the starter had undergone beyond the yield strain, the bars became permanently elongated.

The local bar strains of the two outer longitudinal wall reinforcement along both edges of the wall are shown in Figures 5.65 and 5.66 for the peak positive cycles and Figures 5.67 and 5.68 for the peak negative cycles. There was no yielding of bars either within lap splice region or at the height of 1.5 m above the foundation beams at any testing stage.

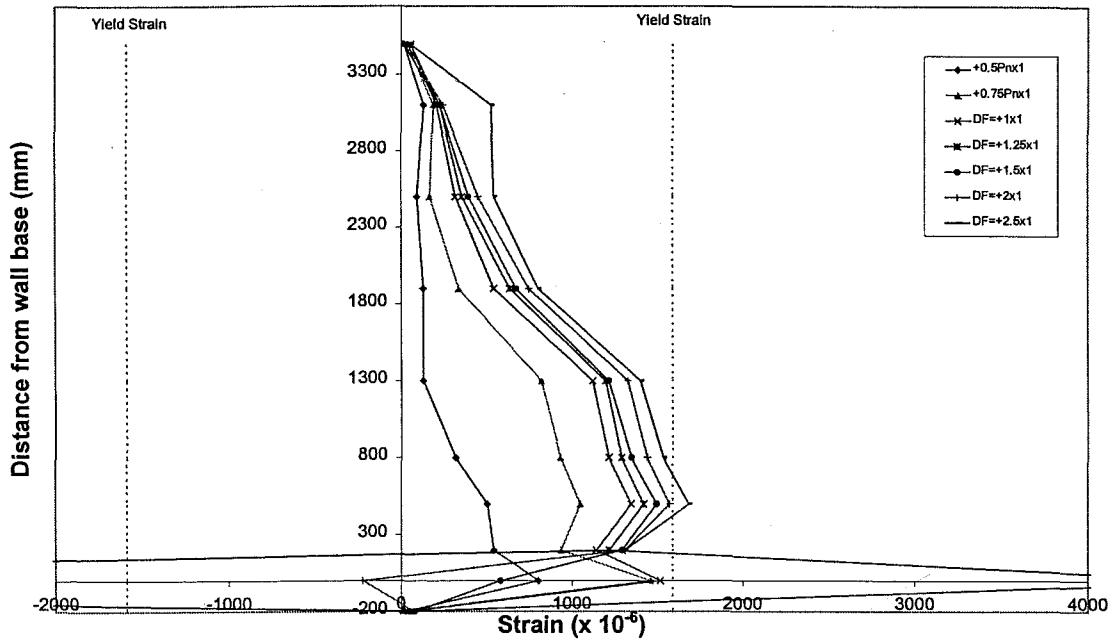

Figure 5.65: Unit 2: Outermost East edge longitudinal reinforcement strains measured at positive peak cycles (Tension edge)

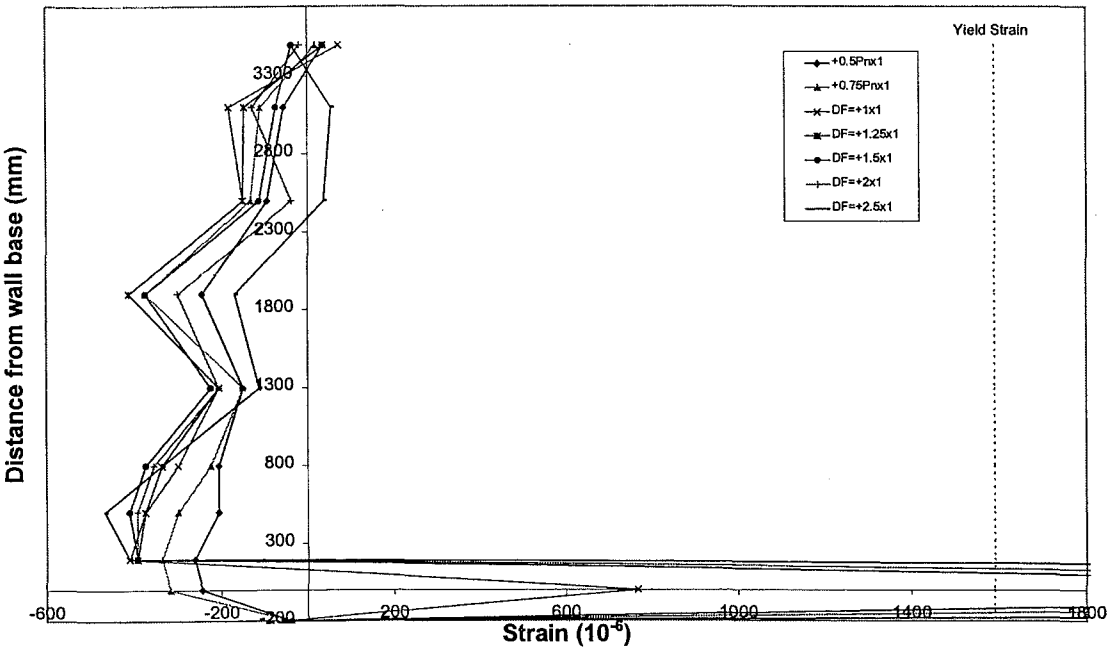

Figure 5.66: Unit 2: Outermost West edge longitudinal reinforcement strains measured at positive peak cycles (Compression edge)

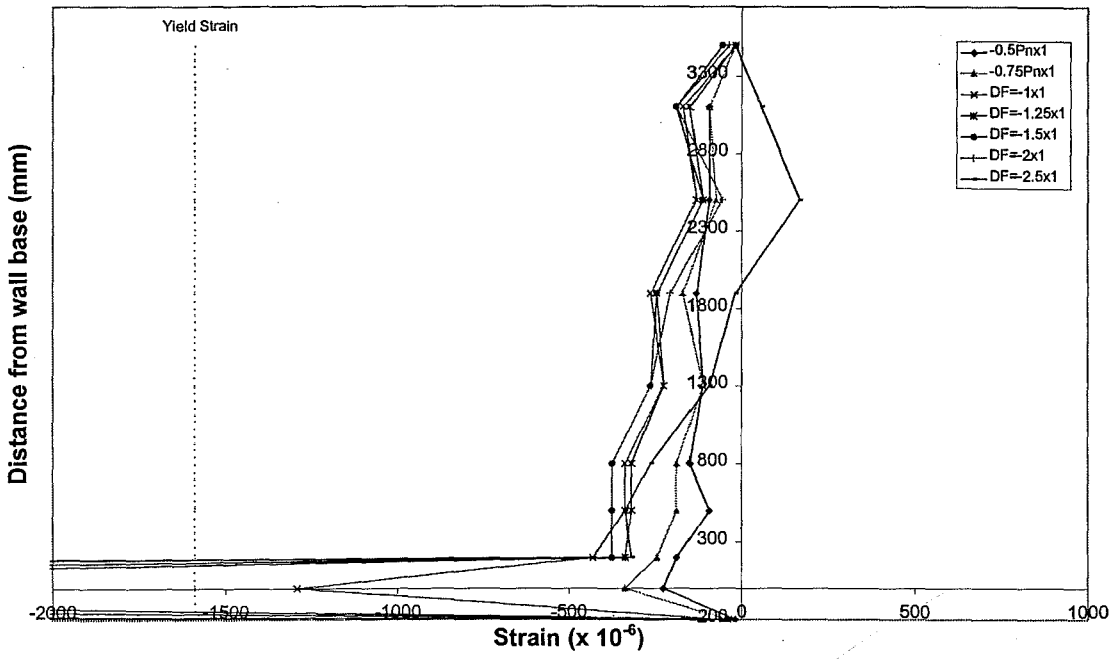

Figure 5.67: Unit 2: Outermost East edge longitudinal reinforcement strains measured at negative peak cycles (Compression edge)

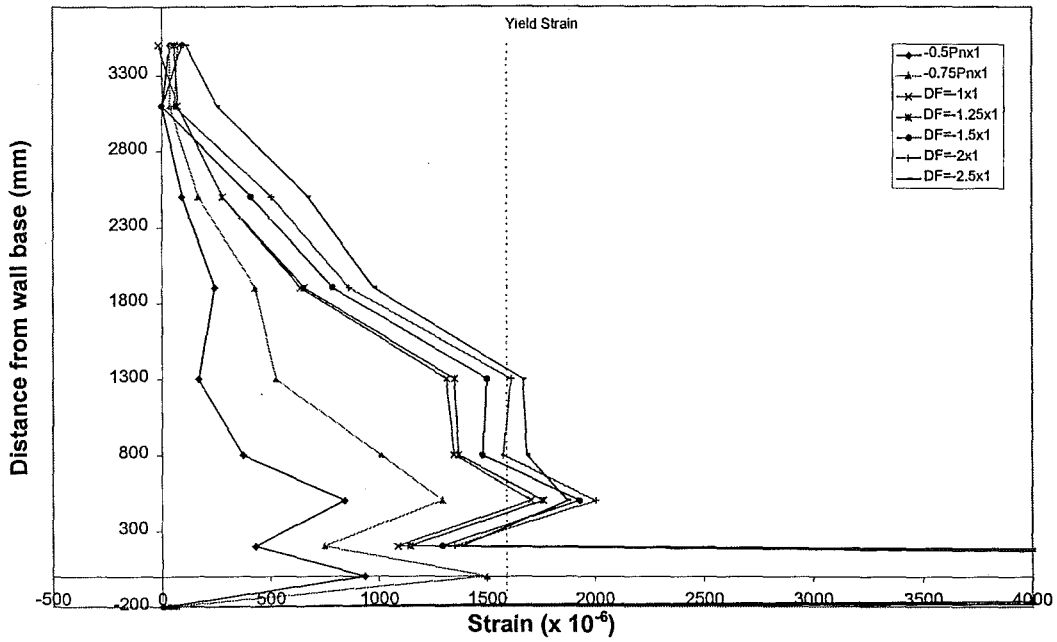

Figure 5.68: Unit 2: Outermost West edge longitudinal reinforcement strains measured at negative peak cycles (Tension edge)

When the wall was subjected to the initial positive peak cycles, the longitudinal reinforcement strains along the East edge (Tension) varied as shown in Figure 5.65. No strains were detected in the starter bars at 200 mm below the wall-foundation interface. As predicted, yielding of longitudinal bars started and concentrated at the wall-foundation interface. As the applied force increased beyond the first yield capacity of the horizontal connection, the starter bars were permanently elongated. Once the wall was subjected to the reverse direction loading, those starter bars went into compression. This scenario occurred at μ_Δ = +2×1 and higher when the local bar strain at the wall-foundation connection shows negative value as shown in Figure 5.65.

There was yielding taken place at the location immediate above the lap splice until $\mu_\Delta = \pm 2$ was reached (see Figures 5.65 and 5.68). The wall was softened around this region and caused some instability. This resulted in a rapid increase of out-of-plane displacements

Similarly, the first yielding occurred at the wall-foundation interface on the West edge (Compression). The compression reinforcement reached the yield strain later than the tension reinforcement because concrete takes most of the internal compressive force. The measured local bar strains at the wall-foundation interface changed from negative strain to positive strain as soon as $\mu_\Delta = +1\times1$ was reached (see Figure 5.66). This could be interpreted exactly the same way as what happened on the East edge when subjected to tension.

Figure 5.69 illustrates the development of the starter strains at the wall-foundation interface across the wall panel during the elastic cycles. The neutral axis depth moved towards the extreme compression fibre as the applied force increased. The outermost tension steel approached yield strain when the wall was subjected to the first yield capacity. Once μ_Δ = -1×2 was achieved, most of the tension reinforcement yielded causing strain gauges became unusable.

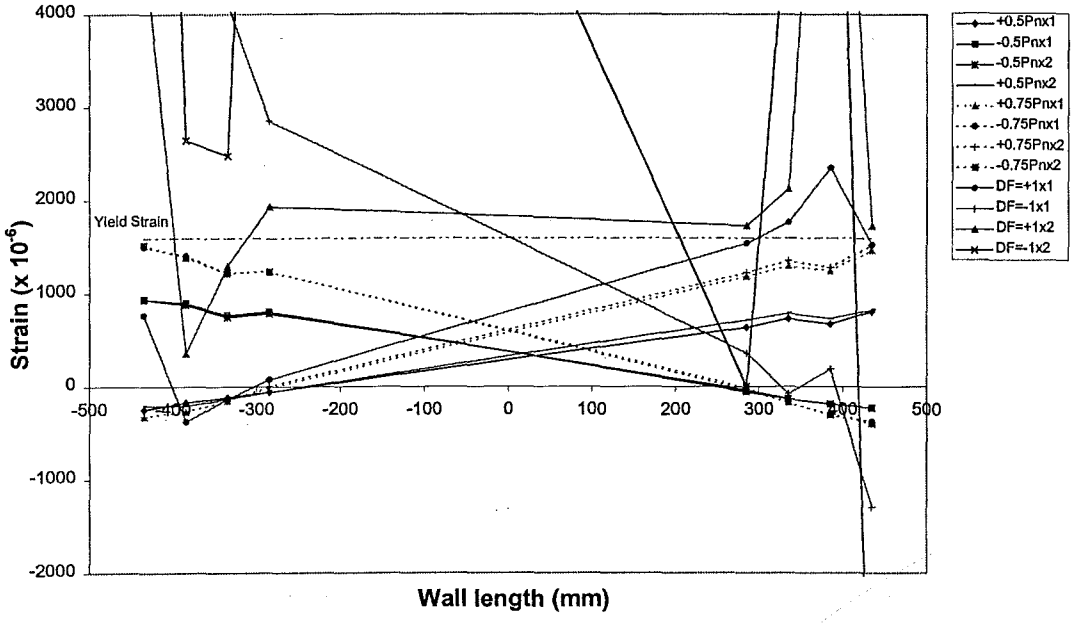

Figure 5.69: Unit 2: Strains of starter bars across the wall-foundation interface during the test

Considering the local bar strains within lap splice region, no yielding occurred during the load-controlled cycles or the "Elastic cycles". Strain profiles were symmetrical in both loading directions. This could be illustrated in Figure 5.70. At $0.5P_n$, the strain profiles were approximately linear. The second cycle of the same load level did not have much effect on the strain profiles. They became steeper when applied load level approached $0.75P_n$. Strain profile gradient increased when $\mu_\Delta = 1$ was approached. There was no sign of strength degradation occurred during the "Elastic cycles". The local bar strains at the higher level of ductility were not shown because the strain gauges were damaged.

Figure 5.71 shows the strain of the reinforcement in the region immediately above lap splice. The strength degradation became more significant under the repetition of the same applied load level. However, the strain profiles were still approximately symmetrical for both loading directions. The strain of the extreme tension fibre in this region approached the yield strain much faster compared the strain in lap splice region at the same applied load level.

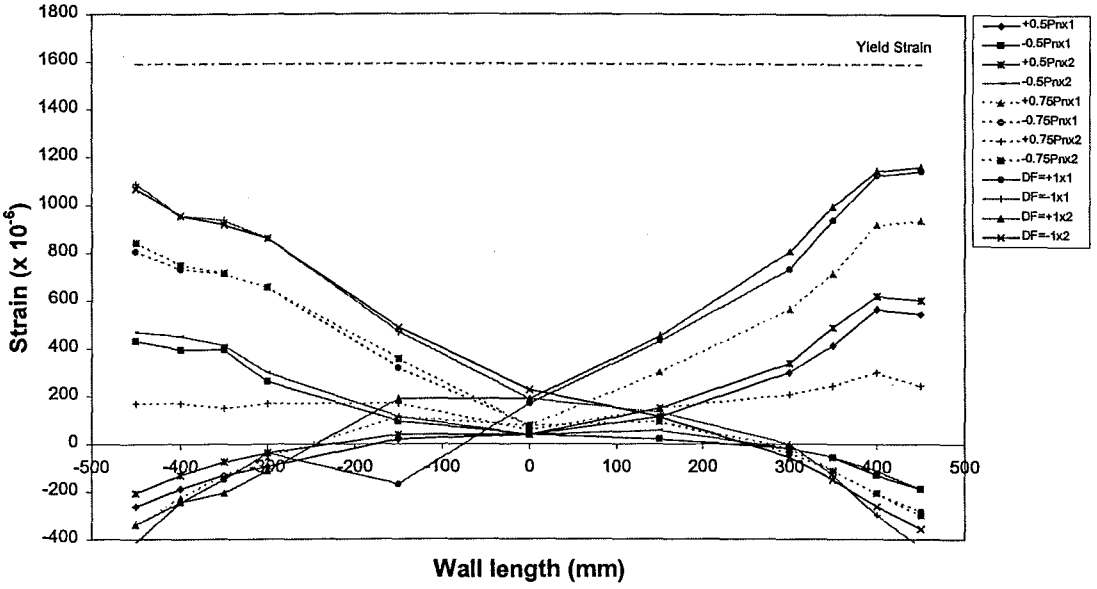

Figure 5.70: Unit 2: Strains of wall reinforcement within lap splice region (200 mm above the foundation beam) during the peak elastic cycles

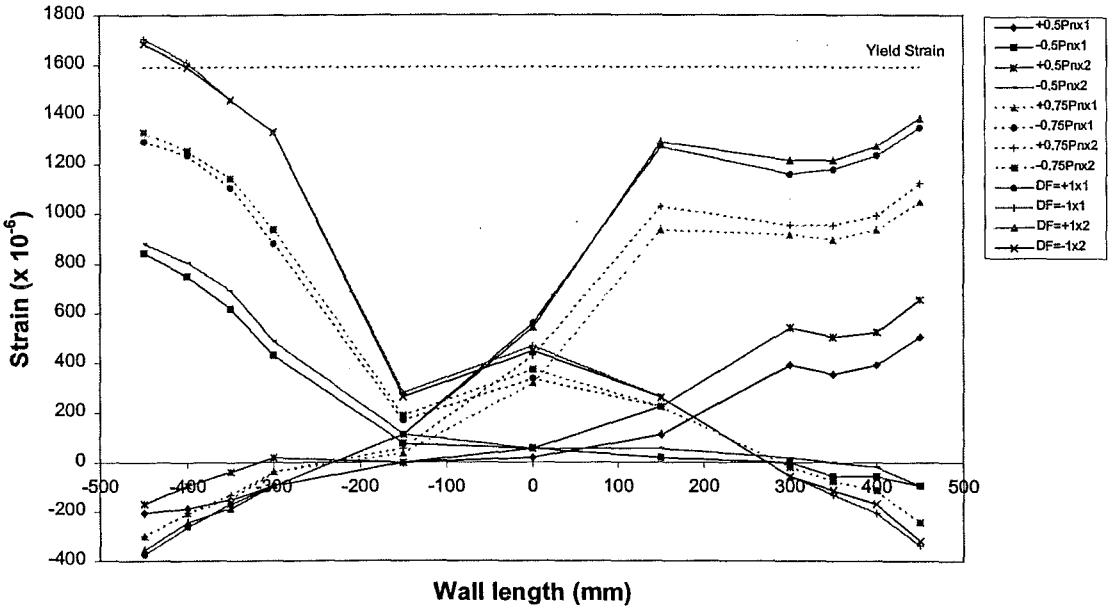

Figure 5.71: Unit 2: Strains of wall reinforcement above the region of lap splice (500 mm above the foundation beam) during the peak elastic cycles

5.2.3.4 Concrete Strains : Unit 2

Concrete strain variation at the level of wall-to-foundation connection during the test is illustrated in Figures 5.72, 5.73, 5.76 and 5.77. Spalling was observed during the first cycle of μ_Δ = +2.5×1 with the spalling concrete strain ε_{cu} = -0.0072 (see Figure 5.72).

Longitudinal concrete strain on West edge when subjected to compression is shown in Figure 5.72. When the West edge subjected to tension, North and South clip gauges extended in the same order of magnitude and trend (see Figure 5.73). The magnitude of concrete strain measured at the wall base was always greater that the concrete strain at the region of immediately above lap splice when subjected to compression and tension as shown in Figures 5.74 and 5.75, respectively.

Longitudinal concrete strain on East edge which was measured by North and South clip gauges indicated tension and compression strains (see Figure 5.76) when subjected to loading at μ_Δ = -1.25×2. The edge should have been nominally in compression under this direction of loading. This indicates that the skewed neutral axis had occurred.

Figure 5.77 illustrates the longitudinal concrete strain on East edge when subjected to tension. The plot shows that this edge always stayed in tension during the test. The concrete strain on East edge at the wall base always smaller than the concrete strain at the region immediately above lap splice (see Figures 5.78 and 5.79).

Constant eccentric vertical load had significantly reduced the amount of lifting at the base compared to Unit 1. However, the amount of curvature variation about the minor axis was much larger compared to Unit 1 due to the eccentric vertical load.

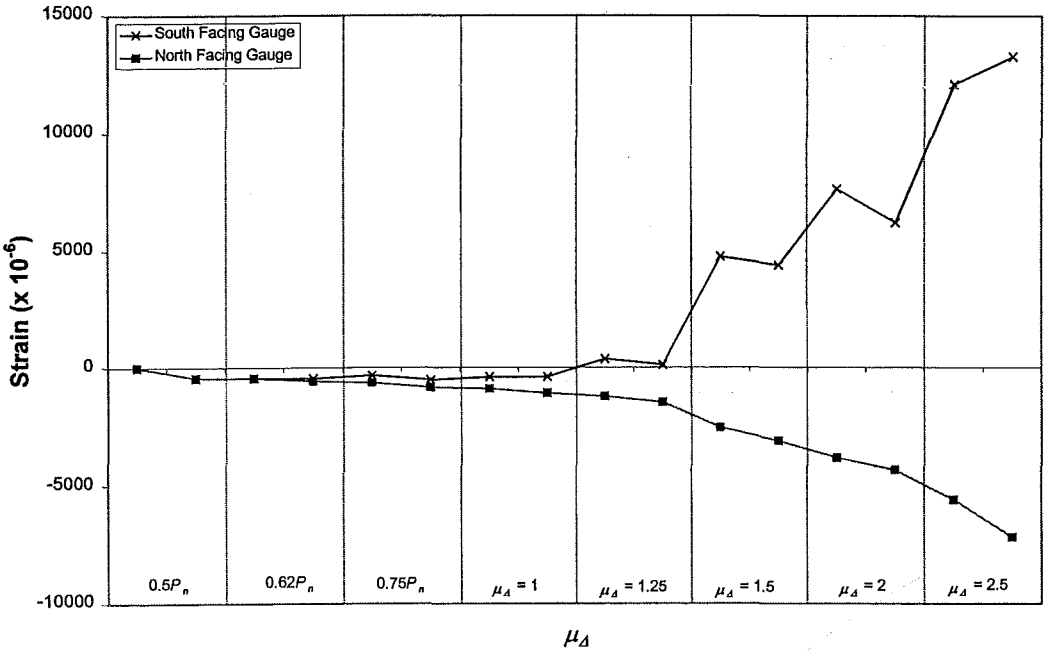

Figure 5.72: Unit 2: Concrete longitudinal strains of West edge when subjected to compression obtained from outermost clip gauges (base of wall)

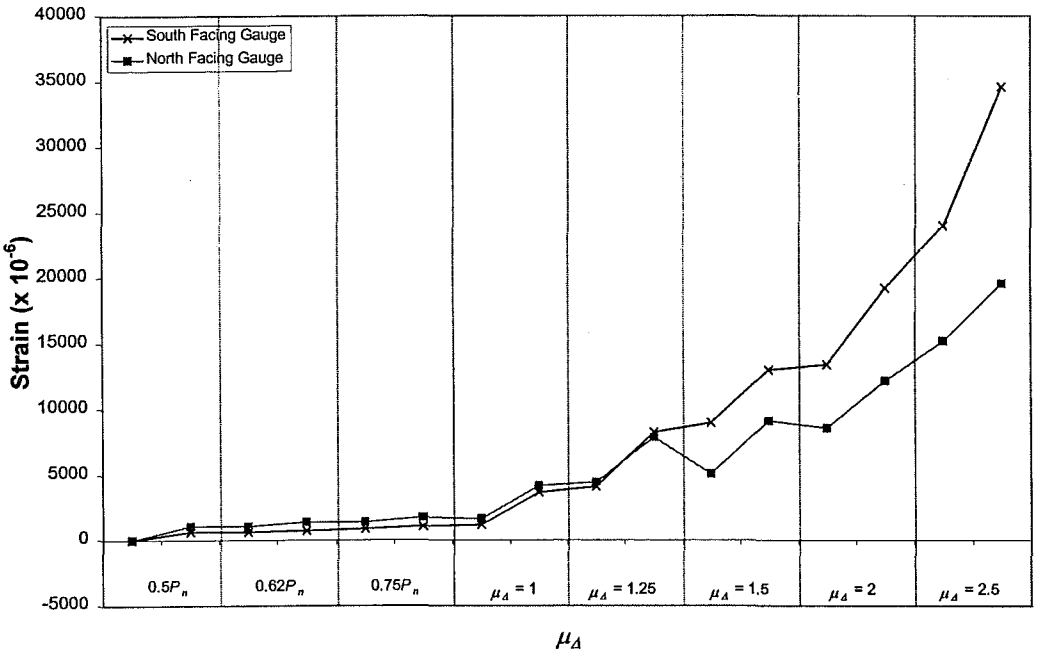

Figure 5.73: Unit 2: Concrete longitudinal strains of West edge when subjected to tension obtained from outermost clip gauges (base of wall)

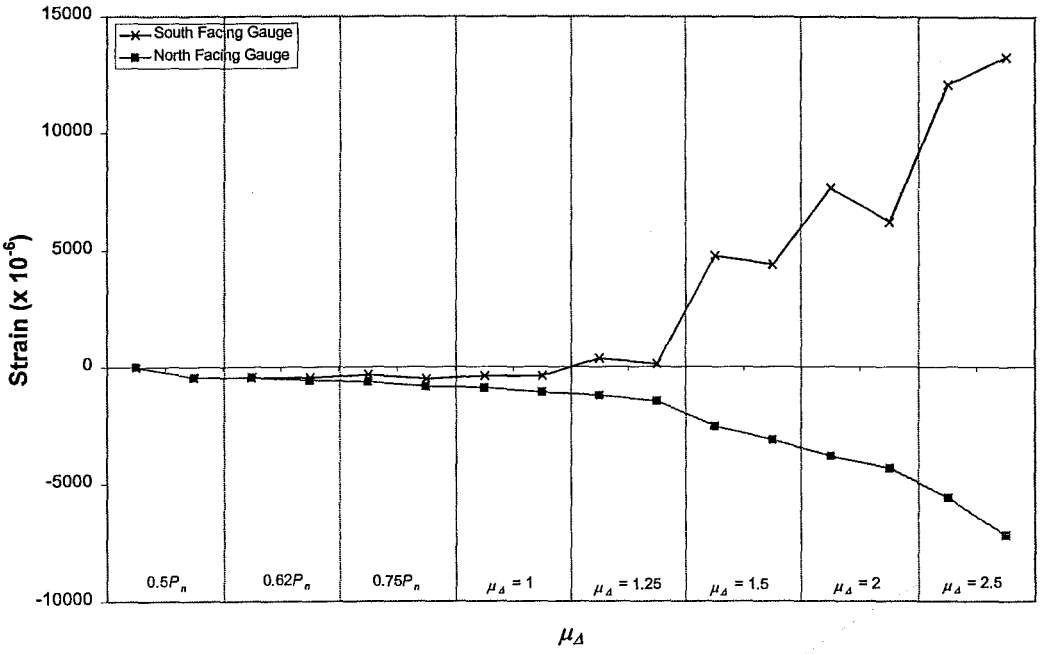

(a) Wall base

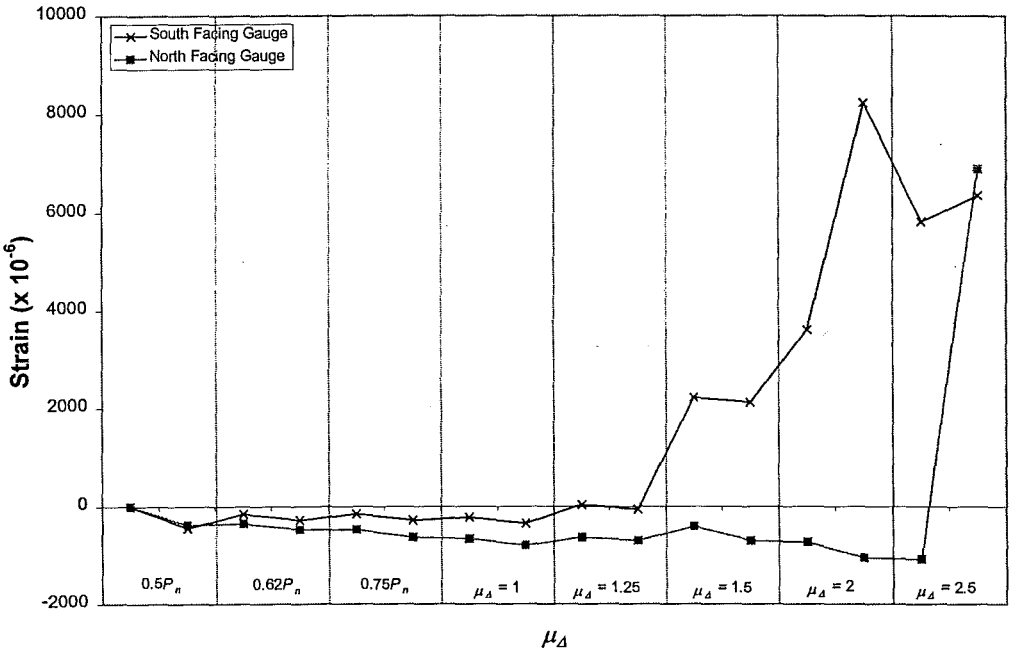

(b) Immediately above lap splice

Figure 5.74: Unit 2: Difference in concrete strains in West edge when subjected to compression obtained from the outermost clip gauges

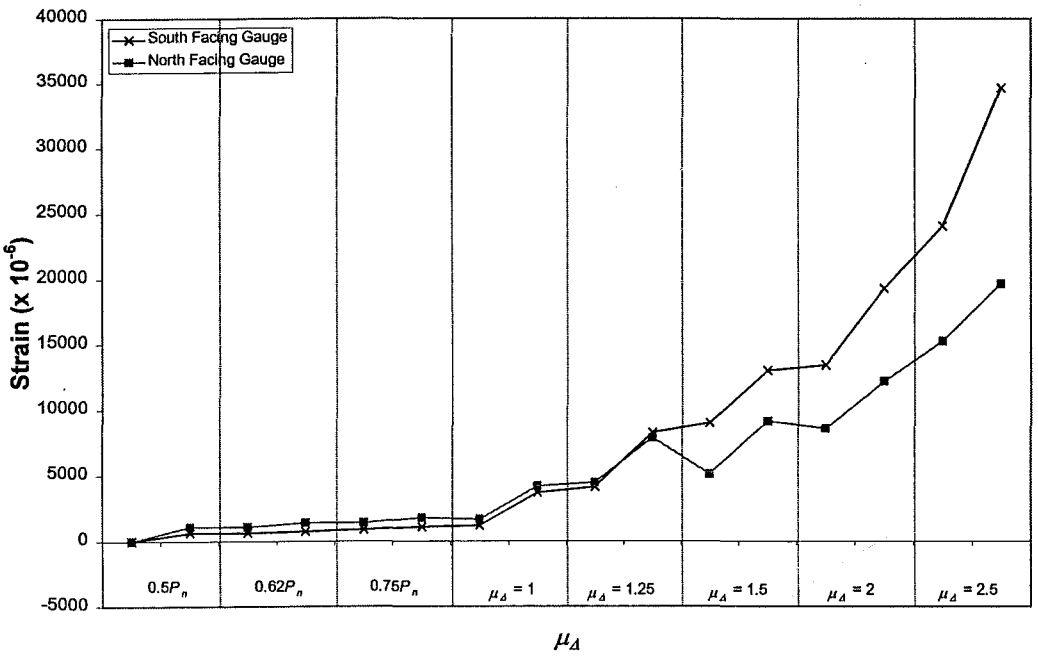

(a) Wall base

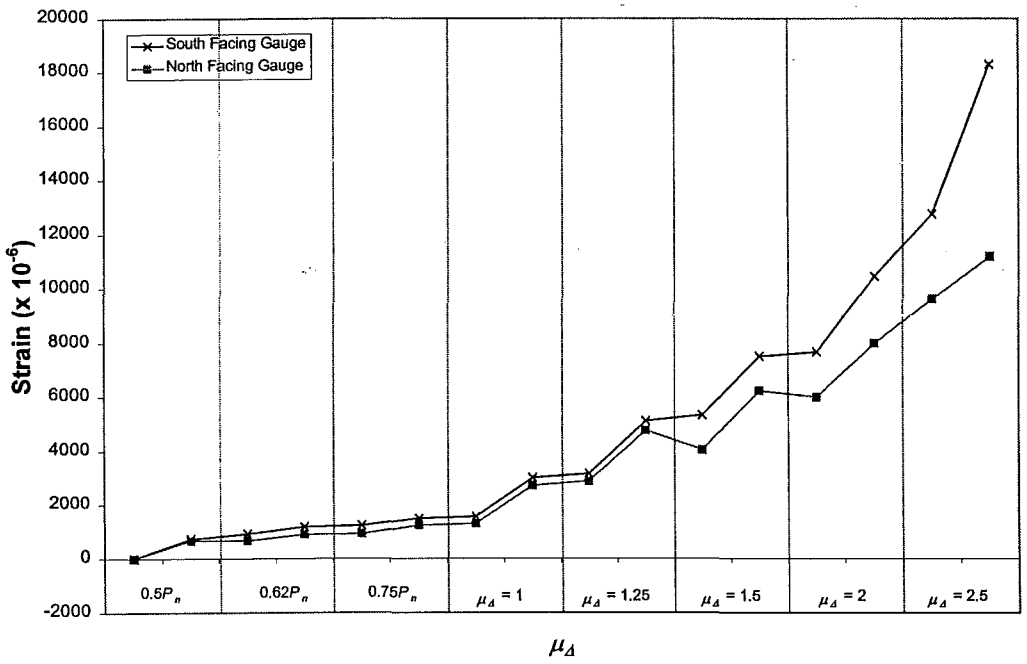

(b) Immediately above lap splice

Figure 5.75: Unit 2: Difference in longitudinal concrete strains in West edge when subjected to tension obtained from the outermost clip gauges

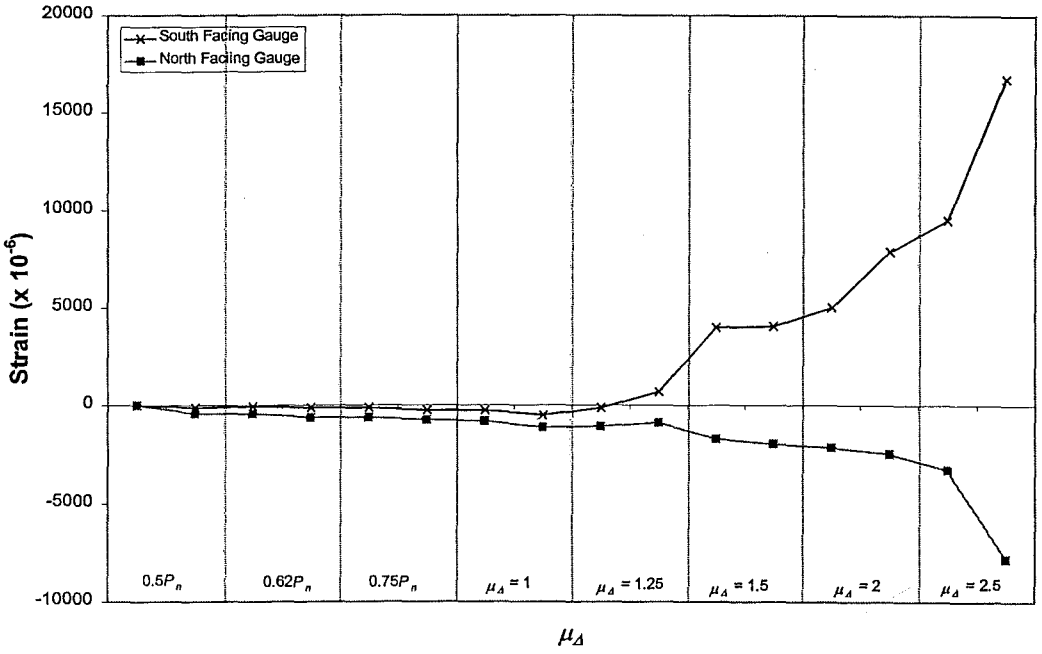

Figure 5.76: Unit 2: Concrete longitudinal strains of East edge when subjected to compression obtained from outermost clip gauges (base of wall)

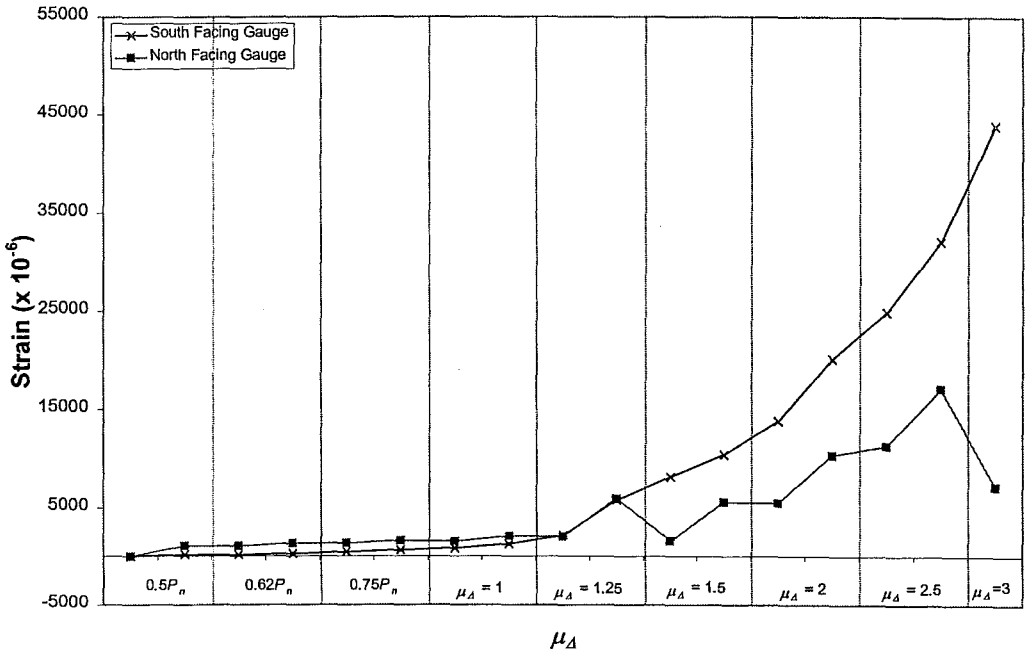

Figure 5.77: Unit 2: Concrete longitudinal strains of East edge when subjected to tension obtained from outermost clip gauges (base of wall)

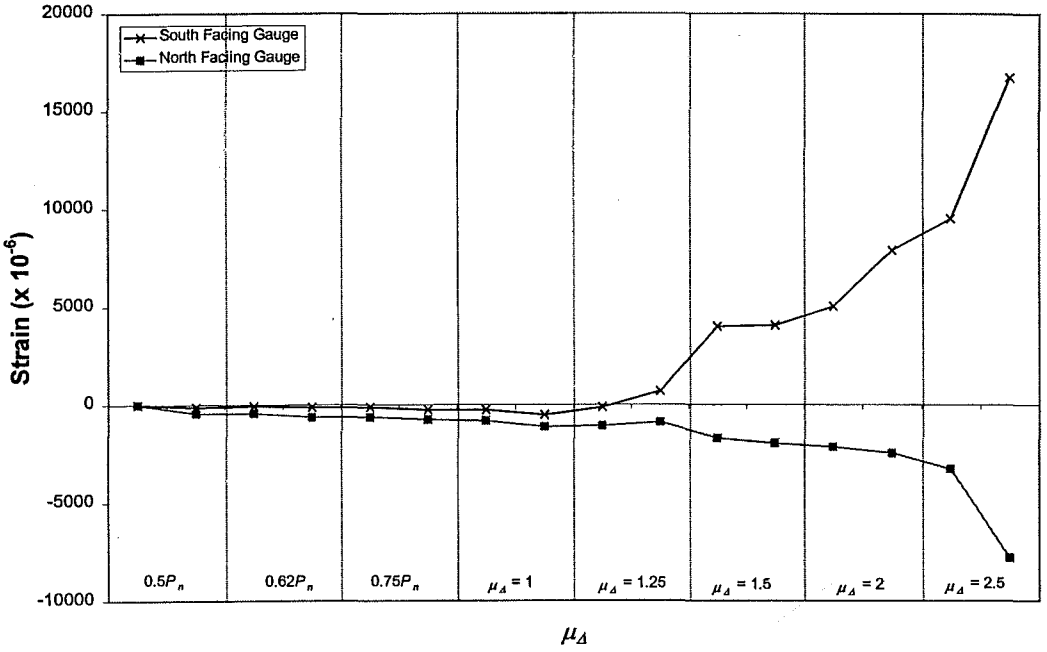

(a) Wall base

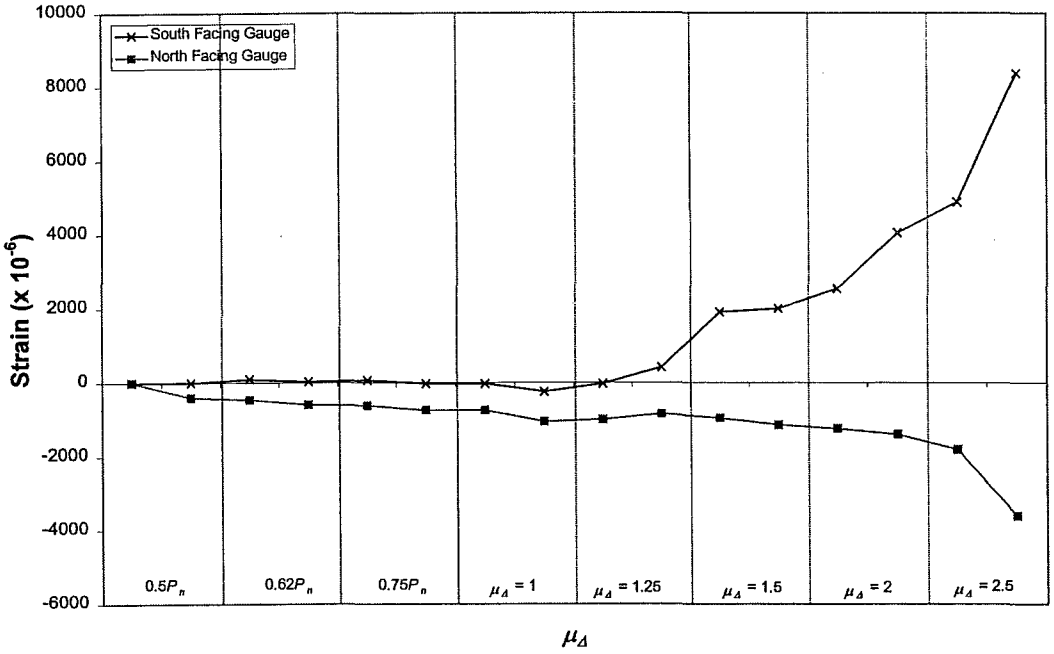

(b) Immediately above lap splice

Figure 5.78: Unit 2: Difference in concrete strains in East edge when subjected to compression obtained from the outermost clip gauges

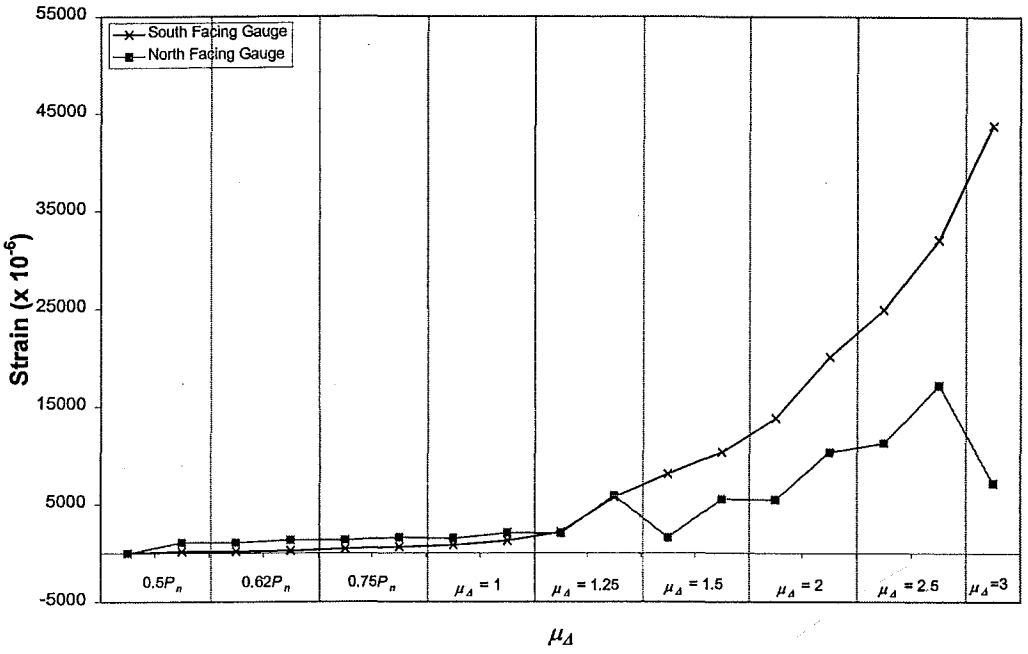

(a) Wall base

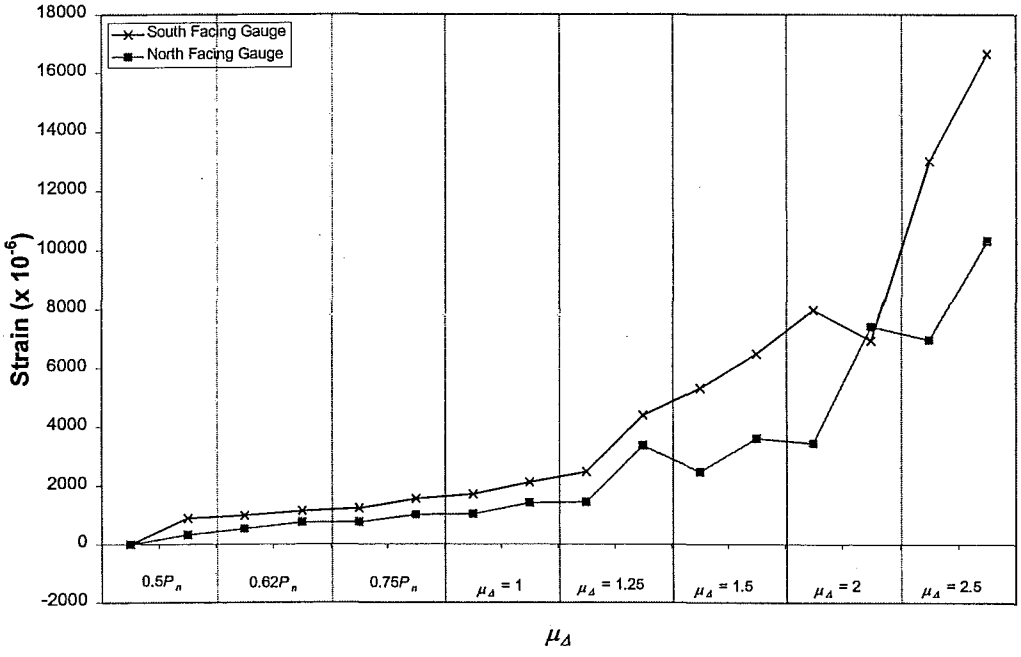

(b) Immediately above lap splice

Figure 5.79: Unit 2: Difference in concrete strains in East edge when subjected to tension obtained from the outermost clip gauges

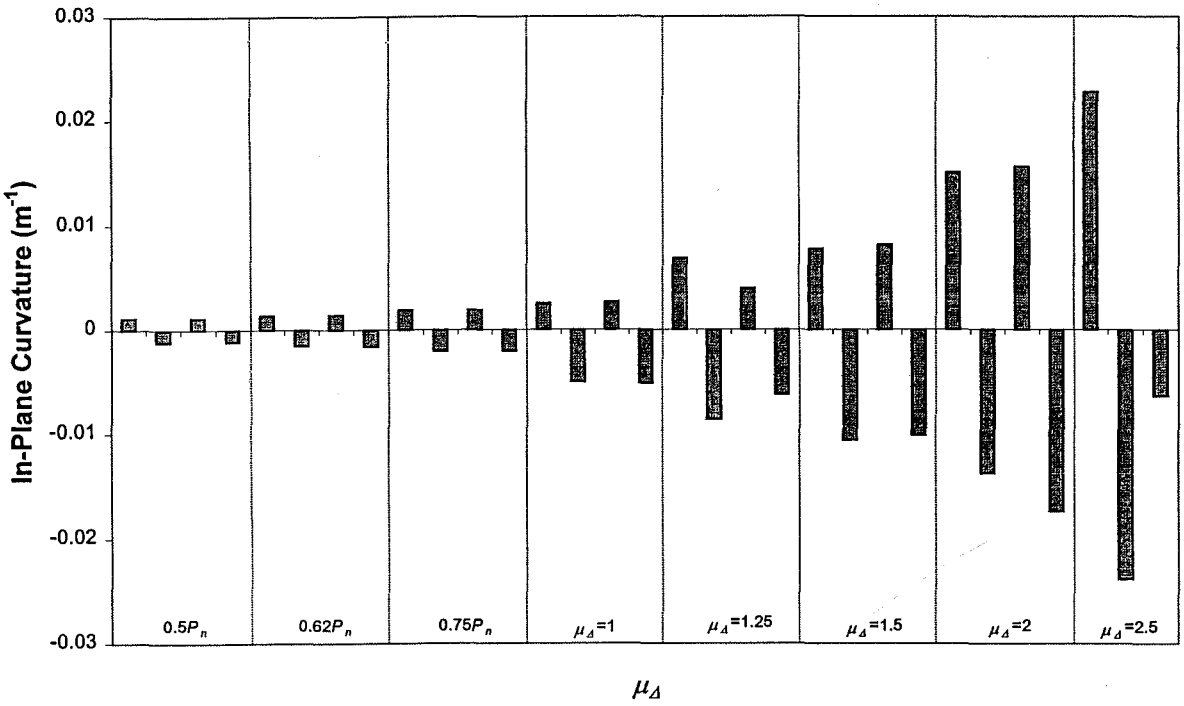

Figure 5.80: Unit 2: In-plane curvature distribution measured at 200 mm above the foundation beam

The measured in-plane curvature along the wall-to-foundation connections followed the applied loading pattern up to when $\mu_\Delta = +2.5\times2$ (see Figure 5.80).

Out-of-plane curvature distribution measured by clip gauges during the test is shown in Figures 5.81 and 5.82. These indicated that the amount of rotation about the horizontal axis increased as the height increased. The most critical region positioned at approximately mid-height of the wall panel. Unlike Unit 1 which the critical region was found to be about 1 m above the foundation beam. This contrast can be explained by the difference of the wall profiles, i.e. double-curvature for Unit 1 and single-curvature for Unit 2.

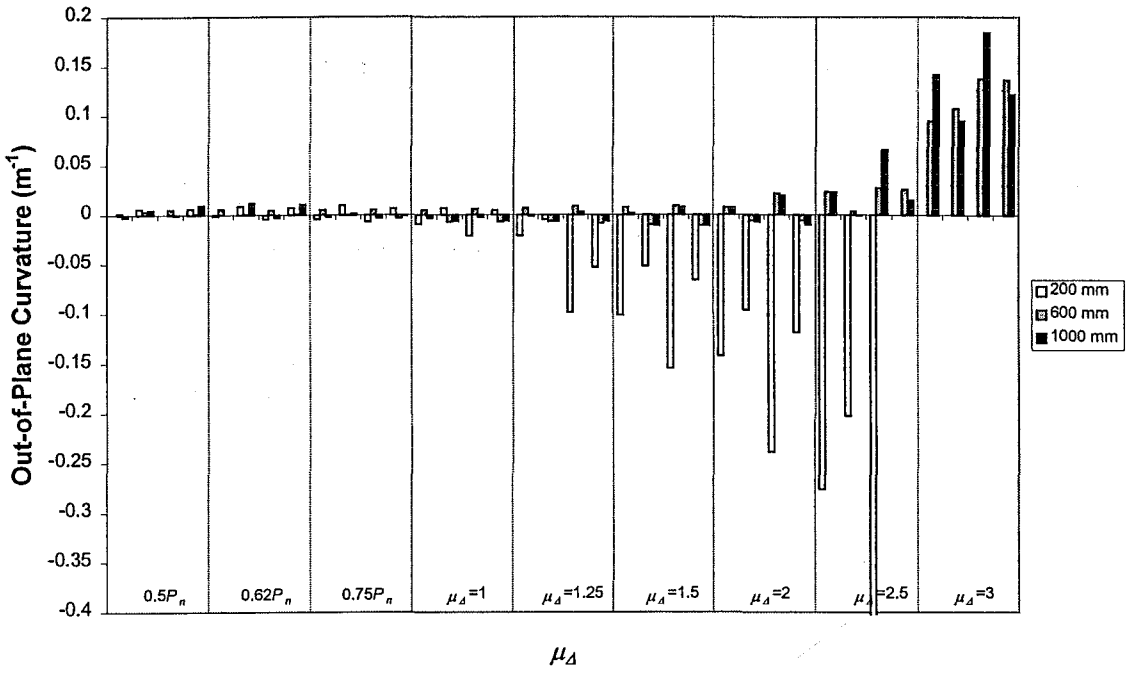

Figure 5.81: Unit 2: Out-of-plane curvature distribution obtained from outermost clip gauges on the West edge during the test

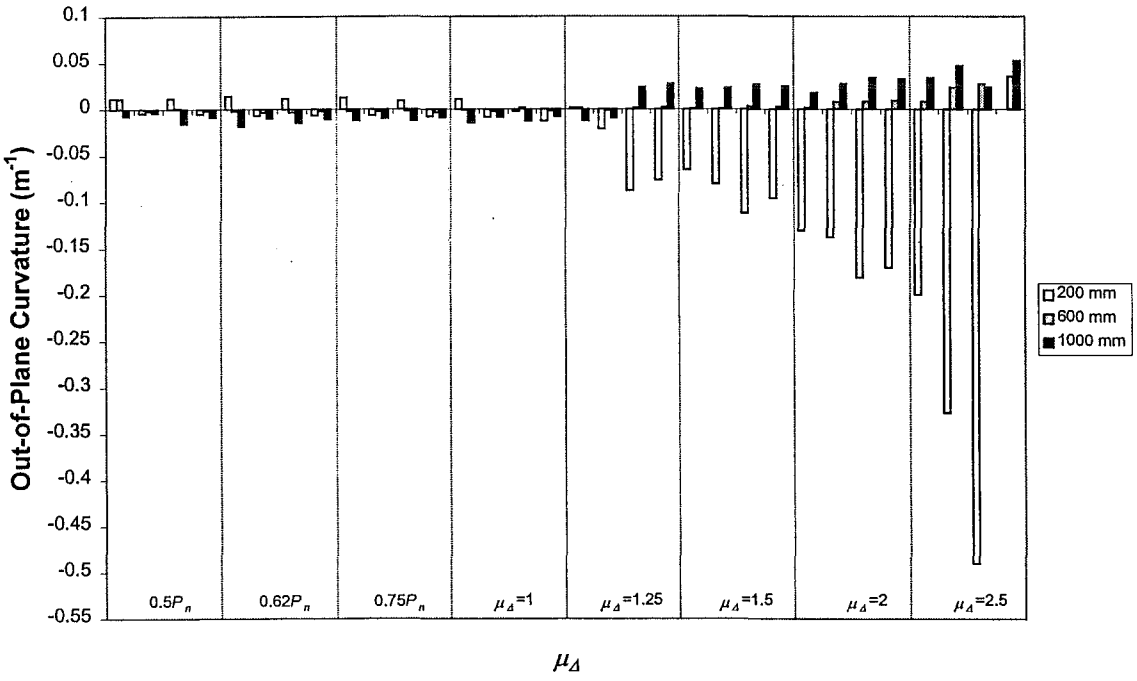

Figure 5.82: Unit 2: Out-of-plane curvature distribution obtained from outermost clip gauges on the East edge during the test

5.2.3.5 Sectional Neutral Axis : Unit 2

The sectional neutral axis was not perpendicular to the longitudinal direction of loading as the result of the out-of-plane curvature of the wall panel. Skewing of the neutral axis appeared to start at μ_Δ = +1.25×1 when concrete strain on convex side was in compression and on concave side became tension (see Figure 5.72).

The amount of concrete strains measured during the test was recorded up to approximately μ_Δ = +3×1 where most clip gauges were removed. This was to prevent any damage to instrumentation which might occur as the test was continued.

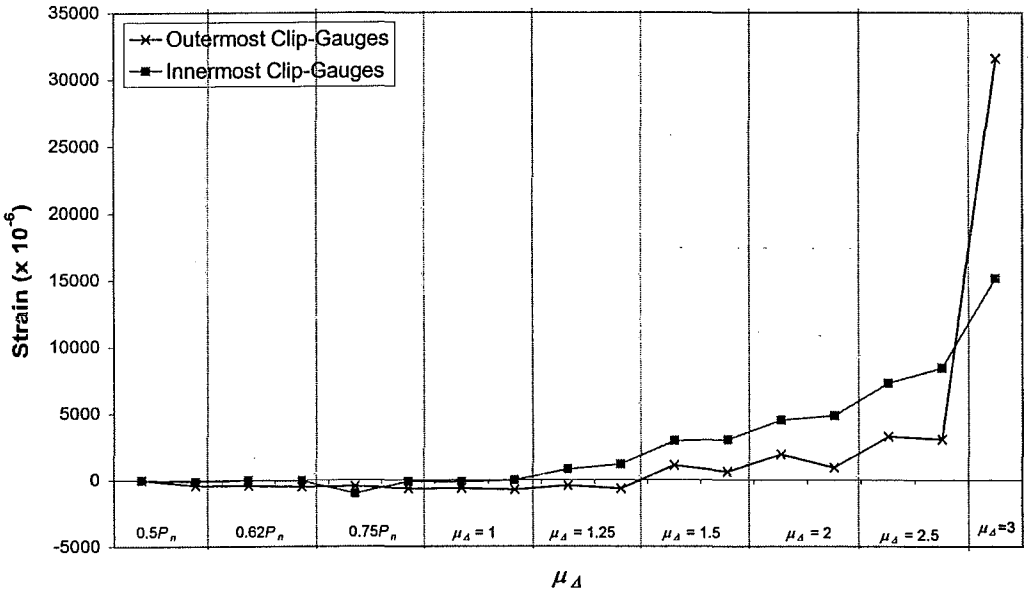

(a) 200 mm

Figure 5.83: Unit 2: Difference in concrete strains in West edge when subjected to compression obtained from the outermost clip gauges at different heights

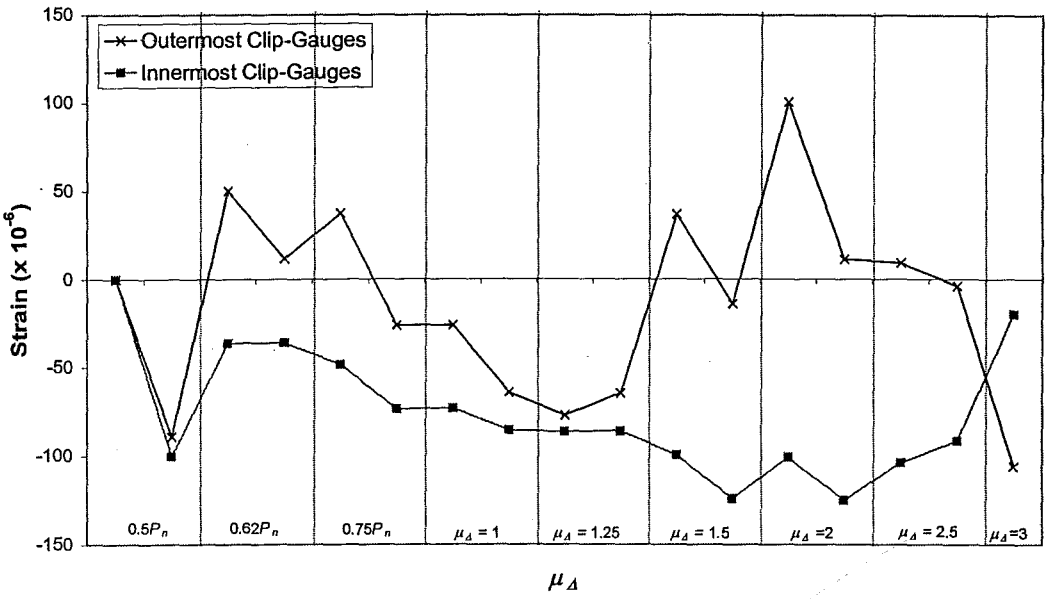

(b) 600 mm

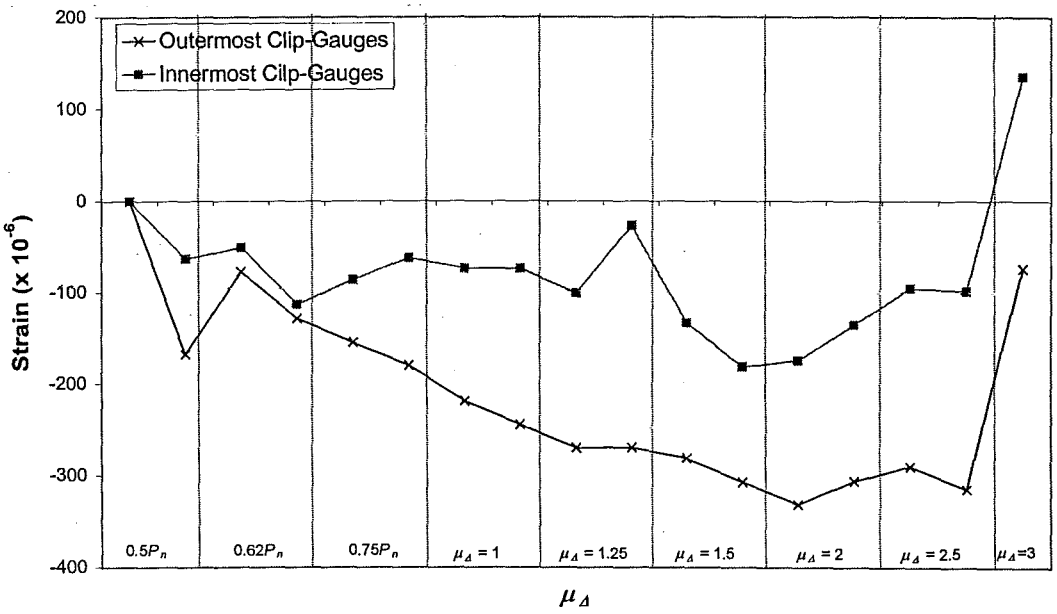

(c) 1000 mm

Figure 5.83 (cont.): Unit 2: Difference in concrete strains in West edge when subjected to compression obtained from the outermost clip gauges at different heights

The position of neutral axis at the height of 200 mm above the foundation beam was between the outermost and the innermost clip gauges when the wall subjected to μ_Δ = +1.25× 1 (see Figure 5.83 (a)). At the μ_Δ = +1.5×1 the position of neutral axis shifted beyond the outermost clip gauges towards the extreme compression fibre. At 600 mm above the foundation beam, the position of neutral axis was confined within the region between the outermost and the innermost clip gauges during the test (see Figure 5.83 (b)). At 1000 mm above the foundation beam, the neutral axis lay in the region towards the middle of the wall (see Figure 5.83 (c)).

When the West edge of the wall became subjected to tension, both outermost and innermost clip gauges always indicated tensile concrete strain during the test (see Figure 5.84). However, the magnitude of the measured concrete strain decreased as the height increased

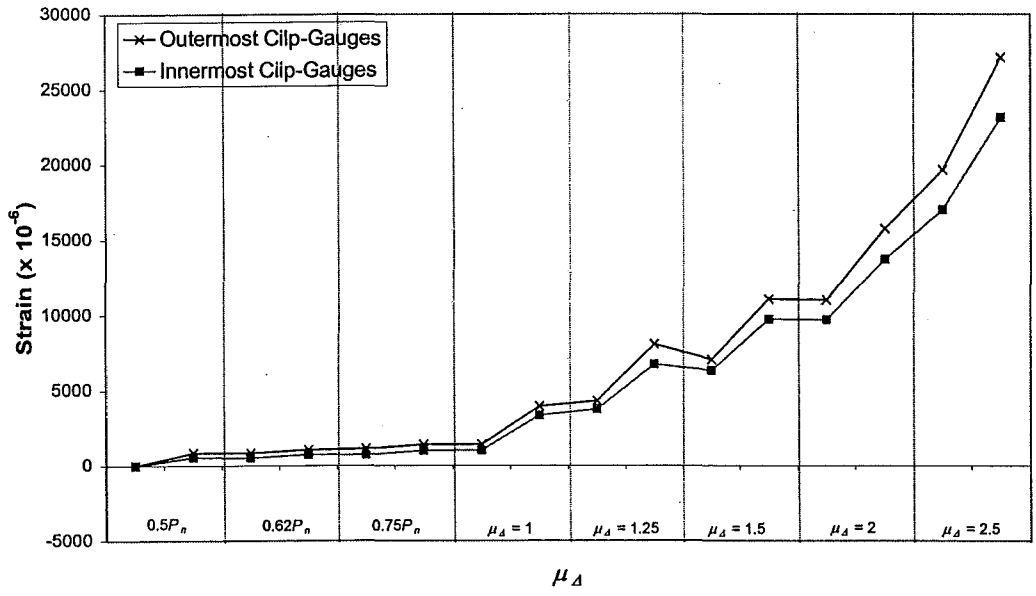

(a) 200 mm

Figure 5.84: Unit 2: Difference in concrete strains in West edge when subjected to tension obtained from the outermost clip gauges at different heights

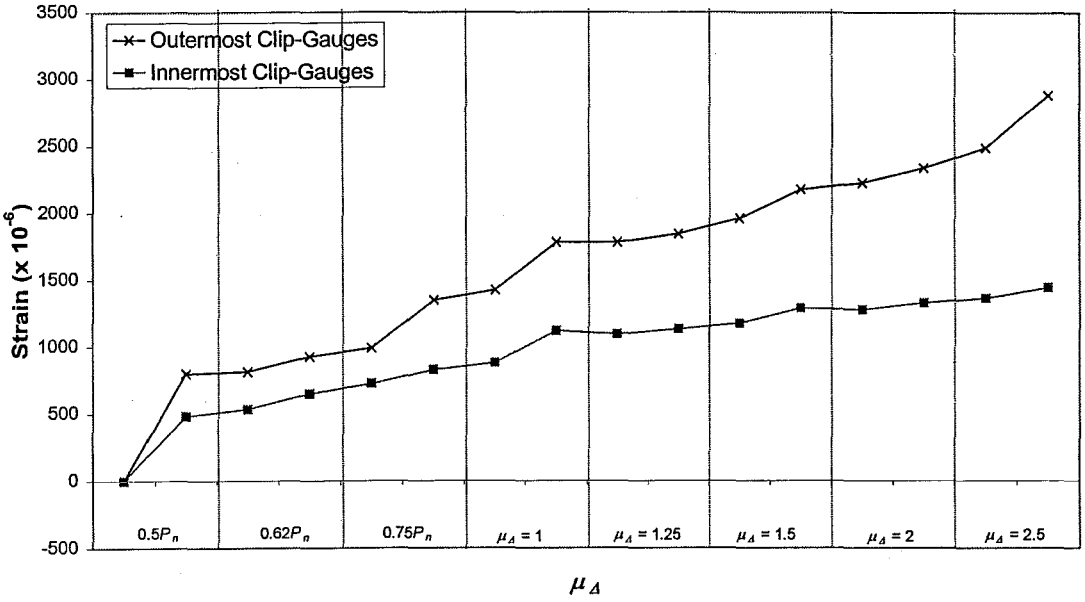

(b) 600 mm

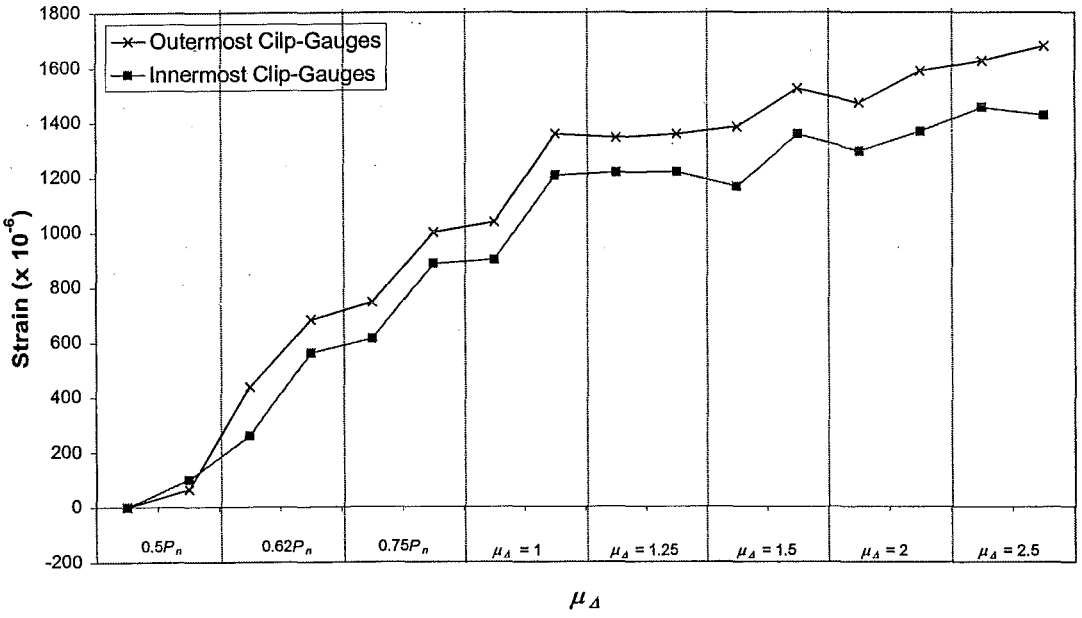

(c) 1000 mm

Figure 5.84 (cont.): Unit 2: Difference in concrete strains in West edge when subjected to tension obtained from the outermost clip gauges at different heights

5.3 Unit 3

5.3.1 Unit 3 Properties

The properties of Unit 3 are illustrated in Table 5.3. All measured values were calculated with the material properties measured on the day of test, and the nominal values were calculated using the nominal material properties.

Table 5.3: Measured properties of Unit 3

Property			Nominal value	Measured value
Reinforcing ratio	p	%	1.26	N/A
Longitudinal reinforcing yield strength*	f_y	MPa	300	318
Concrete compressive strength*	f'_c	MPa	30	23
Modulus of rupture	f_r	MPa	4.38	3.84
Axial load level	$N^*/A_g f'_c$		0.0031	0.0041
Cracking load	P_{crack}	kN	9.7	8.5
First yield strength	P_{yield}	kN	18.8	18.7
Nominal strength	P_n	kN	24.0	23.37

* At the day of testing

The secant stiffness at $0.75P_n$ was k_{75} = 1.97 kN/mm and the estimated reference yield displacement was Δ_y = 11.9 mm (see Appendix B).

5.3.2 General Behaviour and Observations : Unit 3

At the first cycle of $0.5P_n$, horizontal flexural cracks started to appear in the region immediately above the lap splice where starter bars were terminated. The height of cracking was approximately 1 m above the foundation beam (see Figure 5.85). These cracks were expected to occur on the concave side of the wall only because the wall tended to stretch out when subjected to tension. The extreme tension fibre tended to straighten when subjected to tension producing tensile cracks on the concrete surface of the wall.

The height of cracking increased to 1.7 m above the foundation beam when the applied force of $0.62P_n$ was reached. More cracks appeared only on the concave side of the wall.

Once the force of $0.75P_n$ was applied, the cracks above lap splice region commenced to incline diagonally towards the construction joint. The yielding of the starter bars at the connection was detected by the installed strain gauges. At this stage, the height of cracking was approximately 2 m above the foundation beam (see Figure 5.86).

At $\mu_\Delta = +1\times1$, vertical cracks which located at the position of the starter bars became visible. The horizontal joint started to open up from the extreme tension edge to approximately 1 mm.

There were not a lot of cracks initiated or extended after the panel reached $\mu_\Delta = +1.5\times2$. However, the crack along the horizontal joint happened to be approximately 2 mm.

More diagonal cracks had developed near the region where the starter bars were located at $\mu_\Delta = +2\times1$. An identical crack pattern had formed at the other end of the wall when subjected to the same level applied forces in the opposite direction.

At $\mu_\Delta = +2.5\times1$, the existing cracks which located above the lap splice region started to become wider due to the spreading of plasticity in the longitudinal reinforcement (see Figures 5.87 and 5.88).

The twisting at the wall-foundation connection commenced when $\mu_\Delta = +3\times1$ was reached (see Figure 5.89). The extreme compression edge (West edge) twisted in the anti-clockwise direction. The horizontal crack along the joint was widely opened with 5 mm gap.

When approaching μ_Δ = -3.5×1, the concrete spalled under the compression stress (see Figure 5.90). The magnitude of twisting became rather significant especially when subjected to the repetition of the same displacement ductility level.

On going from μ_Δ = -3.5×1 to μ_Δ = +5×1, the out-of-plane displacement measured at the height of 1.8 m above the foundation beam was approximately 11 mm. The out-of-plane displacement on the compression edge of the wall was measured to be between 10 mm to 35 mm under the twisting action at the base (see Figures 5.91 to 5.94).

All the starter bars on the tension edge (East edge) of the wall were ruptured when μ_Δ= +5.5×1 was reached (see Figure 5.95). There were many vertical splitting cracks along the length of the lap splice. A diagonal crack appeared only on the convex side of the wall (see Figure 5.97).

At the end of the test, it was noticed that most cracks were concentrated in the region next to the wall-foundation connection. There was very a small number of cracks in the top half of the wall (see Figures 5.96 to 5.99).

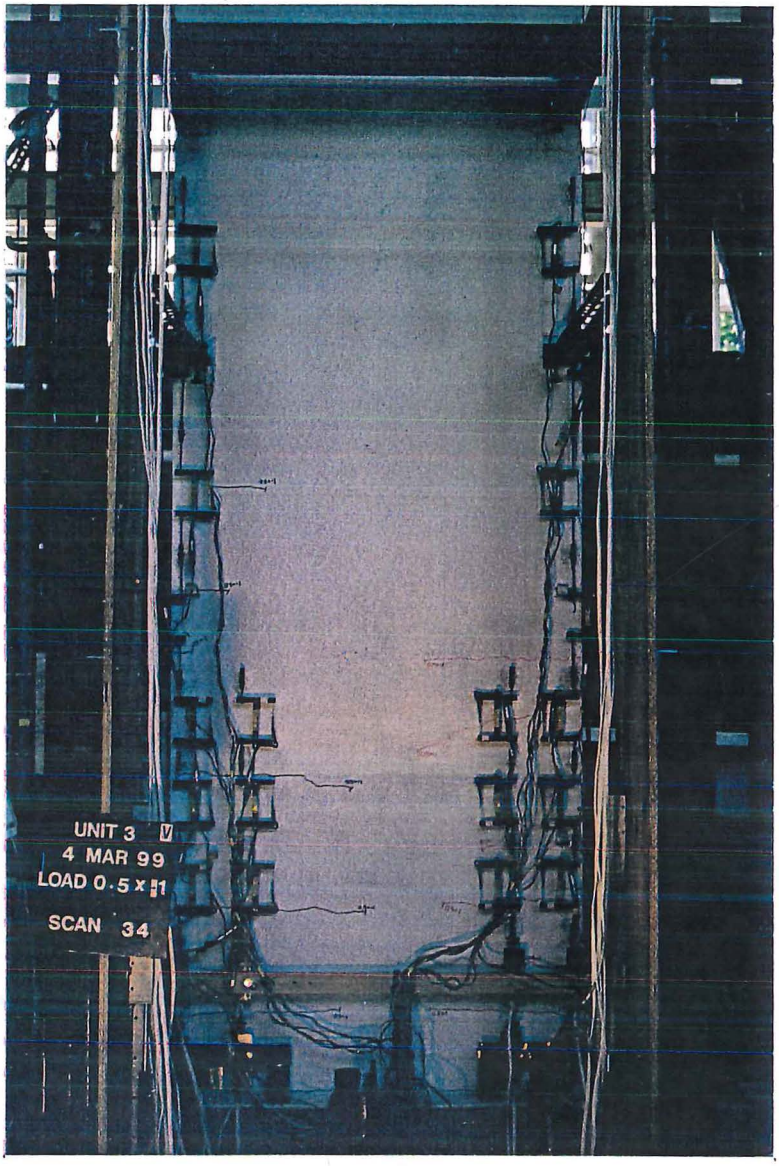

Figure 5.85: View of Unit 3 at cracking strength (South/Concave)

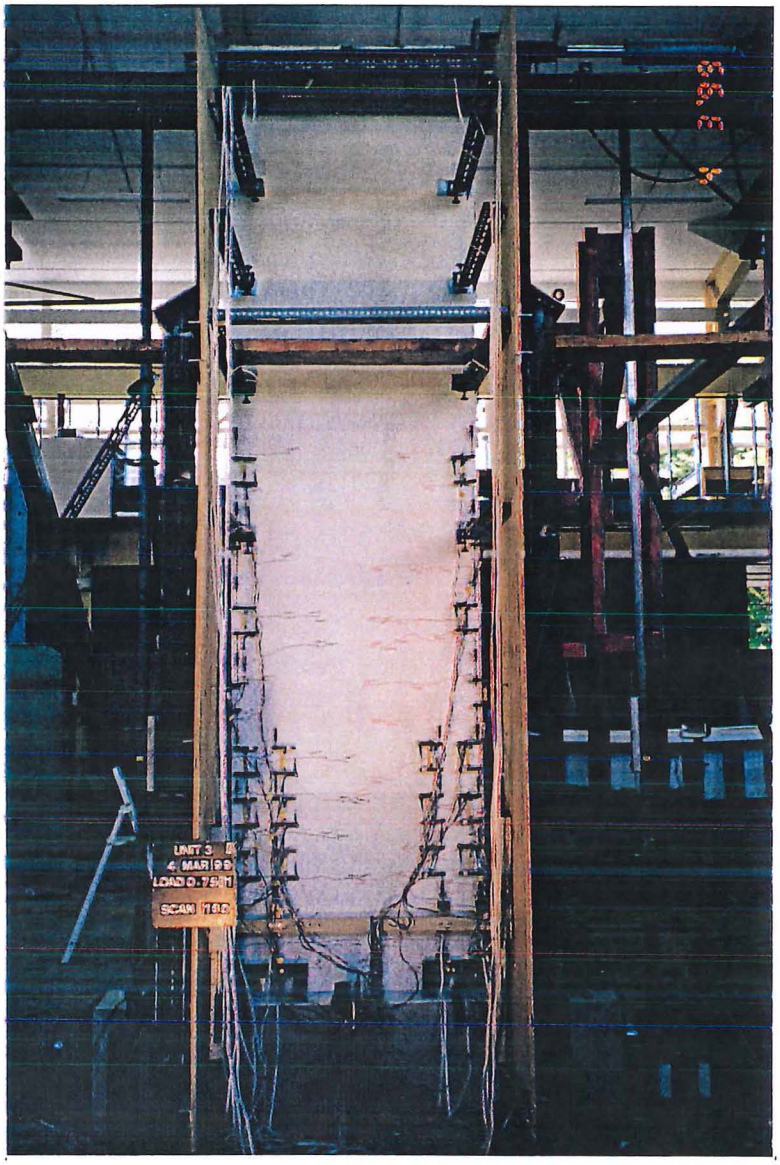

Figure 5.86: View of Unit 3: first yield at positive direction loading (South/Concave)

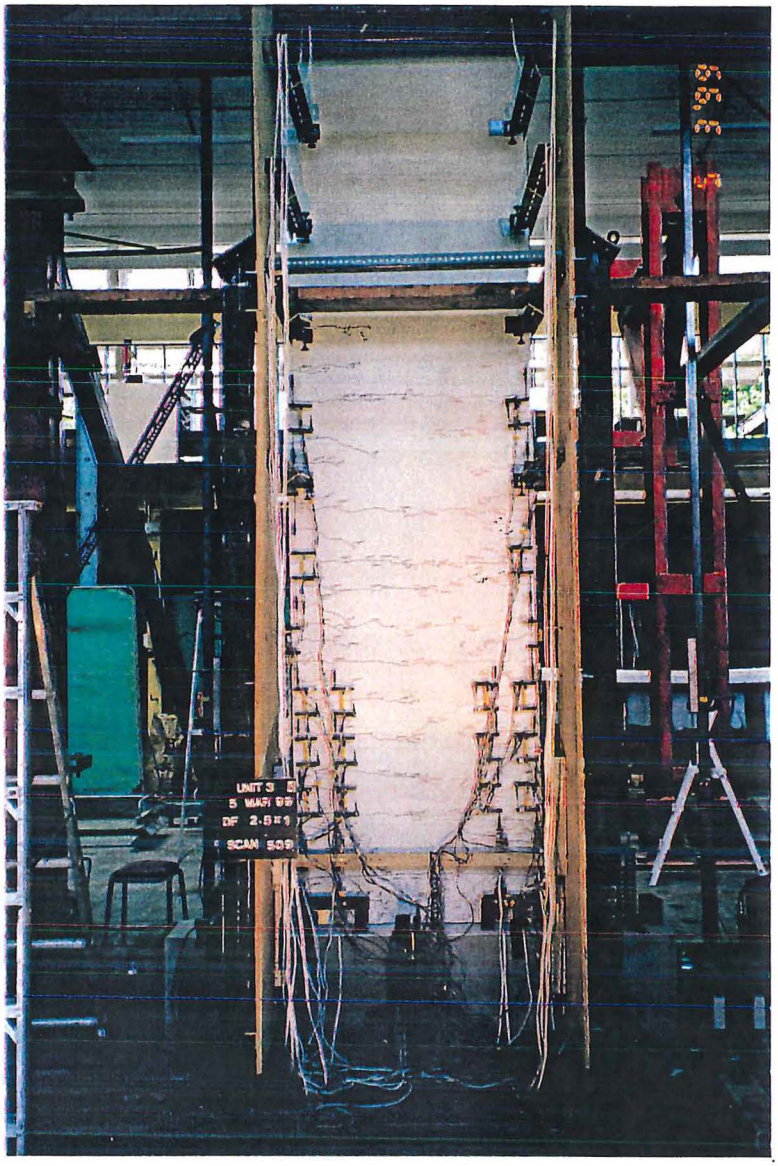

Figure 5.87: View of Unit 3 at μ_Δ = +2.5×1 (South/Concave)

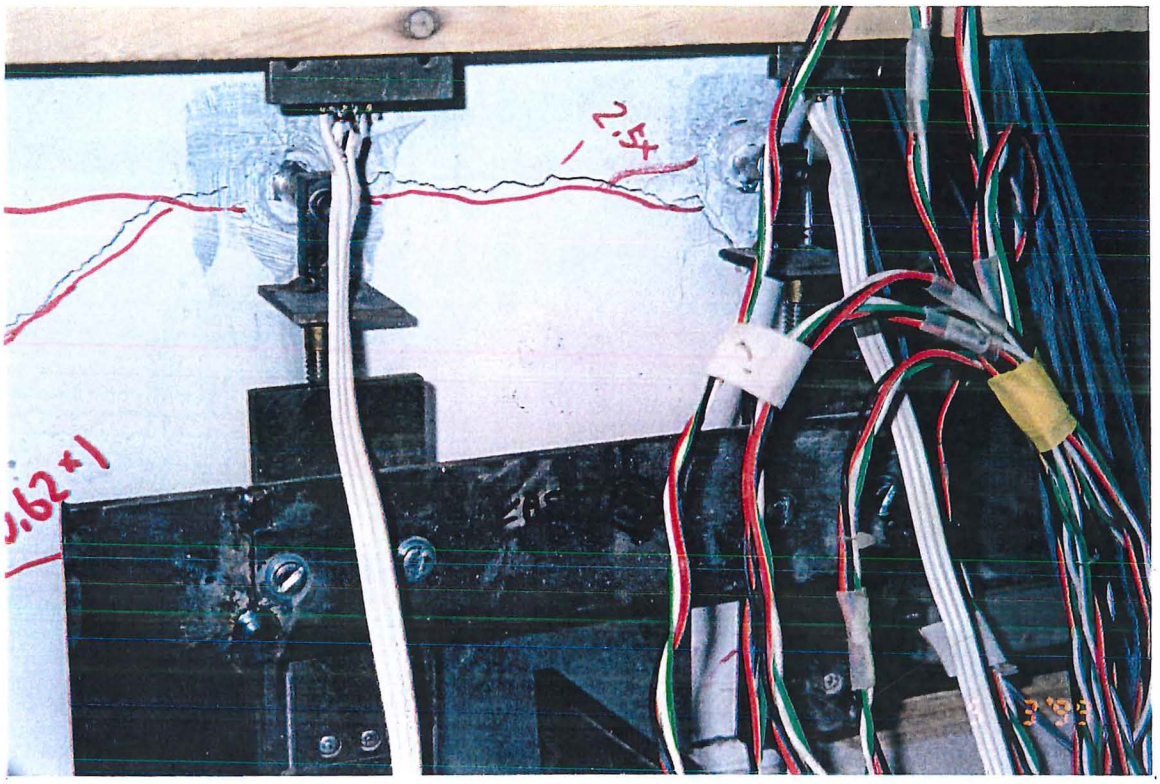

Figure 5.88: Unit 3: Cracking above lap splice due to the spreading of plasticity (South/Concave)

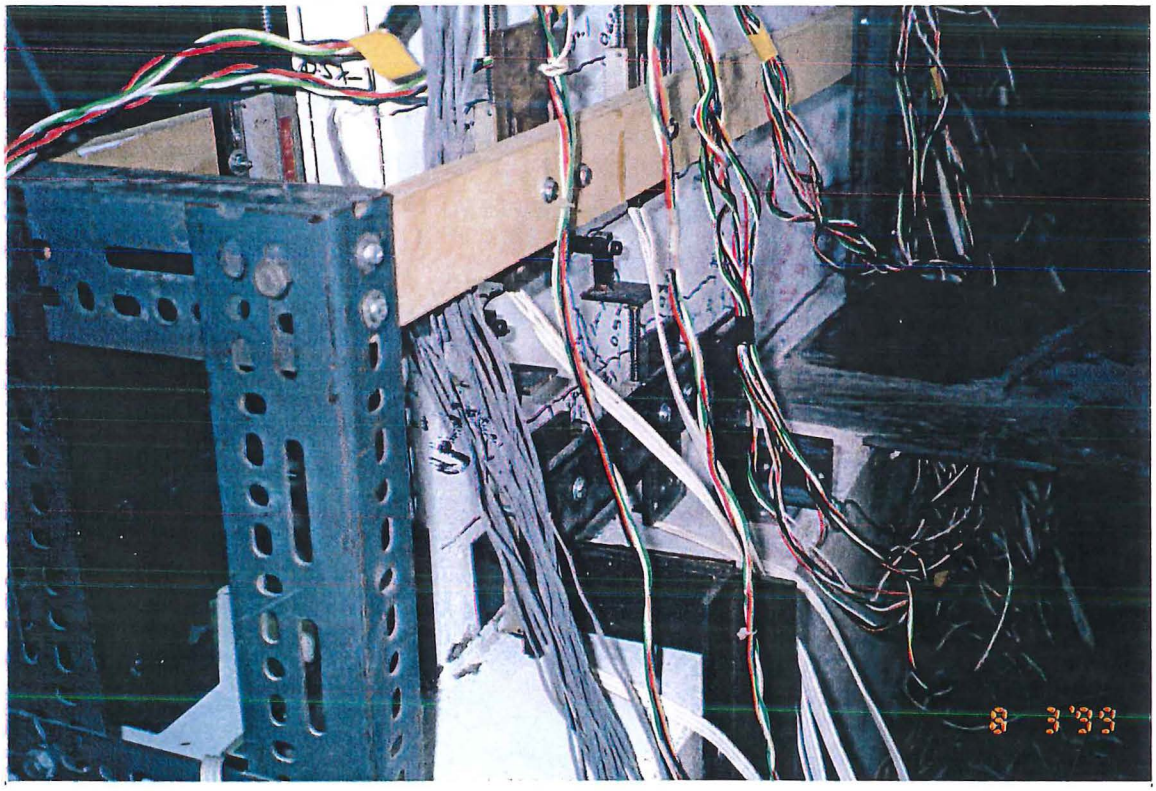

Figure 5.89: Unit 3: Twisting started along the horizontal joint at μ_Δ = +3×1 (West edge)

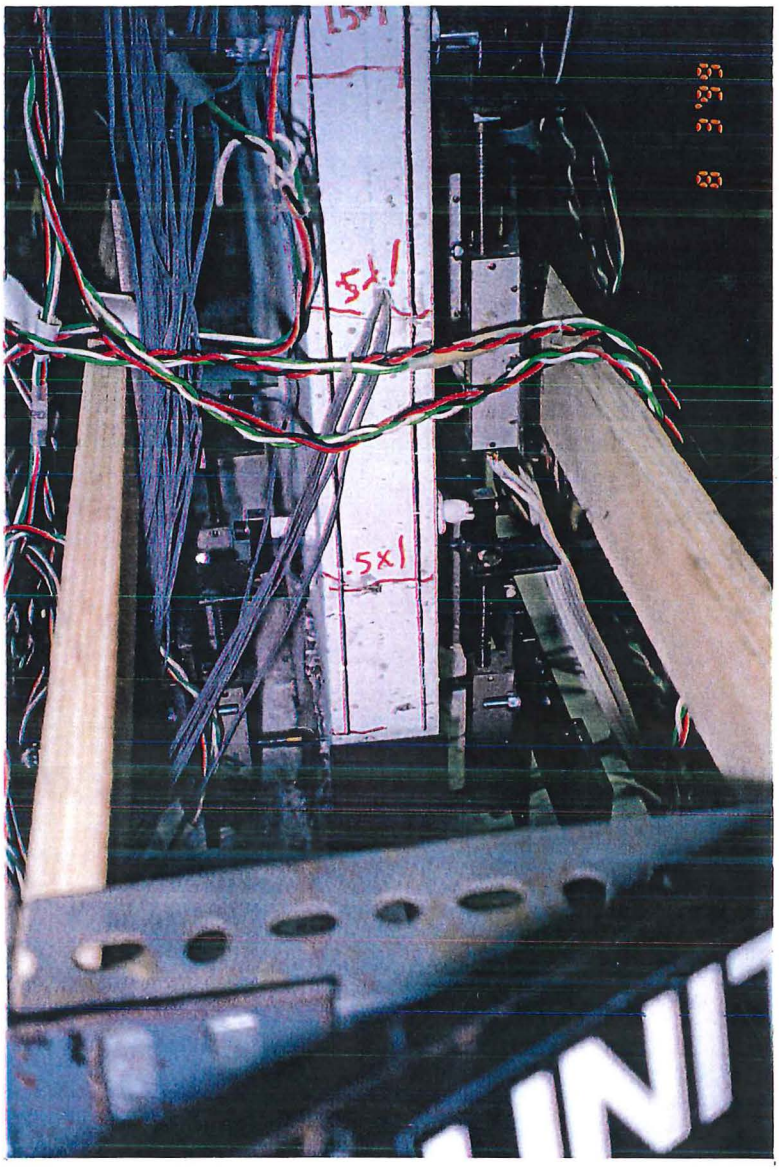

Figure 5.90: Unit 3: Spalling of concrete due to twisting action at μ_Δ = -3.5×1 (East edge)

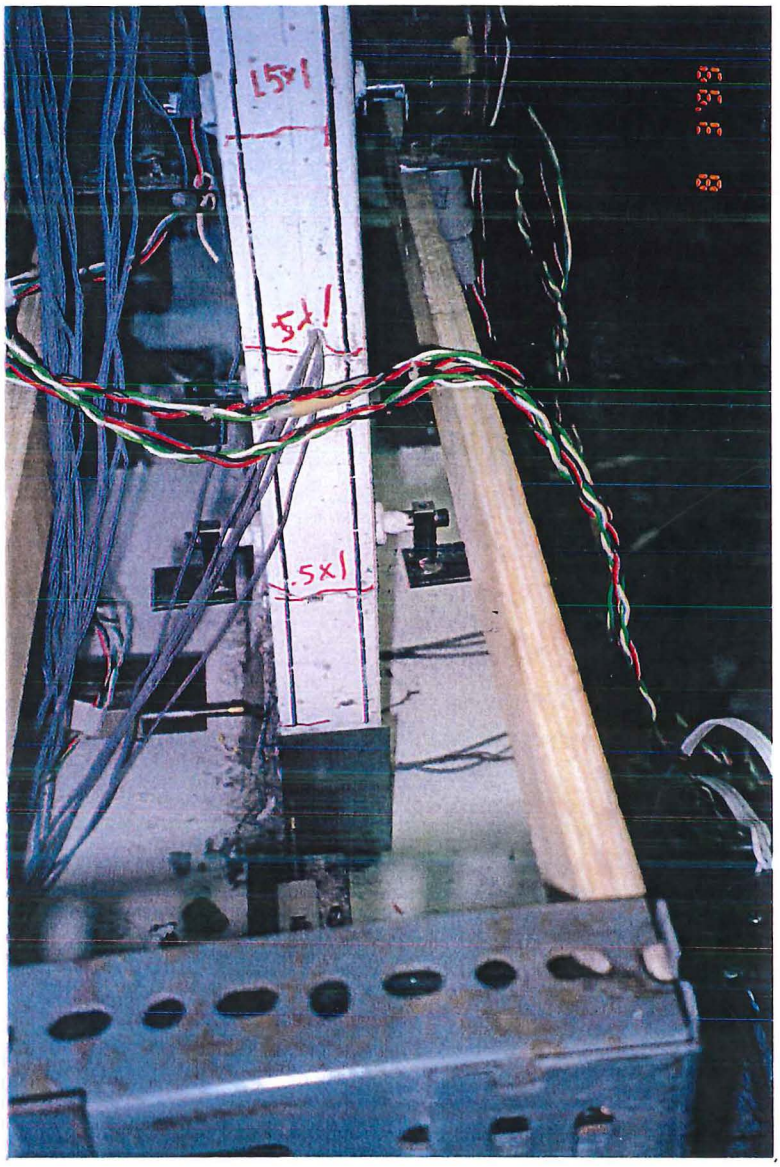

Figure 5.91: Unit 3: Twisting of the base at μ_Δ = +4×1 (East edge)

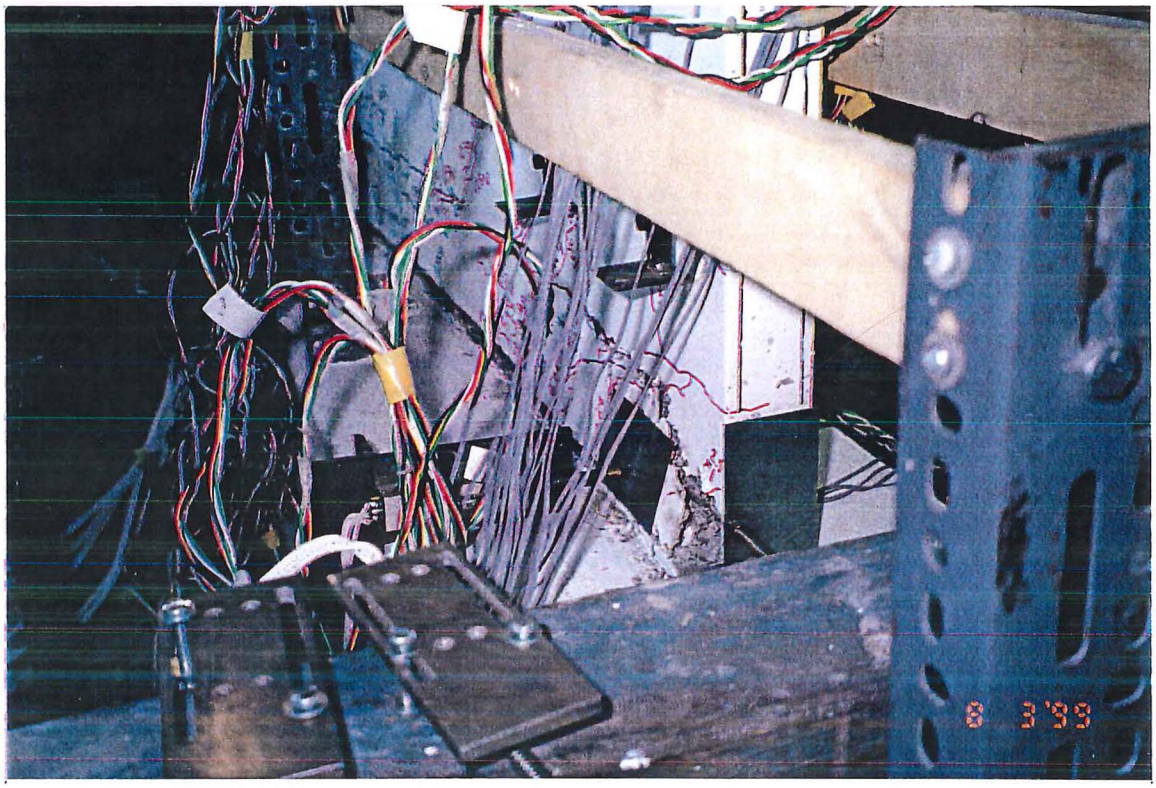

Figure 5.92: Unit 3: Compression concrete spalled at μ_Δ= -4×1 (East edge)

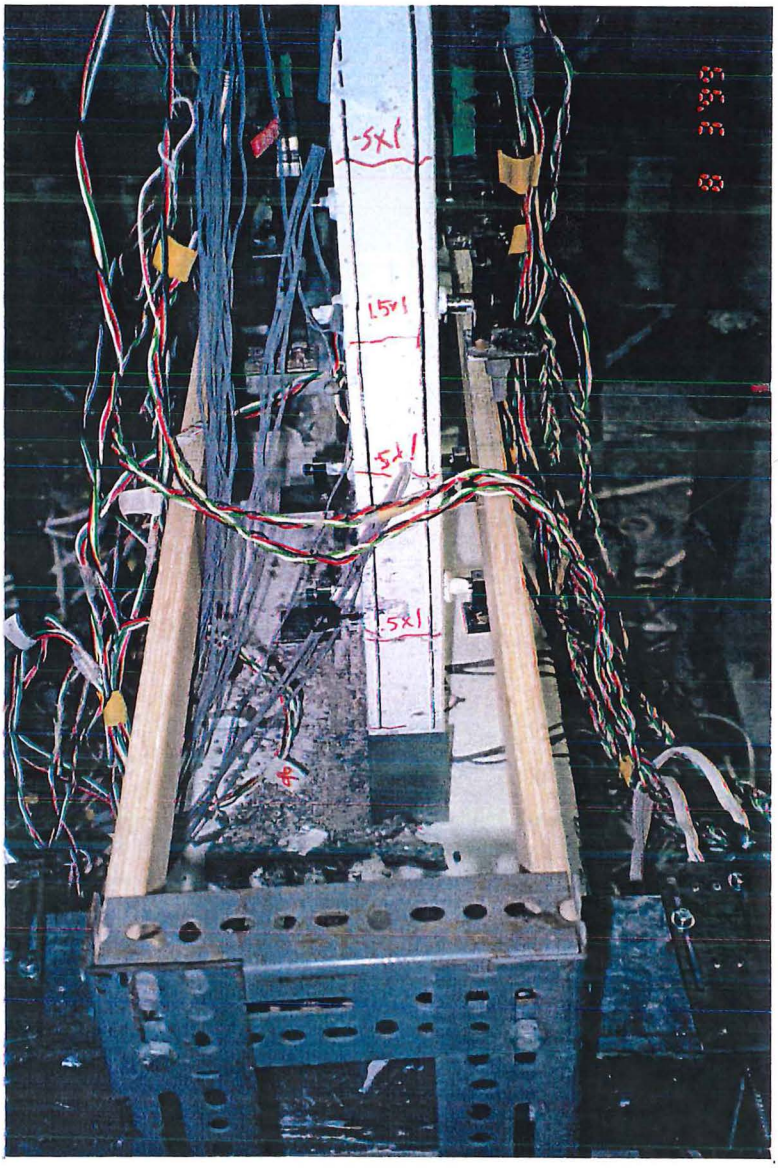

Figure 5.93: Unit 3: Compression concrete spalled at μ_Δ = -4.5×1 (East edge)

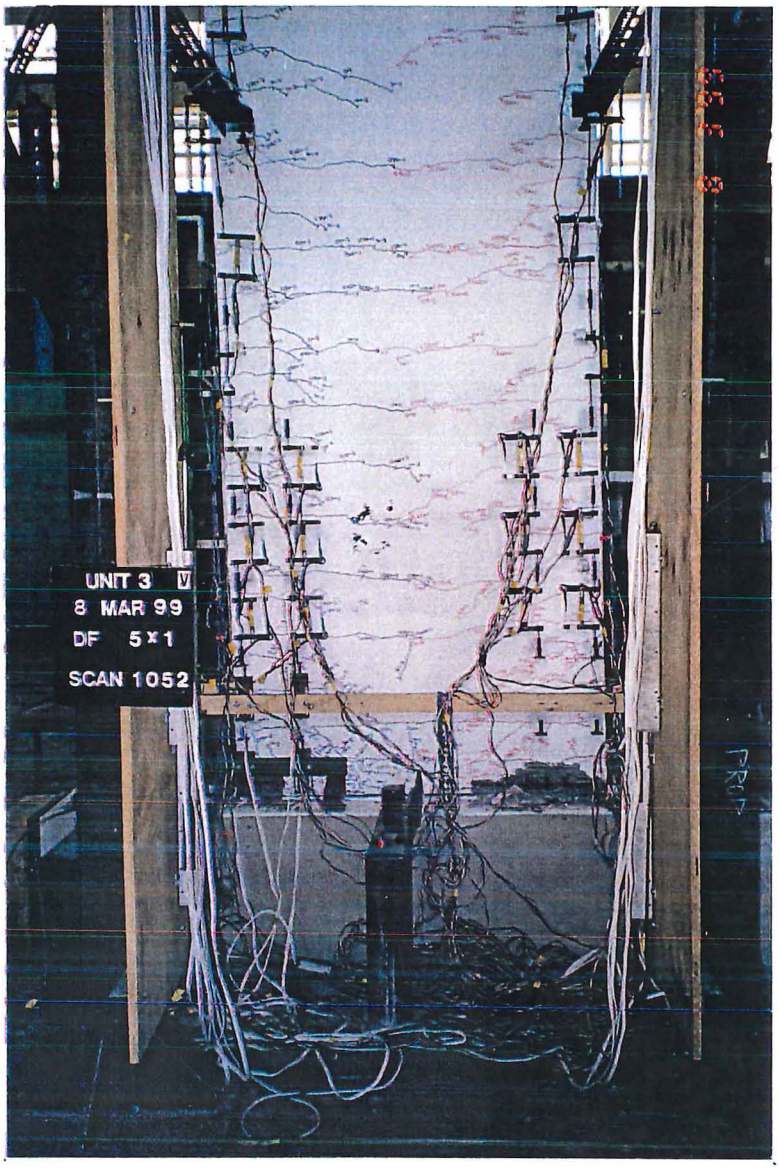

Figure 5.94: Cracking pattern of Unit 3 at μ_Δ = +5×1 (South/Concave)

Figure 5.95: Unit 3: Fracturing of the tension starter bars at μ_Δ = +5.5×1 (South/Concave)

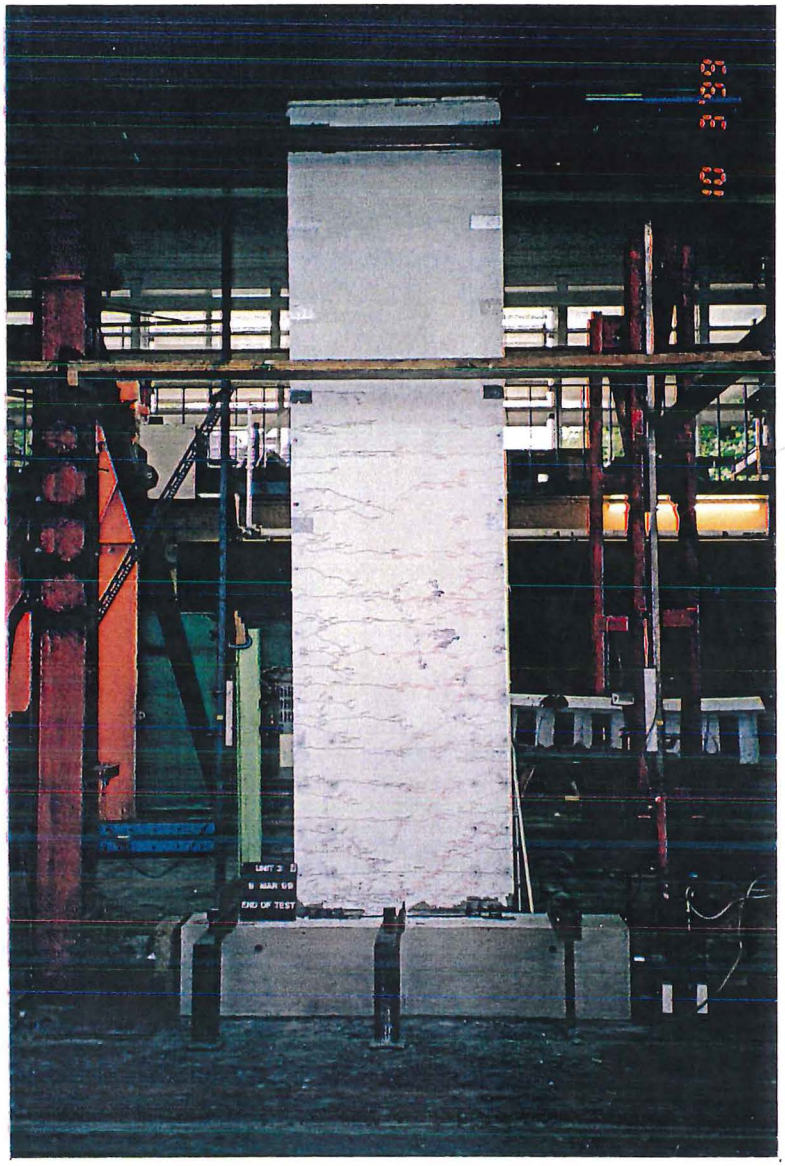

Figure 5.96: Unit 3: Overall cracking pattern on the South/Concave side at the end of test

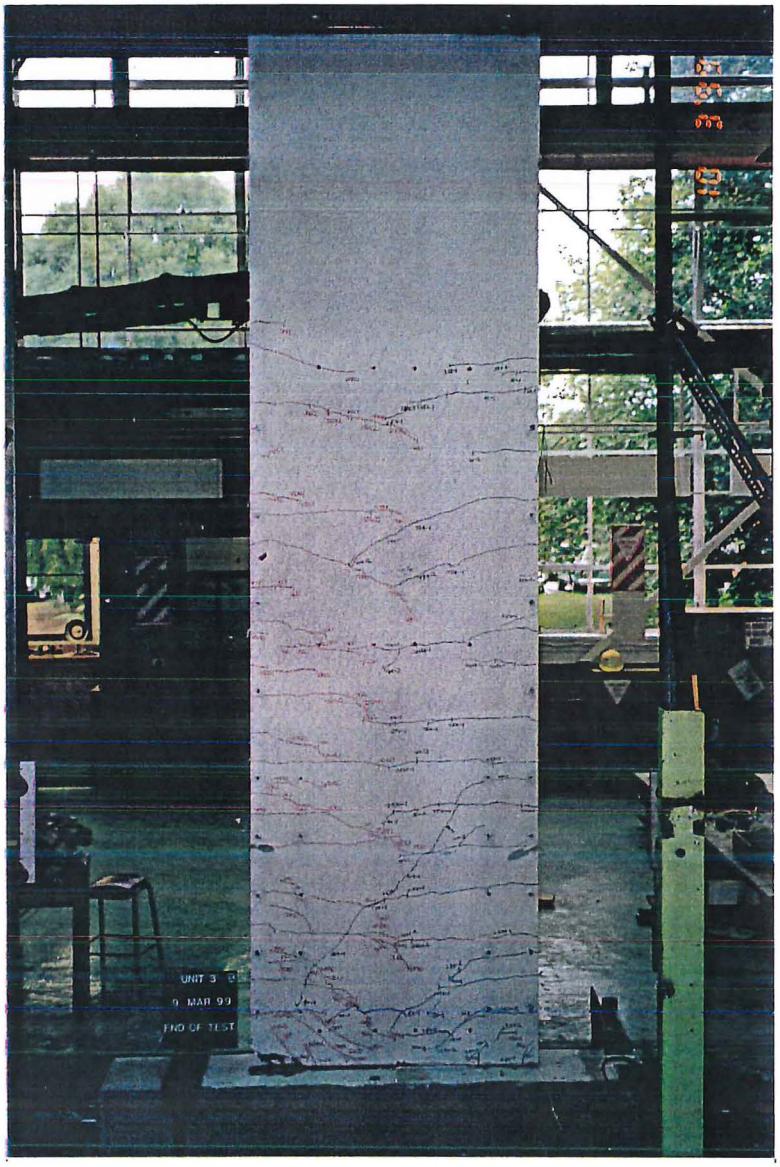

Figure 5.97: Unit 3: Overall cracking pattern on the North/Convex side at the end of test

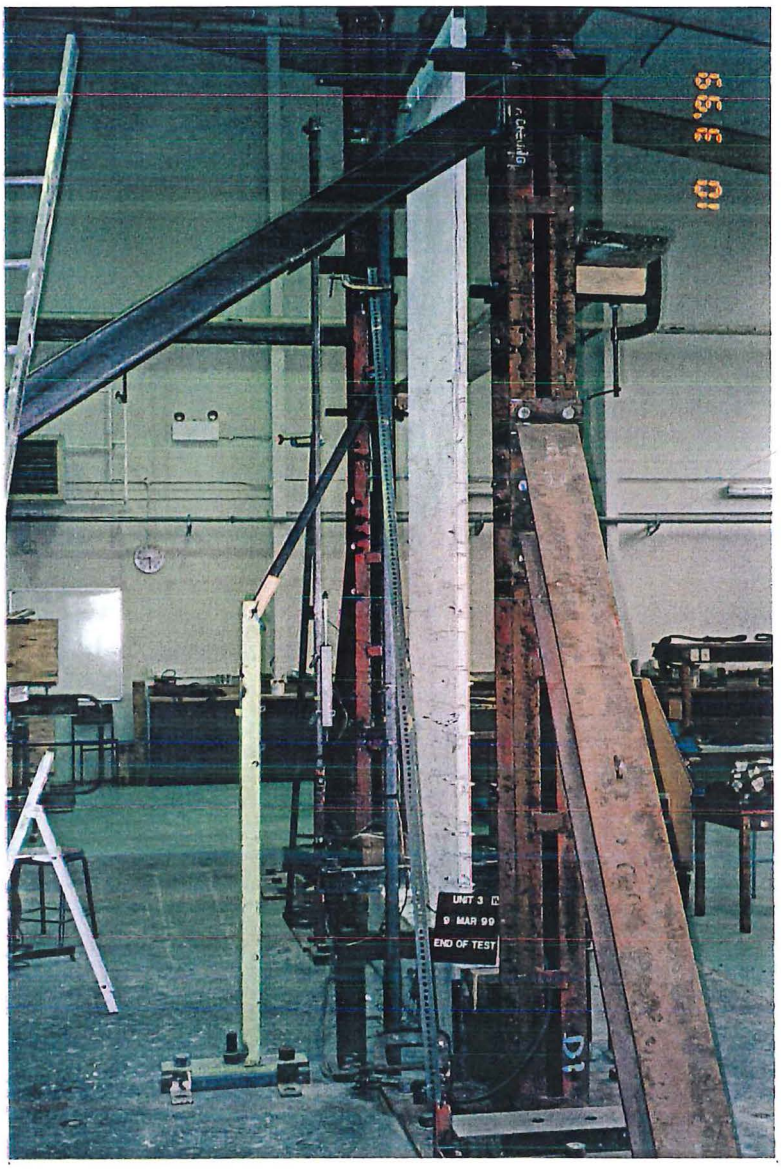

Figure 5.98: Unit 3: West edge view at the end of test

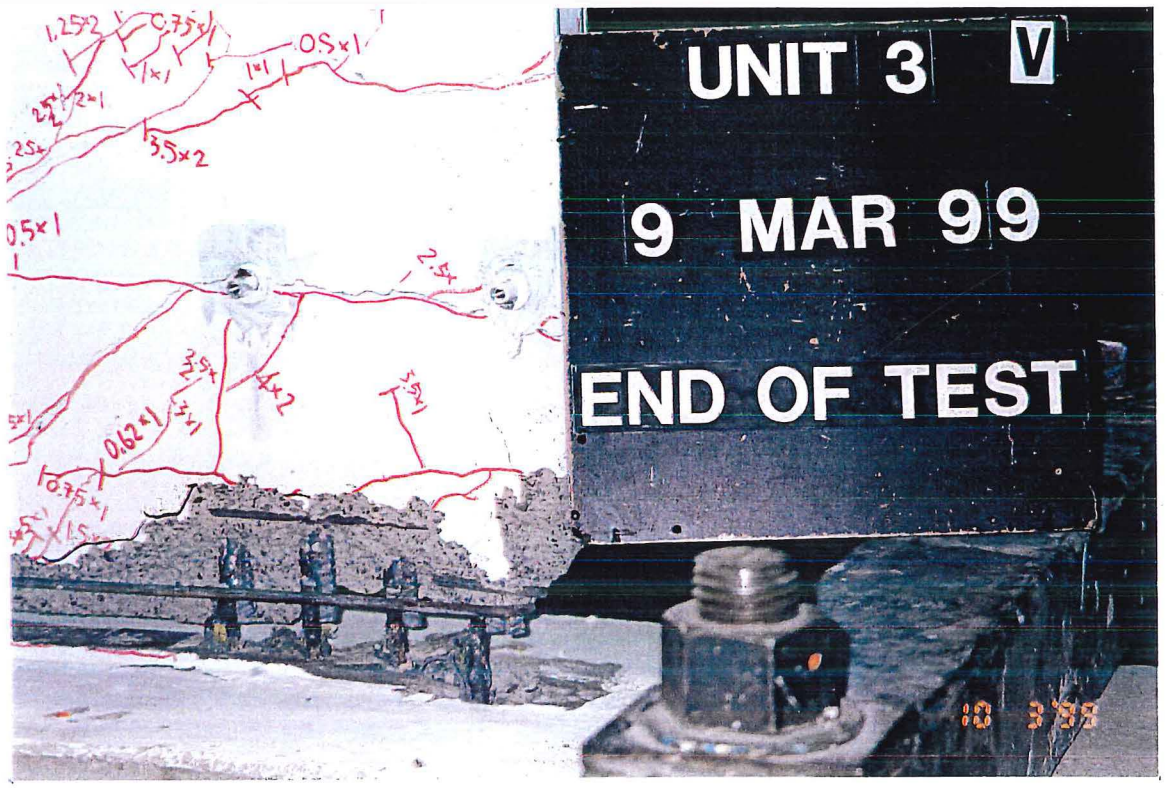

Figure 5.99: Unit 3: Close-up view of fractured starter bars at the end of test (South/Concave)

5.3.3 Analysis of Experimental Results : Unit 3

5.3.3.1 Lateral Force-Lateral Displacement Response : Unit 3

The load-displacement response in Figure 5.100 shows a very good performance of this test specimen under the applied lateral force. The actual maximum flexural capacity was 100.9 kNm which was 15.1% higher than the theoretical nominal flexural capacity. This consequence was the result of overstrength which caused by strain hardening of the reinforcement at the wall-foundation connection. The welding between the starter bars and the longitudinal reinforcement also clearly enhances the flexural strength of the wall-foundation connection. The flexural capacity of the wall dropped down to 80% of the nominal flexural capacity when the applied displacement was equivalent to μ_Δ = -3.5×1. The theoretical moment-curvature curves, plotted in Figure 5.101, represent the behaviour estimated assuming a monotonic loading in each direction.

Unit 3 curves compared to Unit 1, has significantly better performance (flexural strength, energy dissipation and ductility); compare Figures 5.100 and 5.101 to Figures 5.15 and 5.16. In Figure 5.100, the flexural capacity was dropped rapidly, caused by the rupture of starter bars that occurred during the approach of μ_Δ = +5.5×2.

5.3.3.2 Out-of-Plane Displacements : Unit 3

The maximum out-of-plane movement was predicted to occur in the region above the lap splice where the yielding of the longitudinal reinforcement took place due to the spreading of plasticity. As yielding occurred, concrete began to loose stiffness due to a large number of cracks. When the wall was subjected to the applied force in the opposite direction, this cracked region came into compression. Consequently, the susceptibility of out-of-plane buckling increased.

The actual out-of-plane movement of the wall during the test is described in Figures 5.102 to 5.105. All the out-of-plane displacement plots represent "North face" on the right and "South face" on the left. The wall tended to stretch out on the tension edge causing some horizontal cracking on the concave side tension edge of the wall only.

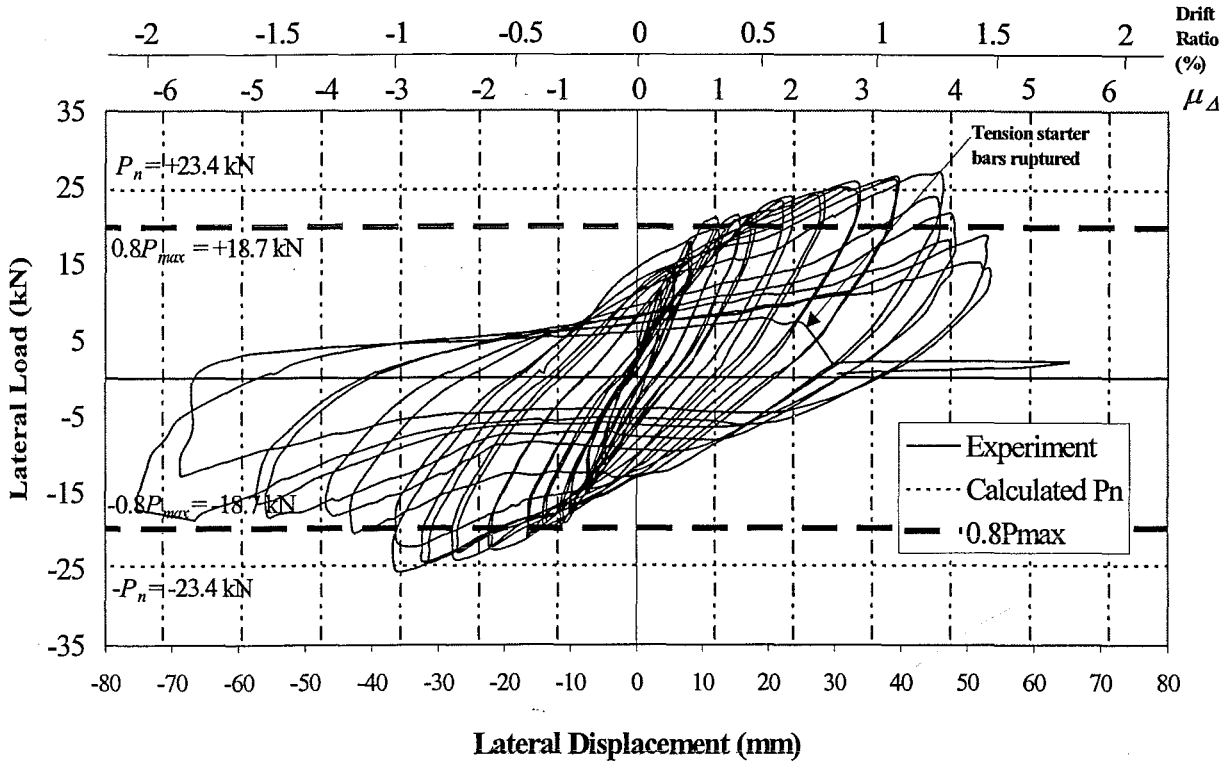

Figure 5.100: In-plane lateral load-lateral displacement response of Unit 3

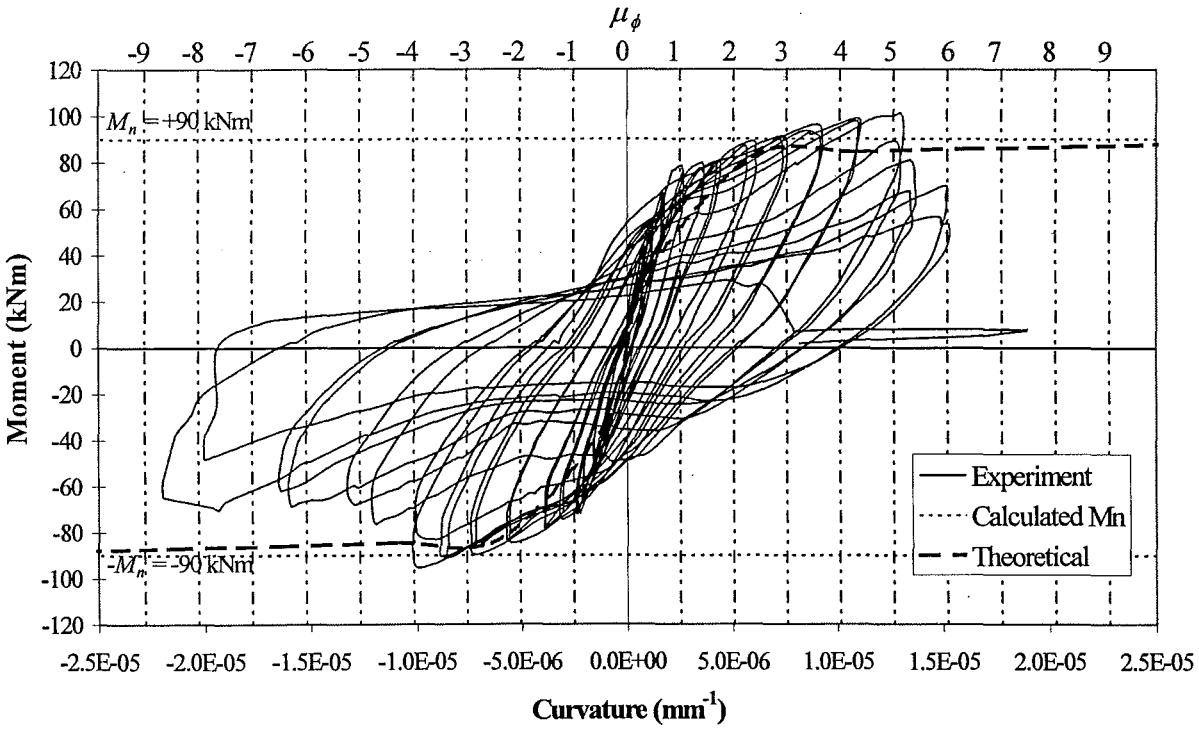

Figure 5101: Moment-curvature response of Unit 3

There were not significant out-of-plane movements occurring on the tension edges of the wall. Although Figure 5.102 shows the measured out-of-plane of 5.5 mm and 8.5 mm at the base when the wall when subjected to μ_Δ= +4×1 and μ_Δ= +4.5×1 respectively, these figures were not an actual movement. The spalling of concrete at this location caused them by relocation of the instrumentation targets.

The out-of-plane movement was a maximum of 12 mm when μ_Δ= +4×1 was reached (see Figure 5.103). The deflected shape of the compression edge of the wall was a double curvature. Some movement was detected at the base at μ_Δ= +3×1 which was caused by twisting action. Most of the out-of-plane movement was taken place on the compression edge above the lap splice as predicted. The maximum out-of-plane displacement at μ_Δ= +4.5×1 was approximately 20 mm at 1 m height above the construction joint.

The East edge became subjected to compression under the negative direction loading. The profile started to change from a single to a double curvature at μ_Δ= -3×1 to μ_Δ= -4×1 where the maximum out-of-plane displacement found to be 22 mm (see Figure 5.104).

The sign of the out-of-plane displacement at the base was different between Figures 5.104 and 5.105. This indicated that twisting of the base had occurred tremendously at μ_Δ= -4×1 and μ_Δ= -4.5×1. The most critical region was found to be at approximately 1 m height above the foundation beam.

5.3.3.3 Local Bar Strains : Unit 3

The development of strains of the most extreme bar taken from East edge of the wall is demonstrated in Figure 5.106. Apparently, the strains in the starter bar approached its yield strains at approximately $0.75P_n$. Once the first yield capacity was reached, the strain gauge data became out of range and unusable due to the damage probably occurring to the strain gauges.

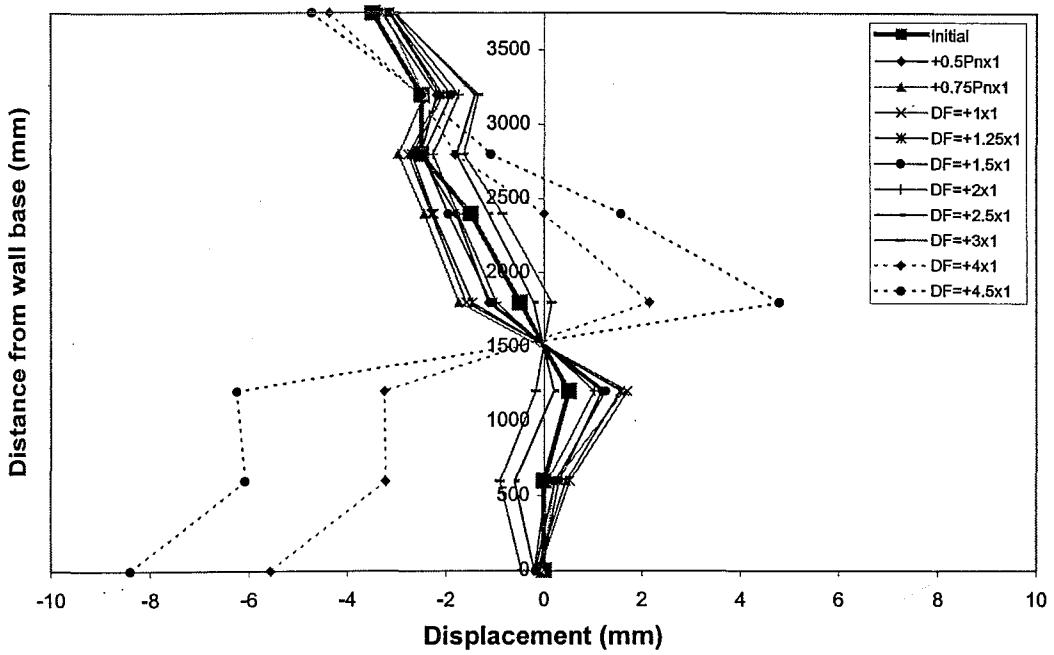

Figure 5.102: Unit 3: Out-of-plane movement on East edge of the wall at positive peak cycles (Tension edge)

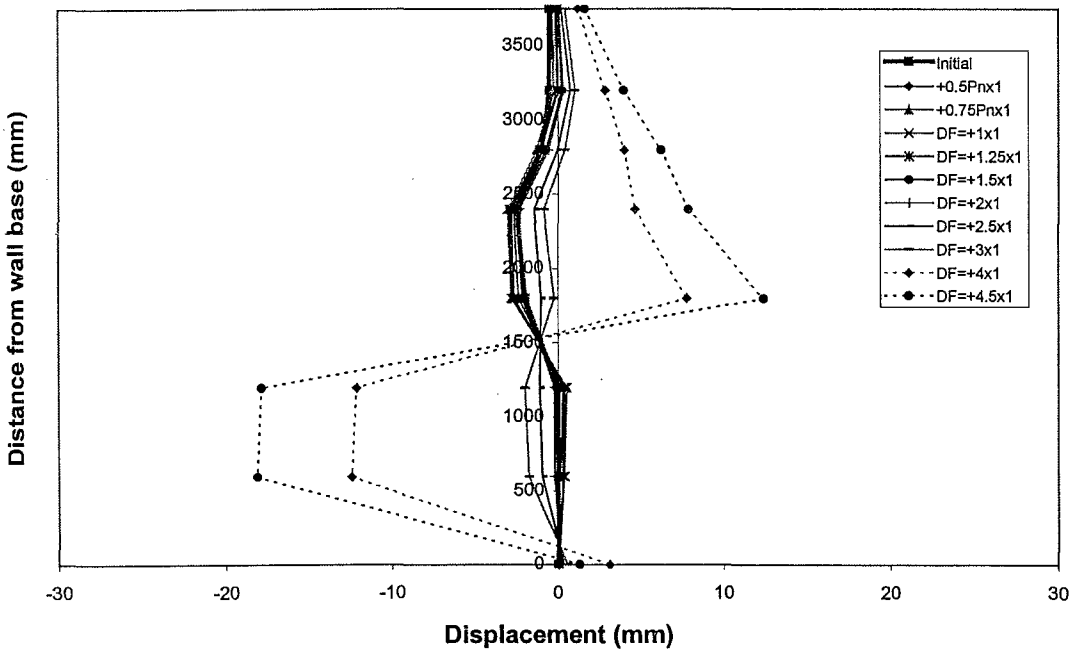

Figure 5.103: Unit 3: Out-of-plane movement on West edge of the wall at positive peak cycles (Compression edge)

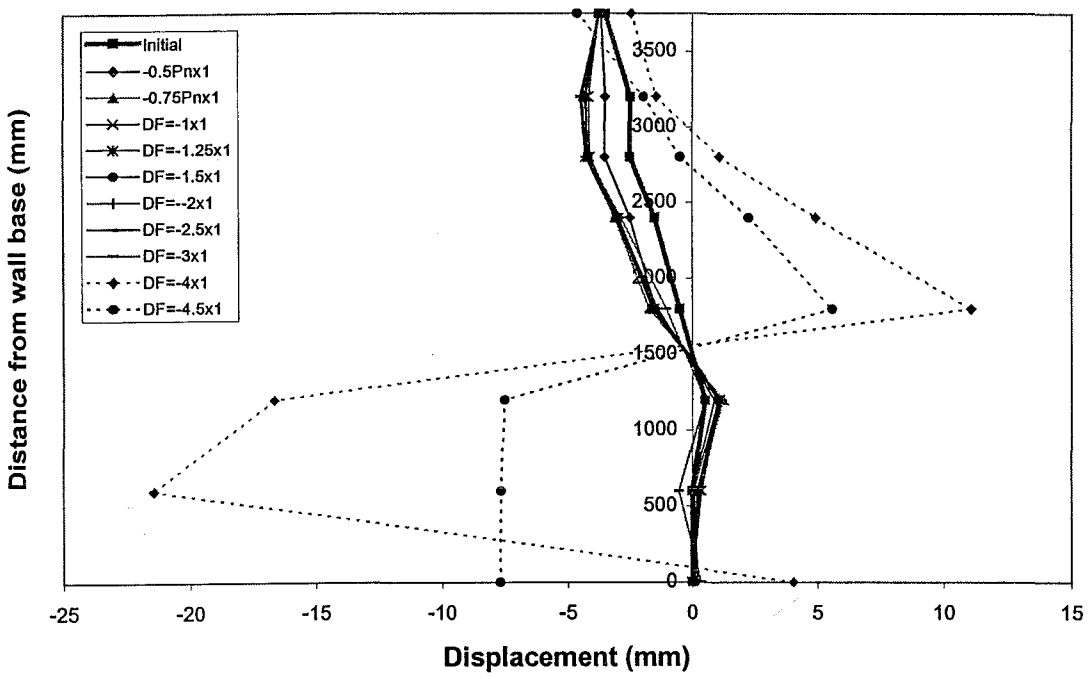

Figure 5.104: Unit 3: Out-of-plane movement on East edge of the wall at negative peak cycles (Compression edge)

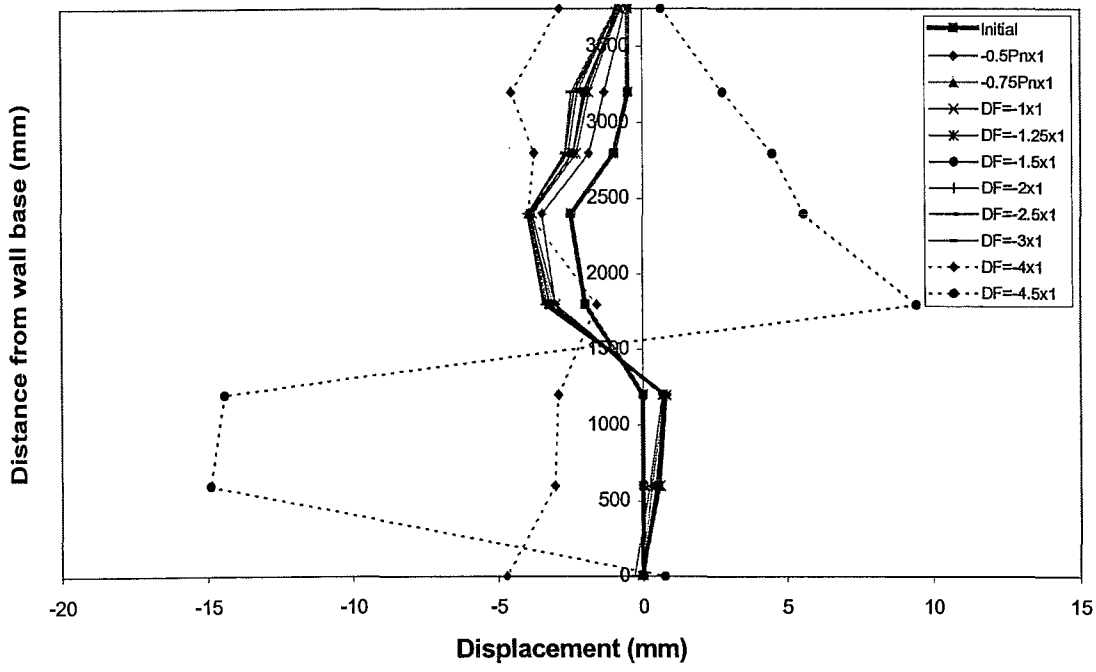

Figure 5.105: Unit 3: Out-of-plane movement on West edge of the wall at negative peak cycles (Tension edge)

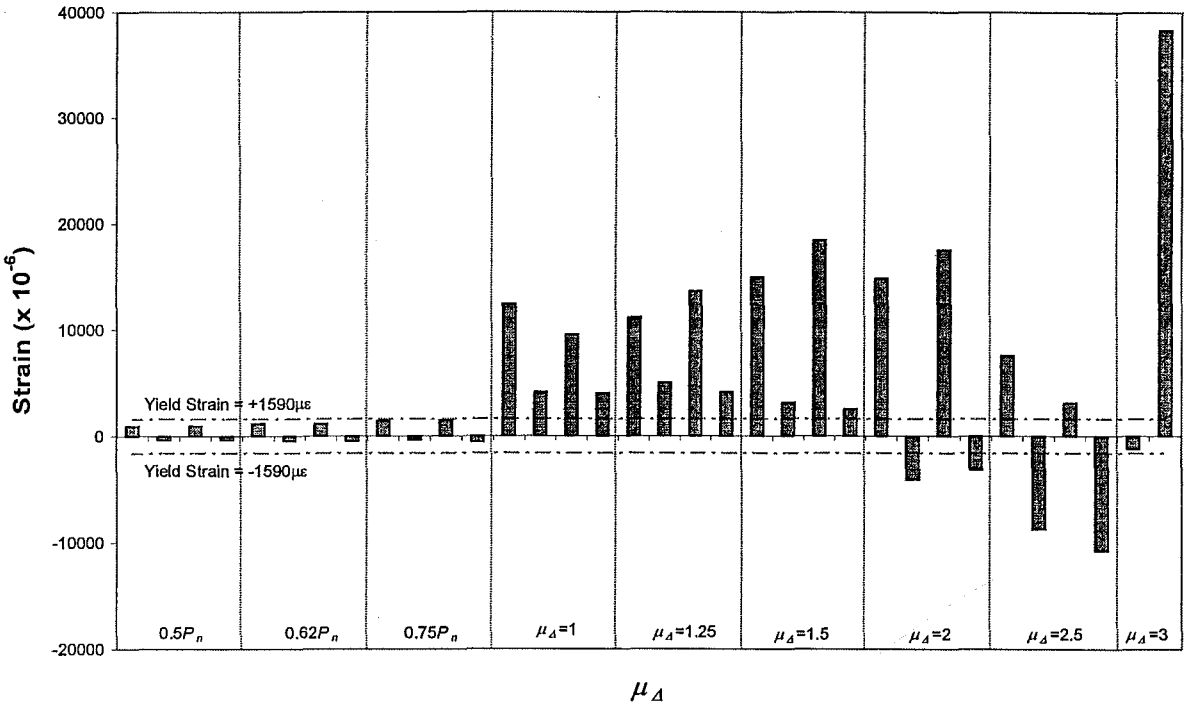

Figure 5.106: Unit 3: Strains of the outermost East edge starter bar measured at the wall-foundation interface during the test

Figure 5.107 shows the local strains in the longitudinal reinforcement on the East edge of the wall under positive cycles. It must be noted that a spread of yielding in the region immediately above lap splice occurred simultaneously with the yielding of the starter bars at the wall-foundation connection. Additionally, the yield spreading covered a larger area compared to Unit1. There was no yielding of the longitudinal reinforcement above the height of 1 m from the foundation beam or at 200 mm below the horizontal connection during the test.

Yielding of the longitudinal compression reinforcement, which was located below the base of the wall, did not occurred at any stage of testing. In Figure 5.108, there was a residual strain from tensile yielding at the wall-foundation connection which was taken place in the previous cycle (see Figure 5.107).

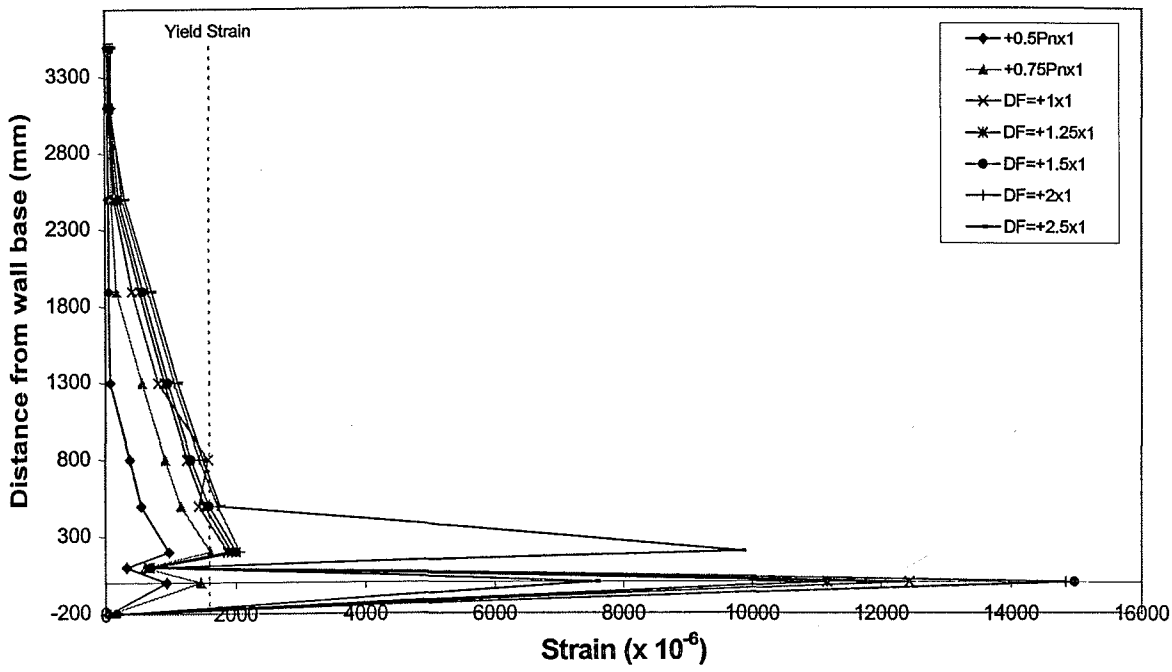

Figure 5.107: Unit 3: Outermost East edge longitudinal reinforcement strains measured at positive peak cycles (Tension edge)

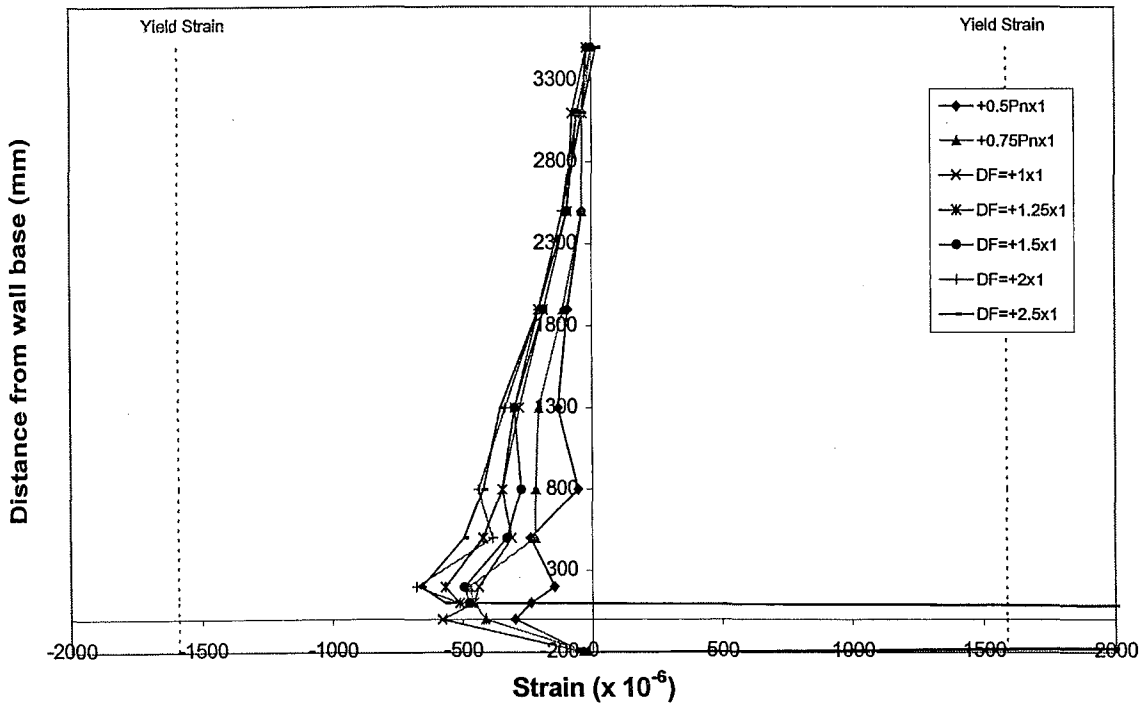

Figure 5.108: Unit 3: Outermost West edge longitudinal reinforcement strains measured at positive peak cycles (Compression edge)

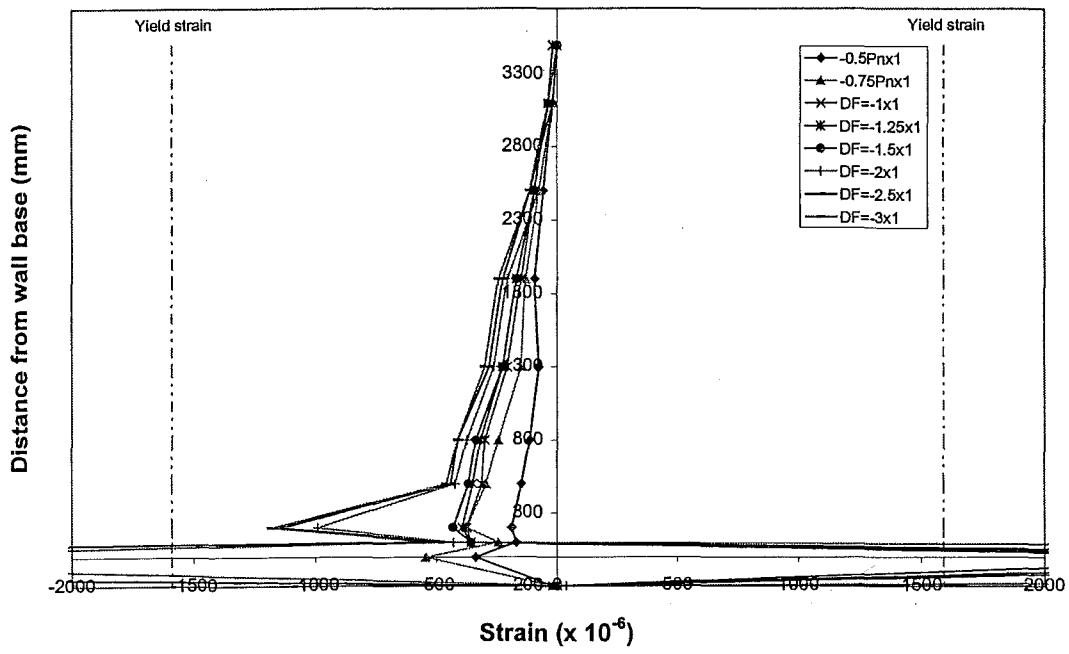

Figure 5.109: Unit 3: Outermost East edge longitudinal reinforcement strains measured at negative peak cycles (Compression edge)

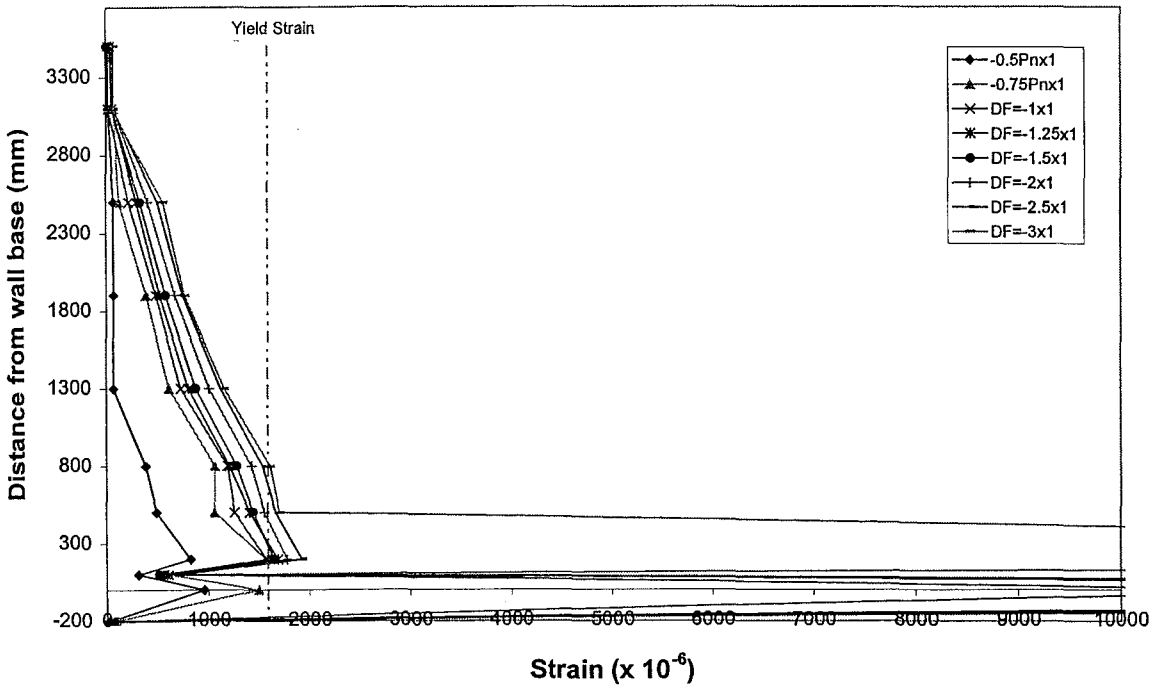

Figure 5.110: Unit 3: Outermost West edge longitudinal reinforcement strains measured at negative peak cycles (Tension edge)

Figures 5.109 and 5.110 shows the local strains of the longitudinal reinforcement when subjected to the peak negative cycles. The wall behaved exactly the same way as it was imposed by the peak positive cycles. The local strain at the position where the starter bars were terminated increased rapidly at μ_Δ = -3×1.

During elastic cycles, the starter bars at the West edge yielded in tension at $0.75P_n$ at the wall-foundation connection. The bar strains reached their yield strain as this level μ_Δ = +1×1 was approached, the starter bars became permanently elongated and the data became unusable (see Figure 5.111).

Lap splice provided an additional flexural strength to the region adjacent to the wall-foundation connection. Yielding of the longitudinal reinforcement in the area of the lap was not detected at any instance during the test. Local bar strains of the reinforcement in the lap splice region are shown in Figure 5.112. Strain profiles appear to be rather symmetrical about the vertical axis when subjected to the elastic loading in both directions. The local bar strains at the higher level of ductility were not shown because the strain gauges were damaged.

As the result of the short lap splice length, yielding of the longitudinal reinforcement in the region immediately above lap splice occurred simultaneously with the starter bars. This caused cracking of concrete on the extreme tension fibre and allowed for yield penetration to take place as the applied forces increased. In Figure 5.113, it shows the development of the longitudinal bar strain in this region when subjected to the elastic cycles. Again, the repetition of the same level of applied force tended to have an influence in the flexural strength degradation.

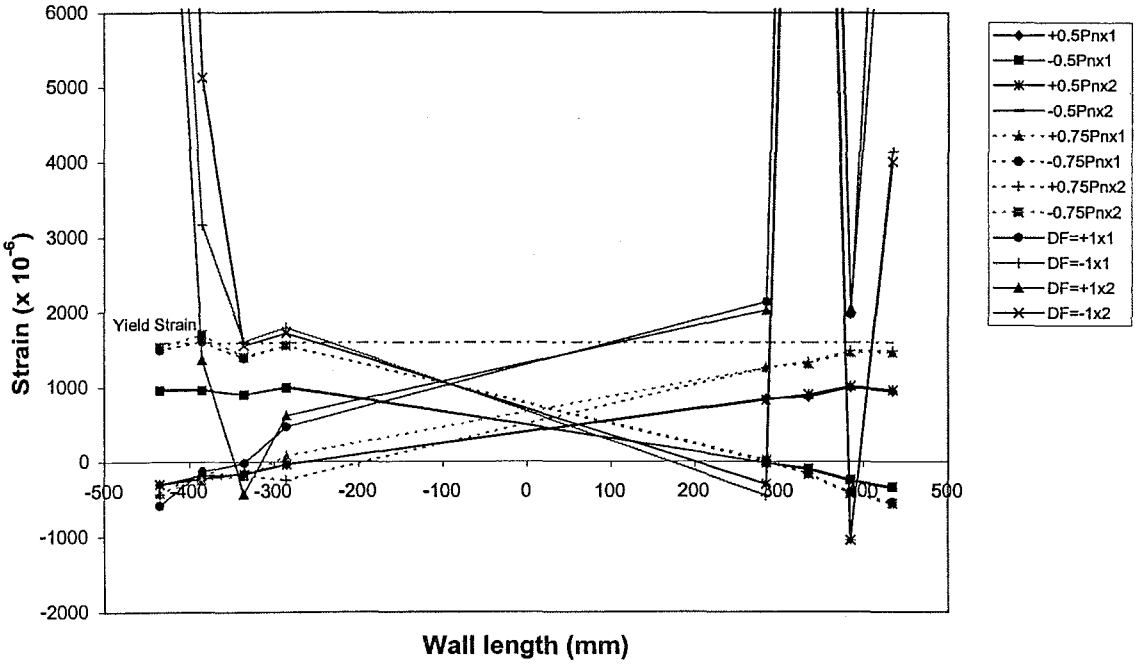

Figure 5.111: Unit 3: Strains of starter bars across the wall-foundation interface during the test

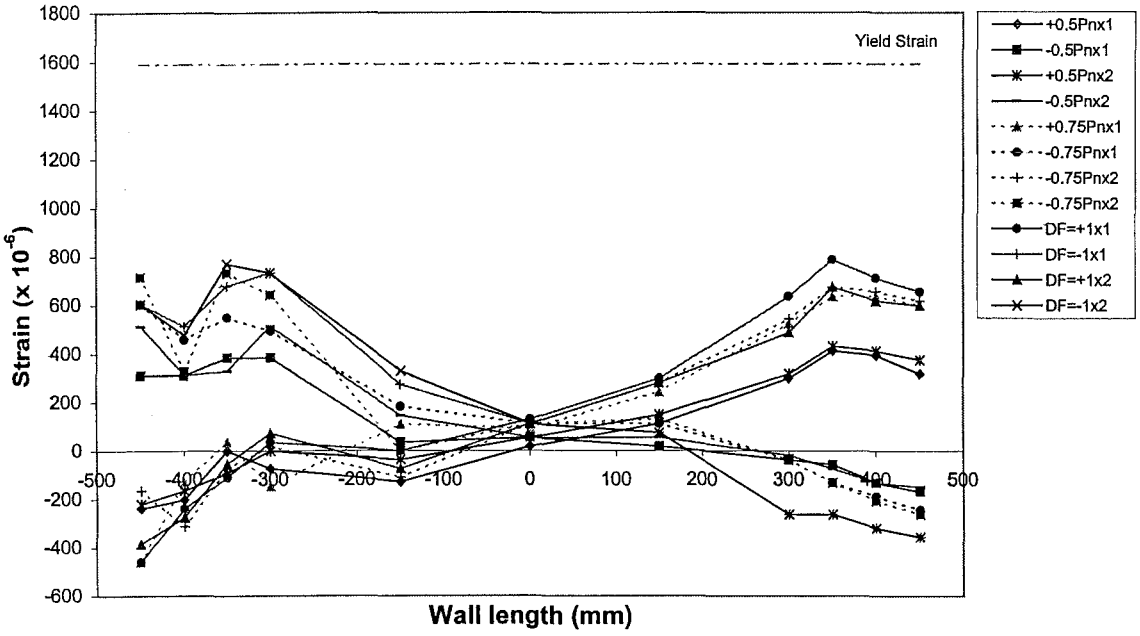

Figure 5.112: Unit 3: Strains of wall reinforcement within lap splice region (100 mm above the foundation beam) during the peak elastic cycles

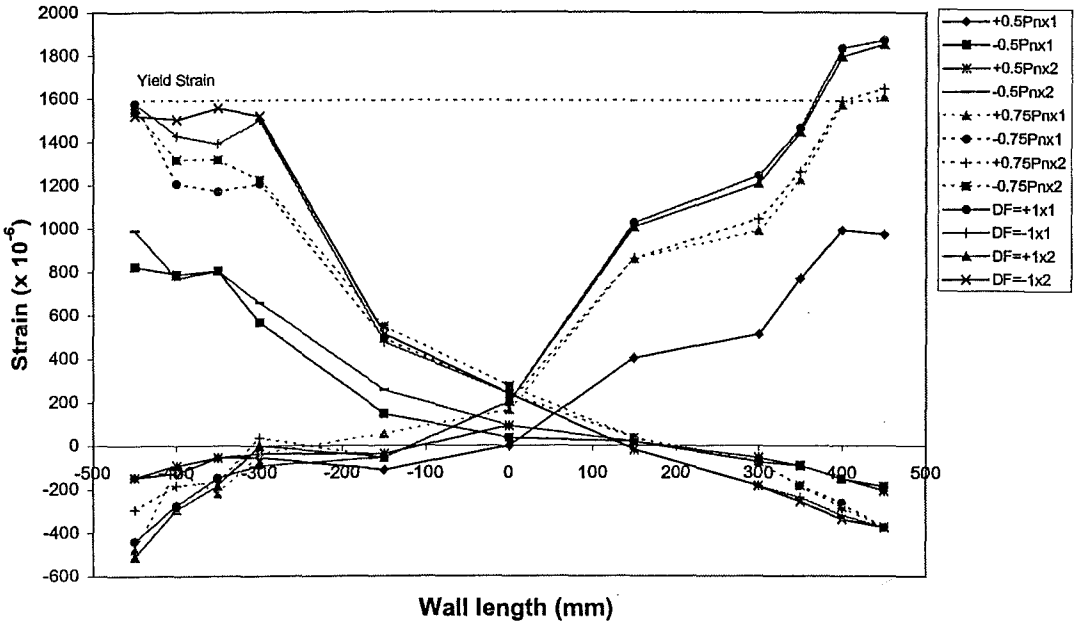

Figure 5.113: Unit 3: Strains of wall reinforcement above the region of lap splice (200 mm above the foundation beam) during the peak elastic cycles

5.3.3.4 Concrete Strains : Unit 3

Figures 5.114, 5.115, 5.118 and 5.119 illustrate concrete strain history, which was taken from two edges of the specimen, during the test. The behaviour of the test specimen was very similar to Unit 1 which that the entire panel exhibiting residual tensile strains along the construction joint. The measured concrete strain indicated that uplifting of the wall has often occurred once the test progressed beyond μ_Δ = -1×1 (see Figure 5.118).

Spalling of concrete in the compression block was found at μ_Δ = -3.5×2 with the spalling concrete strain, ε_{cu} = -0.005. Clip gauges became unusable beyond this point of testing.

The longitudinal concrete strain measured on the West edge when subjected to compression by clip gauges located at two different faces of the wall detected the out-of-plane movement about the horizontal axis (see Figure 5.114). The similar results are also shown in Figure 5.118 when the East edge was subjected to compression. The magnitude of compressive concrete strain at the wall base for both West and East

edges was greater than the measured compressive concrete strain in the region immediately above lap splice (see Figures 5.116 and 5.120).

When West edge and East edge were subjected to tension, both gauges at the wall base underwent into tension with same order of magnitude. However, the tensile concrete strain in the region immediately above lap splice was smaller than the measured longitudinal concrete strain at the wall base (see Figures 5.117 and 5.121).

In-plane curvature at the height of 200 mm above the foundation beam was measured as shown in Figure 5.122. An in-plane stiffness of the wall in the negative direction seemed to be greater than the positive direction. During the post-elastic cycles, the repetition of the same load level resulted in the lower value of in-plane curvature. Other displacement components were suspected to have some contribution on this effect.

Out-of-plane curvature was measured using clip gauges which were attached on the surface of the concrete directly opposite to each other. The maximum out-of-plane curvature on the wall panel, disregarding any rotation at the horizontal connection, occurred at approximately 1 m height from the foundation beam (see Figures 5.123 and 5.124). Softening of concrete was expected around this region that caused by the yield spreading and the overstrength.

5.3.3.5 Sectional Neutral Axis : Unit 3

During a few initial "elastic" cycles, the neutral axis at the construction joint was approximately perpendicular to the in-plane loading direction. At μ_Δ = -3×1, the position of the neutral axis started to alter and skew where the strength rapidly dropped (see Figure 5.100).

As the displacement ductility increased, the skewness of the neutral axis became very large and difficult to make an accurate prediction due to a large margin of errors induced in the measuring devices. The data, which obtained from clip gauges, were too coarse at the high displacement ductility. Therefore, the evaluation of these data was neglected beyond this point.

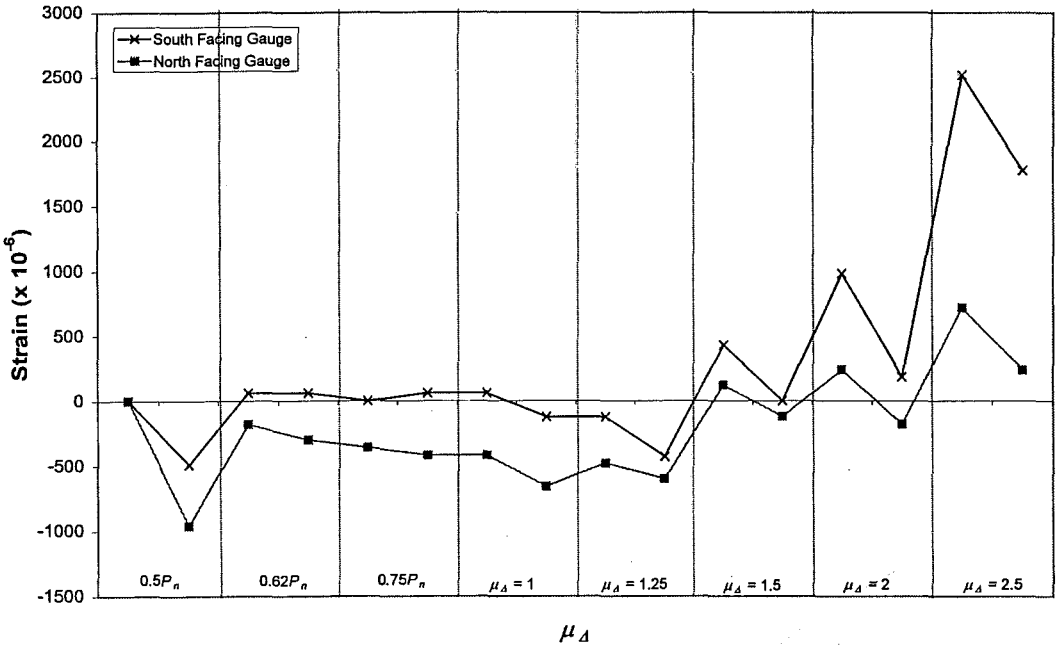

Figure 5.114: Unit 3: Concrete longitudinal strains of West edge when subjected to compression obtained from outermost clip gauges (base of wall)

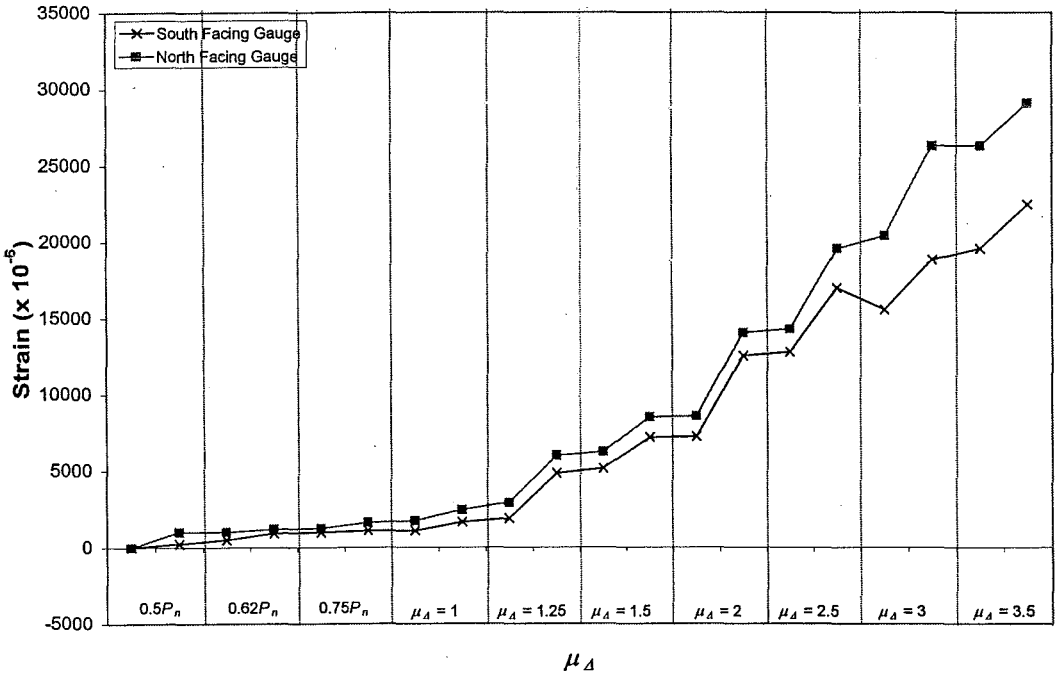

Figure 5.115: Unit 3: Concrete longitudinal strains of West edge when subjected to tension obtained from outermost clip gauges (base of wall)

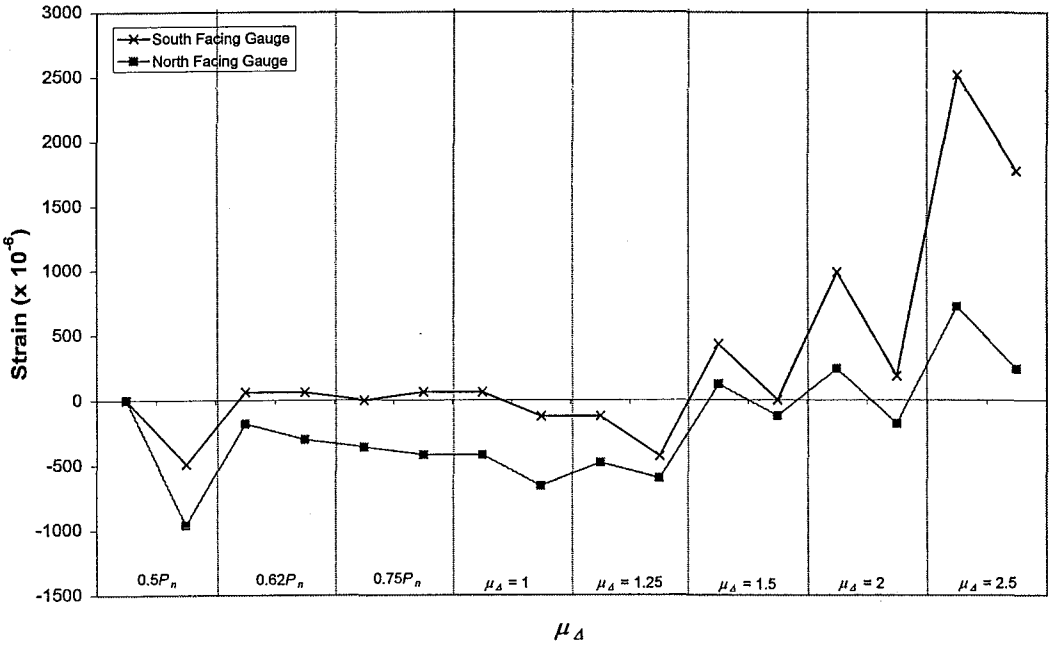

(a) Wall base

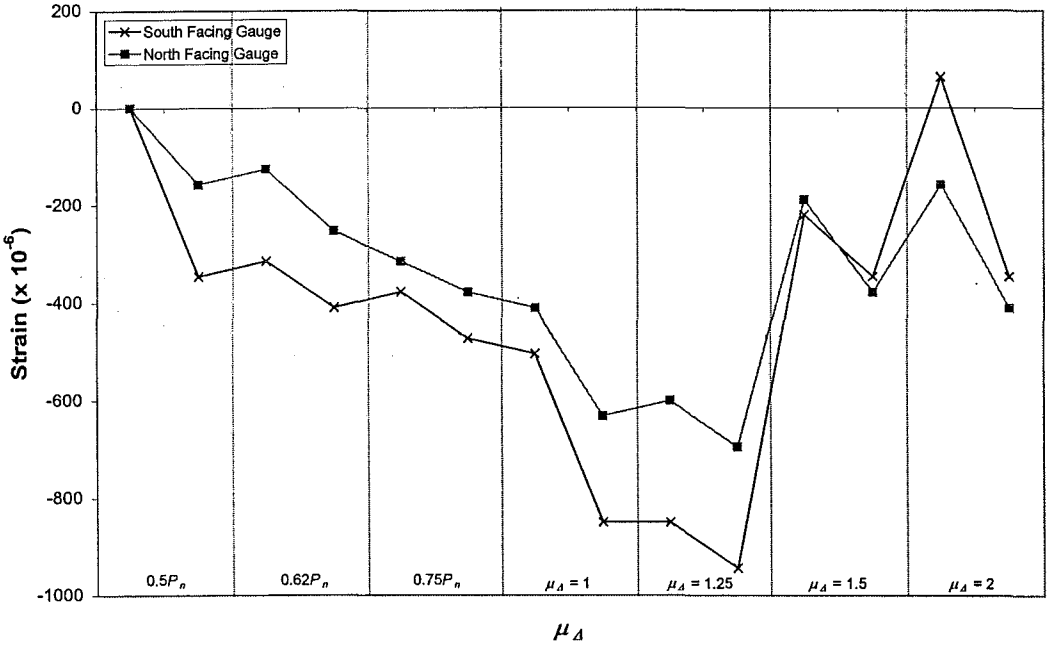

(b) Immediately above lap splice

Figure 5.116: Unit 3: Difference in concrete strains in West edge when subjected to compression obtained from the outermost clip gauges

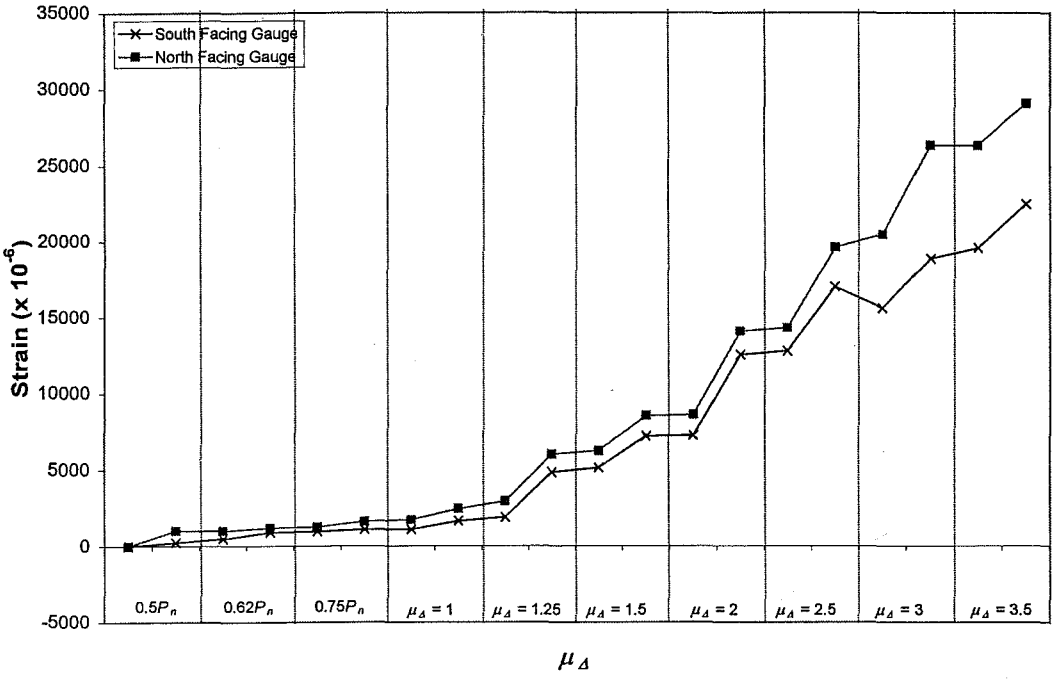

(a) Wall base

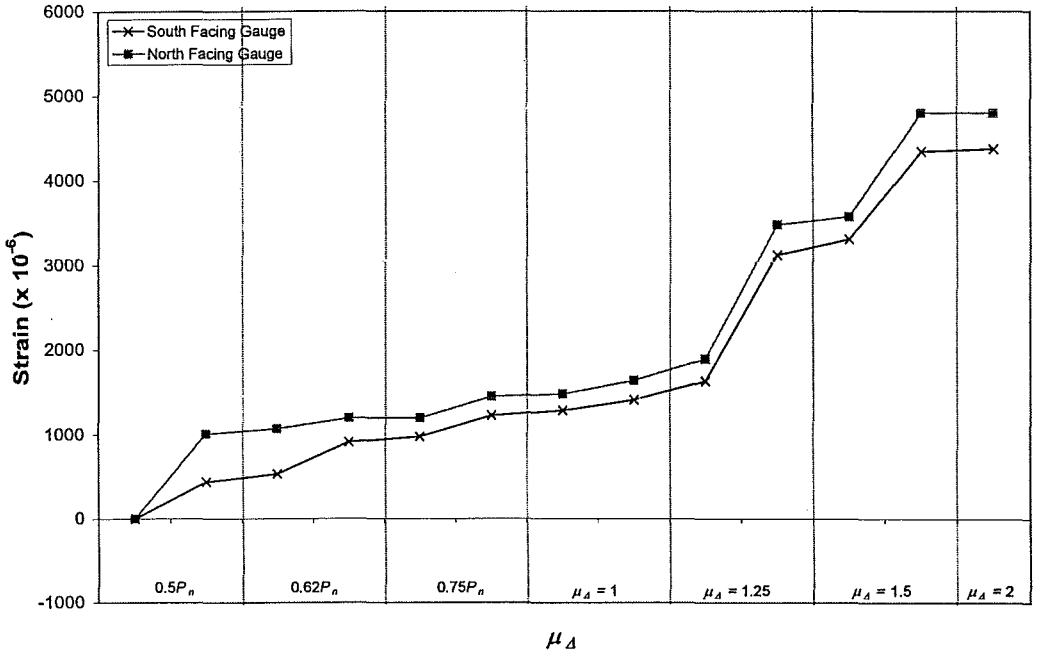

(b) Immediately above lap splice

Figure 5.117: Unit 3: Difference in longitudinal concrete strains in West edge when subjected to tension obtained from the outermost clip gauges

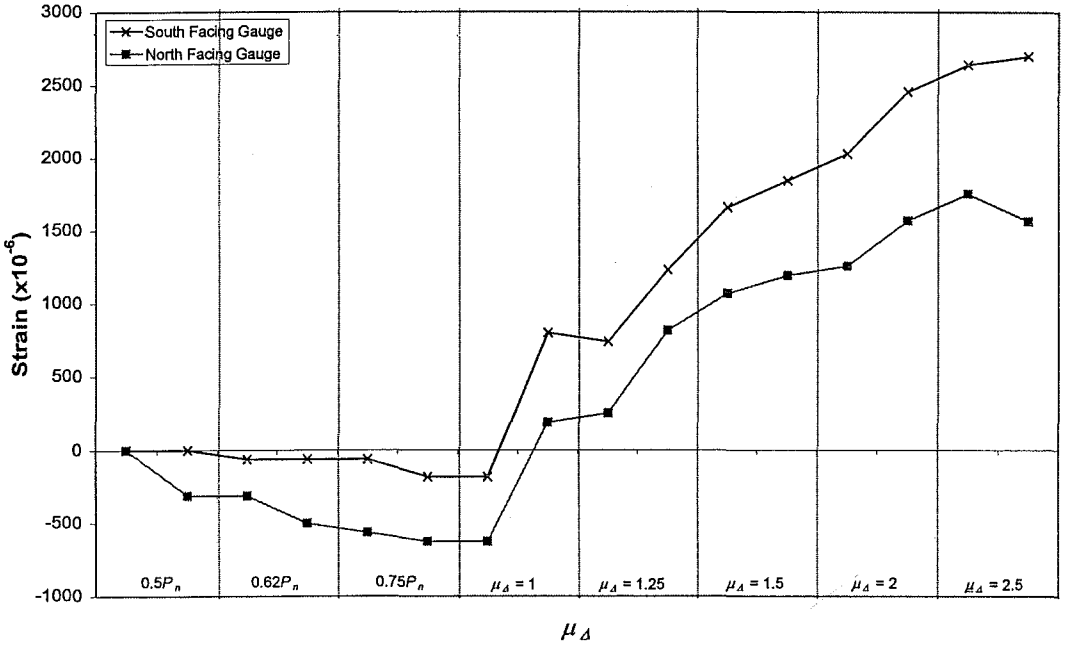

Figure 5.118: Unit 3: Concrete longitudinal strains of East edge when subjected to compression obtained from outermost clip gauges (base of wall)

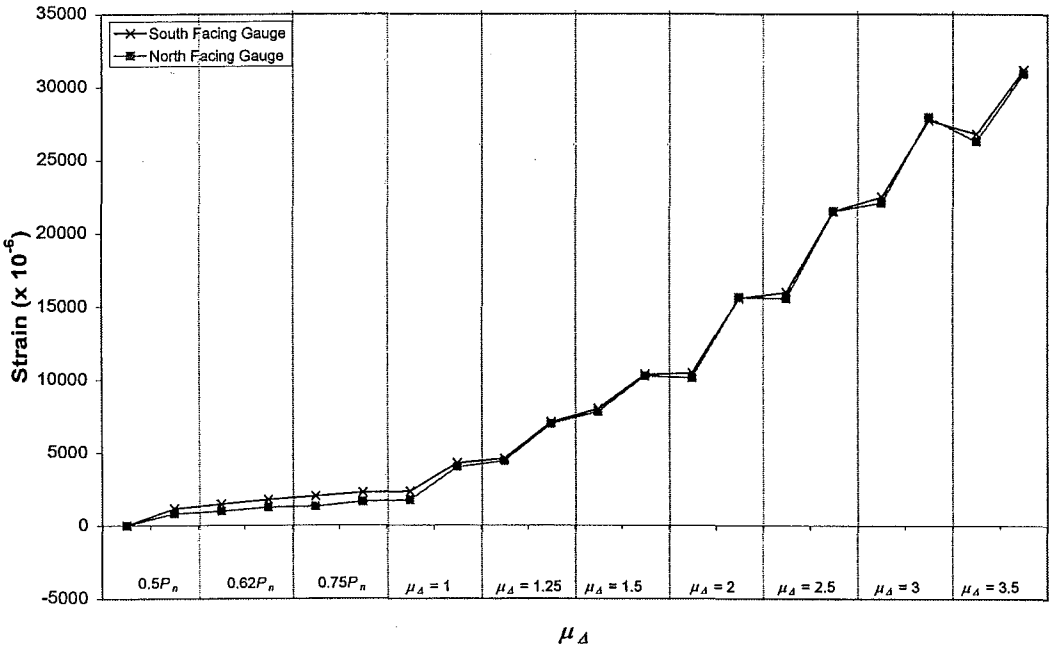

Figure 5.119: Unit 3: Concrete longitudinal strains of East edge when subjected to tension obtained from outermost clip gauges (base of wall)

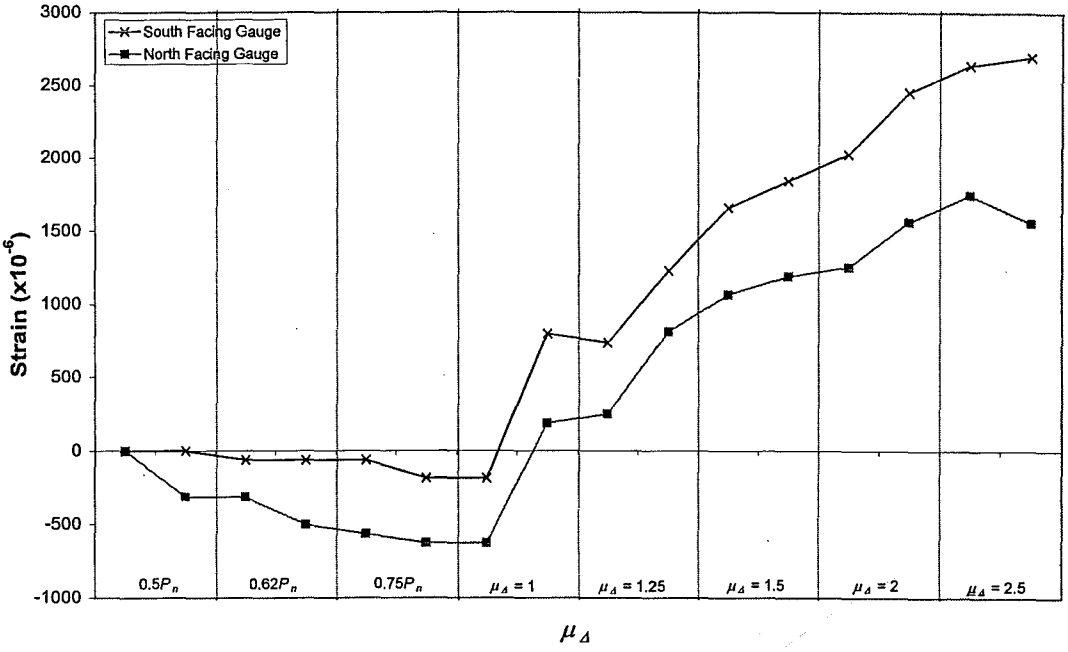

(a) Wall base

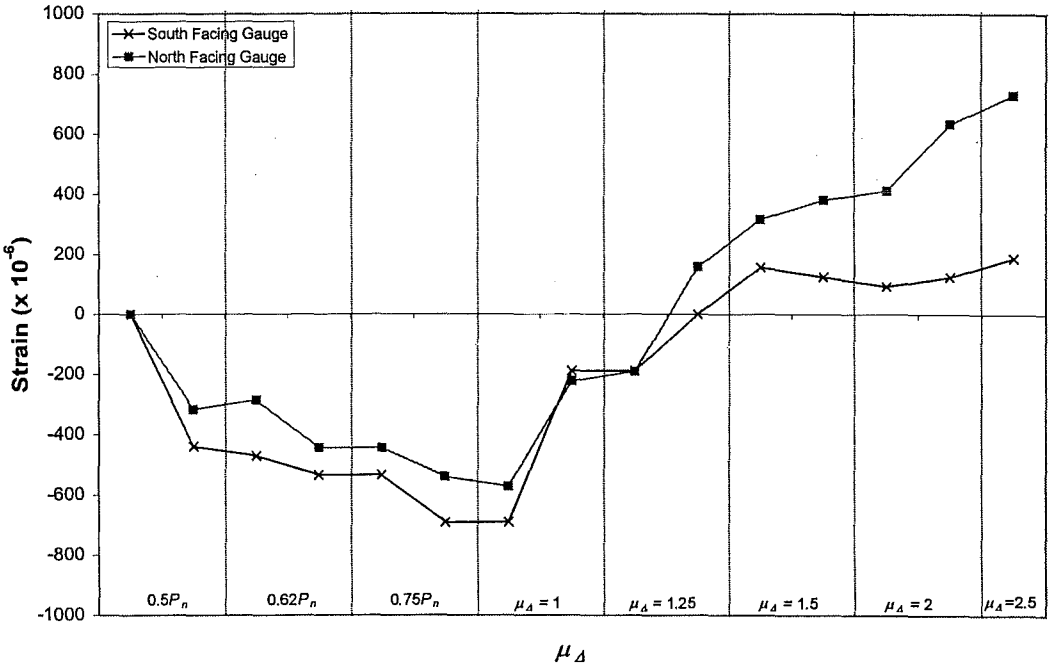

(b) Immediately above lap splice

Figure 5.120: Unit 3: Difference in concrete strains in East edge when subjected to compression obtained from the outermost clip gauges

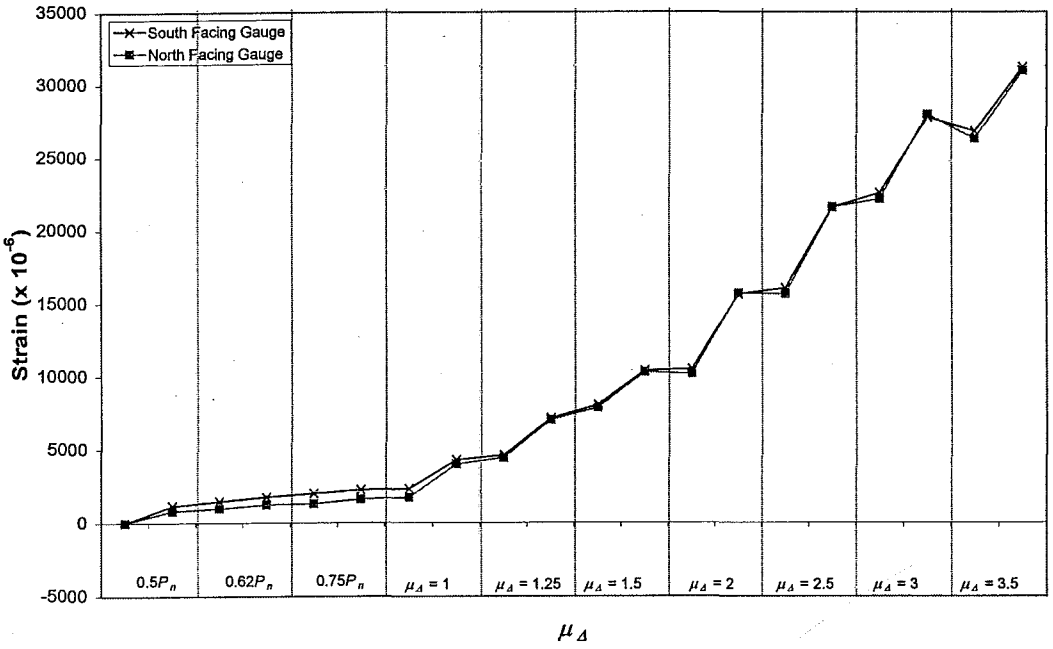

(a) Wall base

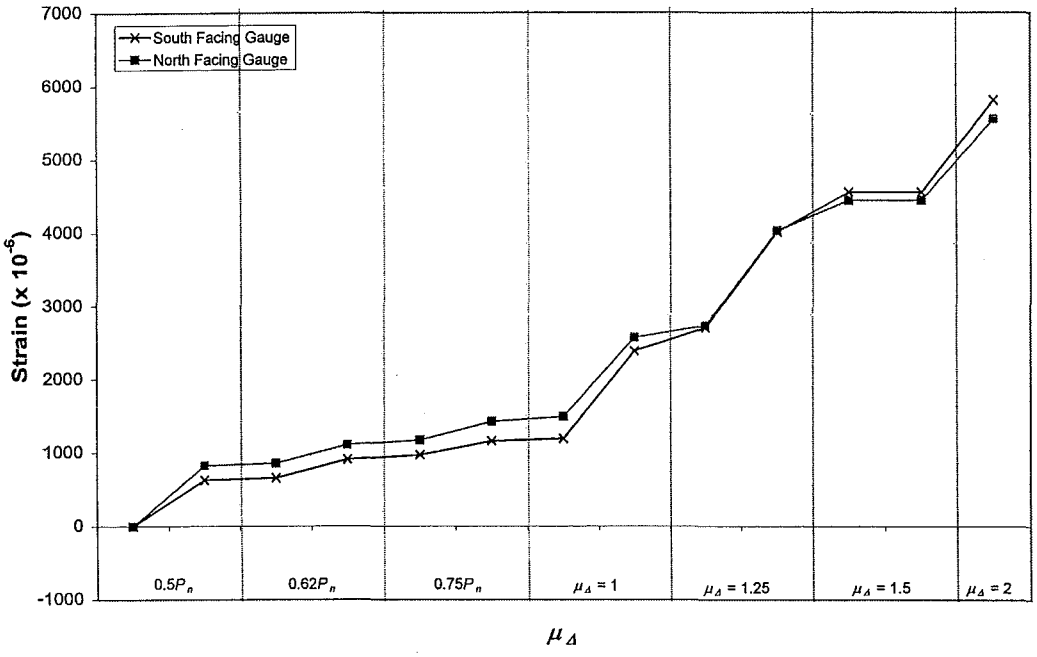

(b) Immediately above lap splice

Figure 5.121: Unit 3: Difference in concrete strains in East edge when subjected to tension obtained from the outermost clip gauges

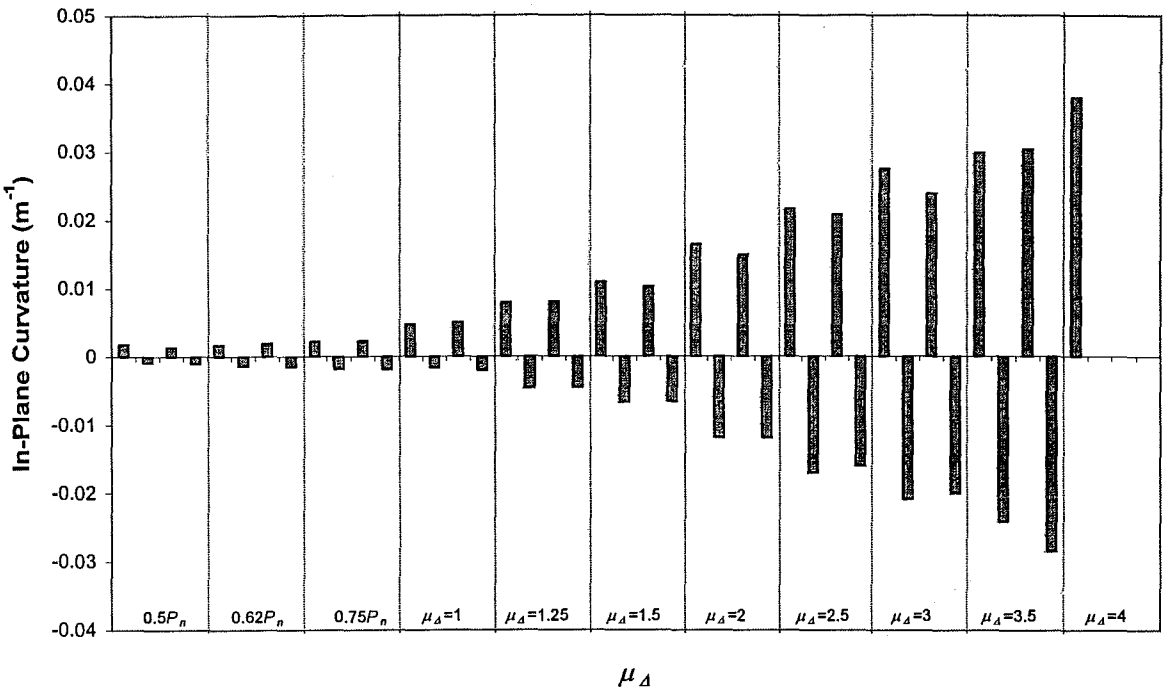

Figure 5.122: Unit 3: In-plane curvature distribution measured at 200 mm above the foundation beam

Figure 5.125 shows the average longitudinal concrete strain measured by the innermost and the outermost clip gauges taken when West edge was subjected to compression. At 200 mm above the foundation beam, the neutral axis depth lay between the innermost and the outermost clip gauges until $\mu_\Delta = +1.5\times1$ was reached. Then position of neutral axis shifted towards the outside of the outermost clip gauges (see Figure 5.125 (a)). At 600 mm and 1000 mm above the foundation beam, the neutral axis positioned on the inside of the innermost clip gauges throughout the test (see Figures 5.125 (b) and 5.125 (c)).

When the West edge subjected to tension under the negative longitudinal direction loading, both innermost and the outermost clip gauges indicated tensile concrete strain (see Figure 5.126). The readings appeared to be at the same order of magnitude. However, both compressive and tensile concrete strains decreased as the height increased.

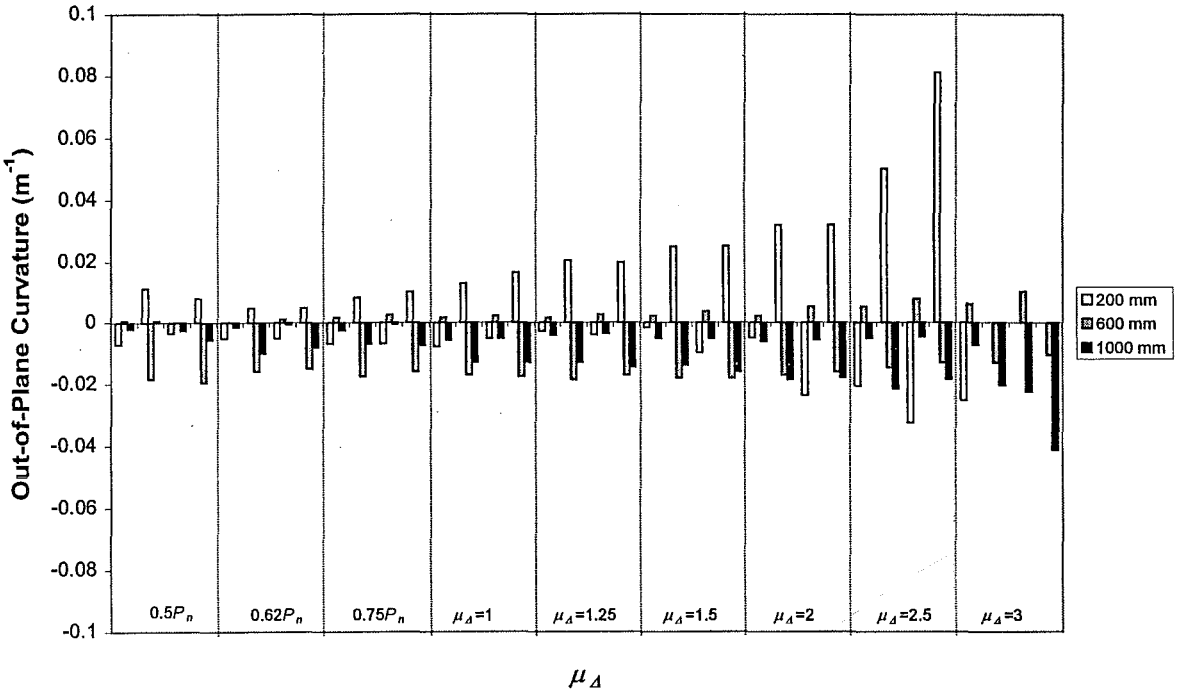

Figure 5.123: Unit 3: Out-of-plane curvature distribution obtained from outermost clip gauges on the West edge during the test

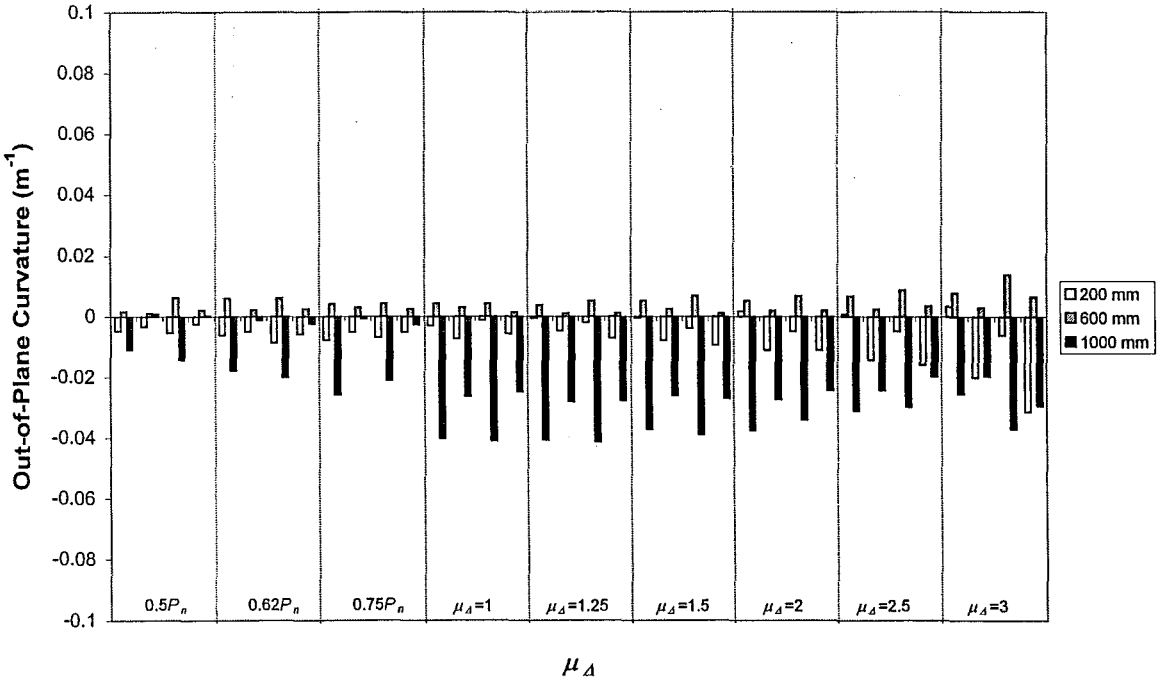

Figure 5.124: Unit 3: Out-of-plane curvature distribution obtained from outermost clip gauges on the East edge during the test

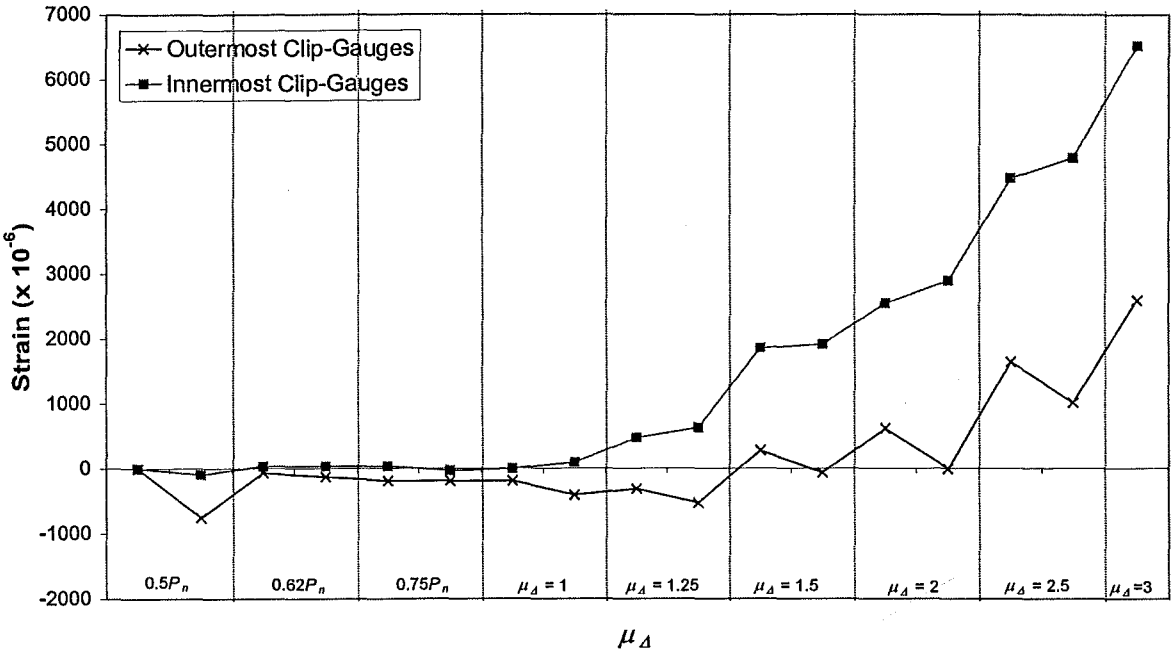

(a) 200 mm

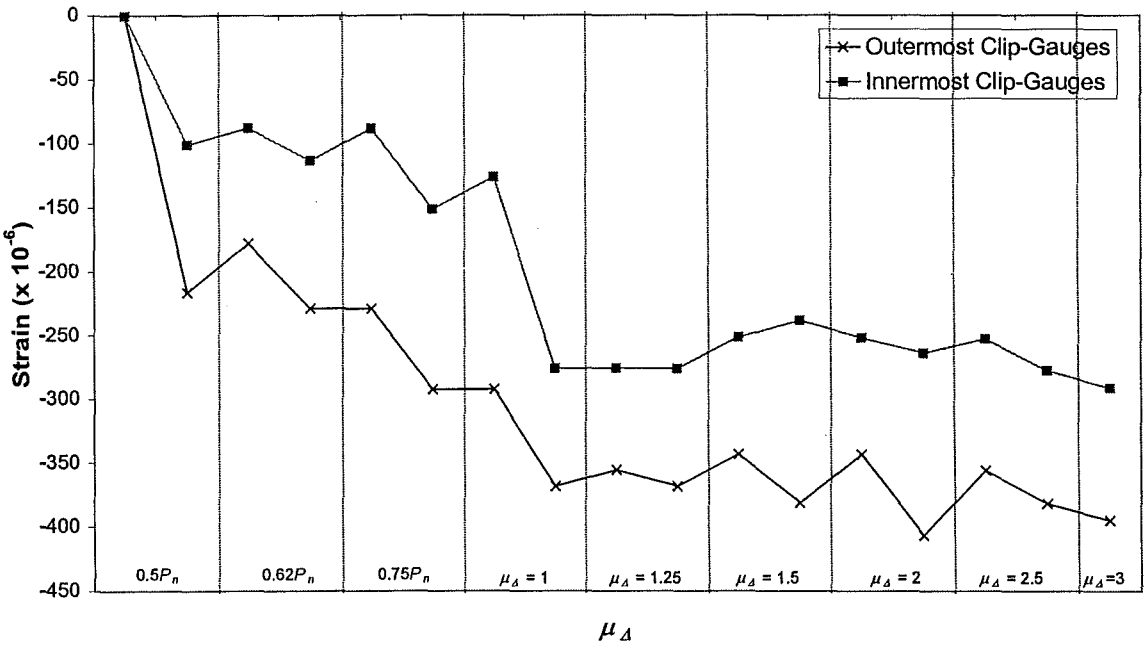

(b) 600 mm

Figure 5.125: Unit 3: Difference in concrete strains in West edge when subjected to compression obtained from the outermost clip gauges at different heights

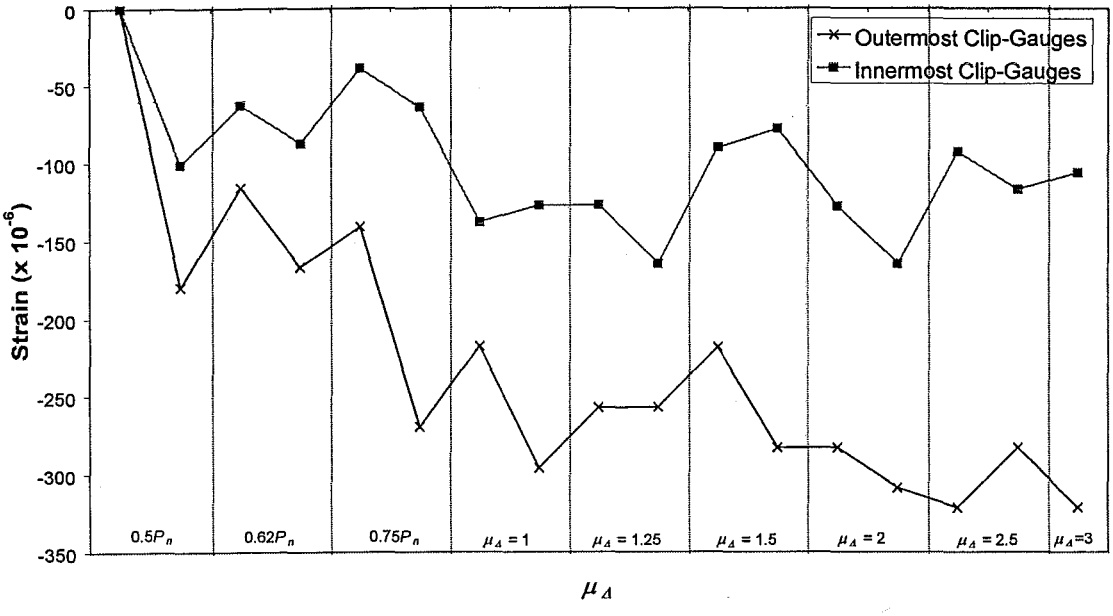

(c) 1000 mm

Figure 5.125 (cont.): Unit 3: Difference in concrete strains in West edge when subjected to compression obtained from the outermost clip gauges at different heights

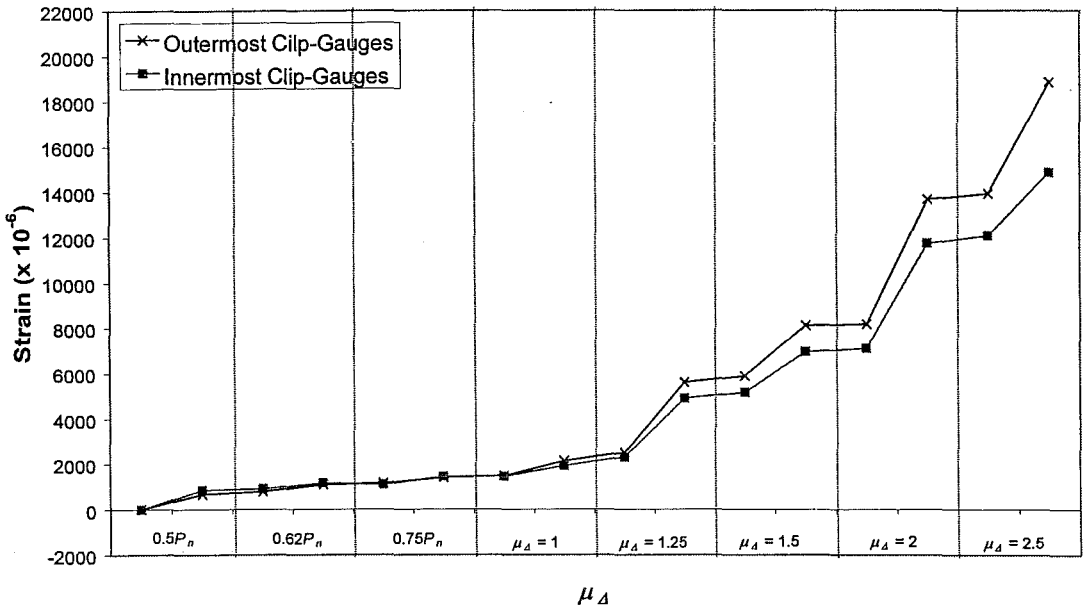

(a) 200 mm

Figure 5.126: Unit 3: Difference in concrete strains in West edge when subjected to tension obtained from the outermost clip gauges at different heights

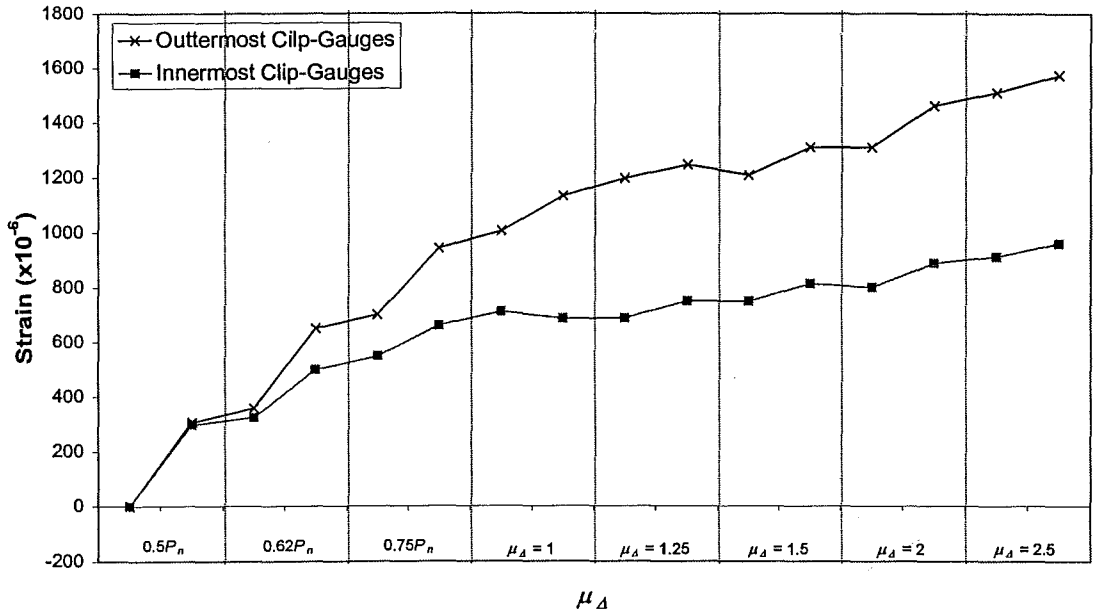

(b) 600 mm

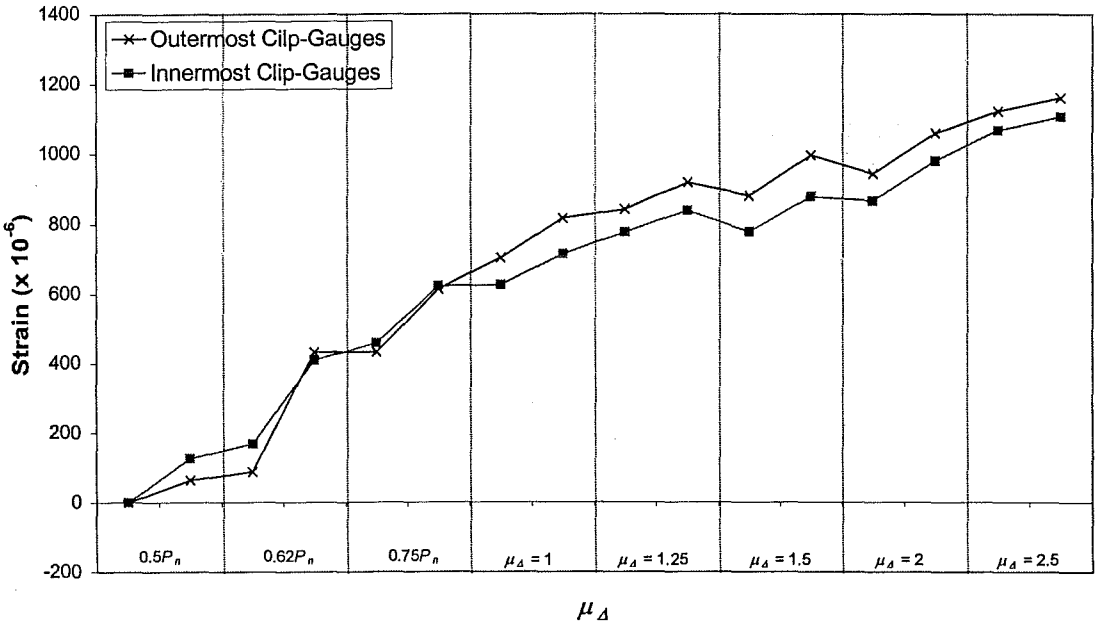

(c) 1000 mm

Figure 5.126(cont.): Unit 3: Difference in concrete strains in West edge when subjected to tension obtained from the outermost clip gauges at different heights

5.4 Unit 4

5.4.1 Unit 4 Properties

The properties of Unit 4 are illustrated in Table 5.4. All measured values were calculated with the material properties measured on the day of test, and the nominal values were calculated using the nominal material properties.

Table 5.4: Measured properties of Unit 4

Property			Nominal value	Measured value
Reinforcing ratio	p	%	1.26	N/A
Longitudinal reinforcing yield strength*	f_y	MPa	300	318
Concrete compressive strength*	f'_c	MPa	30	30.3
Modulus of rupture	f_r	MPa	4.38	4.40
Axial load level	$N^*/A_g f'_c$		0.0127	0.0125
Cracking load	P_{crack}	kN	9.7	9.8
First yield strength	P_{yield}	kN	18.9	20.1
Nominal strength	P_n	kN	24.1	25.4

* At the day of testing

The secant stiffness at $0.75P_n$ was $k_{75} = 2.37$ kN/mm and the estimated reference yield displacement was $\Delta_y = 10.7$ mm (see Appendix B).

5.4.2 General Behaviour and Observations : Unit 4

Flexural cracks initiated at the horizontal joint and the location where the starter bars were terminated during $+0.5P_n \times 1$. These cracks started at the edge which subjected to tension and propagated to reach the length of 0.5 m (see Figure 5.127). A few cracks developed on the concave side of the wall and reached the height of 1 m above the foundation beam. In the third cycle, i.e. $0.62P_n \times 1$, cracks initiated within the lap-splice region and propagated towards the horizontal joint. At this stage, the height of cracking was approximately 1.8 m. Figure 5.128 shows cracking pattern at the first yield capacity of the wall.

At μ_Δ = +1.25×1, a few vertical cracks approximately 180 mm length, developed at the location of the starter bars which subjected to tension. Interestingly, more vertical cracks developed at the location above the lap splice where the longitudinal reinforcement was when μ_Δ = -1.5×2 was reached (see Figure 5.129).

Sliding shear at the horizontal joint occurred at all stages of the test. However, it became more significant when the wall was subjected to μ_Δ = +2×1. This implies that inadequate bond strength developed between the wall panel and the cement-based grout. It must be noted that more cracks developed on the convex side caused by the eccentricity effect from the vertical load at the top of the wall.

At μ_Δ = +2.5×1, yield penetration happened to spread from the end of the lap splice upwards. Consequently, two large cracks developed along the end of the lap splice and at the height of 300 mm above the foundation beam respectively (see Figures 5.130 and 5.131). These cracks became wider as the applied displacement ductility increased.

Cement-based grout between the wall panel and the foundation beam started to crush at the compression edge of the wall when subjected to μ_Δ = +3×1.

The base of the wall panel twisted clockwise at μ_Δ = -4×1 with the magnitude, measured at both ends of the wall, between 2 mm (West edge) and 10 mm (East edge). Concrete started to crush and spall on the compression side of the wall. It is interesting to note that this only occurred at one end of the wall, i.e. East edge.

At μ_Δ = -4.5×1, a vertical splitting initiated and propagated with the total length of lap-splice i.e. 180 mm on the East edge of the wall (see Figure 5.132). This was the result of concrete crushing and twisting at the base under compression. The crack width was measured to be approximately 10 mm (see Figures 5.133 and 5.134) and the out-of-plane movement at the base on the tension edge (East edge) was 25 mm due to twisting action in clockwise direction. Many small cracks joined up and formed a few diagonal cracks starting from the West edge of the wall propagated towards the bottom of the East edge.

The starter bars on the compression edge (West edge) buckled and the vertical crack at the East edge widened to approximately 20 mm when the wall subjected to μ_Δ = -5×2 (see Figures 5.135 to 5.137). The magnitude of twisting action was measured to be 35 mm at the East edge in clockwise direction.

The test continued until the starter bars fractured at μ_Δ = +5.5×1. Fracture failure occurred at the end of the welds where the starter bars were subjected to cyclic loading (see Figures 5.138 and 5.138). This caused by the retensioning and buckling of the starter bars. Again, it is important to note that this only happened on the East edge of the wall. Neither crushing, spalling of concrete nor fracturing of the starter bars occurred on the West edge of the wall. Overall cracking patterns are shown from Figures 5.140 to 5.142.

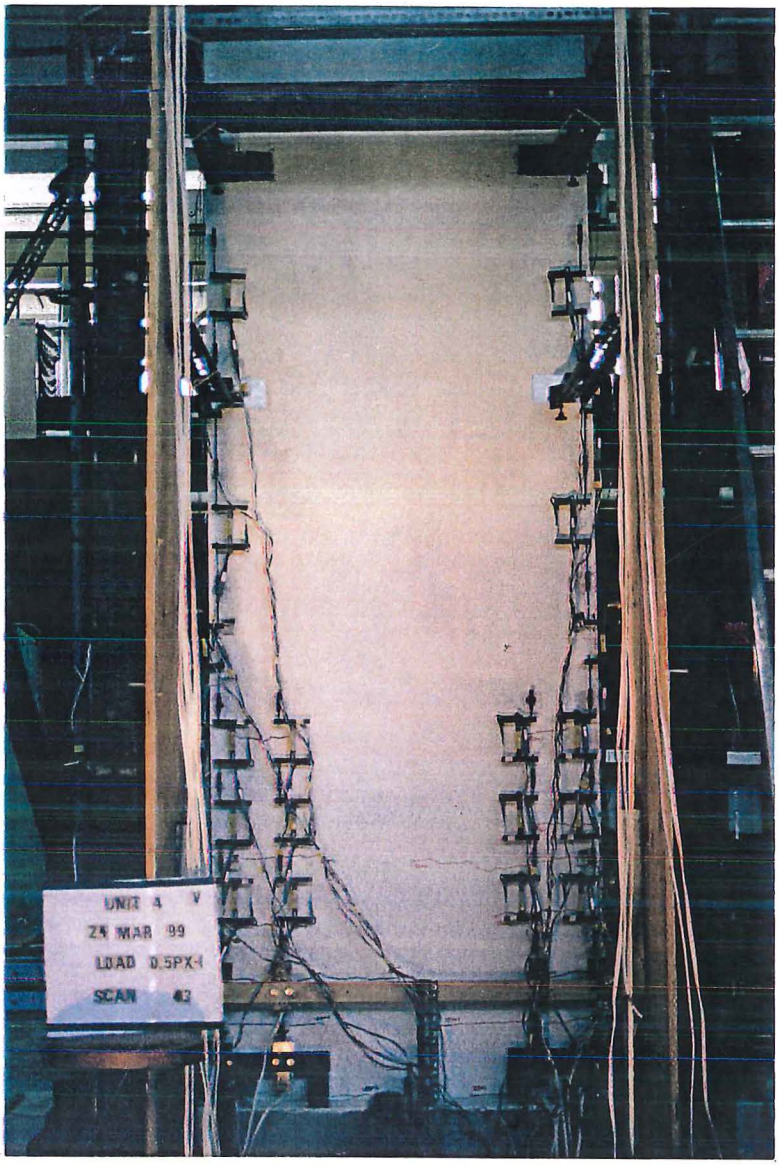

Figure 5.127: View of Unit 4 at cracking strength (South/Concave)

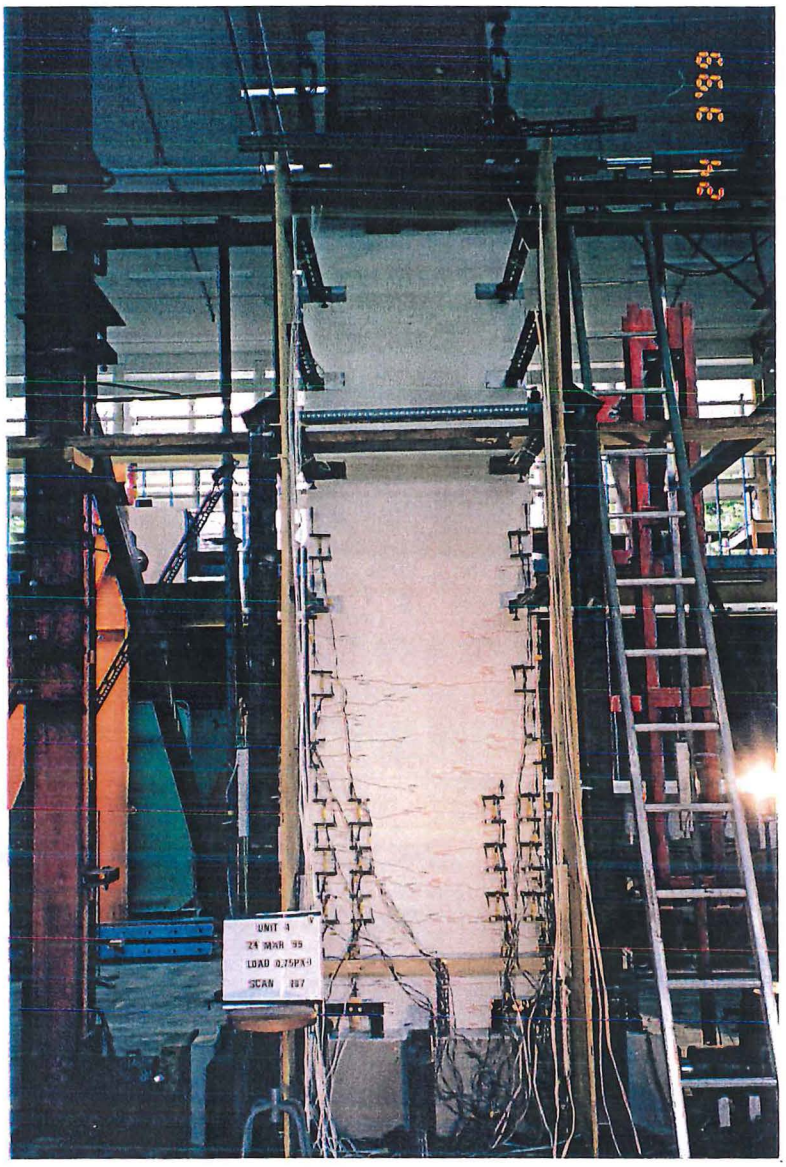

Figure 5.128: View of Unit 4: first yield at the positive direction loading (South/Concave)

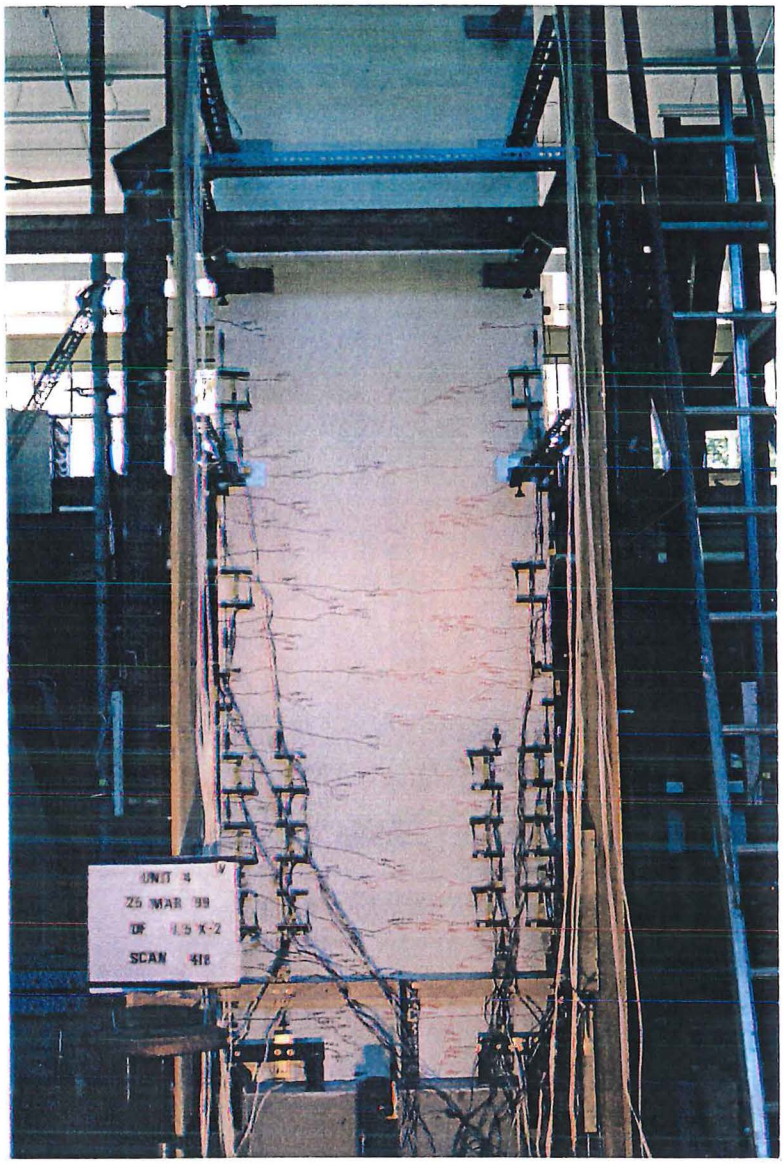

Figure 5.129: Unit 4: Cracking pattern on the South/Concave side at μ_Δ = -1.5×2

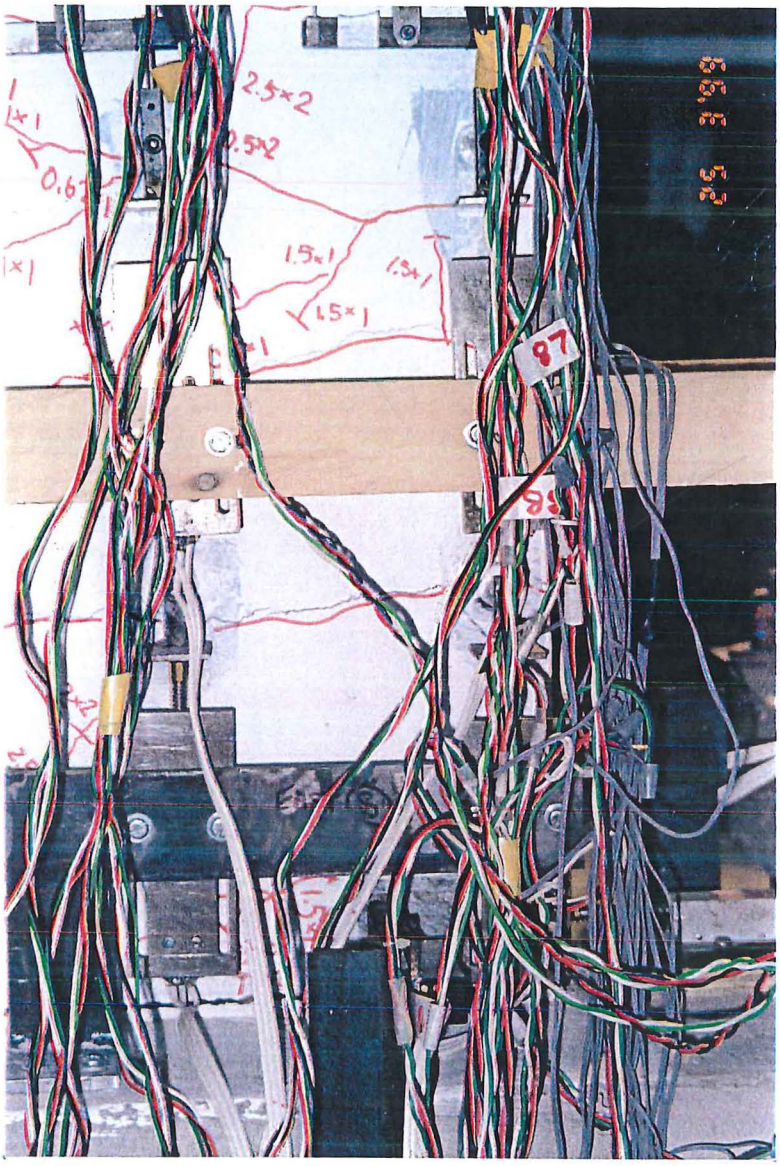

Figure 5.130: Unit 4: Spreading of plasticity at 300 mm above the foundation beam at μ_{Δ}= +2.5×1 (South/Concave)

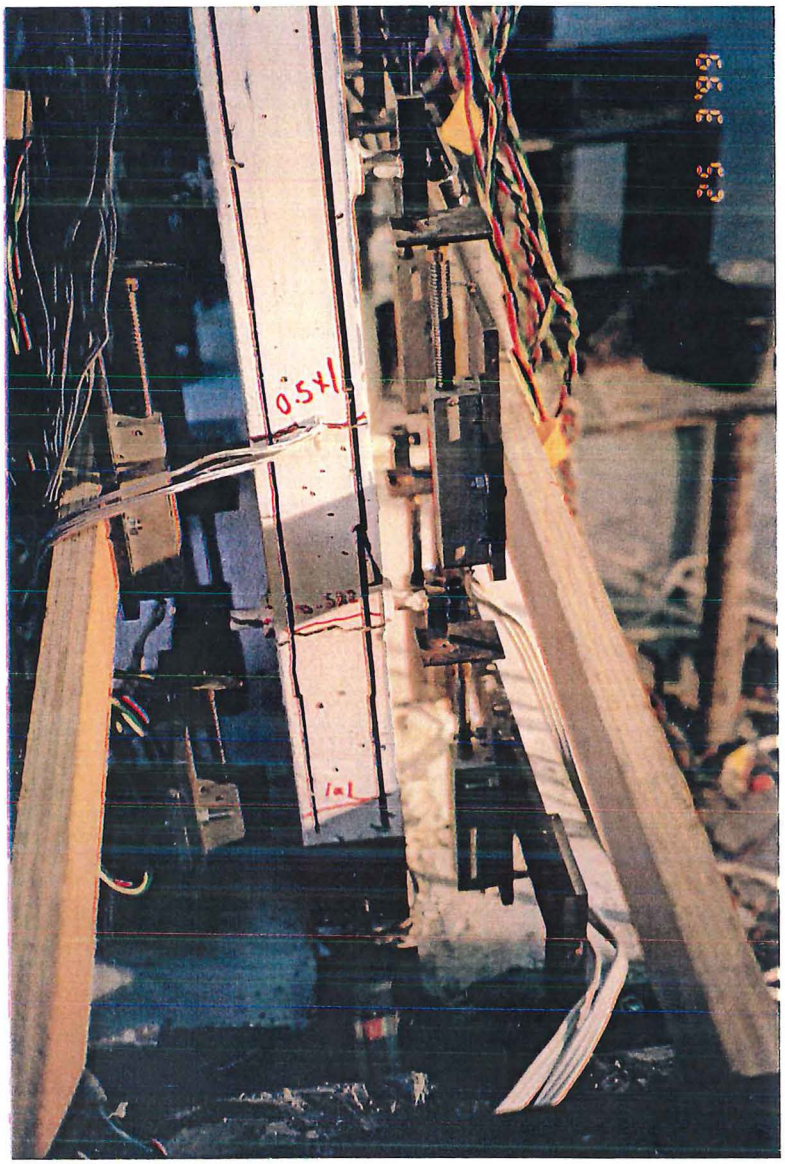

Figure 5.131: Unit 4: East edge view of cracking caused by spreading of plasticity at 300 mm above the foundation beam at μ_Δ = +2.5×2

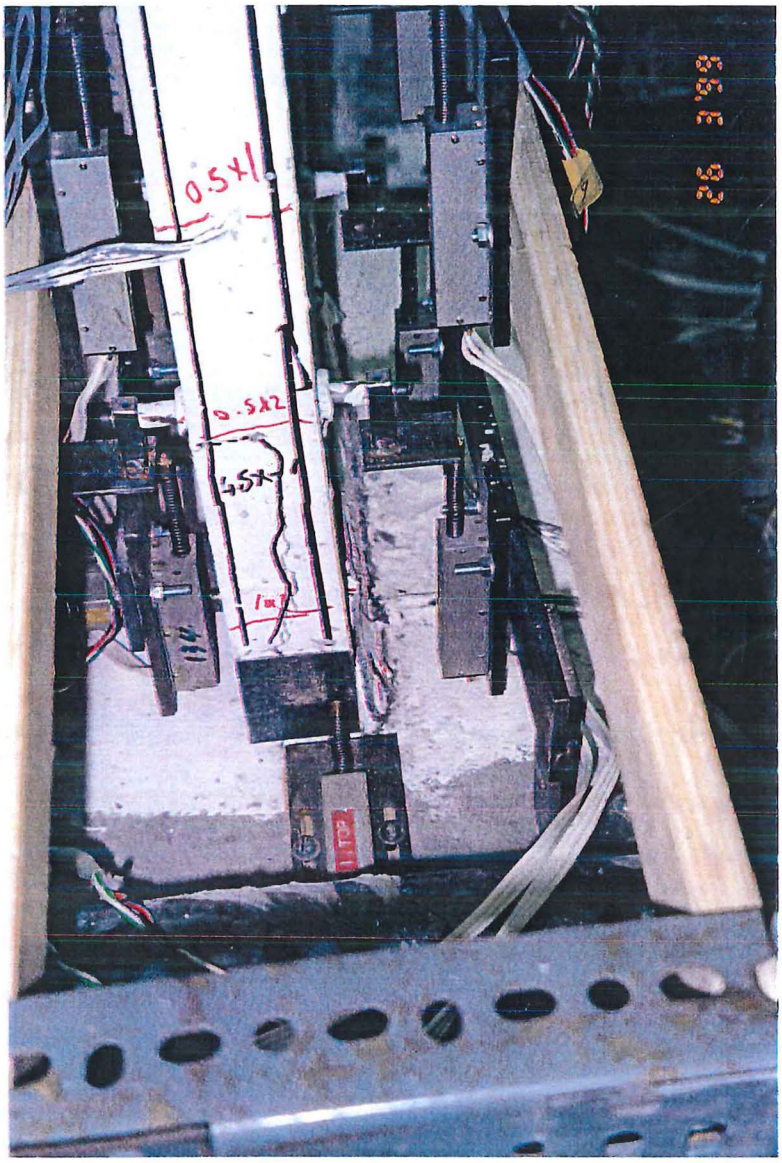

Figure 5.132: Unit 4: Initiation of vertical splitting at East edge of the wall at μ_Δ= -4.5×1

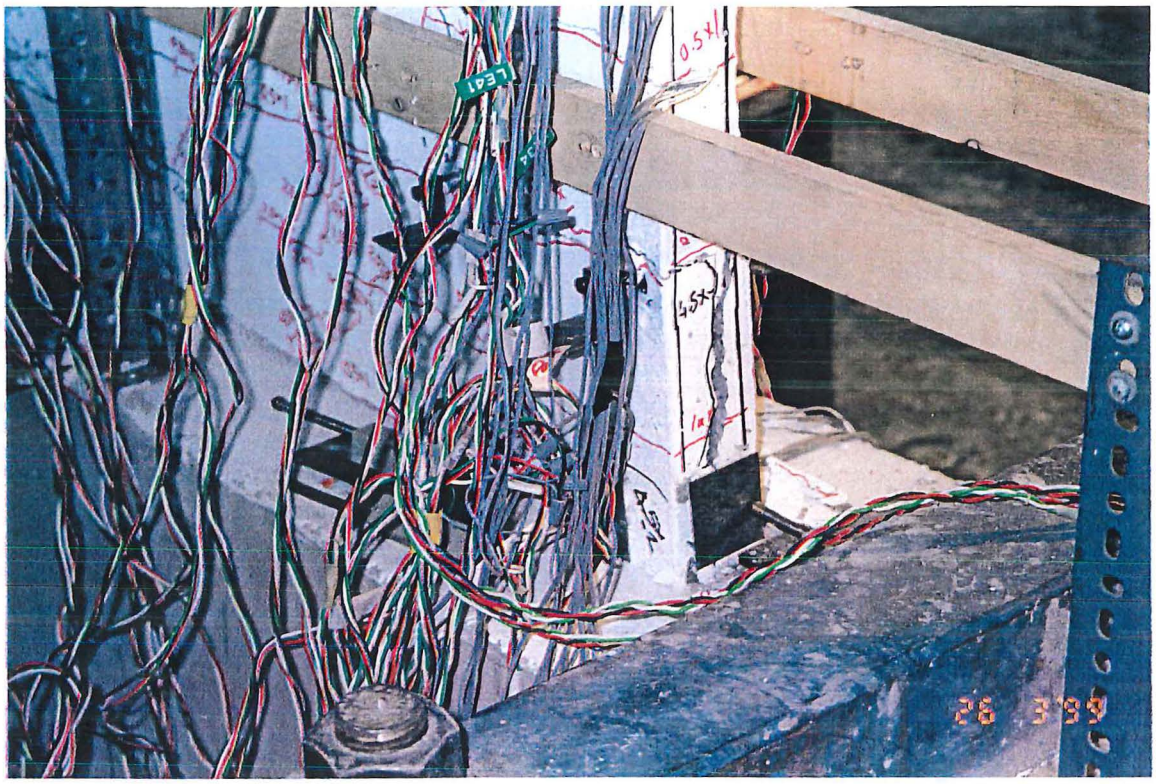

Figure 5.133: Unit 4: Vertical splitting opened up to approximately 10 mm at μ_Δ = -4.5×2 (East edge)

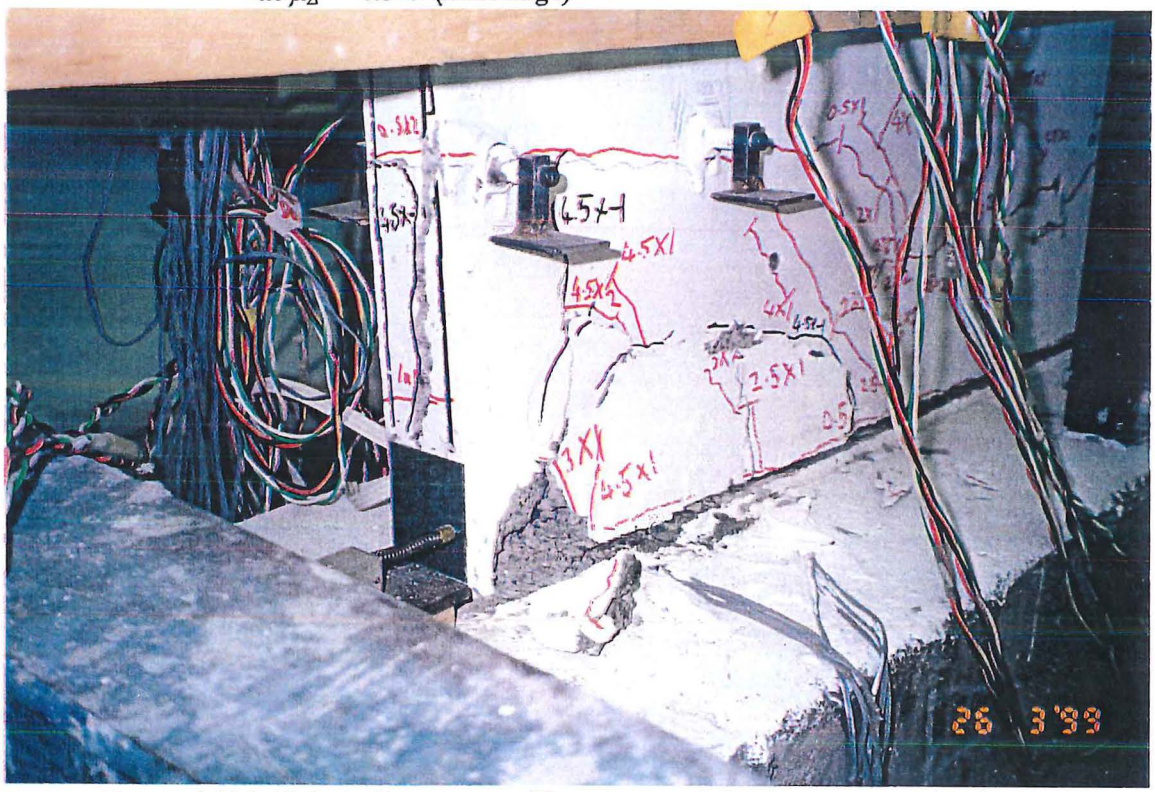

Figure 5.134: Unit 4: Concrete spalling occurred simultaneously with the occurrence of vertical splitting at μ_Δ = -4.5×2 (East edge)

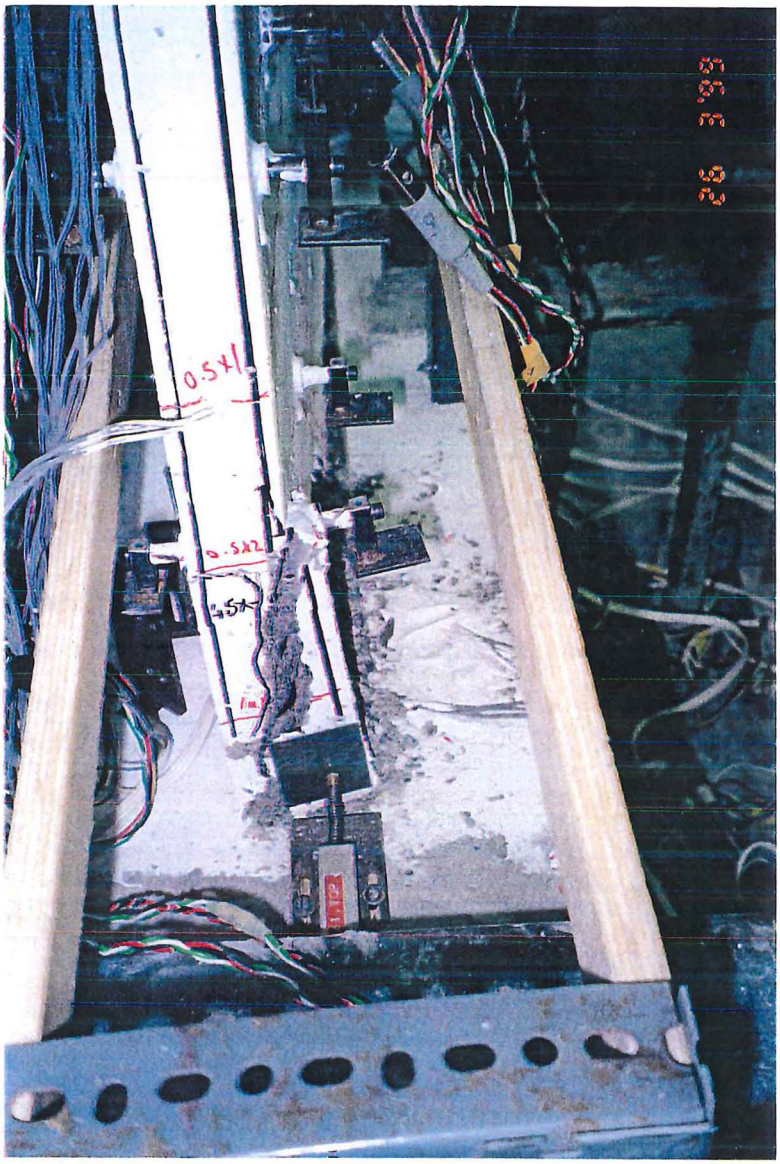

Figure 5.135: Unit 4: Reduction of compressive block caused by vertical splitting at μ_Δ = -5×1 (East edge)

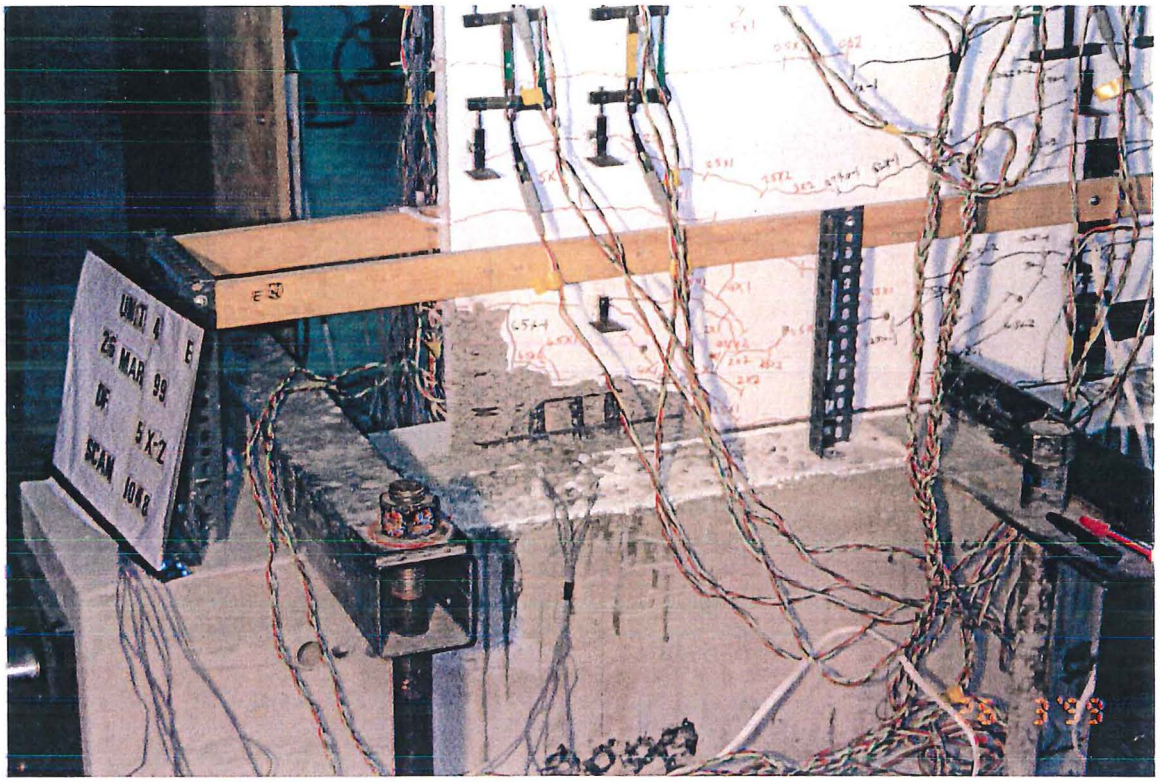

Figure 5.136: Unit 4: Buckling of compression starter bars at μ_Δ = -5×2 (North/Convex)

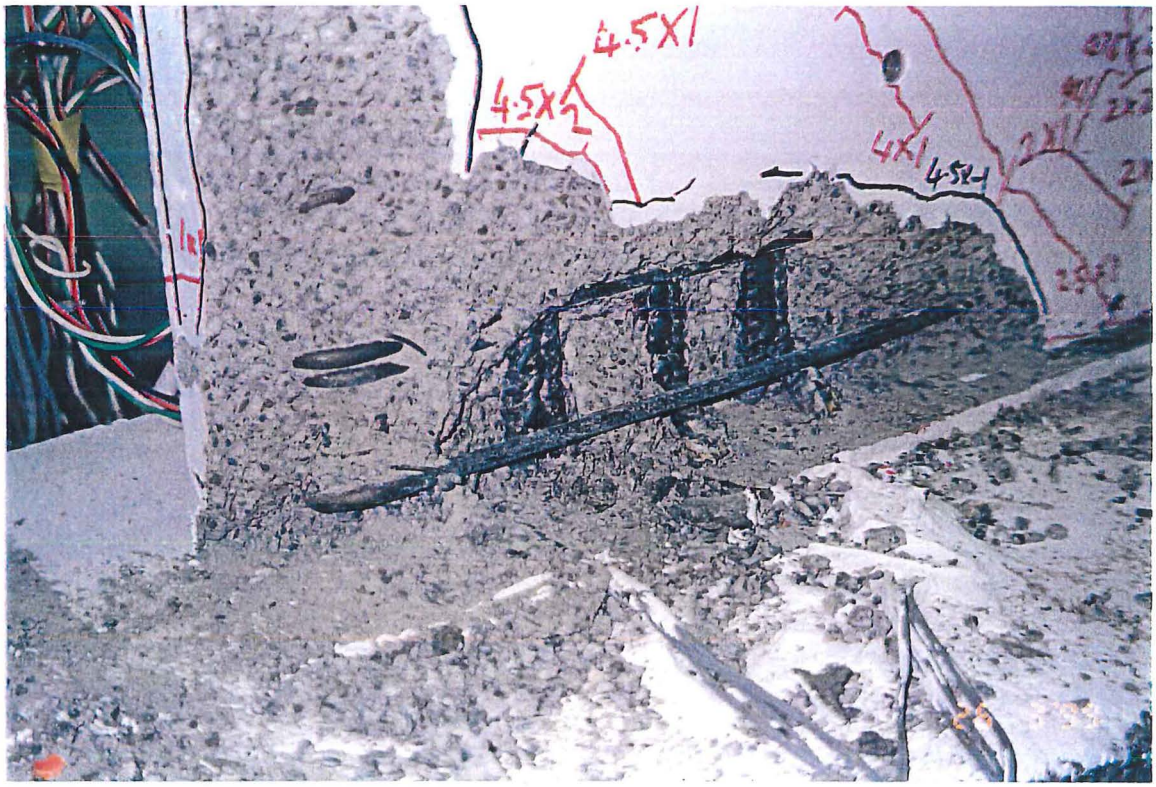

Figure 5.137: Unit 4: Buckling of compression starter bars at μ_Δ = -5×2 (North/Convex)

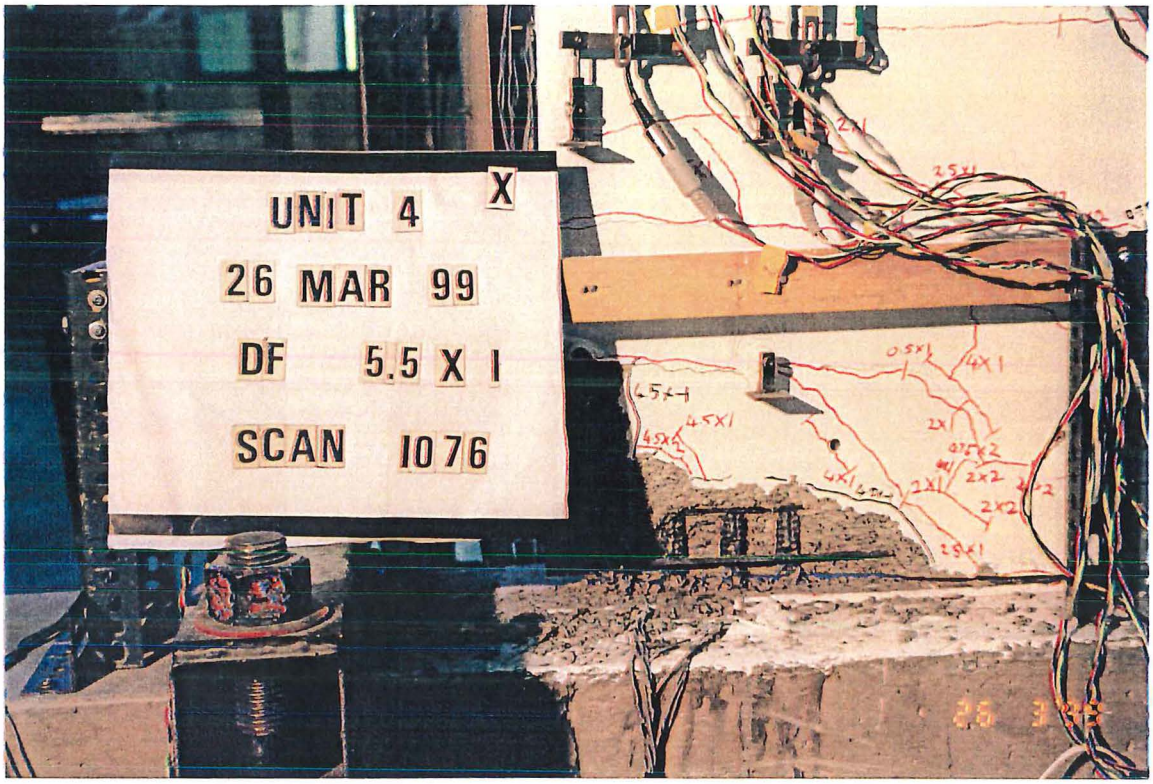

Figure 5.138: Unit 4: Fracturing of tension starter bars at μ_Δ = +5.5×1 (North/Convex)

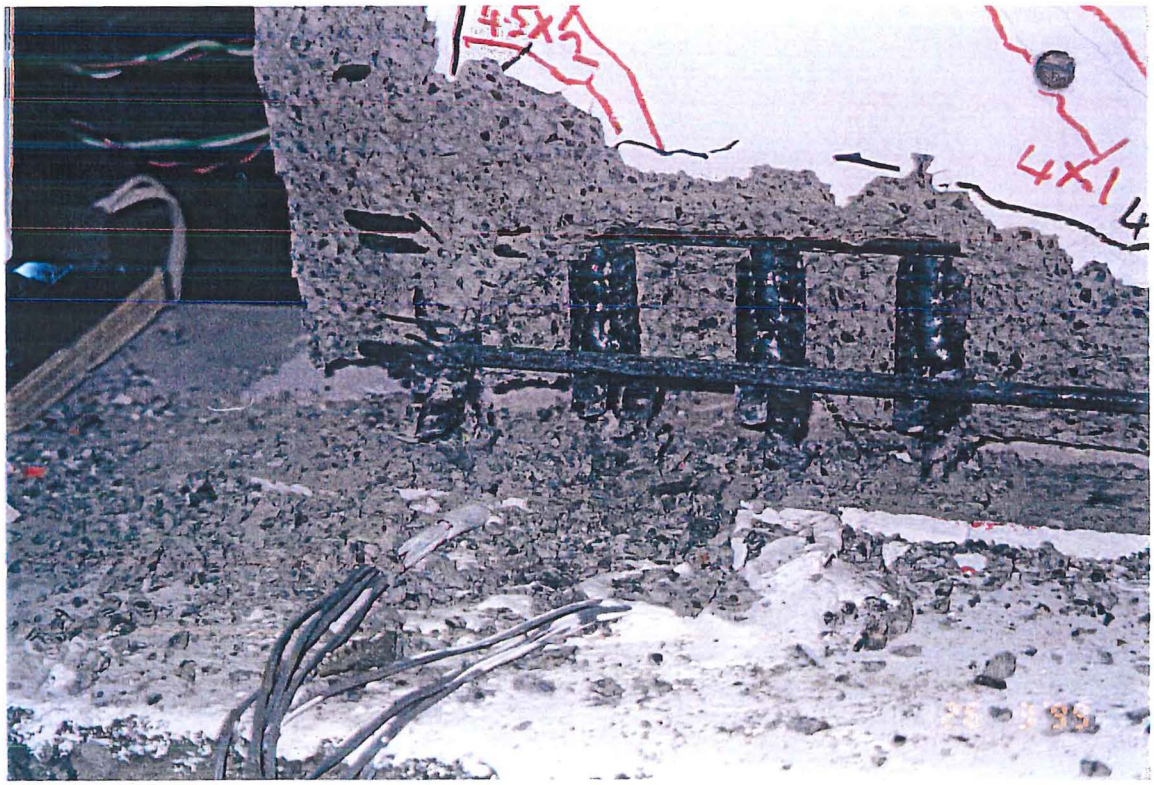

Figure 5.139: Unit 4: Fracturing of tension starter bars at μ_Δ = +5.5×1 (North/Convex)

Figure 5.140: Unit 4: Overall cracking pattern on the South/Concave side at the end of test

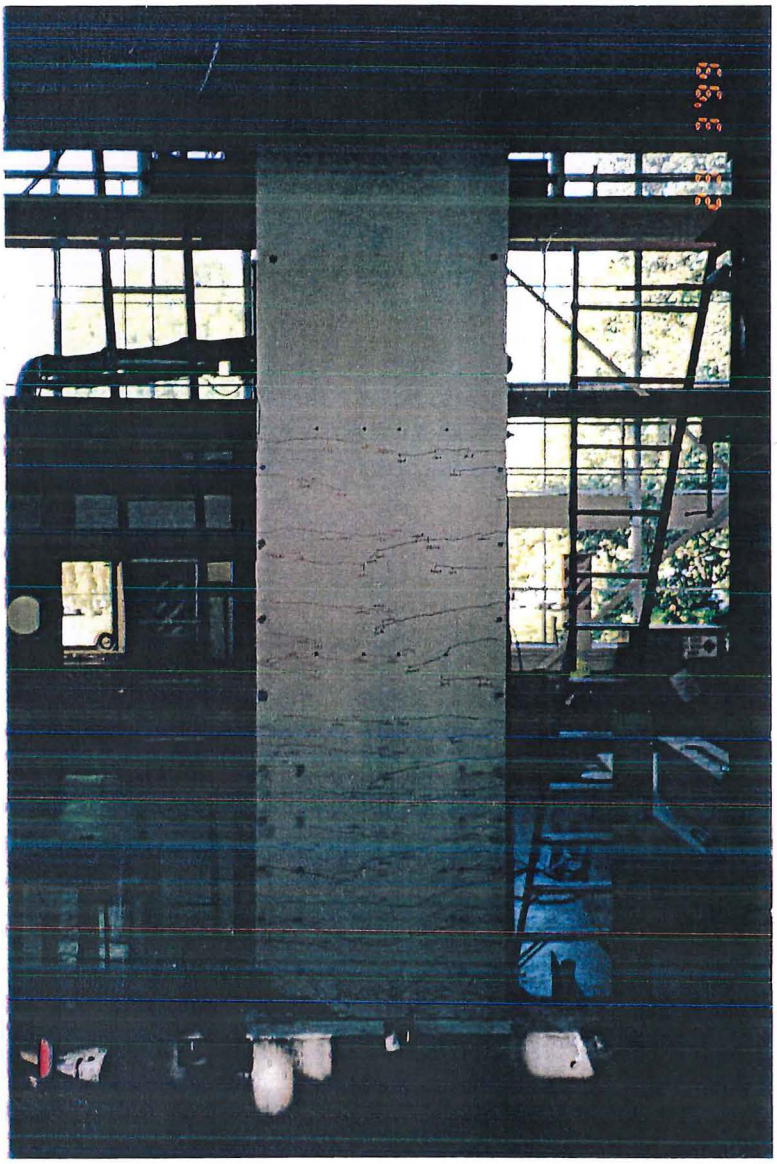

Figure 5.141: Unit 4: Overall cracking pattern on the North/Convex side at the end of test

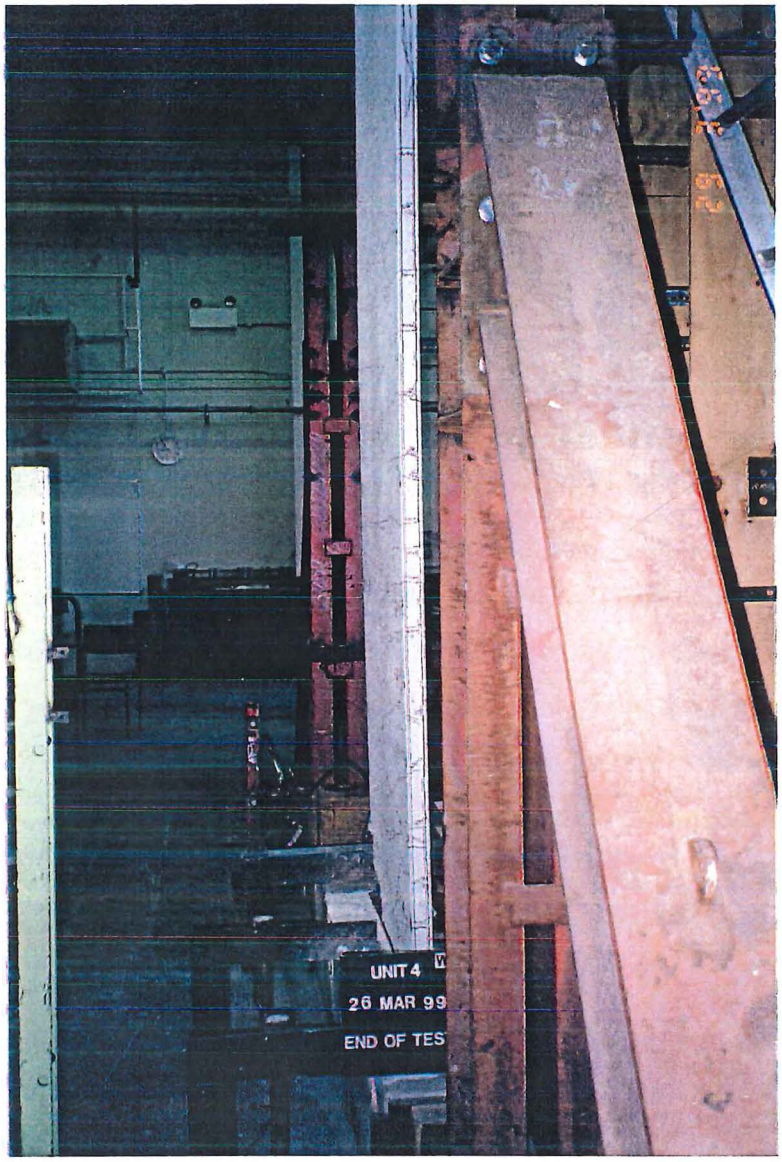

Figure 5.142: Unit 4: West edge cracking pattern at the end of test

5.4.3 Analysis of Experimental Results : Unit 4

5.4.3.1 Lateral Force-Lateral Displacement Response : Unit 4

The overall lateral applied force versus lateral displacement response is illustrated in Figure 5.143. The first initial cycles in the "elastic" range, i.e. initial cycles before μ_Δ = 1 was achieved, non-linear inelastic behaviour was exhibited mainly by the formation of cracks at the wall-foundation connection. The displacements in the negative direction were larger than those in the positive direction at the same applied in-plane force. Consequently, an unsymmetrical response of the specimen resulted. It was caused by the damage at one end of the construction joint. The theoretical moment-curvature curves, plotted in Figure 5.144, represent the behaviour estimated assuming a monotonic loading in each direction.

During the initial cycles, the lateral load-lateral displacement response indicated some pinching but with a reasonable amount of energy dissipation capacity. This pinching gradually increased as the applied force increased. Sliding shear occurred at the interface between the base of wall panel and the cement-based grout. At the reloading branch of the hysteresis loops, the wall slid with a reduced amount of shear resistance. Then, the wall started to gain strength and stiffness when the dowel action mechanism from the starter bars began to activate.

The repetition of cycles to the same displacement ductility had an influence on lateral strength reduction. This effect was significant at the high displacement ductilities.

The maximum strength of the wall also increased by 15% of the nominal flexural strength in the strain hardening stage at $\mu_\Delta = +4.5\times1$.

Obviously, the first strength reduction had taken place when the vertical splitting of the concrete occurred and followed by spalling of concrete which resulted in the loss of length of wall acting as the compression stress block. However, the wall regained the strength from the dowel action of the starter bars. The second strength

reduction occurred when tension starter bars ruptured during the second cycles attempting to achieve $\mu_\Delta = +5.5\times2$ (see Figure 5.143).

5.4.3.2 Out-of-Plane Displacements : Unit 4

Figures 5.145 to 5.148 illustrate the displacements in the out-of-plane direction on the East edge and West edge when subjected to positive and negative cycles. All the out-of-plane displacement plots represent "North face" on the right and "South face" on the left. These profiles were measured at the positive peak cycles using linear potentiometers, which targeted on the concave side of the wall.

In Figure 5.145, as the positive applied force increased, the lower portion of tension edge of the wall, i.e. East edge, moved to a straight position while the top portion displaced laterally outwards. The edge profile changed from a single curvature to a double curvature at $\mu_\Delta = +1\times1$. The displacement at the top and the bottom of the panel was negligible due to the support details. As seen in Figure 5.145, displacements were measured at the base of the wall. This was the result of the spalling concrete cover pushing against the linear potentiometer.

However, the lower portion of wall on West edge, when subjected to compression, behaved oppositely to that of the East edge (see Figure 5.146). Once more, the wall profile turned from a single to a double curvature where the point of inflection was approximately 1.5 m above the foundation beam. The maximum drift ratio of the compression edge was about 0.3% of the full storey height.

Once the negative cycles were imposed on the wall, the East edge when subjected to compression displaced laterally in the out-of-plane direction greater than when the wall was subjected to the positive cycles. At $\mu_\Delta = -4.5\times1$, the out-of-plane interstorey drift ratio was measured to be approximately 0.6% (see Figure 5.147).

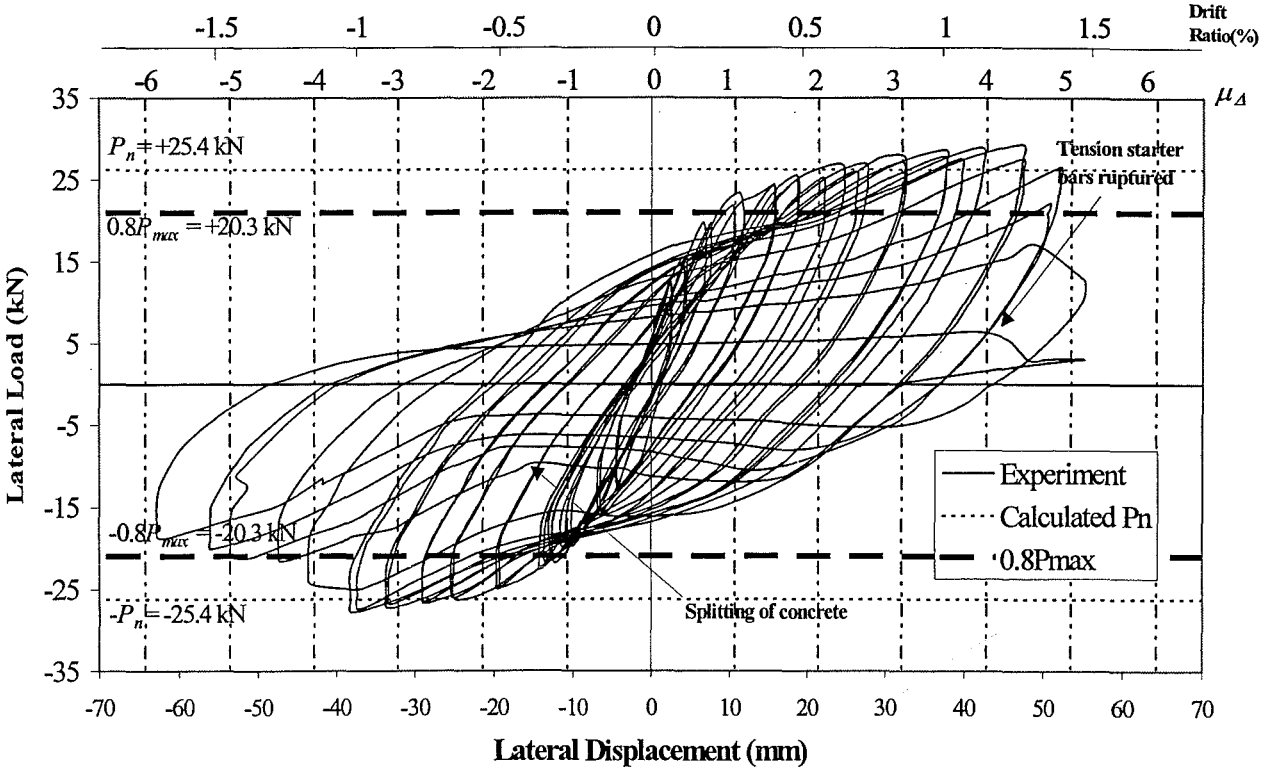

Figure 5.143: In-plane lateral load-lateral displacement response of Unit 4

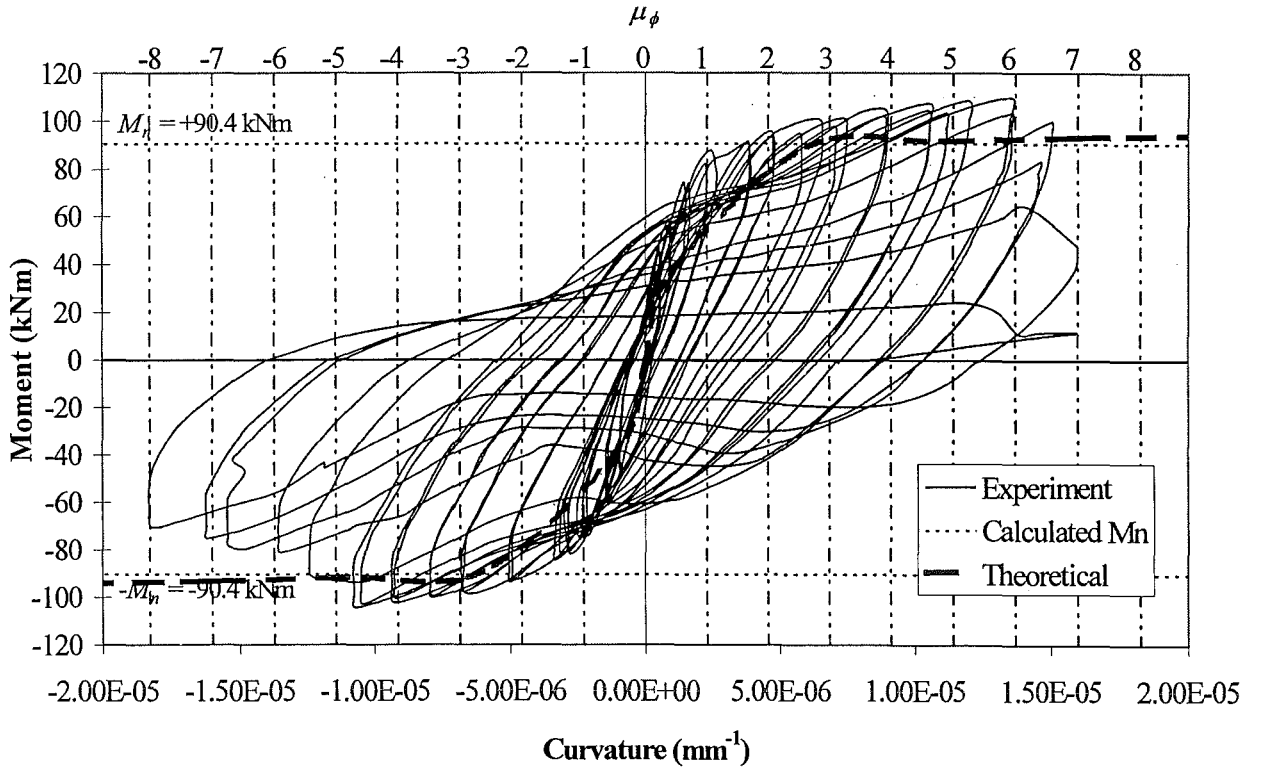

Figure 5.144: Moment-curvature response of Unit 4

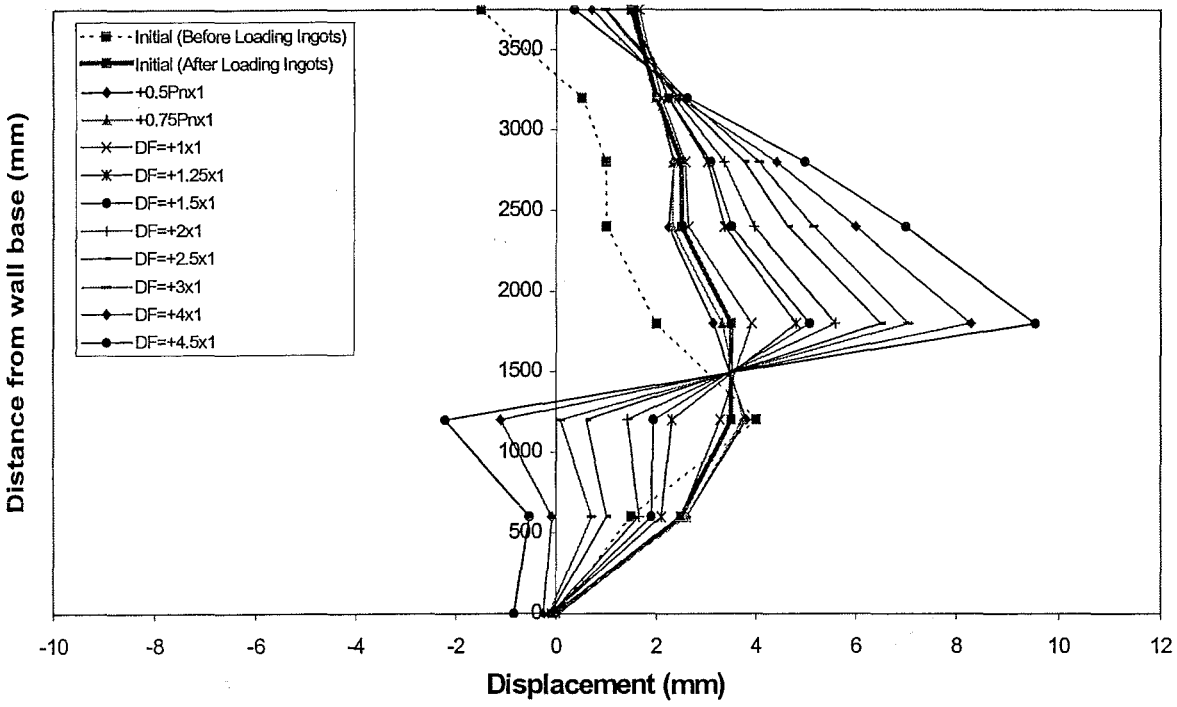

Figure 5.145: Unit 4: Out-of-plane movement on East edge of the wall at positive peak cycles (Tension edge)

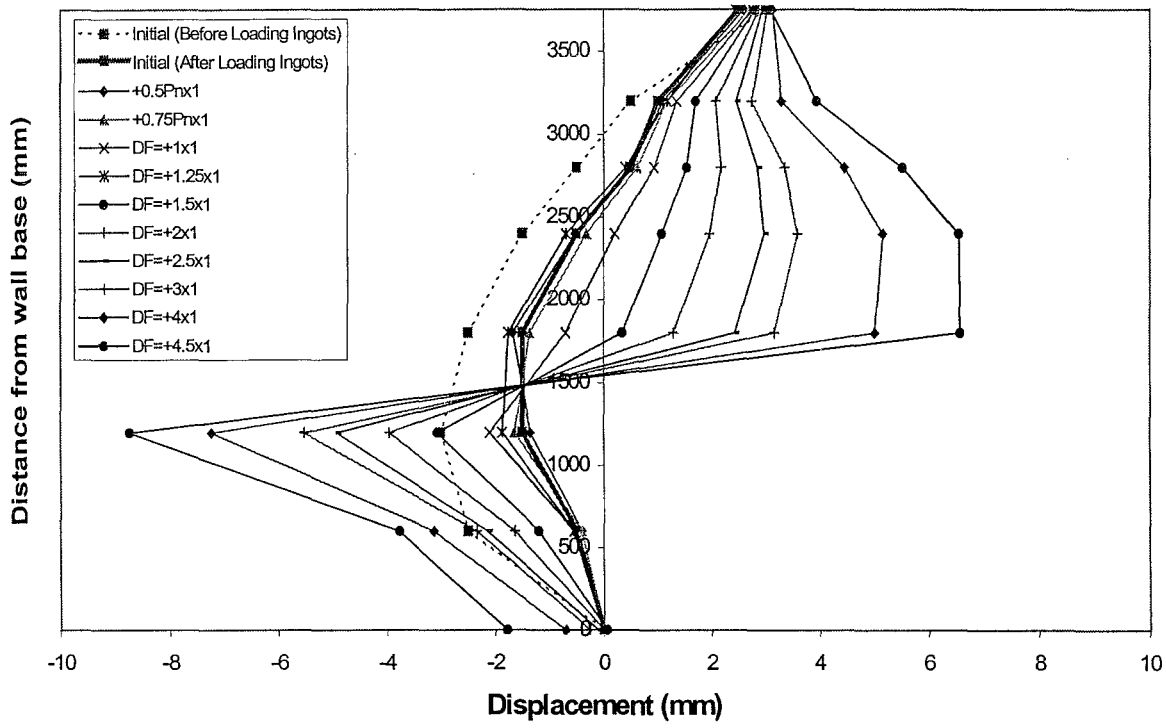

Figure 5.146: Unit 4: Out-of-plane movement on West edge of the wall at positive peak cycles (Compression edge)

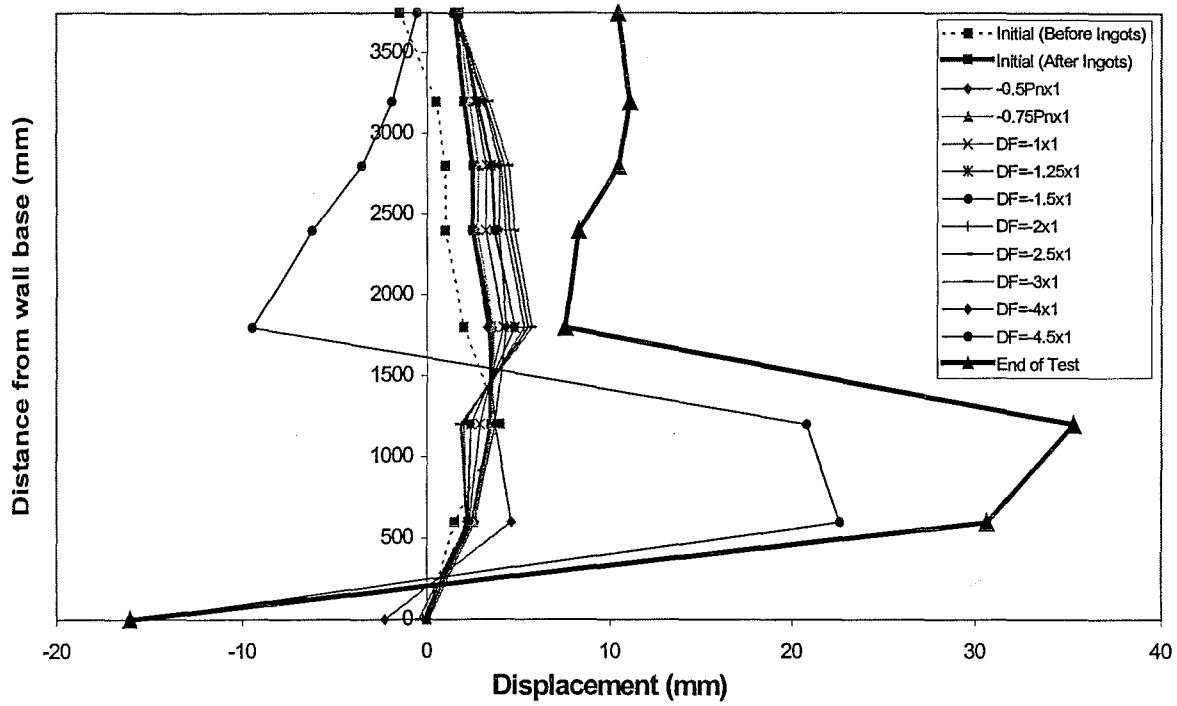

Figure 5.147: Unit 4: Out-of-plane movement on East edge of the wall at negative peak cycles (Compression edge)

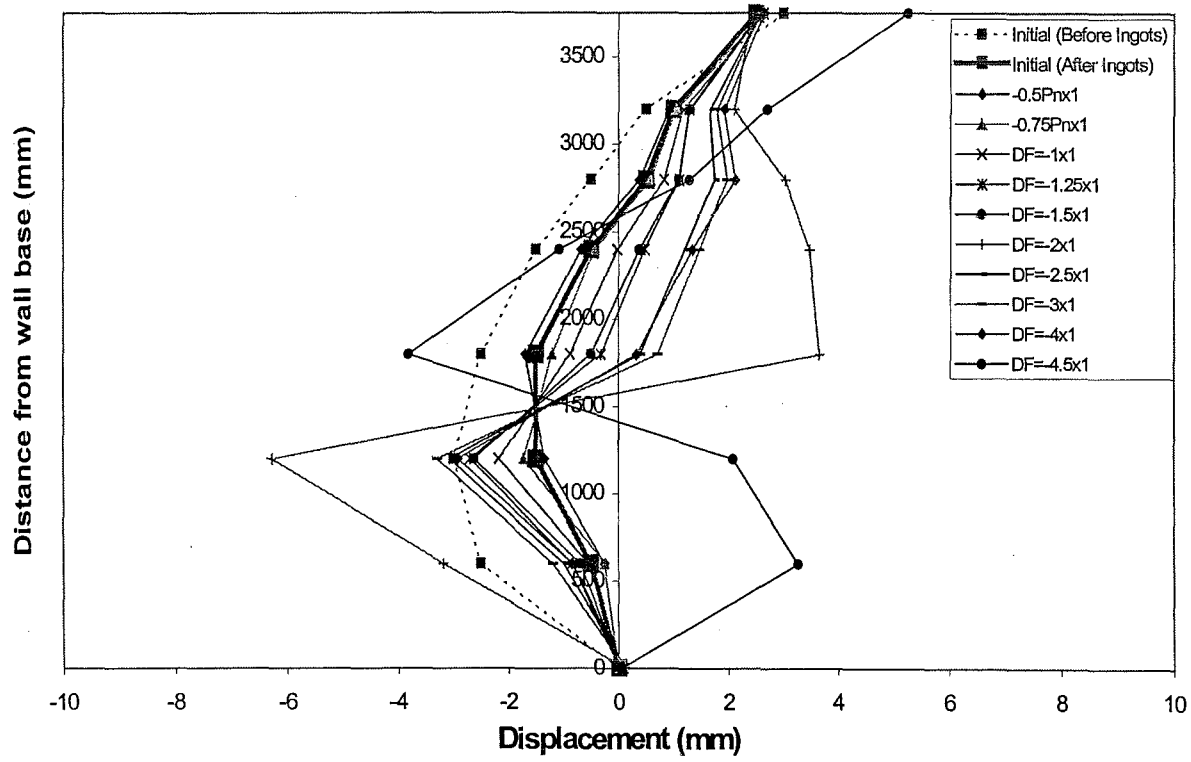

Figure 5.148: Unit 4: Out-of-plane movement on West edge of the wall at negative peak cycles (Tension edge)

5.4.3.3 Local Bar Strains : Unit 4

The variation of the local bar strains measured from the most extreme starter bars, i.e. East edge, during the test is shown in Figure 5.149. The graph only represents the strains in the wall-foundation connection where yielding was expected to take place. During the first two applied force level, i.e. $0.5P_n$ and $0.62P_n$, the strains at this location always stay below yield strain. Strains reached its yield strain when $0.75P_n$ was applied to the wall. After the twelfth cycle, large tensile strains developed in these starter bars and exceeded the yield strain limit. These maximum strains at each cycle always increased with the higher applied maximum lateral displacement. When reversing the loading direction, strains decreased a plastic elongation remained from the previous loading cycle.

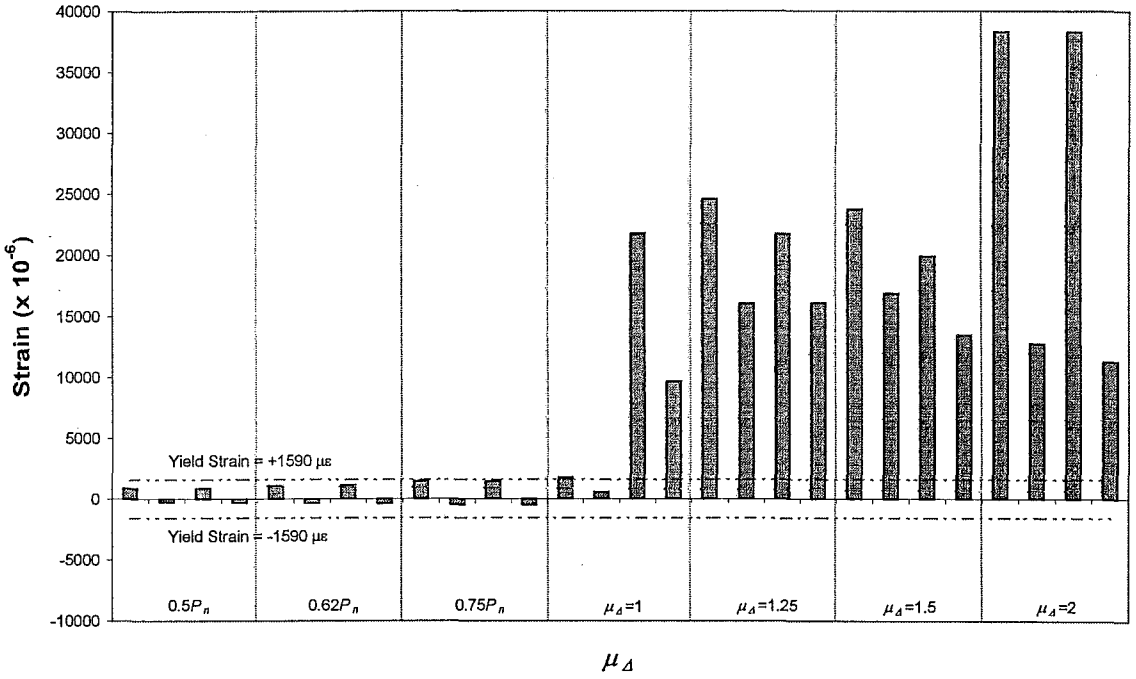

Figure 5.149: Unit 4: Strains of the outermost East edge starter bar measured at the wall-foundation interface during the test

The variation of the strains along the height of the wall was measured using strain gauges, which where attached to the longitudinal reinforcement. The local bar strains for the longitudinal reinforcement on both edges are shown in Figures 5.150 to 5.153. There were no strain variations found on the starter bars at the depth of 200 mm below the horizontal connection. Strains varied the most at the wall-foundation

interface as predicted. The strains were measured only to $\mu_\Delta \approx$ 2.5-3 where most strain gauges started to detach from the reinforcing steel.

Lap splices actually provided additional capacity around the horizontal connection. However, cracking of concrete still occurred without any yielding developed in this region at any stage of testing.

Strains of compression reinforcement always lie below yield strain except strains at the horizontal connection. Figure 5.154 shows some tensile strains occurred at the horizontal connection. These were the residual strains which taken place by the previous imposed tension. At μ_Δ = +1×1, one of the strain gauge started to become unusable, hence the reading must be ignored.

Yielding of the longitudinal reinforcement developed in the region immediately above the lap splice as shown in Figure 5.156. Yielding at this location occurred simultaneously at the horizontal joint due to a short lap splice length. However, these strains increased slower compared to the horizontal joint during the displacement controlled loading. These strain profiles were assumed to be linear between each strain gauge. Therefore, the integration of these strain variations can be used as an estimation of the total change in the height of the wall during the test.

At the wall-foundation interface, strain profile measured during an "Elastic" range had a linear shape. The neutral axis depth at yield capacity, i.e. $0.75P_n$, was approximately 215 mm from the extreme compression fibre as shown in Figure 5.154. The predicted neutral axis depth at yield capacity was 225 mm which agreed with the actual results. The local bar strains at the higher level of ductility were not shown because the strain gauges were damaged.

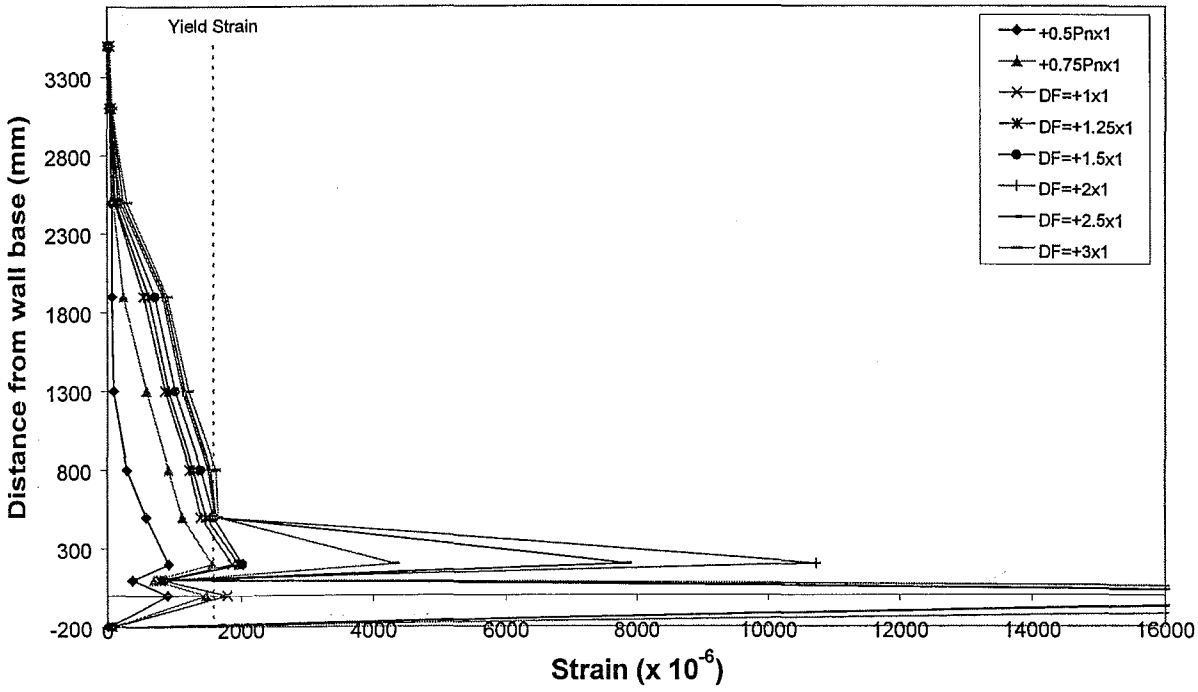

Figure 5.150: Unit 4: Outermost East edge longitudinal reinforcement strains measured at positive peak cycles (Tension edge)

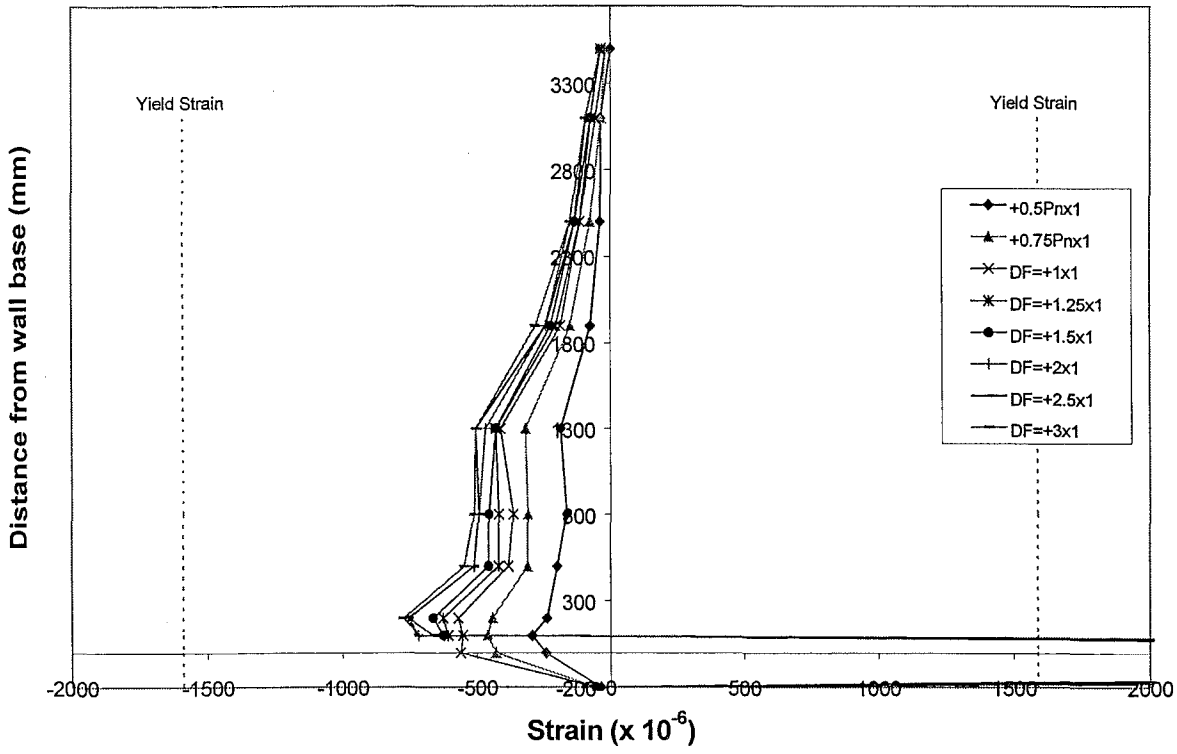

Figure 5.151: Unit 4: Outermost West edge longitudinal reinforcement strains measured at positive peak cycles (Compression edge)

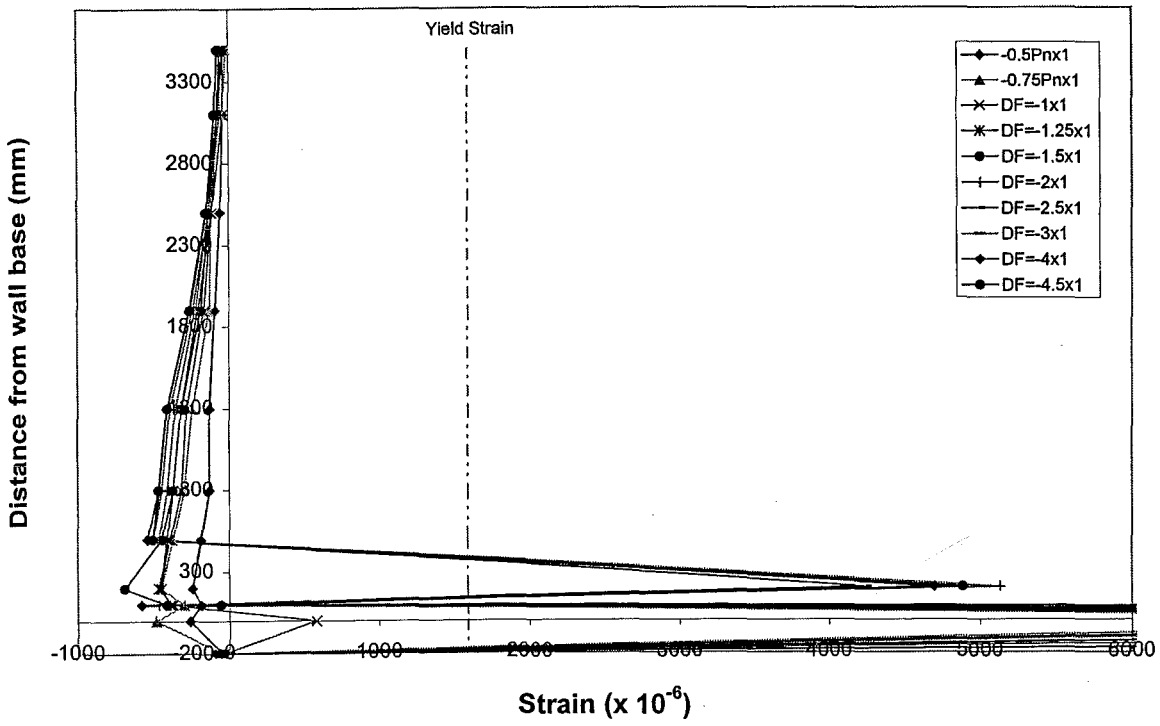

Figure 5.152: Unit 4: Outermost East edge longitudinal reinforcement strains measured at negative peak cycles (Compression edge)

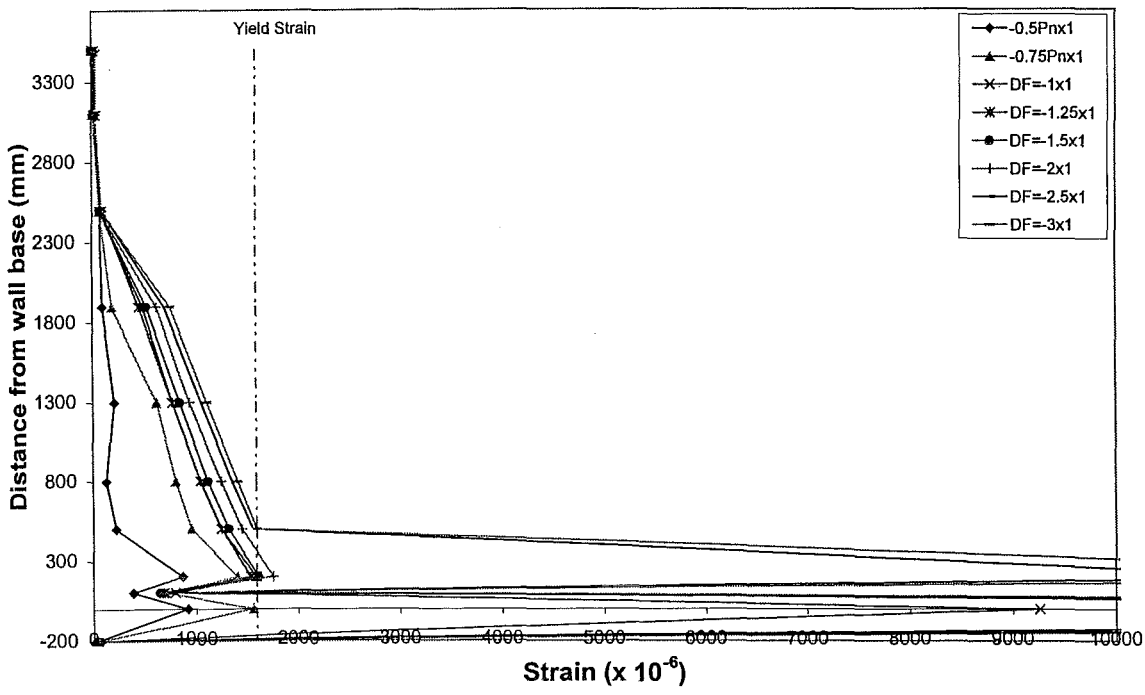

Figure 5.153: Unit 4: Outermost West edge longitudinal reinforcement strains measured at negative peak cycles (Tension edge)

In the lap splice region, the strain profiles were symmetrical about the vertical axis of the wall when subjected to the "Elastic Cycles" in both loading directions. Figure 5.155 confirmed that the repetition of the same load did not cause any strength degradation in this area during the initial cycles. The maximum tensile strain also lay well below yield strain at yield capacity, i.e. $0.75P_n$.

At the top of lap splice, strains approached yield strain at the first yield capacity, i.e. $0.75P_n$. The repetition of the same load level had more contribution on the strength degradation in this region due to the amount of cracking occurred (see Figure 5.156). The strain profile was more symmetrical about the vertical axis at $0.5P_n$ compare to the profile at the first yield capacity.

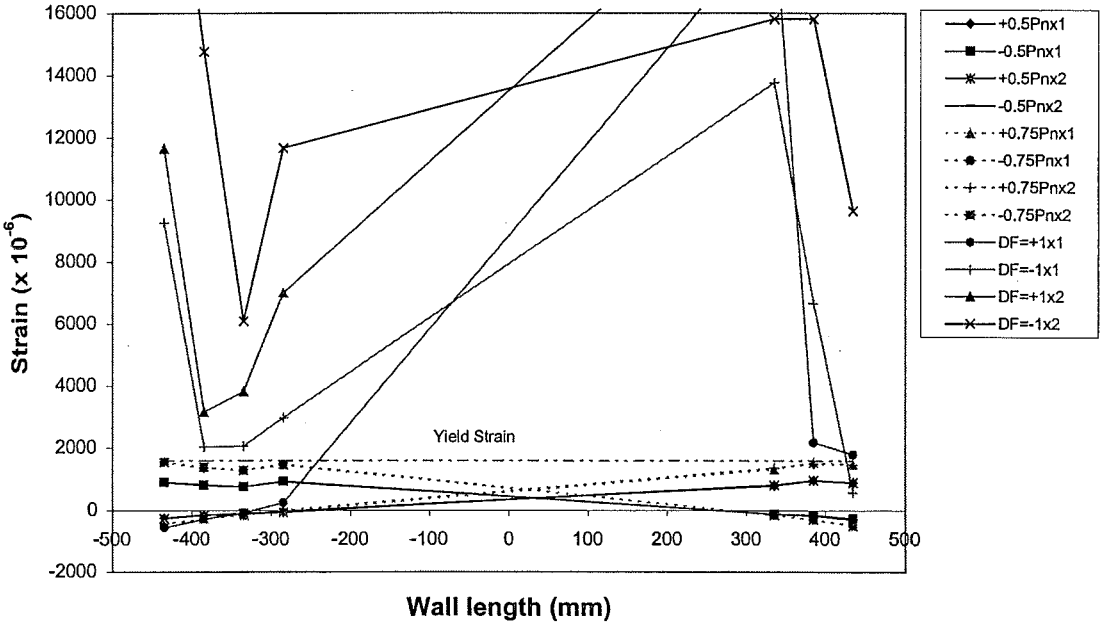

Figure 5.154: Unit 4: Strains of starter bars across the wall-foundation interface during the test

5.4.3.4 Concrete Strains : Unit 4

Figures 5.157, 5.158, 5.161 and 5.162 show the concrete strain history at the construction joint when subjected to compression and tension.

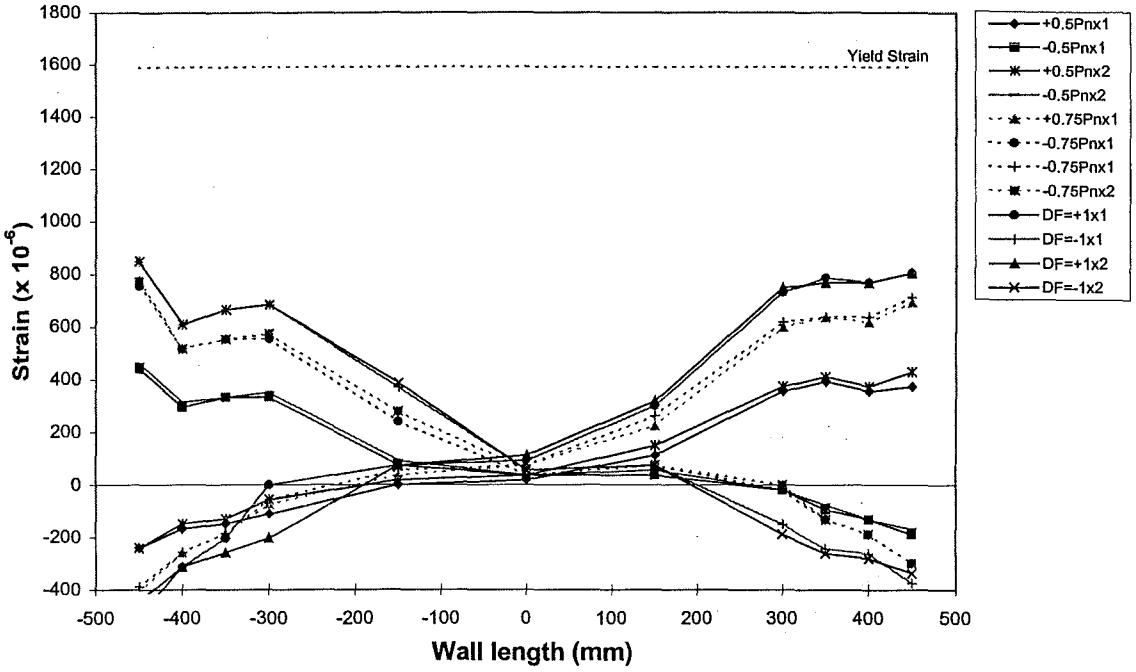

Figure 5.155: Unit 4: Strains of wall reinforcement within lap splice region (100 mm above the foundation beam) during the peak elastic cycles

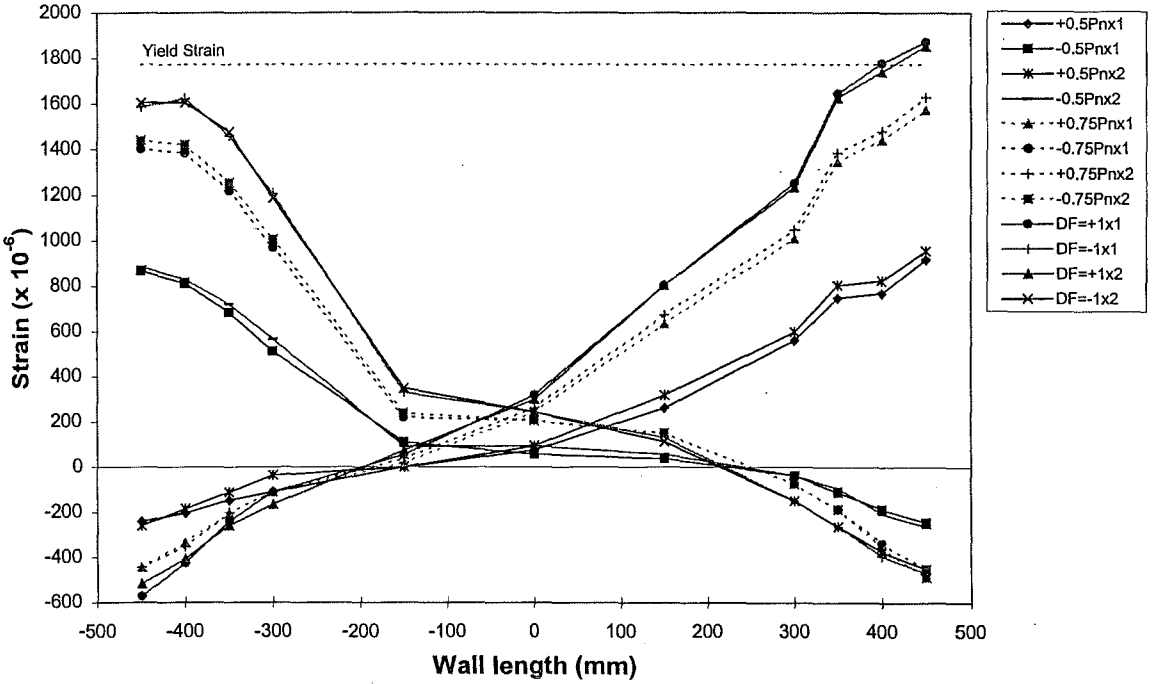

Figure 5.156: Unit 4: Strains of wall reinforcement above the region of lap splice (200 mm above the foundation beam) during the peak elastic cycles

The longitudinal concrete strain on the West edge when subjected to compression does not show residual uplift imposed at the wall base (see Figure 5.157). The neutral axis started to become skew when $\mu_\Delta = +1.25\times1$ was reached. At the region immediately above lap splice, the neutral axis commenced to skew at $\mu_\Delta = +2.5\times1$ (see Figure 5.159 (b)).

When the East edge was subjected to compression, the vertical splitting of concrete had an effect on the concrete strain. A severe damage caused the rapid drop of the concrete strain on the South facing gauge at $\mu_\Delta = -2.5\times1$ (see Figure 5.161). The measured concrete strain in the region above lap splice was less than the measured value at the wall base (see Figure 5.163).

Figures 5.158 and 5.162 show the concrete strain when the wall was subjected to tension. The two readings were reasonably close implying both faces had the approximately the same tensile concrete strain. They started to deviate when subjected to the higher displacement, i.e. $\mu_\Delta = -2.5\times2$ for West edge and $\mu_\Delta = +2.5\times1$ for East edge.

The entire panel was subjected to an uplift force until $\mu_\Delta = +2\times2$ was reached. Severe cracking occurred mostly on the East edge during the negative cycles. Concrete started to spall at $\mu_\Delta = -4.5\times1$ and the spalling concrete strain $\varepsilon_{cu} = -0.006$.

In-plane curvature in the negative loading direction was greater than the measured values during the positive loading direction (see Figure 5.165). The unsymmetrical effect of an in-plane curvature became very significant during the post-elastic cycles.

Out-of-plane curvature history is shown in Figures 5.166 and 5.167. There was not a significant rotation about the horizontal axis on the West edge. The location of maximum out-of-plane curvature was at 1 m height above the foundation beam.

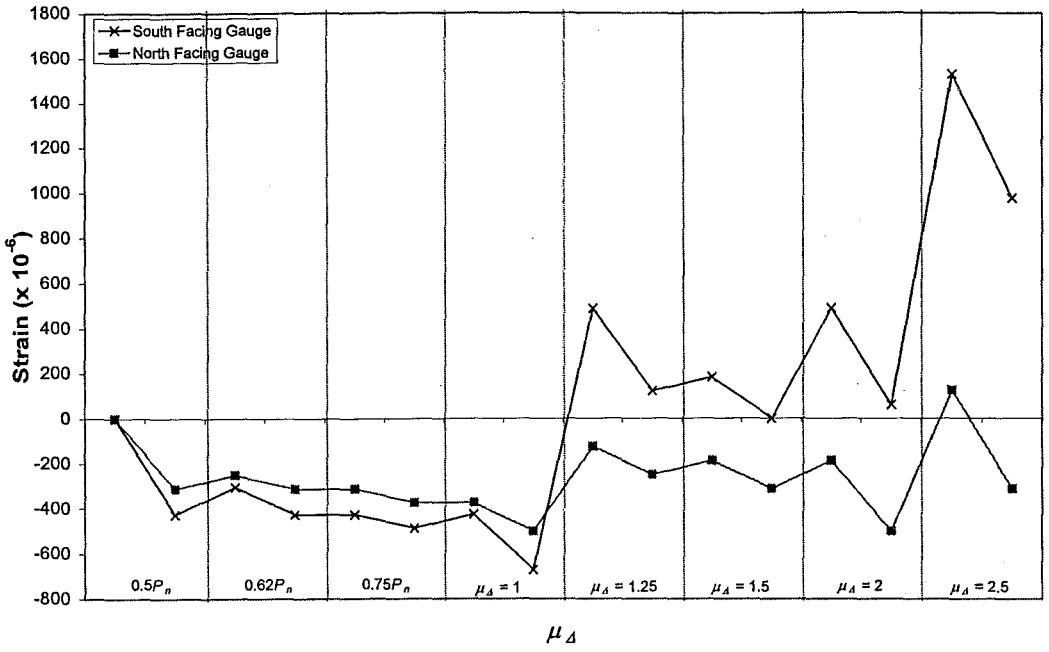

Figure 5.157: Unit 4: Concrete longitudinal strains of West edge when subjected to compression obtained from outermost clip gauges (base of wall)

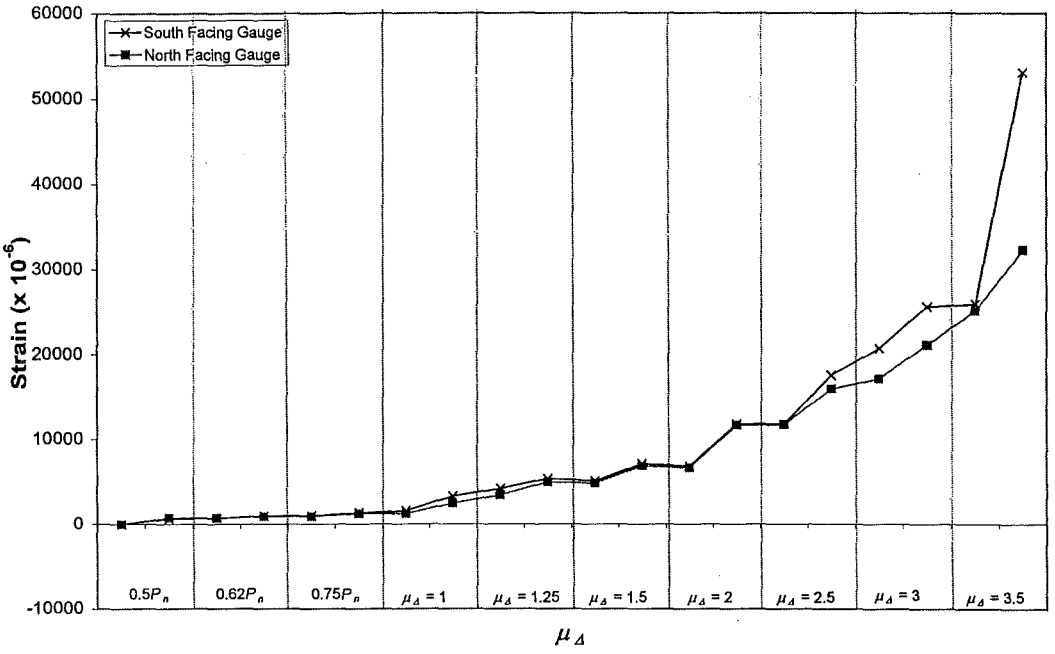

Figure 5.158: Unit 4: Concrete longitudinal strains of West edge when subjected to tension obtained from outermost clip gauges (base of wall)

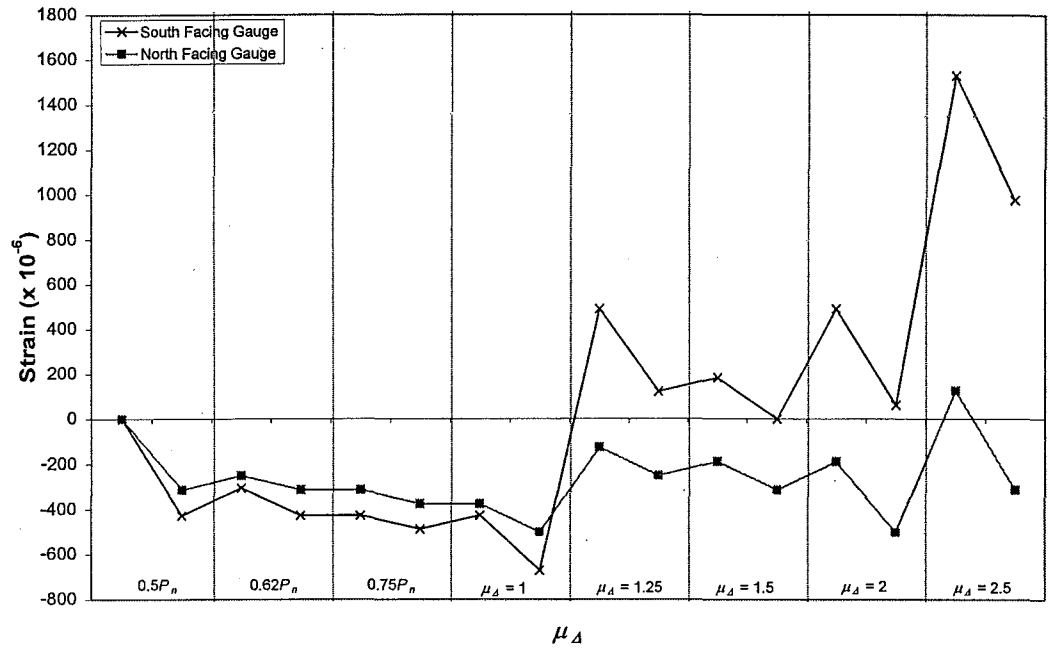

(a) Wall base

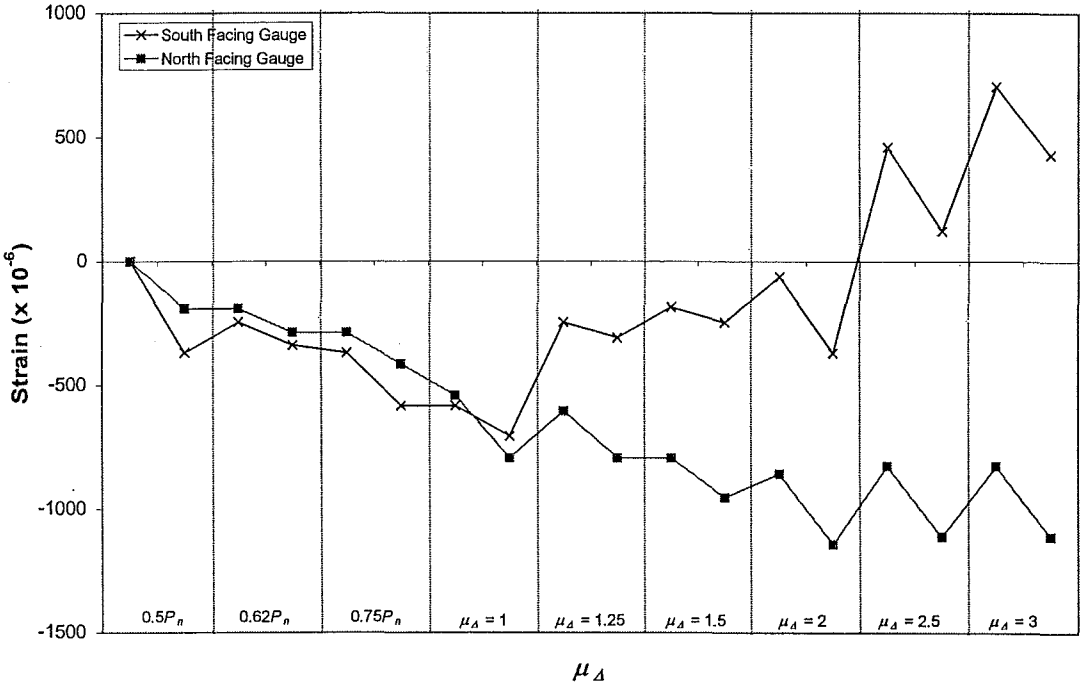

(b) Immediately above lap splice

Figure 5.159: Unit 4: Difference in longitudinal concrete strains in West edge when subjected to compression obtained from the outermost clip gauges

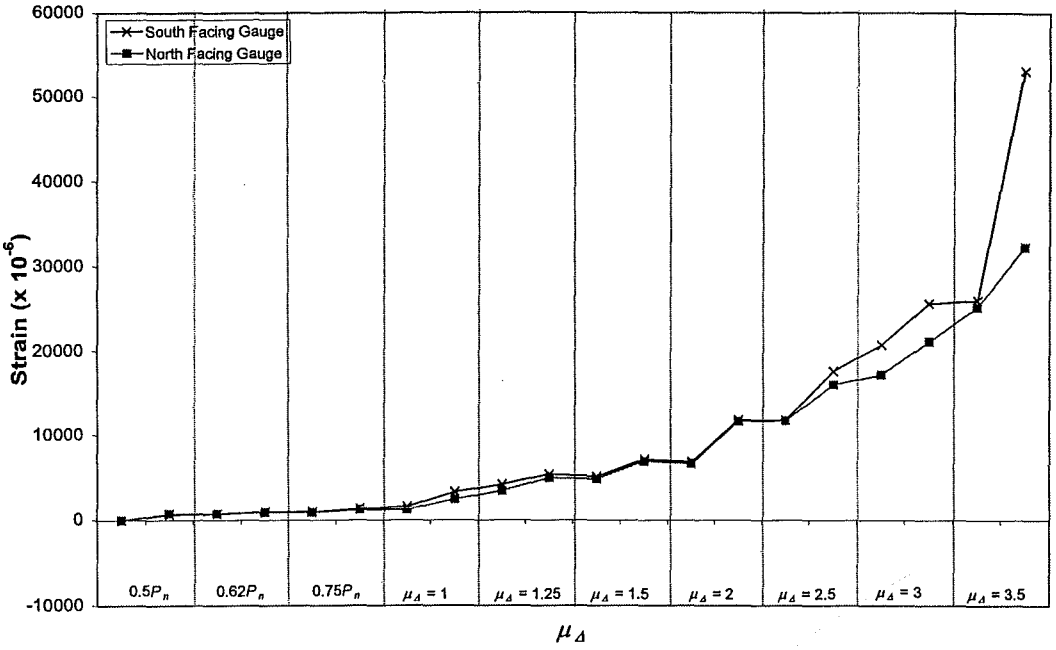

(a) Wall base

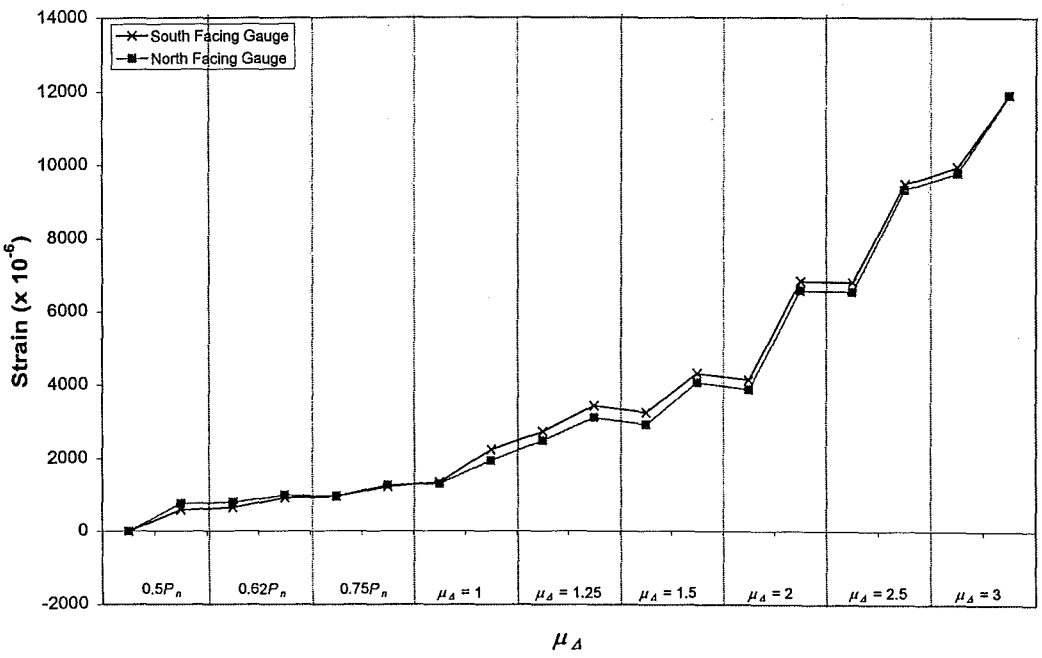

(b) Immediately above lap splice

Figure 5.160: Unit 4: Difference in longitudinal concrete strains in West edge when subjected to tension obtained from the outermost clip gauges

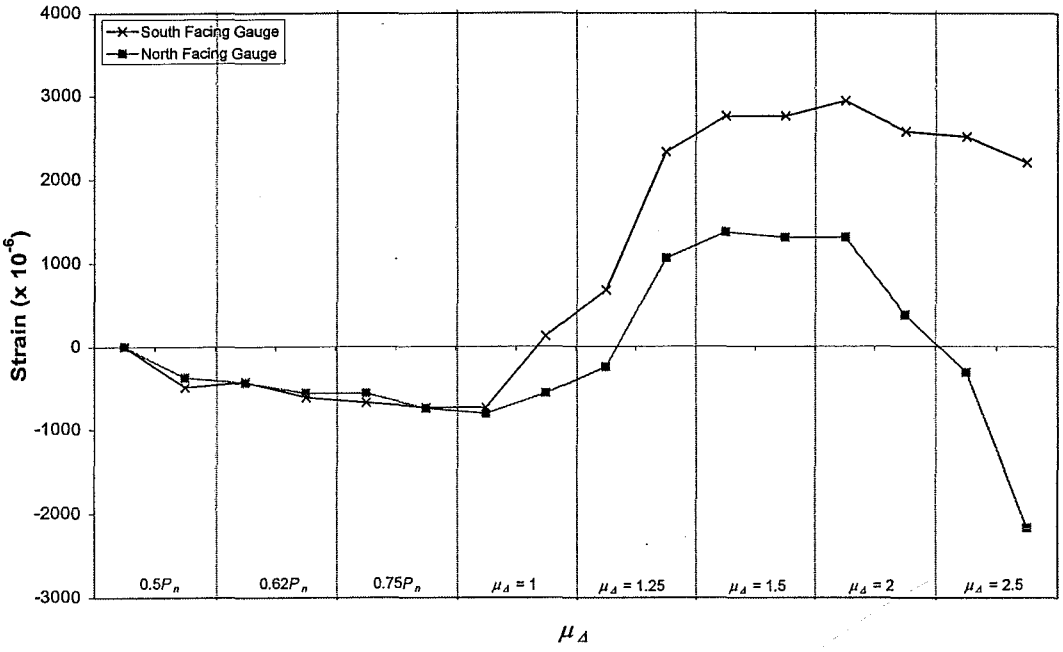

Figure 5.161: Unit 4: Concrete longitudinal strains of East edge when subjected to compression obtained from outermost clip gauges (base of wall)

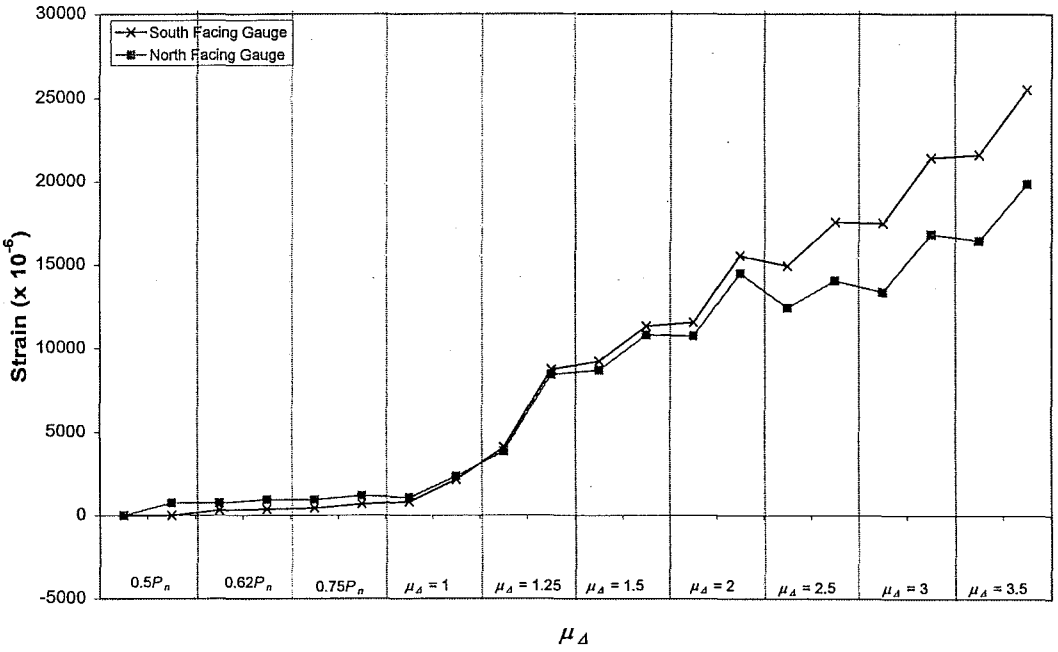

Figure 5.162: Unit 4: Concrete longitudinal strains of East edge when subjected to tension obtained from outermost clip gauges (base of wall)

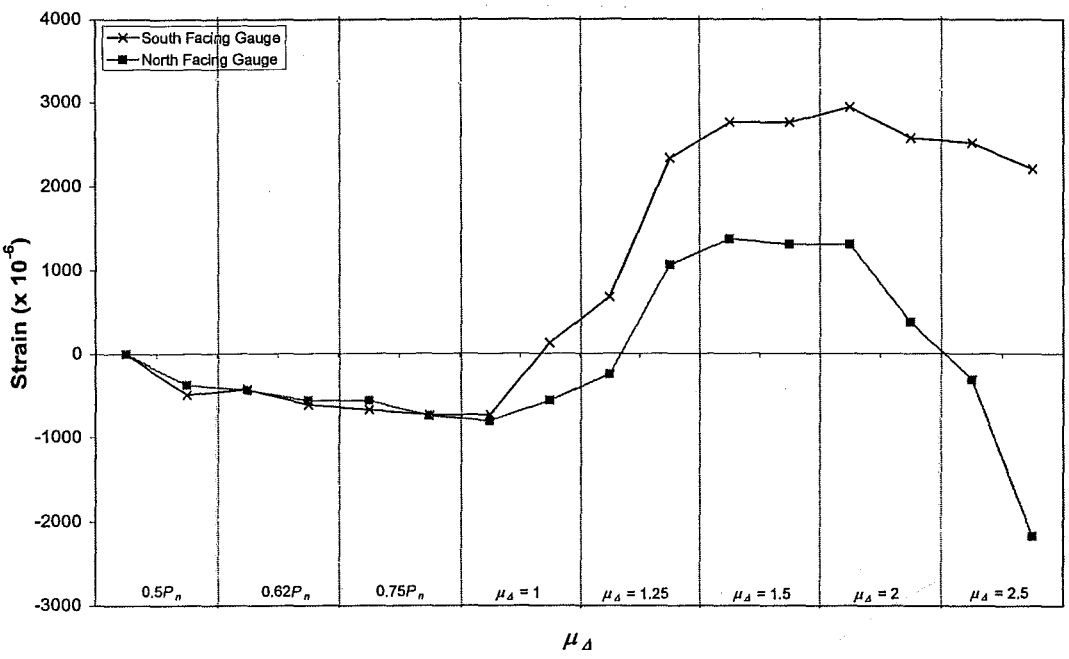

(a) Wall base

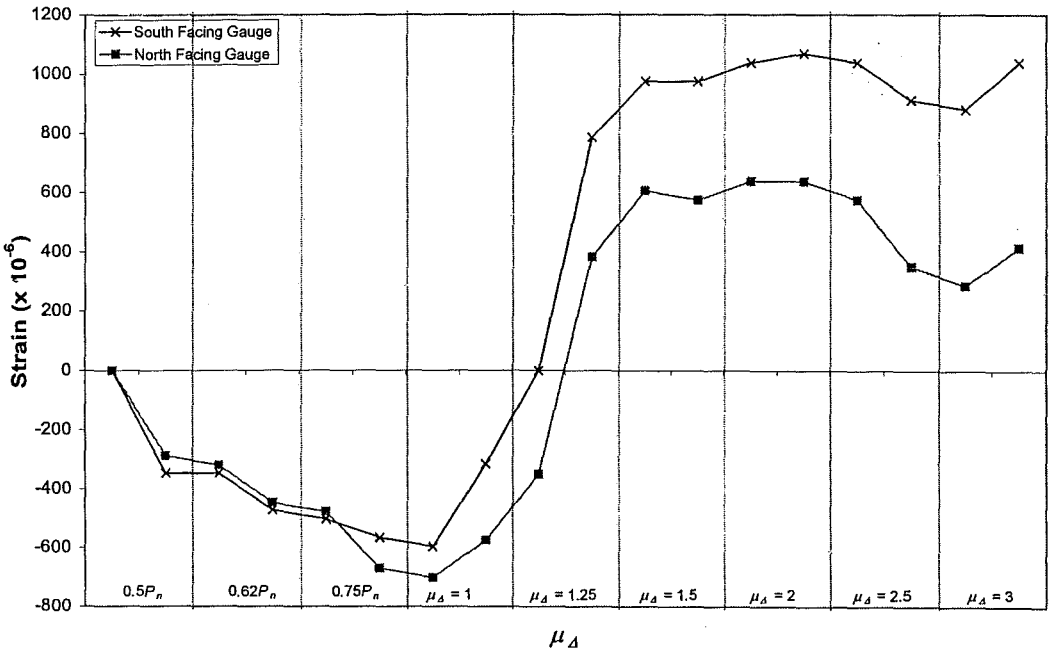

(b) Immediately above lap splice

Figure 5.163: Unit 4: Difference in longitudinal concrete strains in East edge when subjected to compression obtained from the outermost clip gauges

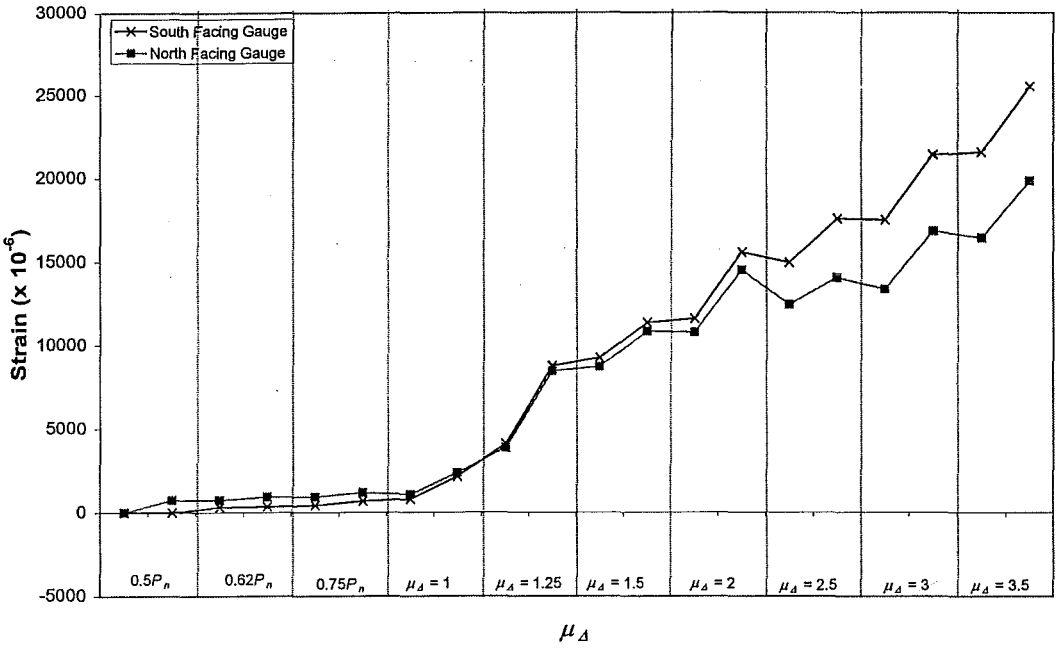

(a) Wall base

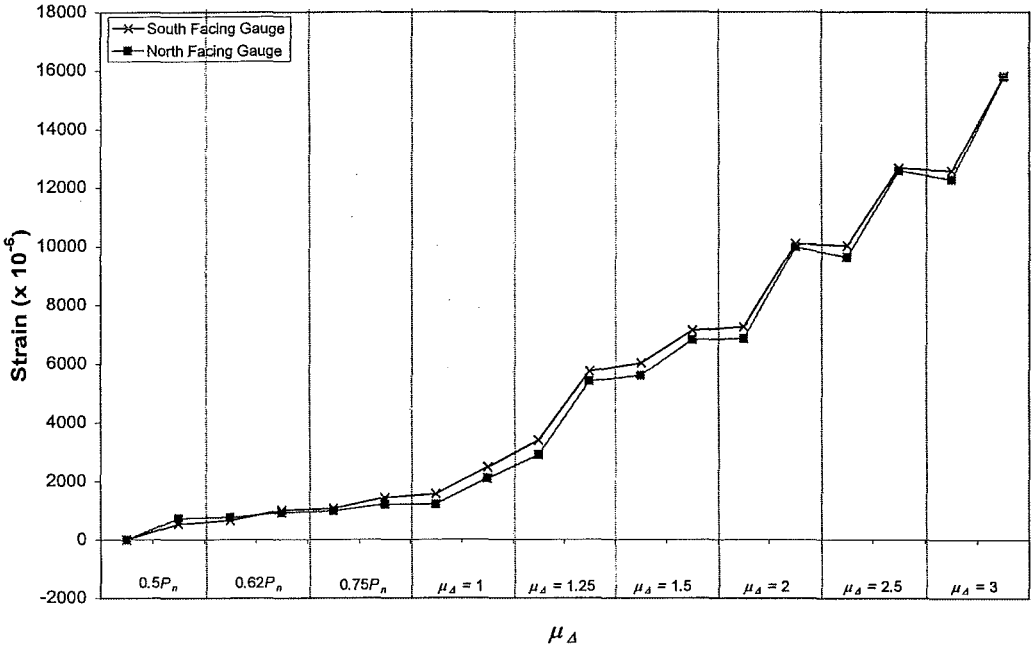

(b) Immediately above lap splice

Figure 5.164: Unit 4: Difference in concrete strains in East edge when subjected to tension obtained from the outermost clip gauges at different heights

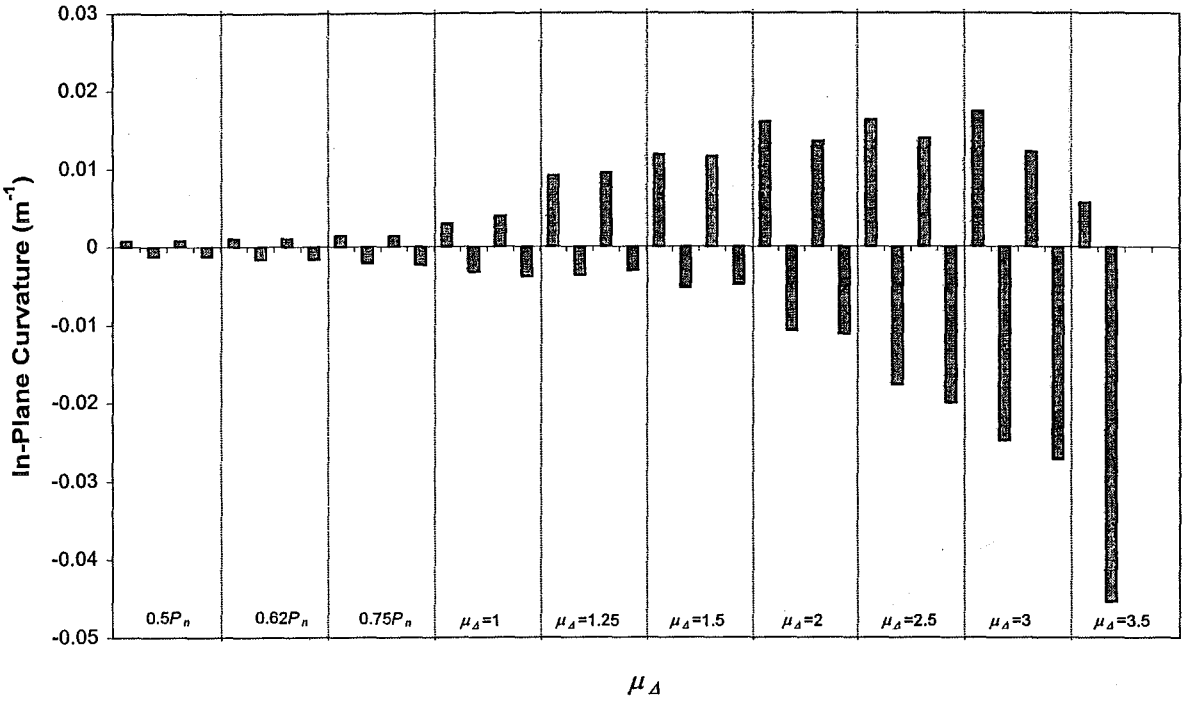

Figure 5.165: Unit 4: In-plane curvature distribution measured at 200 mm above the foundation beam

5.4.3.5 Sectional Neutral Axis : Unit 4

The neutral axis of this test specimen changed its position more rapidly compared to Unit 3 because of an effect of the applied eccentric vertical load at the top of the wall. This induced a biaxial action which catalysted the skewness of the neutral axis to occur at the lower applied horizontal forces.

When West edge was subjected to compression, the neutral axis at 200 mm above the foundation beam moved to the outside of the outermost clip gauges when $\mu_\Delta = +1.25\times1$ was reached. At 600 mm and 1000 mm above the foundation beam, the neutral axis was on the inside of the innermost clip gauges throughout the test (see Figure 5.168). When West edge became into tension, the clip gauges indicated tensile concrete strain (see Figure 5.169). The measured concrete strain decreased when the height increased.

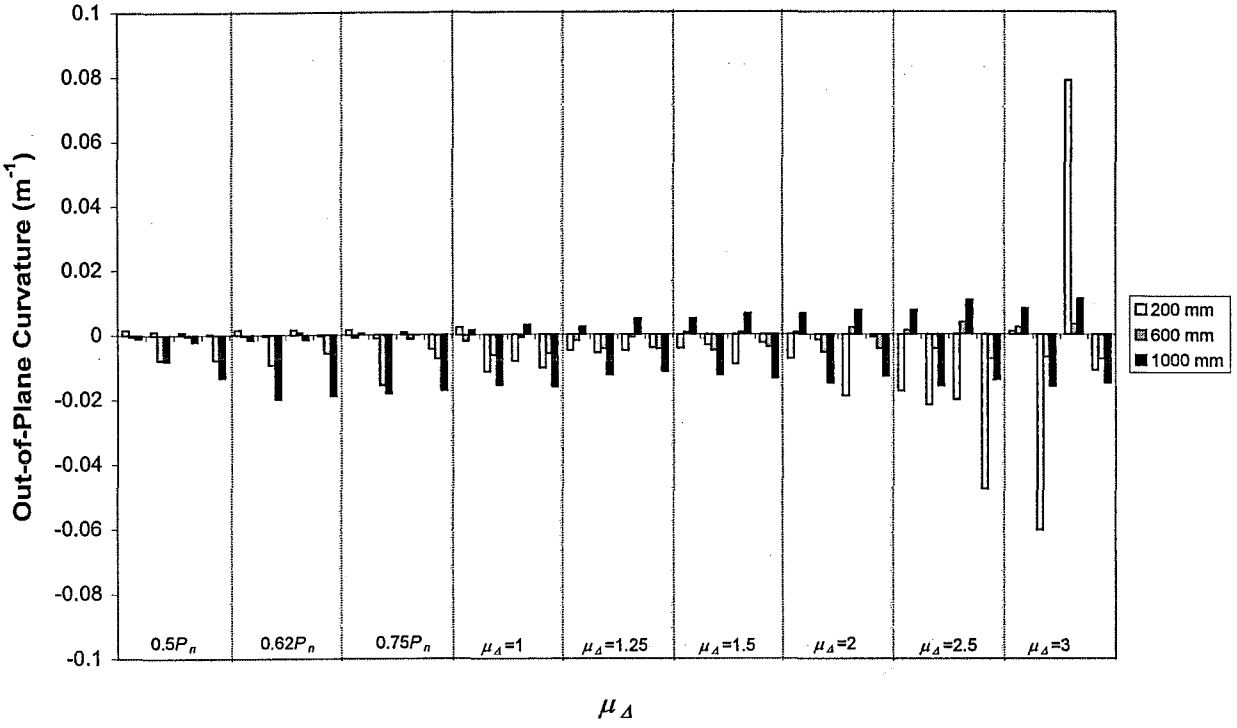

Figure 5.166: Unit 4: Out-of-plane curvature distribution obtained from outermost clip gauges on the West edge during the test

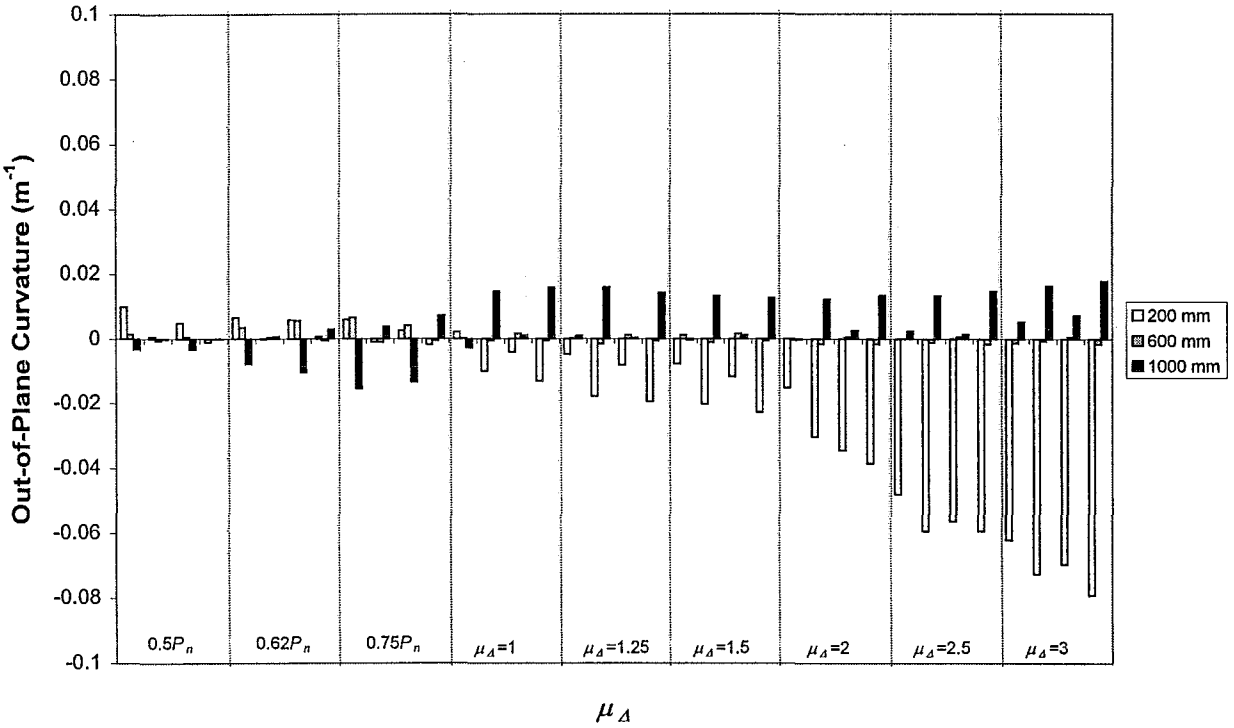

Figure 5.167: Unit 4: Out-of-plane curvature distribution obtained from outermost clip gauges on the East edge during the test

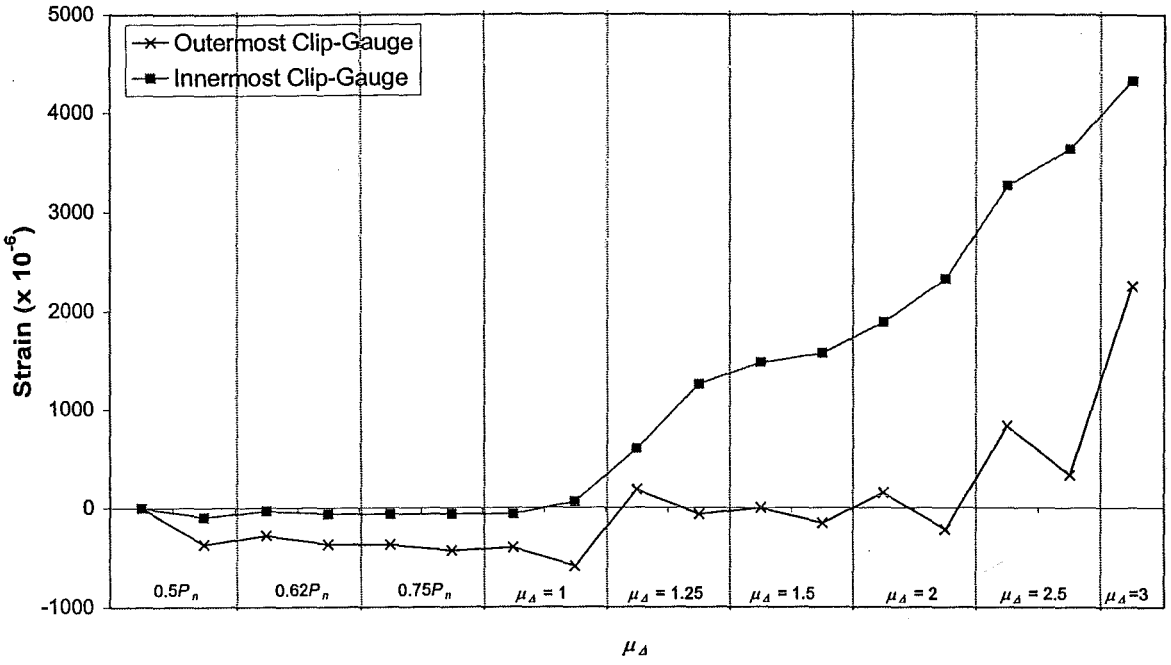

(a) 200 mm

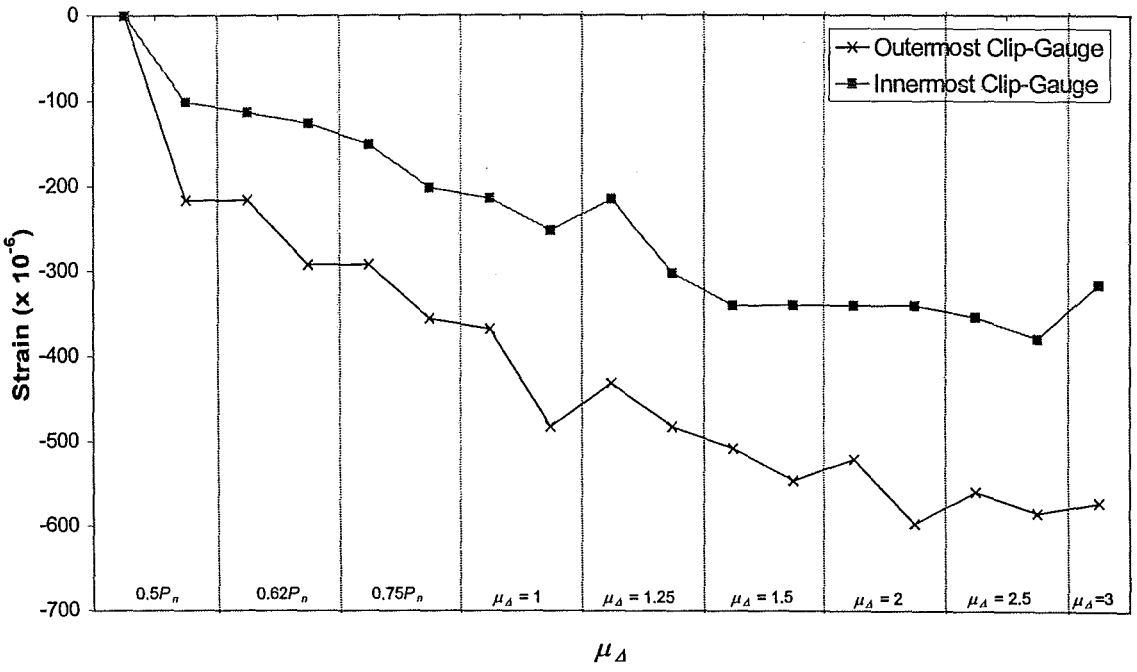

(a) 600 mm

Figure 5.168: Unit 4: Difference in concrete strains in West edge when subjected to compression obtained from the outermost clip gauges at different heights

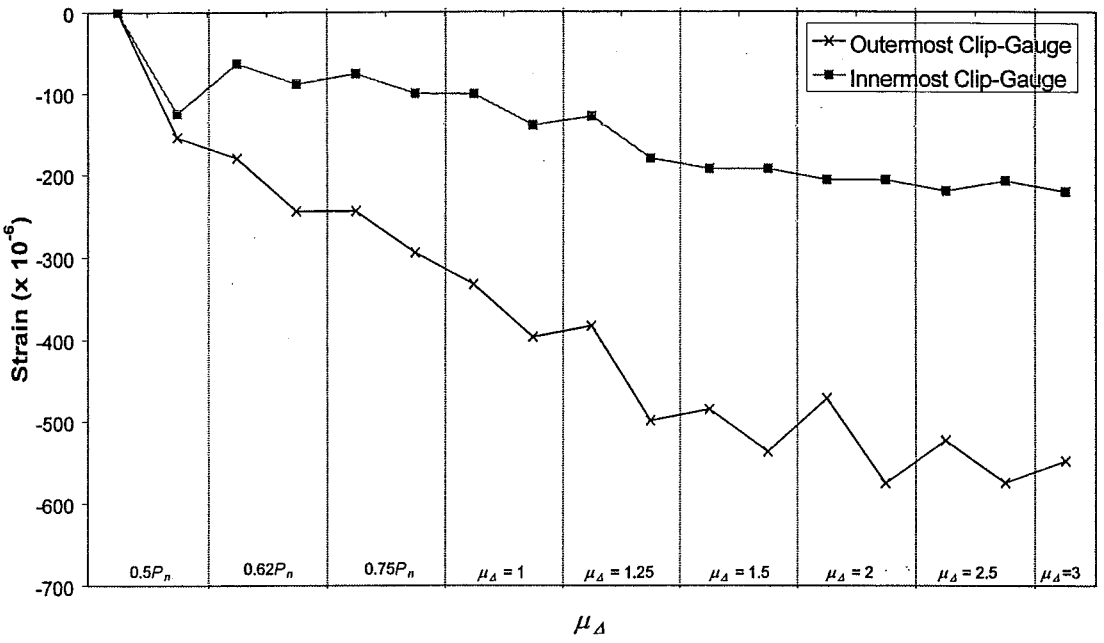

(c) 1000 mm

Figure 5.168 (cont.): Unit 4: Difference in concrete strains in West edge when subjected to compression obtained from the outermost clip gauges at different heights

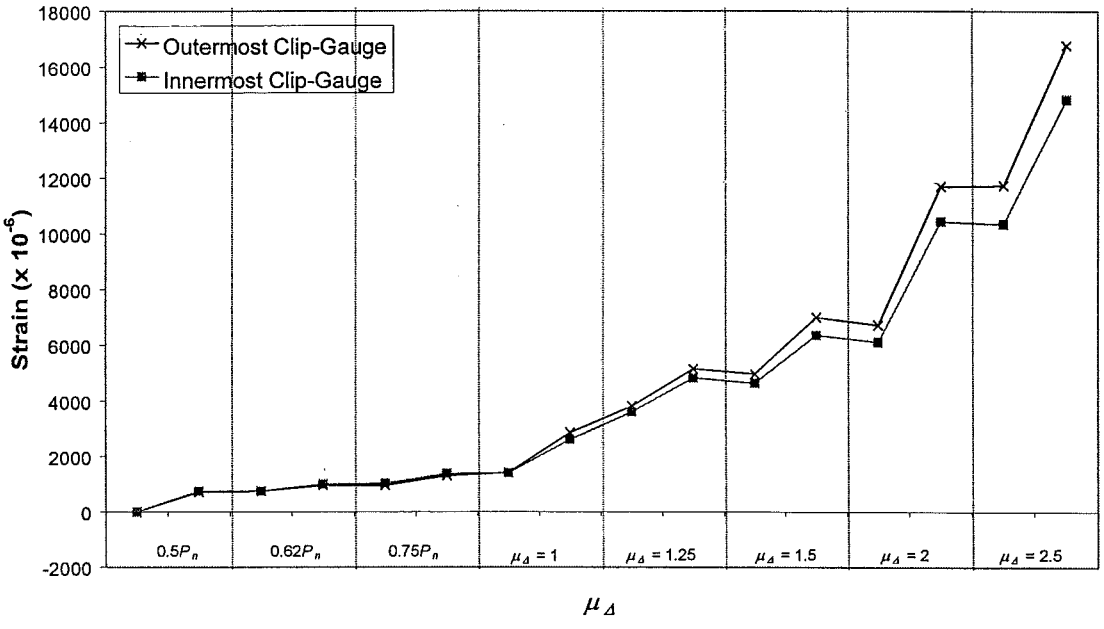

(a) 200 mm

Figure 5.169: Unit 4: Difference in concrete strains in West edge when subjected to tension obtained from the outermost clip gauges at different heights

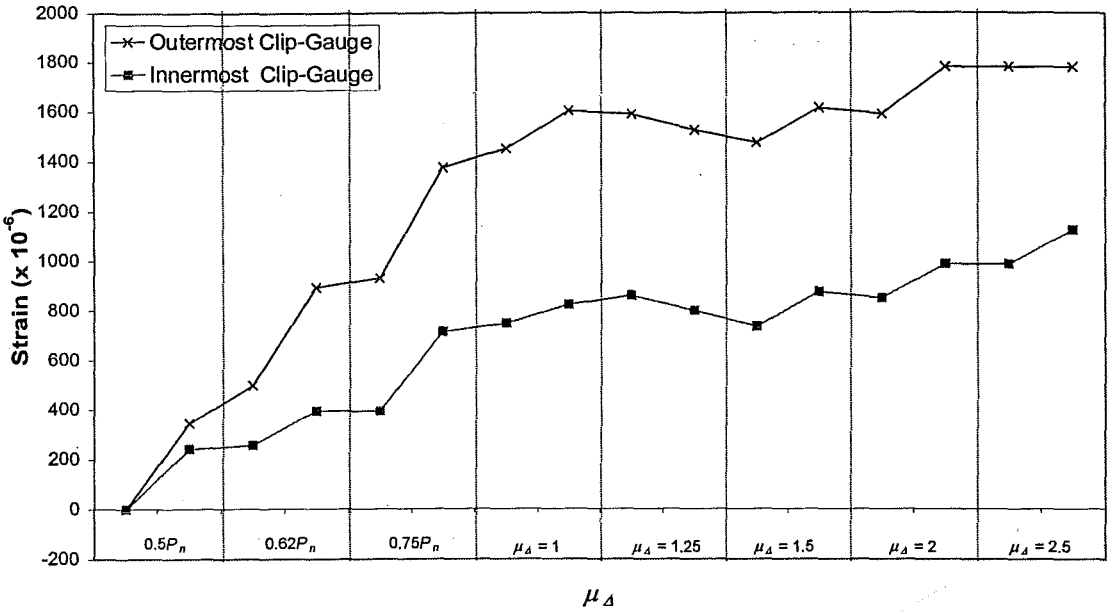

(b) 600 mm

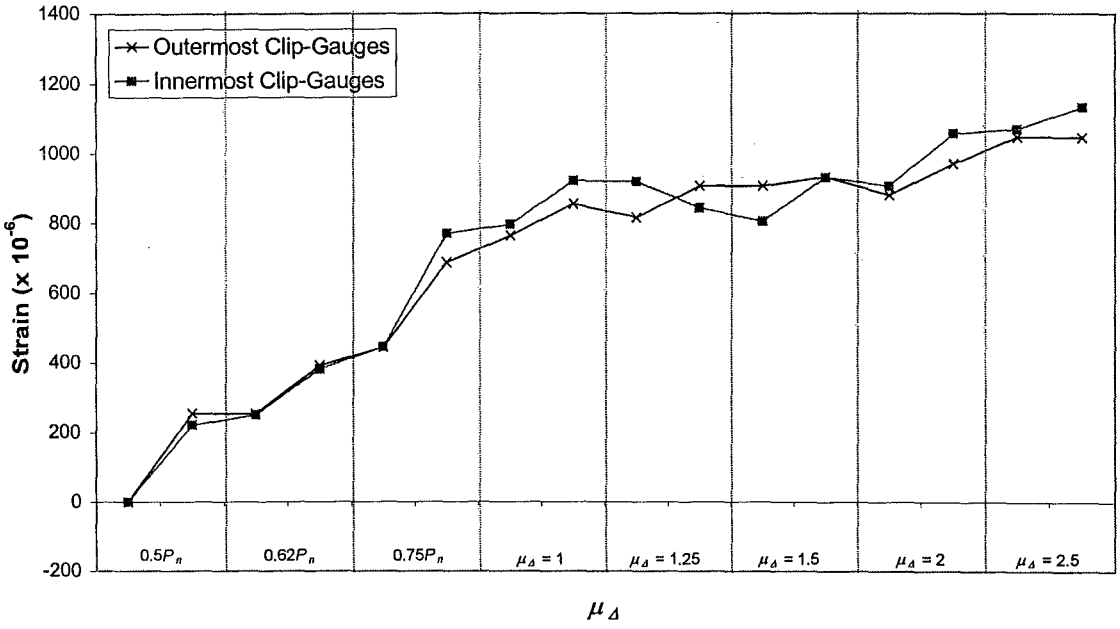

(c) 1000 mm

Figure 5.169 (cont.): Unit 4: Difference in concrete strains in West edge when subjected to tension obtained from the outermost clip gauges at different heights

CHAPTER 6
DISCUSSION

6.1 Experimental Performance

6.1.1 Overview

None of the test units failed by out-of-plane buckling. Only Unit 2 suffered by an excessive out-of-plane displacement at mid-height of the compression edge. This could lead to the lateral buckling failure occurring. Units 1, 3 and 4 were apparently stable. Strength reduction caused in these units due to the change of the neutral axis positions, fracturing of the starter bars and reduction of the lengths of walls due to crushing of the edges of the walls.

Table 6.1 shows the amount of maximum out-of-plane displacements measured during the test at $\mu_\Delta = 1.25$ and $\mu_\Delta = 4$ for the test units. It can be seen that the amount of out-of-plane displacements for Unit 2 was extremely larger than the other three test units at both μ_Δ=1.25 and $\mu_\Delta = 4$.

Table 6.1: Out-of-plane displacement

Unit	Out-of-plane displacement (mm)	
	$\mu_\Delta = 1.25$	$\mu_\Delta = 4$
1	1.5	-
2	9.0	253
3	2.8	12.5
4	7.1	8.3

Note: Wall thickness of test specimens was 50 mm.

Twisting at the base was found for Units 1, 3 and 4 when subjected to displacement ductility ranging between 2.5 and 4 as shown in Table 6.2. This was caused

by the buckling of compression starter bars and pushed the wall section sidesway, while the starter bars on tension side straightened under loading. Units 3 and 4 had greater $\mu_{\Delta,twist}$, i.e. displacement ductility level at which the wall panel commenced to twist at the base, presumably enhanced by the welding of the lap splices which prevented lateral movements that would cause buckling of the starter bars and loss of bond along the starter bars which would have occurred at an earlier stage.

Table 6.2: Displacement ductility at the onset of twisting

Unit	$\mu_{\Delta,twist}$
1	2.5
2	-
3	3
4	4

A conclusion could be drawn from the above discussion of how twisting action affected the amount of out-of-plane displacements. A large out-of-plane displacement in Unit 2 may have been associated with the lack of twisting motion at the base (which restrained any movements in the out-of-plane direction (1^{st} mode or a single curvature)). Whereas all other Units shifted to the second mode, i.e. double curvatures at higher displacement ductilities.

The available ductility of test units which was evaluated at the maximum displacement ductility, where the strength degradation of 20% of the maximum peak capacity occurred, is shown in Table 6.3.

The magnitude of sliding shear at the base was less for Units 2 and 4 compared to Units 1 and 3, respectively (see Appendix D). This was probably due to the presence of axial compression resulting from the simulated roof gravity load.

Table 6.3: Available displacement ductility at 20% reduction of maximum capacity

Unit	μ_Δ
1	2
2	2.5
3	3.5
4	4

Overstrength action occurred in Units 3 and 4 with approximately 15% increase in the in-plane flexural strength from strain hardening of the starter bars. Reiterating that the welding of the splices in Units 3 and 4 was probably the factor that permitted enhanced flexural strengths, as compared to Units 1 and 2. The real flexural strength of each wall was evaluated using two different methods, i.e. a conventional sectional analysis and a moment-curvature analysis, which are compared to the actual strength measuring from the experiment (see Table 6.4).

Table 6.4: Theoretical and experimental peak flexural strength

Unit	In-plane flexural strength (kNm)			Measured peak flexural strength / Predicted flexural strength*
	Experimental (Measured)	Sectional Analysis	Moment-curvature Analysis	
1	91	92	89	0.99
2	101	98	95	1.03
3	101	88	85	1.15
4	110	95	93	1.16

* The predicted flexural strength was taken from "Sectional Analysis Method"

It must be noted that the flexural strength of Units 1 and 2 were predicted accurately using the conventional sectional analysis and the moment-curvature analysis.

The walls with short lap splice length, which represented smaller size diameter of reinforcement, performed better than the one with long lap splice length. However, there was no crack within the top half of the panel in Units 3 and 4 with the well-defined plastic hinge region near the wall-foundation connection.

Table 6.5 shows the measured spalling concrete strain for Units 1 to 4 (measured over a 200 mm gauge length at the base of the wall). It must be noted that these values are greater than what is given in for an unconfined ultimate concrete strain in New Zealand Concrete Structures Standard [N1].

Table 6.5: Measured spalling concrete strain

Unit	Spalling Concrete Strain, ε_{cu}
1	-0.004
2	-0.007
3	-0.005
4	-0.006

6.1.2 Unit 1

Unit 1 started to lose its lateral load resisting capacity during the twisting at the base at the compression edge as subjected to in-plane loading. The twisting motion occurred simultaneously with the spalling of the concrete cover that allowed the starter bars to buckle under compression. At μ_Δ = +5×1 the resisting flexural capacity had dropped to approximately 15% of the maximum flexural capacity.

The extensive cracking appeared to take place more on the concave side than convex side of the wall which propagated from the extreme tension fibres. Because of the initial profile of the wall, the concave side of the tension edge was subjected to longitudinal tension stress in conjunction with out-of-plane flexural tension stresses. The result of this biaxial moment lead to the sudden reduction of flexural strength at μ_Δ = +2.5×2. This explains why overstrength did not occur in Unit 1; the extreme

skewing of the neutral axis altered the shape of the contact area of concrete compression zone which shifted the centroidal position of internal concrete compression force and reduced the internal lever arm.

The maximum out-of-plane displacement was approximately 0.1% of the storey height. This magnitude of the out-of-plane displacement would not be able to trigger lateral buckling failure to this type of wall panel. Additionally, large cracks did not occur in the region immediately above lap splice where lateral buckling be expected to start.

6.1.3 Unit 2

Unit 2 was the most critical test specimen which must be considered very carefully due to the significant amount of out-of-plane displacement. The test was ended when the panel was visually unstable to avoid any unexpected accidents during the test. The resisting flexural capacity at the end of the test was 45% of the maximum flexural capacity.

The cracking extended over the whole panel on the convex side and concentrated in the top half region of the wall except at the base of the wall where plasticity was concentrated. These cracks reduced the stiffness of the whole panel as the applied displacement ductility increased. Combined with the effects of biaxial response of the eccentric vertical load, the out-of-plane displacement became extremely large compared to the out-of-plane displacement of Unit 1.

Twisting of the base was not detected in Unit 2 at any stage of testing. As mentioned earlier, this would have a major effect on the crack patterns. Therefore cracking would be expected everywhere on the panel, while the connection of Unit 1 twisted which relieved some of the out-of-plane moments imposed by the eccentric gravity loads.

The strength of this unit decreased during the out-of-plane rotation at the base of the wall at $\mu_{\Delta} = 2$. The neutral axis became skew similarly to Unit 1 and contributed to

the strength reduction. However, the rate of strength degradation for Unit 2 was faster due to the applied secondary moment from the eccentric vertical load. Unfortunately, there was no instrumentation provided to measure the out-of-plane shear induced by the eccentric vertical load. Therefore, out-of-plane shear was not determined in the experiment.

6.1.4 Units 3 and 4

These test units were displaced and undergone deformation mainly due to flexural cracking which was confined within 1 m height above the foundation beam. The failure of these test units caused by fracturing of starter bars in the region adjacent to the lap-splice welds when subjected to cyclic loading. There was no sign of lap splice bond failure because of the welded connections.

Welds along the lap-splice certainly enhanced the performance of both walls by eliminating crushing of cement-based grout as observed in Units 1 and 2. Lateral displacement of lap splice never happened at any stage of testing which minimised the magnitude of twisting at the base and consequently increased displacement ductility of twisting ($\mu_{\Delta,twist}$) to 3 and 4 for Units 3 and 4, respectively. The lap splice welds also had an effect on an increase of the amount of energy dissipation that can be shown on the hysteresis loops for Units 3 and 4 (see Figures 5.100 and 5.143).

Flexural cracking seemed to govern the behaviour of Units 3 and 4. Most cracks were concentrated in the region near the wall-foundation connection where the potential plastic hinge zone was defined. No cracking was found in the region above the mid-height of the panel. As a result of a large plastic deformation of the starter bars at the wall-foundation connection, overstrength and yield penetration were allowed to occur at the higher imposed displacement ductility caused the wall panel to deform mainly in flexural mode.

Cracking above lap splice implied that there was a yield penetration spreading along the longitudinal reinforcement. However, these cracks did not have much effect on

the out-of-plane displacement or any sign that lateral buckling failure that might occur. The amount of out-of-plane displacement on the compression edge was minimised by twisting action at the base which was moving in the same direction as the out-of-plane displacement as mentioned previously.

Eccentric vertical load did have some contribution on the behaviour of Unit 4 but not very significant. Vertical splitting of the compression end of the wall was found when attempting to achieve the first cycle of μ_Δ = -4.5×1 at concrete strain ε_{cu} = -0.006. This confirmed that the confining reinforcement should be provided in order to increase spalling strain of concrete and hence at displacement ductility of vertical splitting.

6.2 Analytical Methods

6.2.1 Wall Stiffness

The stiffness of the walls was calculated using a moment-curvature analysis with different sectional and material properties. The value of wall stiffness was taken as the slope of the straight line that went from the origin through the point of the first yield capacity. The first yield capacity was defined as the wall capacity at which tensile reinforcement attains the yield strain or the extreme concrete compression fibre attains a strain, ε_{cu} = -0.002, whichever yields the lowest value. The specific name for this type of stiffness is "Secant Stiffness, k_{75}".

The modulus of elasticity of concrete, E_c was calculated using Equation 3-7 assuming the concrete density was equal to 2300 kN/m^3. Concrete strength for this analysis was equal to 30 MPa as normally specified in the design.

Three different grades of reinforcement, which are 300, 430 and 500, were used to ensure that the effects of the reinforcement variation, f_y, are covered in the analysis. The size and location of the reinforcing steels were arbitrarily chosen to simulate the condition of different reinforcing steel content, p_s. Subsequently, the theoretical effective second moment of inertia was calculated by back substitution of the theoretical secant stiffness, from a moment-curvature analysis, into Equation 6-2.

A graph of the ratio of the effective second moment of inertia to the gross second moment of inertia, I_e/I_g, was plotted against reinforcing steel content, p_s, with the variations of the strength of reinforcing steel, f_y, as shown in Figure 6.1. The second graph was plotted between the effective second moment of inertia to the gross second moment of inertia, I_e/I_g, and the strength of reinforcing steel, f_y, with the variation of reinforcing steel contents (see Figure 6.2). Figure 6.2 shows little difference as predicted. Hence, an equation which can be used to predict the effective second moment of inertia for different reinforcing steel contents can be formulate using Figure 6.1 only.

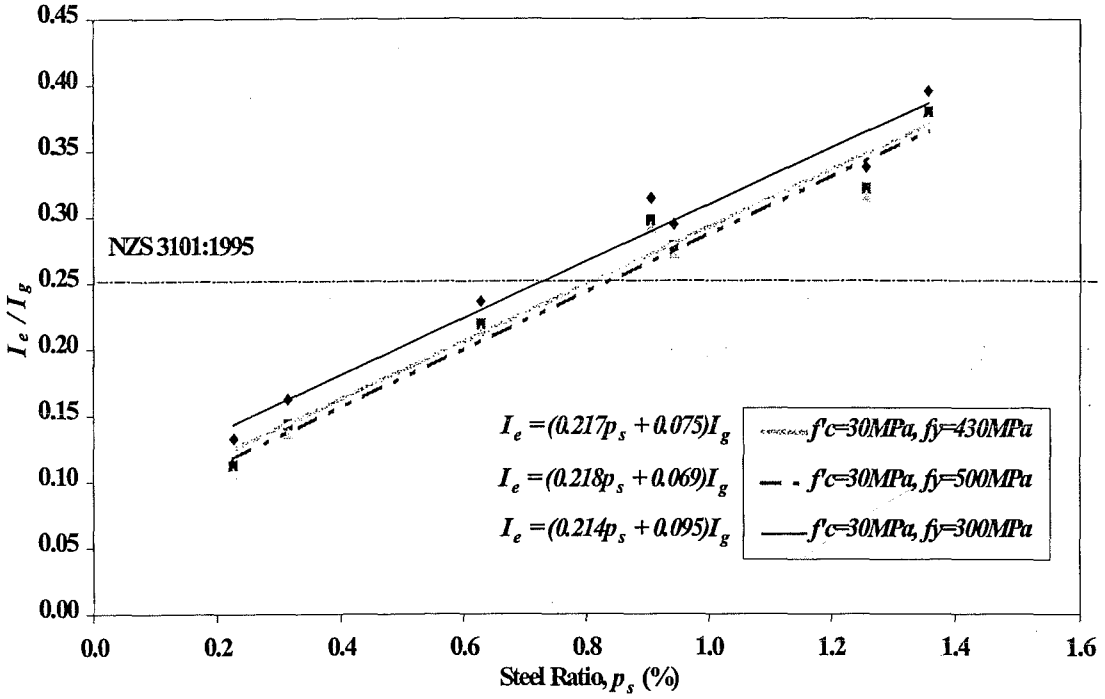

Figure 6.1: Graph I_e/I_g vs. p_s with the variation of reinforcing steel strength

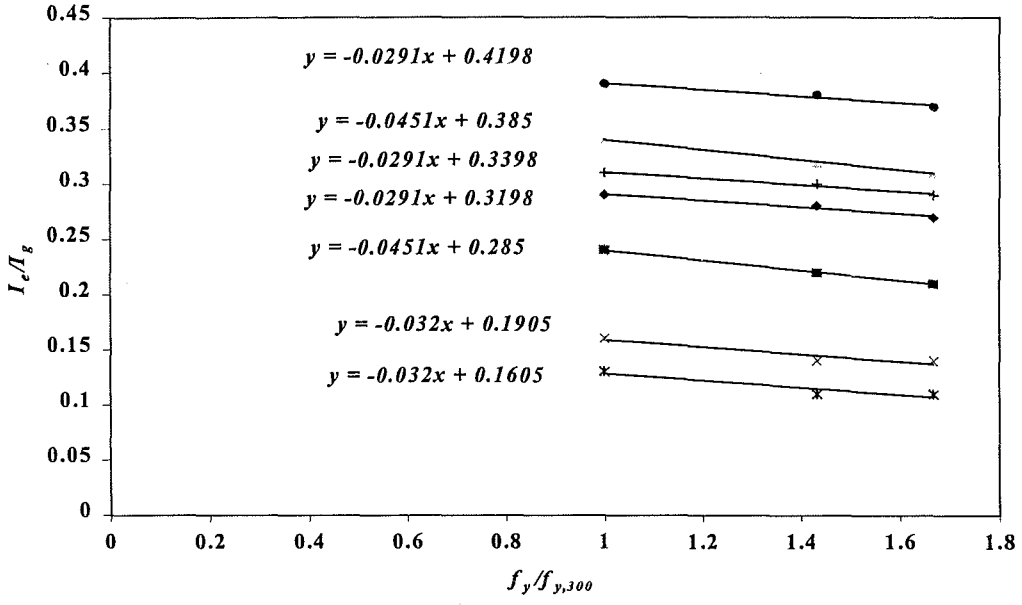

Figure 6.2: Graph I_e/I_g vs. f_y with the variation of reinforcing steel contents.

This equation was derived based on Grade 300 reinforcing steel that was given in Equation 6-1.

$$I_e = (0.21p_s + 0.095)I_g \qquad [6\text{-}1]$$

where

I_e = effective second moment of inertia (mm^4)

I_g = gross second moment of inertia (mm^4)

p_s = reinforcing steel content (%)

f_y = lower characteristic yield strength of non-prestressed reinforcement (MPa)

Table 6.6 shows the comparison of the theoretical wall stiffness and the experimental wall stiffness of the test units of this research and the test results from McMenamin [M1]. The experimental wall stiffness was the secant stiffness taken from the actual moment-curvature plots. Theoretical wall stiffness, $k_{theoretical}$, was calculated from flexural deformations using Equation 6-2 without taking into account of shear deformation and foundation rotation effect. The actual material properties measured at the day of test were used for calculating the predicted wall stiffness.

$$k_{theoretical} = \frac{3E_c I_e}{h_w^3} \qquad [6\text{-}2]$$

where

$k_{theoretical}$ = theoretical wall stiffness (N/mm)

E_c = modulus of elasticity of concrete (MPa)

I_e = effective second moment of inertia (mm^4)

h_w = total cantilever height of wall (mm)

Table 6.6: Comparison of theoretical wall stiffness and experimental wall stiffness

Units Description	h_w (mm)	l_w (mm)	A_r	p_s (%)	f'_c (MPa)	f_y (MPa)	E_c (MPa)	k^*_{calc} (kN/mm)	k_{expt} (kN/mm)	k_{expt}/k^*_{calc}
McMenamin 1	2500	2000	1.25	1.1	49	504	30140	62.8	17.7	0.28
McMenamin 2	2500	2000	1.25	0.6	51	504	30610	43.3	25.7	0.59
McMenamin 3	2500	1500	1.67	0.6	35	504	26540	15.8	10.0	0.63
McMenamin 4	2500	1000	2.50	0.6	61	504	32830	5.8	6.1	1.05
McMenamin 5	2500	1000	2.50	1.1	37	504	27100	7.1	4.0	0.57
Chiewanichakorn 1	3750	1000	3.75	1.2	39	318	27630	2.3	1.4	0.62
Chiewanichakorn 2	3750	1000	3.75	1.2	44	318	28920	2.4	2.0	0.84
Chiewanichakorn 3	3750	1000	3.75	1.2	23	318	22820	1.9	2.0	1.07
Chiewanichakorn 4	3750	1000	3.75	1.2	30	318	25080	2.1	2.4	1.17

* $k_{theoretical}$ using Equation 6-2

It is shown that Equation 6-1 gives a reasonable approximation of the effective second moment of inertia and hence the wall stiffness except for squat walls. The difference between the theoretical and experimental wall stiffness was below 50%, except for McMenamin 1, probably due to the amount of sliding shear. Most test units had the higher theoretical wall stiffness than the measured value because shear deformation and foundation rotation effect were not taken into account in Equation 6-2. Therefore the wall stiffness, i.e. the applied force per unit displacement, must be higher than the experimental wall stiffness.

6.2.2 Design and Assessment Procedure

This section is a guideline for the design of thin precast concrete walls with the ratio of height to thickness, h_w/t_w, does not exceed 50. Although the wall panel with height to thickness ratio $h_w/t_w = 75$ performed reasonably well, three out of four test units showed the second mode (double curvatures) of out-of-plane displacement and two units had enhanced behaviour through welded splices details that would probably not be used in practice. According to the available test results, the height to thickness ratio $h_w/t_w \leq 50$ is recommended.

Buildings of normal occupance in New Zealand are generally designed for earthquakes using a 475 years return period spectrum, which is based on 5% critical damping. Allowance in the derivation of the lateral forces are made for ductility, for example a building in New Zealand can be designed for nominally elastic response for limited ductility response or for fully ductile response.

Low-rise buildings incorporating precast concrete walls are generally low period structures that are designed for either nominally elastic response or limited ductility response. In some cases, the amount of walls in the buildings is such that the probable lateral strength of the building exceeds that required in the New Zealand Loading Standard [N3] for elastic response. On the other hand it needs to be recognised that these buildings many have less damping than the one used to derive the horizontal coefficients in the Standard design spectrum. Also, recent earthquakes have shown peak ground acceleration that far exceeds the design values. Reasons for these high accelerations have been attributed to near field effects, directivity, soft soil and topographical amplifications. It can be said that significant uncertainty still exists in the evaluation of the design forces to ensure elastic response for a given return period, particularly for short period structures.

Design engineers have manifested the need to develop a continuum design approach where the lateral load capacity versus demand can be used as parameter for estimating the likely response of the structure and its structural members. Such approach is proposed, based on the curvature ductility demand μ_ϕ in the critical region of a wall, is formulated below.

Equation 6-3 was derived for the design engineers to make use of during the seismic design of thin walls. The derivation of this equation is shown in Appendix C at the back of this report.

$$\mu_\phi = 13.7\frac{l_p}{l_p'} - \frac{\left(6\frac{l_p}{l_p'} - 1\right)}{1.05}\frac{C_{h,provided}}{S_p C_{h(450)}} - 1.3 \qquad [6\text{-}3]$$

$$C_{h,provided} = \frac{V_{provided}}{W} \qquad [6\text{-}4]$$

where

μ_ϕ	=	curvature ductility demand in the critical wall of a structure (usually the longest wall)
l_p	=	theoretical potential plastic hinge length of the wall from Equation 2-5
l_p'	=	actual potential plastic hinge length
	=	l_p for conventionally reinforced walls and;
	=	$12d_b + t_{gap}$ for walls in which the plastic hinge is constrained to the wall-to-foundation connections, e.g. connected through lap splices
$C_{h,\,provided}$	=	provided coefficient from design process
$C_{h\,(450)}$	=	base shear coefficient for 450 year return period earthquake from [N3]
S_p	=	structural performance factor
	=	0.67
$S_{a(450)}$	=	design lateral force
$V_{provided}$	=	provided base shear capacity in the building
W	=	total building weight
d_b	=	diameter of reinforcement at the connection
t_{gap}	=	height of the gap between the base of wall and the foundation beam

The curvature ductility demand of the designed structural wall for 2000 years return period earthquake can be calculated using Equation 6-3. The moment-curvature analysis should be employed to obtain the curvature ductility which provided by the same sectional properties using the ultimate concrete strain, ε_{cu}, = -0.005. If the provided value of curvature ductility is smaller than the demand curvature ductility then confining

reinforcement is required in the compression zone. Otherwise, the wall has an adequate deformation capacity to resist elastically a 2000 years return period earthquake.

6.3 Summary

None of the test units failed in lateral buckling fashion except Unit 2 that subjected to a significant out-of-planed displacement which would be susceptible to lateral buckling failure. Strength loss for Units 1, 2 and 4 was due to material failure of either concrete crushing or fracturing of reinforcement. The latter case was caused when the starter bars were subjected to cyclic loading and buckled. Hence, this induced fatigue and fractured the starter bars eventually.

Most cracking activity occurred within the region of 1 m height above the foundation beam forming a well defined potential plastic hinge zone in Units 3 and 4. This was the result of twisting action at the base of the wall. The panel in the region above the potential plastic hinge zone deformed as a rigid body mode until failure. Once overstrength mechanism was maintained, yield penetration was allowed to occur where the bending moment exceeded the yield flexural capacity at both wall-foundation connection and above lap splice.

Eccentric vertical load also had a great influence on the crack pattern of Unit 2 and lead to an excessive out-of-plane displacement because the whole panel was cracked. The amount of out-of-plane displacement was not minimised by the twisting of the base as Units 1, 3 and 4. Lateral buckling failure might have occurred if the test was not terminated for safety reasons. The eccentric vertical load did not have a significant effect for Unit 4 which had a shorter lap splice length and subjected to both lateral and gravity loads because of the presence of twisting motion relieving some of the out-of-plane moments imposed by the eccentric gravity loads.

Twisting at the base was caused by side way motion of buckled starter bars when subjected to compression under load reversal after have been stretched in the previous cycle. This occurred during the displacement ductility range between 2.5 to 4.

In the design of precast concrete walls with $h_w/t_w \leq 75$, the assumption of the neutral axis stays perpendicular to the loading direction is not valid once the out-of-plane displacement commences.

CHAPTER 7
CONCLUSIONS AND RECOMMENDATIONS

7.1 CONCLUSIONS

1. The overall behaviour of the seismic test of a very thin single precast concrete walls with height to thickness ratio h_w/t_w = 75 with the construction joint using vertical starter bars grouped at both ends of the wall, performed reasonably well. They were able to achieve the displacement ductility factors ranging between 2 to 4 without strength degradation.

2. The effect of lap splice length was significant. The artificial welded lap splice length in Units 3 and 4 obviously gives the better performance as because the potential plastic hinge can be controlled and predicted. Hence, the provisions on the size of longitudinal reinforcement in New Zealand Concrete Structures Standard [N1] must be strictly followed for both nominally elastic and ductile walls.

3. There are a large differences in the wall behaviour between using uniformly distributed reinforcements at the cast-in-place wall-foundation connection in McMenamin [M1] and grouped starter bars with lap splice at the wall-foundation connection. The latter case appears to preclude flexural-shear crushing problem seen in the McMenamin tests and gives better representative of commonly used precast concrete wall and more practical in term of construction issues.

4. Displacement ductility at commencement of twisting about the vertical axis ($\mu_{\Delta,twist}$) was ranged between 2.5 to 4 and was followed by strength degradation. In order to make an improvement, the double layers of reinforcement with transverse reinforcement should be used for preventing the longitudinal bar from buckling. Alternatively, spiral reinforcement around the starter bars can be used.

5. The bar diameter-to-wall thickness ratio has the significant effects on crack pattern and the amount of yield penetration. According to this research, the wall with the diameter of longitudinal bars of 1/5 of the wall thickness performed such that a relative low level of ductility capacity was achieved without any strength degradation.

6. An effective second moment of inertia is proposed for the elastic analysis of walls except squat walls. In squat walls, allowances should be made in the analysis for shear deformations in the panels and allowing for possible sliding that occurs at the construction joints.

7. A design procedure proposed in this research was derived to ensure that the designed structural wall would survive the most extreme earthquake, i.e. 2000 years return period and to provide a tool for engineers to prevent the collapse of the structure.

8. Units 3 and 4 presented performance that was better than should be expected for walls with lap splice connections, because of the welding of the splices in those units which is not normally undertaken.

9. There is not sufficient evidence to conclude that lap splices have the effect on the performance of the walls.

7.2 DESIGN RECOMMENDATIONS

1. Nominally elastic design, $\mu_\Delta \leq 1.25$, is highly recommended for this type of thin precast concrete walls in order to prevent any strength reduction caused by twisting at the base, or excessive lateral deformation due to eccentric gravity loads.

2. The size of the longitudinal reinforcement should be strictly followed by the provisions in Concrete Structures Standard, NZS 3101:1995, Clause 17.3.6.3 for limited ductile walls ($3 \leq \mu_{\Delta} \leq 6$) and Clause 12.4.3.3 for fully ductile walls ($\mu_{\Delta} = 6$).

3. Ultimate concrete strain ε_{cu} = -0.005 is recommended as a spalling strain for a conventional sectional analysis and a moment-curvature analysis. Such high value is due to the confinement effect provided by the foundation beam.

4. The design engineers should always ensure that the design precast concrete wall would be able to resist a maximum credible earthquake with 2000 years return period using Equation 6-3. Confining reinforcement must be provided in the concrete compression zone when the curvature ductility demanded calculated from Equation 6-3 is smaller than the curvature ductility provided from the moment-curvature analysis of the section.

7.3 RECOMMENDATIONS FOR FURTURE RESEARCH

1. Other types of building configuration and boundary conditions should be investigated. For example, precast concrete walls with regular and irregular openings, different connection details at the base and wall panel with connected floor slabs.

2. The use of fibre and spiral as the reinforcement for crack control could be investigated.

3. The effects of the combination of in-plane lateral loading, vertical loading and out-of-plane face loading.

4. The proposed equation for the effective second moment of inertia may need to be refined as there might be other variables that have not covered in this research.

REFERENCES

[A1] ASTM Standard C939-94a, *Standard Test Method for Flow of Grout for Preplaced-Aggregate Concrete (Flow Cone Method)*, 1994 Annual Book of ASTM Standards, Vol. 04.02, Philadelphia, 473-475 p.

[A2] ACI Compilation No. 7, *Connections for Tilt-up Construction*, by Weiler G., American Concrete Institute, Michigan, 11-15 p.

[A3] ACI Committee 318, *Building Code Requirements for Reinforced Concrete (ACI 318-89) and Commentary*, American Concrete Institute, Detroit, 1989, 111 p.

[A4] Azizinamini, A., Glikin, J.C. and Oesterle, R.G., *Tilt-up Walls Test Results*, RP322D, Portland Cement Association, Skokie, Illinois, U.S.A., 1994, 16 p.

[A5] Andriono, Takim, *Properties of Reinforcing Steel Used In Seismic Design*, Research Report 86-9, Department of Civil Engineering, University of Canterbury, Christchurch, New Zealand, 1986, 187p.

[B1] Brown, B.J., *Some Stability Issues For Tilt-Up Precast Panels Under In-Plane Seismic Loading*, Journal of the New Zealand Structural Engineering Society (SESOC), Vol.10, No.1, June 1997, 34-42 p.

[C1] Crisafulli, F.J., Restrepo, J.I. and Park, R., *Earthquake Resistance of Structures: The Design and Construction of Tilt-Up Reinforced Concrete Buildings*, Research Report 96-11, Department of Civil Engineering, University of Canterbury, Christchurch, New Zealand, 1996, 138 p.

[E1] *Examples of Concrete Structural Design to New Zealand Standard 3101 (Red Book)*, Cement & Concrete Association of New Zealand, August 1998.

[G1] *Guidelines for the Use of Precast Concrete in Buildings,* Report of a Study Group of the New Zealand Concrete Society and the New Zealand National Society for Earthquake Engineering, Editor: Charlesson, A.W., The Printer, University of Canterbury, Christchurch, August 1991, 174 p.

[G2] Goodsir, W.J., *The Design of Coupled Frame-Wall Structures for Seismic Actions*, Research Report 85-8, Department of Civil Engineering, University of Canterbury, Christchurch, New Zealand, 1985, 333 p.

[H1] Hollings, J.P., *Reinforced Concrete Seismic Design*, Bulletin of New Zealand, National Society for Earthquake Engineering, Vol. 2, No. 3, 217-250p.

[M1] McMenamin, A., *The Performance of Slender Precast Reinforced Concrete Cantilever Walls With Roof Level Lateral Displacement Restraint Under Simulated In-Plane Seismic Loading*, Research Report 99-4, Department of Civil Engineering, University of Canterbury, Christchurch, New Zealand, 1999, 275p.

[N1] NZS 3101: 1995, Concrete Structures Standard, *Part 1: The Design of Concrete Structures* and *Part 2: Commentary on the Design of Concrete Structures*, Standards Association of New Zealand, Wellington, 1995.

[N2] NZS 3109: 1997, *Concrete Construction Standard, Part 1 & 2*, Standards Association of New Zealand, Wellington, 1997.

[N3] NZS 4203: 1992, New Zealand Loading Standard, *General Structural Design and Design Loadings for Buildings, Parts 1 & 2*, Standards Association of New Zealand, Wellington, 1992.

[N4] NZS 3101: 1982, *Part 1: New Zealand Standard Code of Practice for the Design of Concrete* and *Part 2: Commentary NZS 3101*, Standards Association of New Zealand, Wellington, 1982.

[P1] Paulay, T. and Priestley, M.J.N., *Seismic Design of Reinforced Concrete and Masonry Buildings*, John Wiley and Sons, Inc, 1992, 744 p.

[P2] Park, R. and Paulay, T., *Reinforced Concrete Structures*, John Wiley and Sons, New York, 1975, 769 p.

[R1] *Recommended Tilt-Up Design*, Report of Structural Engineers Association of Southern California, June 1979, 18 p.

[S1] Saaticioglu, M., Wood, S.L. and French, C.W., *Deformability of Concrete Members*, Seismic Engineering: Research and Practice, Proceedings of the sessions related to seismic engineering at Structure Congress'89, Editor: Kircher, A. and Chopra, A.K., Publisher: American Society of Civil Engineers, 1989, 845-855 p.

[S2] Gorenc, B., Tinyou, R. and Syam, A., *Steel Designers' Handbook*, 6th Edition, Southwood Press, 1996, 334 p.

[T1] *Tilt-up Technical Manual- TM 34*, Cement & Concrete Association of New Zealand, Editor: Chisholm, D.H., October 1991, 30 p.

[T2] *Tilt-Up Concrete Structures- Reported by ACI Committee (ACI 551R-92)*, American Concrete Institute, Michigan, February 1992, 45 p.

[T3] *Test Report on Slender Walls*, Southern California Chapter American Concrete Institute and Structural Engineers Association of Southern California, 1982, 120 p.

[W1] Wood, S.L., *Minimum Tensile Reinforcement Requirements in Walls*, ACI Structural Journal, Vol. 86, No. 5, September-October 1989, 582-591 p.

[W2] Whitney, C.S., *Plastic Theory of Reinforced Concrete Design*, Proceedings ASCE, December 1940; Transactions ASCE, Vol. 107, 1942, 251-326 p.

APPENDIX A

THE DERIVATION OF CONSTANT APPLIED ECCENTRIC VERTICAL LOADING FOR UNITS 2 AND 4

Gravity Load Calculations

From the idealise building in Figure 3.1, span length is 10 m long.

Prototype wall dimensions: -

Height	=	9.375 m
Width	=	2.5 m
Thickness	=	125 mm

Loads

	Roof dead load	=	25 kN/m^3 × 0.160 m
		=	4.0 kPa for concrete slab
∴	UDL (Roof)	=	4.0 kPa × 5 m
		=	20 kN/m
∴	Stress (Roof)	=	20 kN/m ÷125 mm
		=	0.160 MPa
∴	UDL (Wall weight)	=	24 kN/m^3 × 9.375 m × 0.125 m
		=	28.125 kN/m
∴	Stress (Wall weight)	=	28.125 kN/m ÷ 125 mm
		=	0.225 MPa
	Total stress	=	0.160 + 0.225
		=	0.385 MPa
Therefore, N^*/f'_cA_g		=	0.385/30
		=	0.0128

Maximum eccentricity is approximately 80 mm from the face of the idealise wall.

Scale factor is 1 : 2.5, hence maximum eccentricity is 32 mm.

Model wall dimensions: -

	Height	=	3.75 m
	Width	=	1 m
	Thickness	=	50 mm
∴	UDL (Wall weight)	=	24 kN/m^3 × 3.75m × 0.05m
		=	4.5 kN/m
∴	Stress (Wall weight)	=	4.5 kN/m ÷ 50 mm
		=	0.09 MPa
Additional wall weight		=	(0.225- 0.09) MPa × 50 mm × 1000
		=	6750 N or 675 kg
Additional roof weight		=	0.16 MPa × 50 mm × 1000
		=	8000 N or 800 kg

Each lead ingot weighs approximately 26 kg. Therefore,

No. of lead ingots for wall weight	=	675 kg ÷ 26 kg/ingot
	=	*26 ingots for wall weight*
No. of lead ingots for roof weight	=	800 kg ÷ 26 kg/ingot
	=	*31 ingots for roof weight*

NOTE: Weight of lead ingot "container" has not been taken into account in the above calculation (approx. 75 kg).

APPENDIX B

SECANT STIFFNESS AND REFERENCE YIELD DISPLACEMENT CALCULATIONS

The secant stiffness was calculated from the measured lateral loads and lateral displacement from hysteresis loops at each cycle of $\pm 0.75P_n$ lateral load level. Table B-1 shows the summary of the both measured values for all test units.

Table B-1: Average stiffness (k_{75}) calculation

Unit	Description	Load P (kN)	Displacement 1 Δ_1 (mm)	Displacement 2 Δ_2 (mm)	Average Displacement Δ_{ave} (mm)	Stiffness k (kN/mm)	Average Stiffness k_{75}(kN/mm)
1	$+0.75P_n \times 1$	18.3	-	-	-	-	1.406
	$-0.75P_n \times 1$	18.0	11.30	14.10	12.7	1.42	
	$+0.75P_n \times 2$	18.3	12.70	12.90	12.8	1.43	
	$-0.75P_n \times 2$	17.8	11.60	14.40	13.0	1.37	
2	$+0.75P_n \times 1$	19.4	10.56	10.10	10.33	1.88	1.987
	$-0.75P_n \times 1$	19.3	10.26	9.78	10.02	1.93	
	$+0.75P_n \times 2$	19.3	9.45	7.94*	9.45	2.04	
	$-0.75P_n \times 2$	19.2	9.85	8.39	9.12	2.10	
3	$+0.75P_n \times 1$	17.6	7.85	7.55	7.70	2.29	1.970
	$-0.75P_n \times 1$	17.3	9.87	10.05	9.96	1.74	
	$+0.75P_n \times 2$	17.7	8.46	8.00	8.23	2.15	
	$-0.75P_n \times 2$	17.5	10.37	10.45	10.41	1.68	
4	$+0.75P_n \times 1$	19.7	7.00	6.08	6.54	3.01	2.373
	$-0.75P_n \times 1$	19.7	10.30	9.60	9.95	1.98	
	$+0.75P_n \times 2$	19.7	7.93	7.05	7.49	2.63	
	$-0.75P_n \times 2$	19.9	11.05	10.28	10.67	1.87	

* This value was ignored in the calculation

Table B-2: Reference yield displacement for all test units

Unit	1	2	3	4
Nominal Flexural Strength, P_n (kNm)	24.4	26.1	23.4	25.4
Reference Yield Displacement, Δ_y (mm)	17.3	13.1	11.9	10.7

Example for Unit 2

From Table B-1, find the "Average Lateral Displacement" from "Displacement 1" and "Displacement 2".

At $+0.75P_n \times 1$, the average displacement Δ_{ave} is: -

$$\frac{10.56+10.10}{2} = 10.33 \text{ mm}$$

Stiffness k is calculated by dividing the average displacement Δ_{ave} from the load P as the following: -

$$\frac{19.4}{10.33} = 1.88 \text{ kN/mm}$$

Then, find the average value of "In-plane stiffness, k_{75}", Hence, calculate reference yield displacement (refer Table B-2).

$$\frac{P_n}{k_{75}} = \frac{26.1}{1.987} = 13.1 \text{ mm}$$

APPENDIX C

CURVATURE DUCTILITY DEMAND OF STRUCTURE FOR 2000 YEARS RETURN PERIOD EARTHQUAKE

From NZS 4203:1992 Part 2: Commentary [N3], Figure C-1 illustrates the relationship of risk factor and return period or annual probability of exceedence of the earthquake.

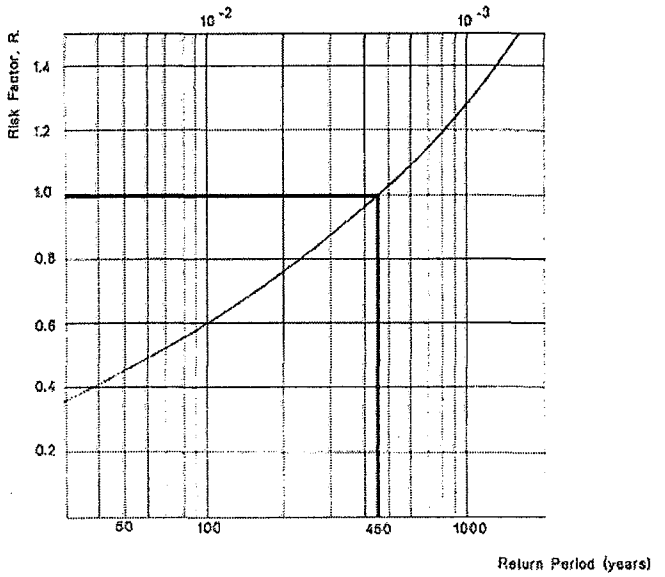

Figure C-1: Relationship between risk factor and return period [N3]

Design lateral force is normally derived from the response spectrum with specified soil conditions and damping which is probabilistically equivalent to 450 years return period earthquake [N3].

The provided flexural strength of structure ($C_{h,\ provided}$) must be always greater than the design strength ($C_{h\ (450)}$) at least 1.35 times to allow for the overstrength mechanism when designing structures with limited ductility [A5]. Equation C-1 is thus:

$$\frac{C_{h,provided}}{S_p C_{h(450)}} = 1.35 \qquad [C\text{-}1]$$

where S_p is the structural performance factor

The curvature ductility demand (μ_ϕ) for wall designed for nominally elastic response is normally given as Equation C-2 where the shorter potential plastic hinge length is taken into account due to lap-splice above the horizontal connection.

$$\mu_\phi = 6\frac{l_p}{l_p'} \qquad \text{[C-2]}$$

where l_p and l_p' are theoretical and experimental potential plastic hinge length for wall respectively.

For the same wall to be able to resist 2000 years return period earthquake, Equation C-3 and C-4 must be satisfied.

$$\frac{C_{h,provided}}{S_p C_{h(450)}} = \lambda \frac{C_{h(2000)}}{C_{h(450)}} \qquad \text{[C-3]}$$

where λ is an amplification factor taking into account for local amplification effects possibly lower damping and to recognise that for low period structures, the lateral displacement demand of an inelastic system is greater than the demand for an elastic system .

Assuming $\lambda = 1.5$, hence: -

$$\frac{C_{h,provided}}{S_p C_{h(450)}} = 1.5 \times 1.6$$

$$= 2.4$$

Equation C-4 represents curvature ductility demand for 2000 years return period earthquake which is equivalent to elastic response.

$$\mu_\phi = 1 \qquad \text{[C-4]}$$

Therefore, combination of Equations C-1 to C-4 lead to: -

$$\mu_\phi = \frac{6\frac{l_p}{l_p'} - 1}{1.35 - 2.4}\left(\frac{C_{h,provided}}{S_p C_{h(450)}} - 1.35\right) + 6\frac{l_p}{l_p'}$$

$$= \frac{\left(-6\frac{l_p}{l_p'} + 1\right)}{1.05}\frac{C_{h,provided}}{S_p C_{h(450)}} - \frac{1.35}{1.05}\left(-6\frac{l_p}{l_p'} + 1\right) + 6\frac{l_p}{l_p'}$$

$$= \frac{\left(-6\frac{l_p}{l_p'} + 1\right)}{1.05}\frac{C_{h,provided}}{S_p C_{h(450)}} + 6\frac{l_p}{l_p'}\left(\frac{1.35}{1.05} + 1\right) - \frac{1.35}{1.05}$$

$$= \frac{\left(1 - 6\frac{l_p}{l_p'}\right)}{1.05}\frac{C_{h,provided}}{S_p C_{h(450)}} + 13.7\frac{l_p}{l_p'} - 1.3$$

Hence, $$\mu_\phi = 13.7\frac{l_p}{l_p'} - \frac{\left(6\frac{l_p}{l_p'} - 1\right)}{1.05}\frac{C_{h,provided}}{S_p C_{h(450)}} - 1.3 \qquad \text{[C-5]}$$

From experimental work of this research, the reduced potential plastic hinge length (l_p') due to lap splice is given by Equation C-6.

$$l_p' = 12d_b + t_{gap} \qquad \text{[C-6]}$$

where d_b is diameter of the starter bars and t_{gap} is the height of gap between the wall and the foundation beam.

Finally, the strength provided ($C_{h,\,provided}$) is given by Equation C-7.

$$C_{h,provided} = \frac{V_{provided}}{W} \qquad \text{[C-7]}$$

where $V_{provided}$ is the provided base shear capacity of the specified sectional properties and W is the total gravity weight imposed on the wall.

APPENDIX D

SLIDING SHEAR FOR UNITS 1 TO 4 MEASURED DURING THE TEST

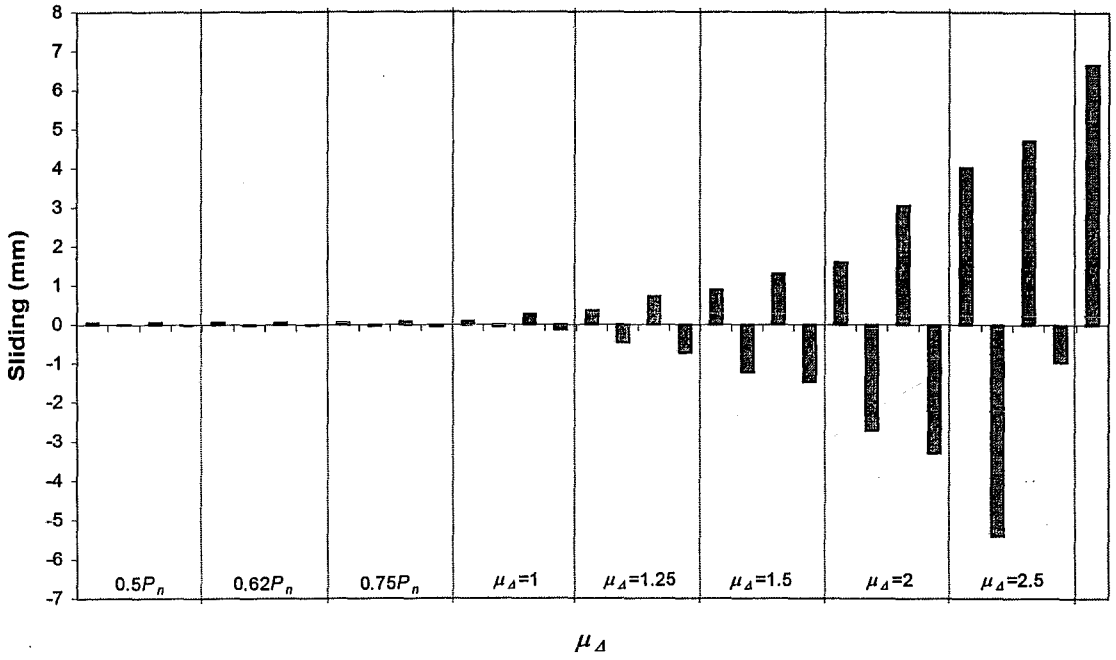

Figure D-1: Sliding shear history measured during the test for Unit 1

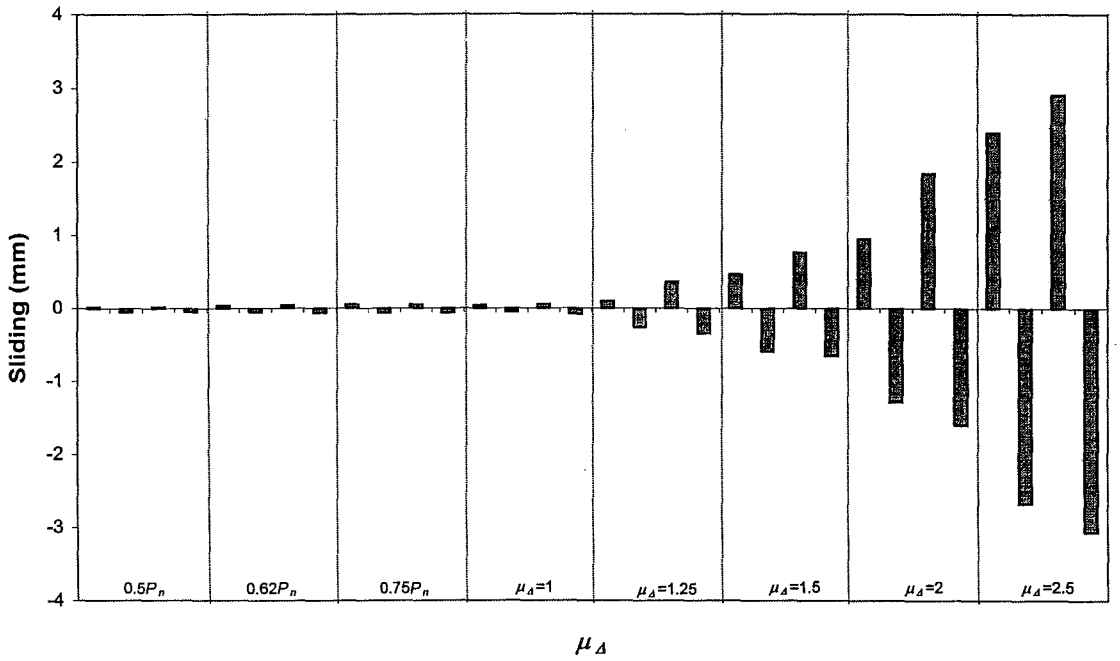

Figure D-2: Sliding shear history measured during the test for Unit 2

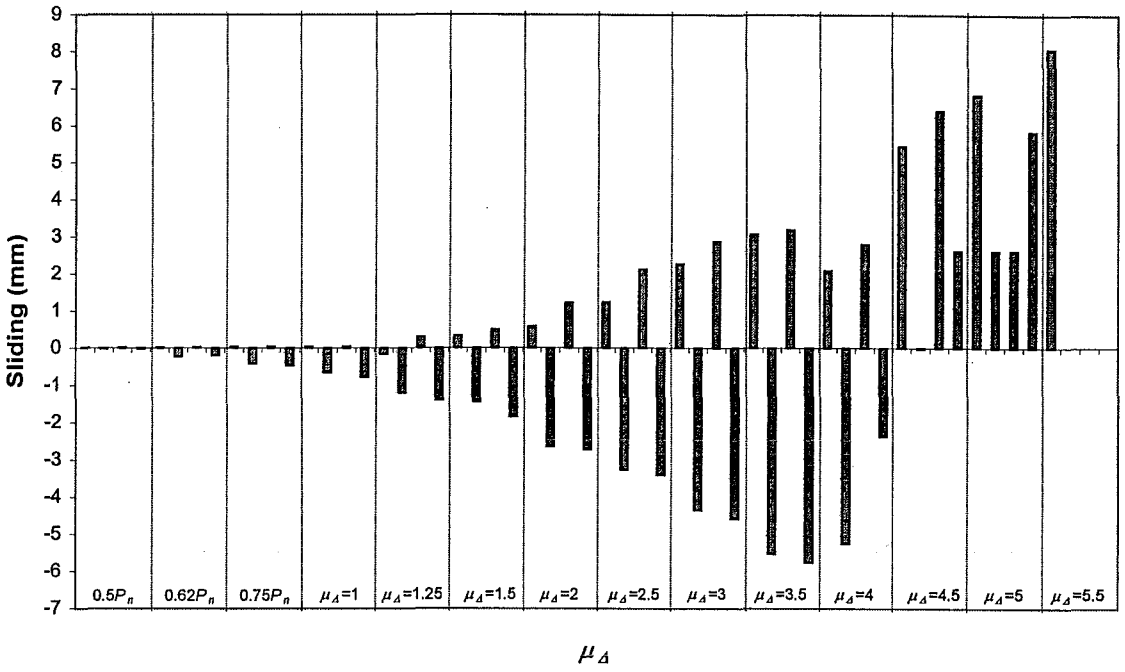

Figure D-3: Sliding shear history measured during the test for Unit 3

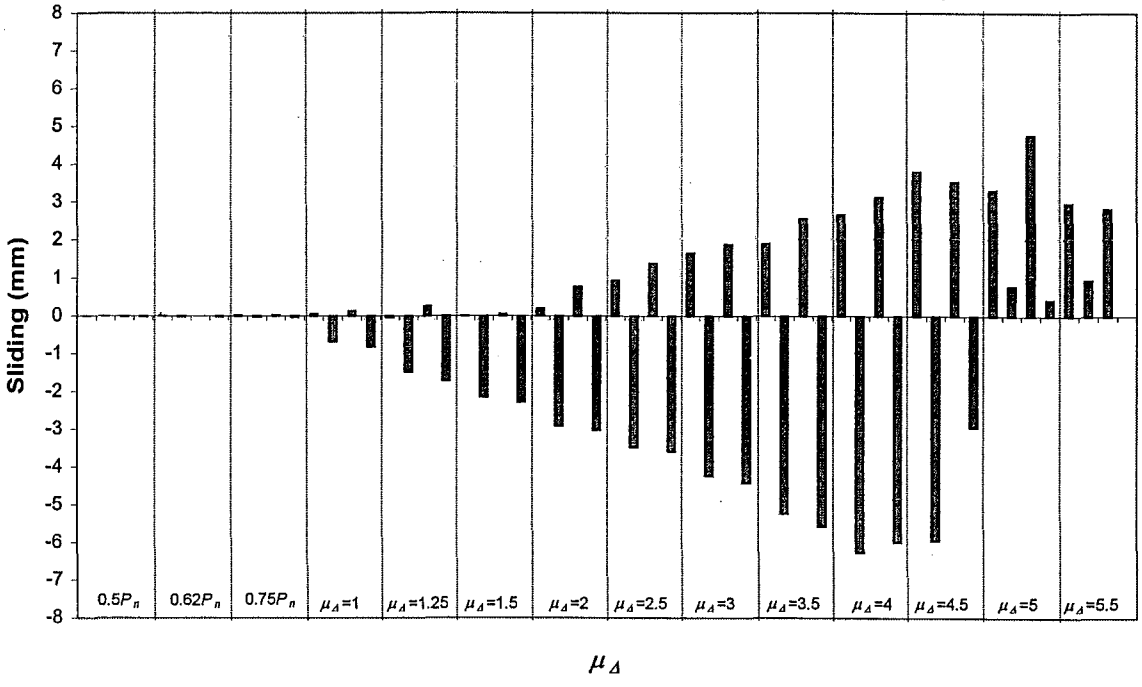

Figure D-4: Sliding shear history measured during the test for Unit 4